Electronic Quantum Transport Simulation for 2D Materials

Ming-Hao Liu (劉明豪)

Department of Physics, National Cheng Kung University, Taiwan

Institut für Theoretische Physik, Universität Regensburg, Germany

17 May 2024

Outline

Basics

- Landauer-Büttiker formalism
- Real-space Green's function method
- Lead self-energy
- Peierls substitution
- Gauge transformation for vector potential
- Semiclassical motion of Bloch electrons
- Electrostatics
- Periodic boundary hopping

Applications

- 2DEG & MoS_2
- Graphene
- Bilayer graphene
- Lieb lattice

Part I

Basics

Landauer-Büttiker formalism[1]

Landauer formula[2,3]

$$G(E) = \frac{2e^2}{h} T(E)$$

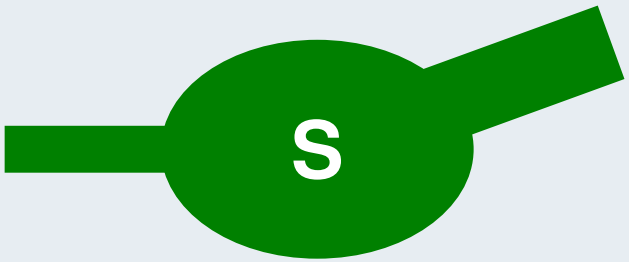

$T(E)$: sum of $|t|^2$ of all involved modes at E.

+

Büttiker formula[4]

$$I_\alpha = \sum_\beta G_{\alpha\beta}(V_\alpha - V_\beta)$$

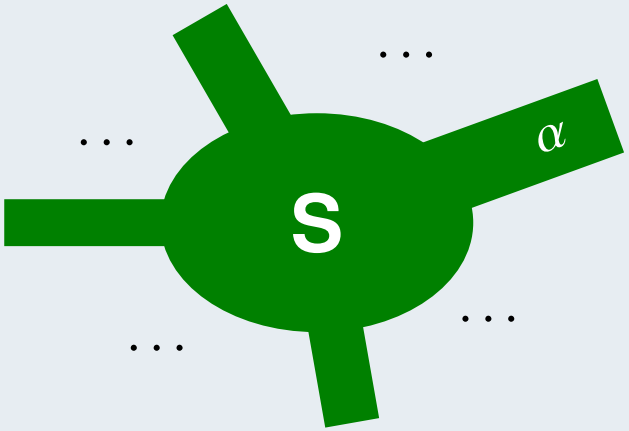

[1] Datta, S., *Electronic Transport in Mesoscopic Systems* (1995)

[2] Landauer, R., Philosophical Magazine **21** (1970) 863

[3] Anderson, P. W., Thouless, D. J., Abrahams, E., and Fisher, D. S., Phys. Rev. B **22** (1980) 3519

[4] Büttiker, M., Physical Review Letters **57** (1986) 1761

4-point resistance

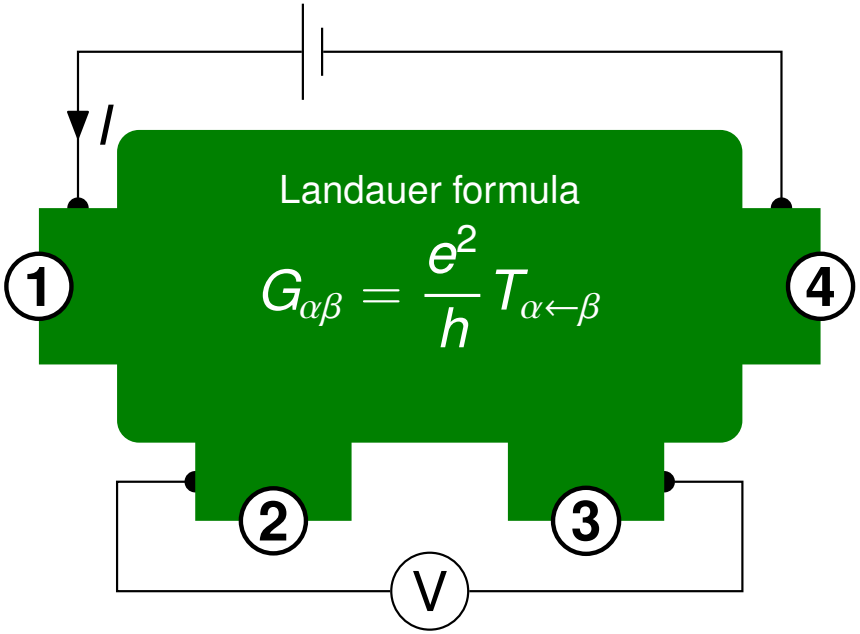

Büttiker formula:

$$I_\alpha = \sum_\beta G_{\alpha\beta}(V_\alpha - V_\beta)$$
$$\alpha, \beta = 1, 2, 3, 4$$

Explicitly:

$$\begin{aligned} I_1 &= G_{12}(V_1 - V_2) + G_{13}(V_1 - V_3) + G_{14}(V_1 - V_4) \\ &= (G_{12} + G_{13} + G_{14})V_1 - G_{12}V_2 - G_{13}V_3 - G_{14}V_4 \\ &= \sum_{\beta\neq 1} G_{1\beta}V_1 - G_{12}V_2 - G_{13}V_3 - G_{14}V_4 \end{aligned}$$

Similarly for I_2, I_3, I_4.

4-point resistance (cont.)

In terms of matrices:

$$\begin{pmatrix} I_1 \\ I_2 \\ I_3 \\ I_4 \end{pmatrix} = \begin{pmatrix} \sum_{\beta\neq 1} G_{1\beta} & -G_{12} & -G_{13} & -G_{14} \\ -G_{21} & \sum_{\beta\neq 2} G_{2\beta} & -G_{23} & -G_{24} \\ -G_{31} & -G_{32} & \sum_{\beta\neq 3} G_{3\beta} & -G_{34} \\ -G_{41} & -G_{42} & -G_{43} & \sum_{\beta\neq 4} G_{4\beta} \end{pmatrix} \begin{pmatrix} V_1 \\ V_2 \\ V_3 \\ V_4 \end{pmatrix}$$

By grounding ④ (i.e., $V_4 = 0$) and looking at only I_1, I_2, I_3:

$$\begin{pmatrix} I_1 \\ I_2 \\ I_3 \end{pmatrix} = \underbrace{\begin{pmatrix} \sum_{\beta\neq 1} G_{1\beta} & -G_{12} & -G_{13} \\ -G_{21} & \sum_{\beta\neq 2} G_{2\beta} & -G_{23} \\ -G_{31} & -G_{32} & \sum_{\beta\neq 3} G_{3\beta} \end{pmatrix}}_{\mathbb{G}} \begin{pmatrix} V_1 \\ V_2 \\ V_3 \end{pmatrix}$$

By matrix inversion:

$$\begin{pmatrix} V_1 \\ V_2 \\ V_3 \end{pmatrix} = \underbrace{\begin{pmatrix} R_{11} & R_{12} & R_{13} \\ R_{21} & R_{22} & R_{23} \\ R_{31} & R_{32} & R_{33} \end{pmatrix}}_{\mathbb{R}=\mathbb{G}^{-1}} \begin{pmatrix} I_1 \\ I_2 \\ I_3 \end{pmatrix}$$

4-point resistance (cont.)

Since V_2, V_3 are voltage probes, $I_2 = I_3 = 0$. Setting $I_1 = I$, we have:

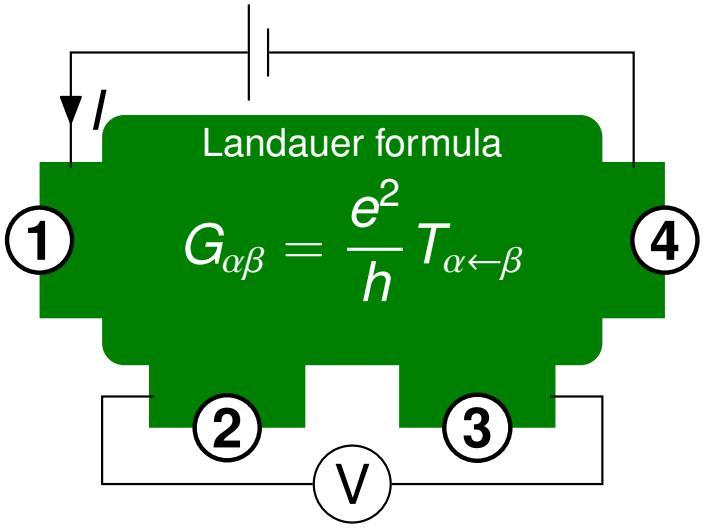

$$\begin{pmatrix} V_1 \\ V_2 \\ V_3 \end{pmatrix} = \begin{pmatrix} R_{11} & R_{12} & R_{13} \\ R_{21} & R_{22} & R_{23} \\ R_{31} & R_{32} & R_{33} \end{pmatrix} \begin{pmatrix} I \\ 0 \\ 0 \end{pmatrix}$$

and hence:

$$V_2 = R_{21} I$$
$$V_3 = R_{31} I$$

Therefore, the four-point resistance is given by:

$$R_{4p} \equiv \frac{V_2 - V_3}{I} = R_{21} - R_{31}$$

Datta, S., *Electronic Transport in Mesoscopic Systems* (1995)

Real-space Green's function method: Recipe

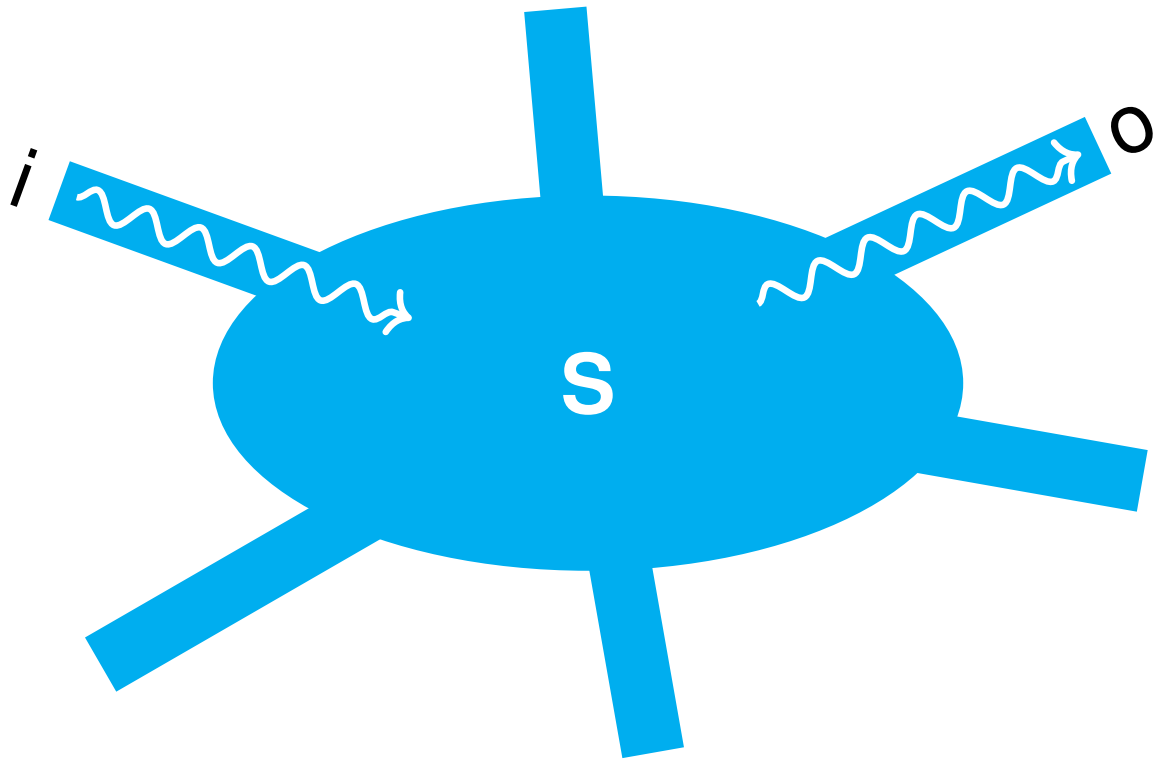

(S: scattering region, i: incoming lead, o: outgoing lead)

Real-space Green's function method: Recipe

Brief summary of the recipe:

$$H_0 = [\cdots]_{N\times N} \qquad \text{(clean tight-binding Hamiltonian)}$$

$$U = [\cdots]_{N\times N} \qquad \text{(onsite energy)}$$

$$\Sigma_p(E) = [\cdots]_{N\times N} \qquad \text{(self-energy at energy } E \text{ for lead } p\text{)}$$

$$H(E) = H_0 + U + \sum_p \Sigma_p(E) \qquad \text{(effective Hamiltonian)}$$

$$G_R(E) = [E\mathbb{1} - H]^{-1} \qquad \text{(retarded Green's function at energy } E\text{)}$$

$$\Gamma_p(E) = -2\mathrm{Im}\Sigma_p(E) \qquad \text{(broadening matrix at energy } E \text{ for lead } p\text{)}$$

$$T_{o\leftarrow i}(E) = \mathrm{Tr}\left[\Gamma_o(E)G_R(E)\Gamma_i(E)G_R^\dagger(E)\right] \qquad \text{(transmission from } i \text{ to } o\text{)}$$

Real-space Green's function method: Recipe

Brief summary of the recipe:

$$H_0 = [\cdots]_{N\times N} \qquad \text{(clean tight-binding Hamiltonian)}$$

$$U = [\cdots]_{N\times N} \qquad \text{(onsite energy)}$$

$$\Sigma_p(E) = [\cdots]_{N\times N} \qquad \text{(self-energy at energy } E \text{ for lead } p\text{)}$$

$$H(E) = H_0 + U + \sum_p \Sigma_p(E) \qquad \text{(effective Hamiltonian)}$$

$$G_R(E) = [E\mathbb{1} - H]^{-1} \qquad \text{(retarded Green's function at energy } E\text{)}$$

$$\Gamma_p(E) = -2\mathrm{Im}\Sigma_p(E) \qquad \text{(broadening matrix at energy } E \text{ for lead } p\text{)}$$

$$T_{o\leftarrow i}(E) = \mathrm{Tr}\left[\Gamma_o(E)G_R(E)\Gamma_i(E)G_R^\dagger(E)\right] \qquad \text{(transmission from } i \text{ to } o\text{)}$$

Matrix size:

$$N = N_{\text{sites}} \times N_{\text{orbitals}}$$

Typically, $O(N) \lesssim 10^4$: easy, $O(N) > 10^8$: out of reach.

Self-energy of semi-infinite leads

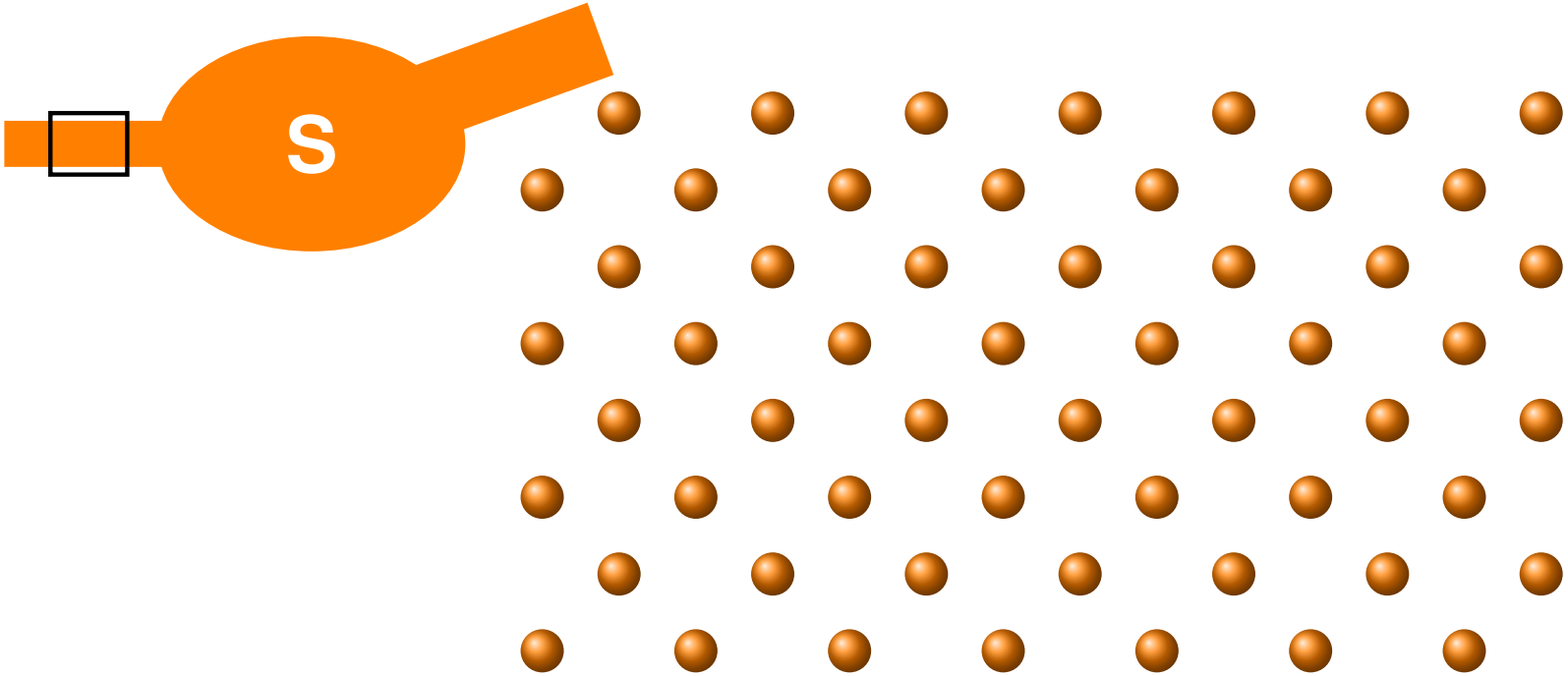

Self-energy of semi-infinite leads

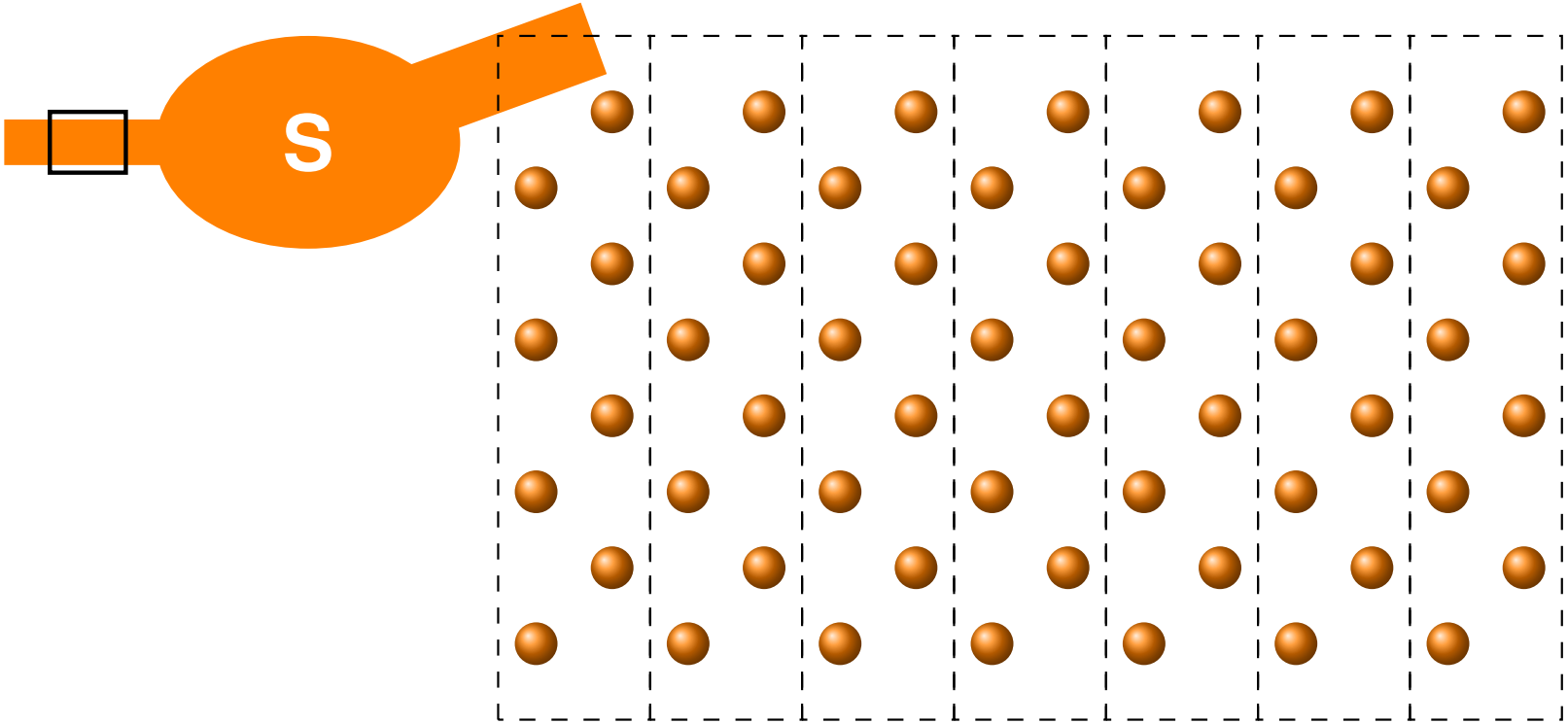

Self-energy of semi-infinite leads

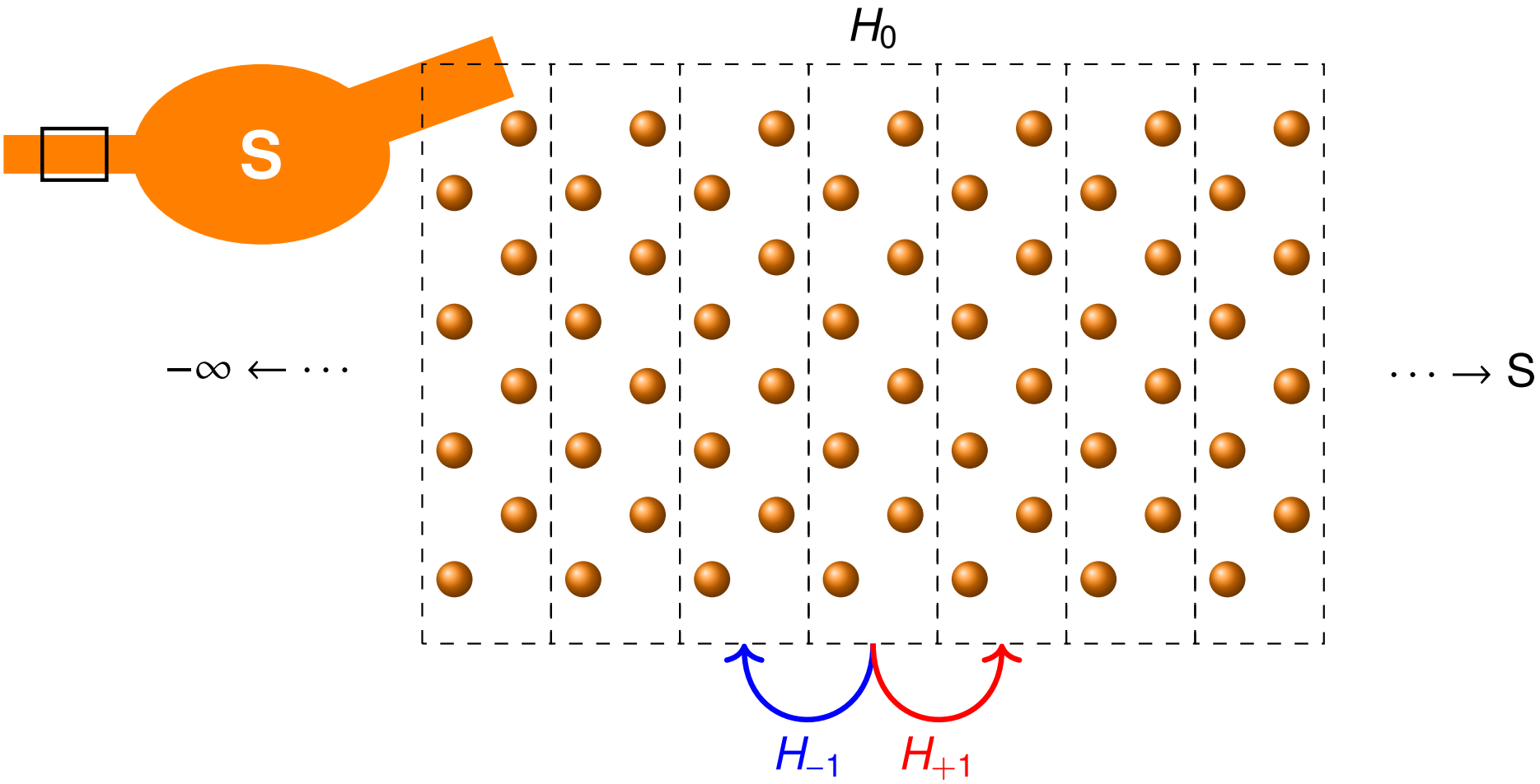

Self-energy of semi-infinite leads

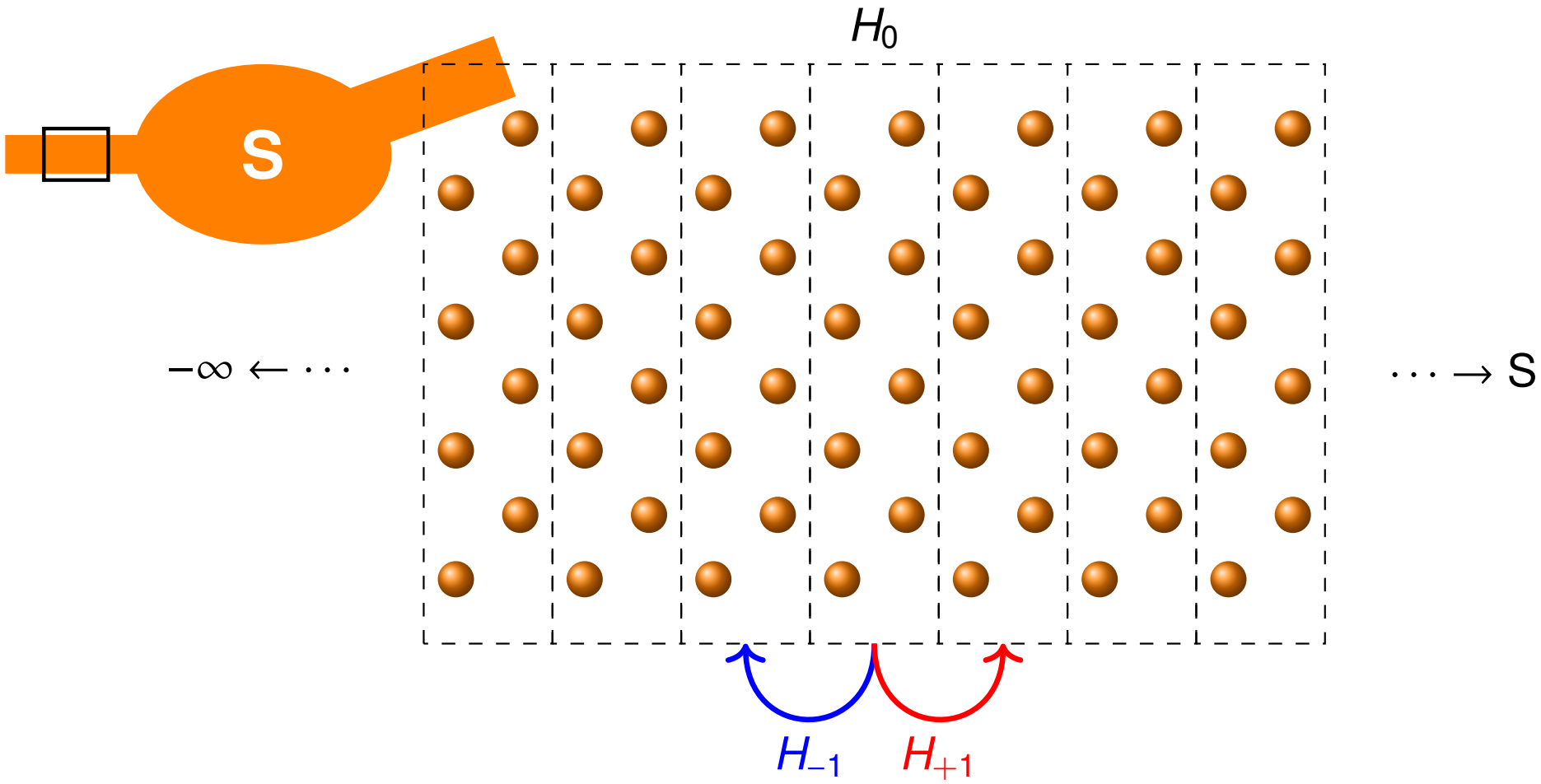

Lead self-energy:

$$\Sigma = \Sigma(E, H_0, H_\pm)$$

(Schur decomposition[1])

[1] Wimmer, M., PhD thesis, Universität Regensburg, 2008

Perpendicular magnetic field

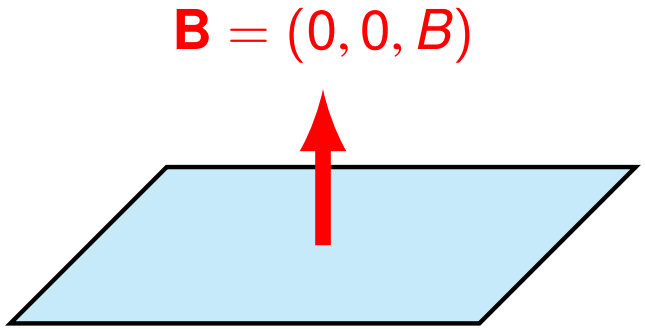

$$\mathbf{B} = \nabla \times \mathbf{A}$$

$$t \to te^{i\Phi} \qquad \text{(Peiers substitution)}$$

$$\Phi = \frac{-e}{\hbar} \int \mathbf{A} \cdot d\mathbf{s} \qquad \text{(Peierls phase)}$$

To maintain translational invariance in the leads:

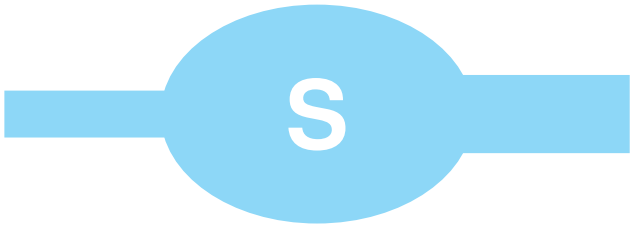

$\mathbf{A} = (-yB, 0)$

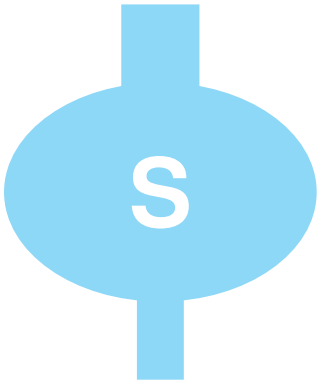

$\mathbf{A} = (0, xB)$

Perpendicular magnetic field

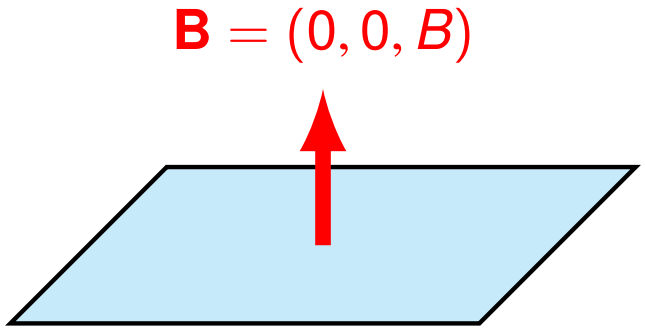

$$\mathbf{B} = \nabla \times \mathbf{A}$$

$$t \to te^{i\Phi} \qquad \text{(Peiers substitution)}$$

$$\Phi = \frac{-e}{\hbar} \int \mathbf{A} \cdot d\mathbf{s} \qquad \text{(Peierls phase)}$$

To maintain translational invariance in the leads:

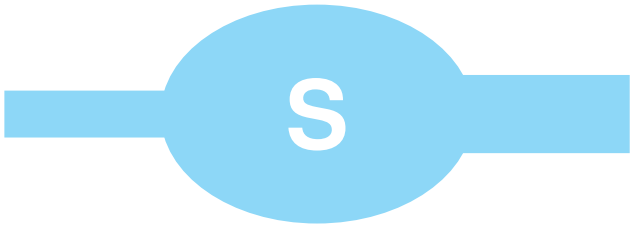

$\mathbf{A} = (-yB, 0)$

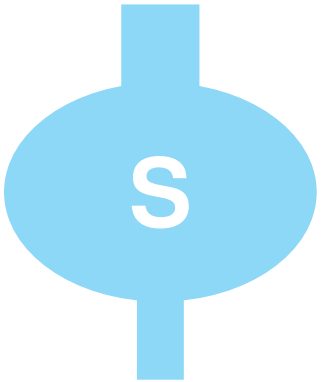

$\mathbf{A} = (0, xB)$

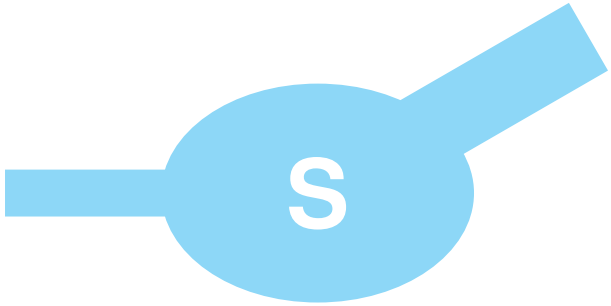

$\mathbf{A} = ?$

Gauge transformation[1]

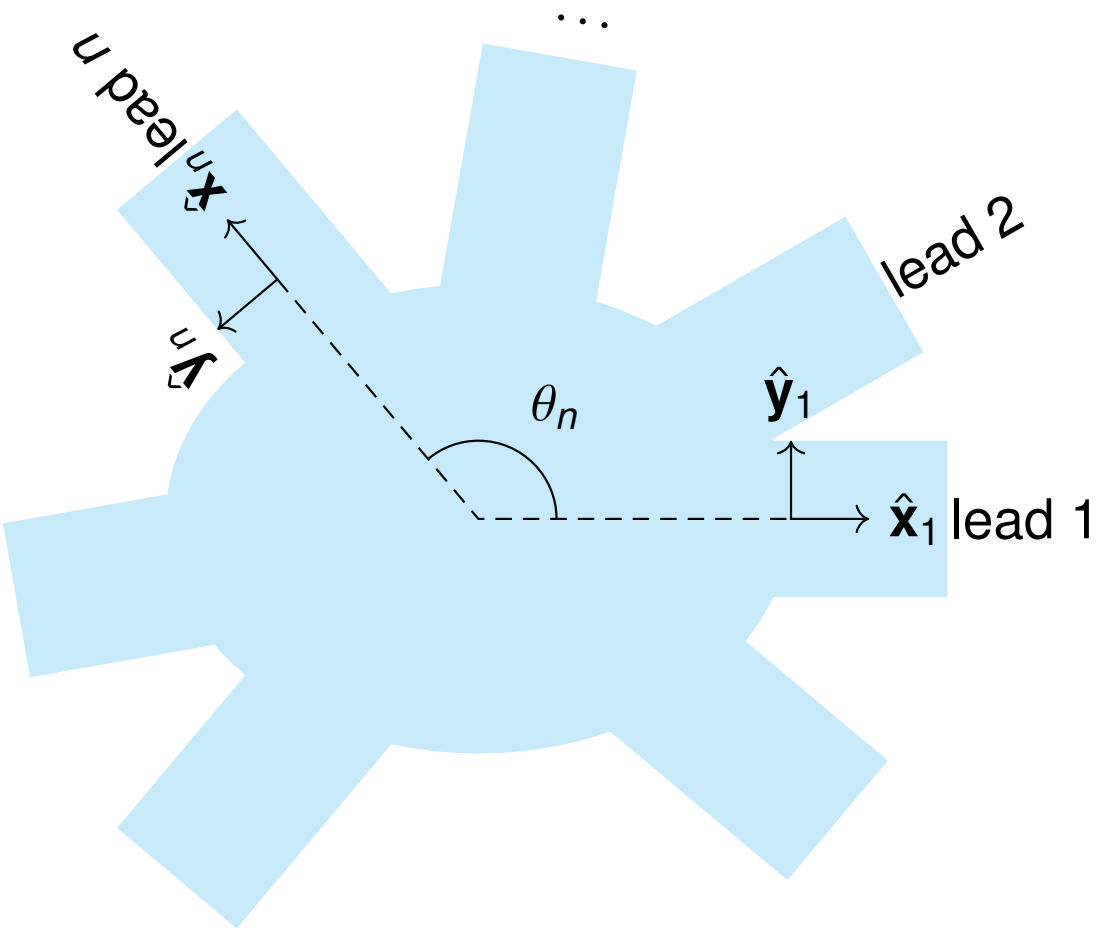

[1] Baranger, H. U. and Stone, A. D., Physical Review B **40** (1989) 8169; Mreńca-Kolasińska, A., Chen, S.-C., and Liu, M.-H., npj 2D Materials and Applications **7** (2023) Article number: 64

Gauge transformation[1]

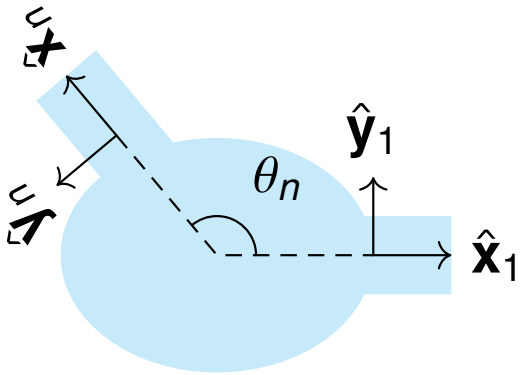

- We adopt

$$\mathbf{A}_1 = -y_1 B \hat{\mathbf{x}}_1 \qquad \text{(in lead 1)}$$

- We wish to have

$$\mathbf{A}_n = -y_n B \hat{\mathbf{x}}_n \qquad \text{(in lead } n\text{)}$$

[1] Baranger, H. U. and Stone, A. D., Physical Review B **40** (1989) 8169; Mreńca-Kolasińska, A., Chen, S.-C., and Liu, M.-H., npj 2D Materials and Applications **7** (2023) Article number: 64

Gauge transformation[1]

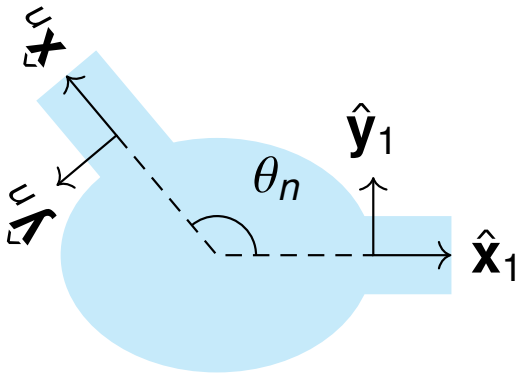

- We adopt

$$\mathbf{A}_1 = -y_1 B \hat{\mathbf{x}}_1 \qquad \text{(in lead 1)}$$

- We wish to have

$$\mathbf{A}_n = -y_n B \hat{\mathbf{x}}_n \qquad \text{(in lead } n\text{)}$$

The answer[1] is:

$$\mathbf{A}_n(x_1, y_1) = \mathbf{A}_1(x_1, y_1) + \nabla f_n(x_1, y_1)$$

$$f_n(x_1, y_1) = B x_1 y_1 \sin^2\theta_n + \frac{1}{2} B (x_1^2 - y_1^2) \sin\theta_n \cos\theta_n$$

[1] Baranger, H. U. and Stone, A. D., Physical Review B **40** (1989) 8169; Mreńca-Kolasińska, A., Chen, S.-C., and Liu, M.-H., npj 2D Materials and Applications **7** (2023) Article number: 64

Gauge transformation[1]

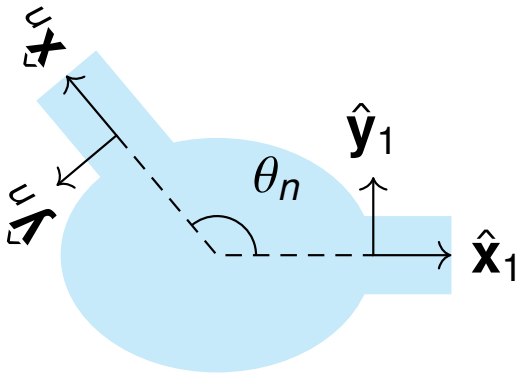

- We adopt

$$\mathbf{A}_1 = -y_1 B \hat{\mathbf{x}}_1 \qquad \text{(in lead 1)}$$

- We wish to have

$$\mathbf{A}_n = -y_n B \hat{\mathbf{x}}_n \qquad \text{(in lead } n\text{)}$$

The answer[1] is:

$$\mathbf{A}_n(x_1, y_1) = \mathbf{A}_1(x_1, y_1) + \nabla f_n(x_1, y_1)$$

$$f_n(x_1, y_1) = B x_1 y_1 \sin^2\theta_n + \frac{1}{2} B (x_1^2 - y_1^2) \sin\theta_n \cos\theta_n$$

If $\theta_1 = 0$, we may simply denote with

$$(x_1, y_1) \to (x, y)$$

[1] Baranger, H. U. and Stone, A. D., Physical Review B **40** (1989) 8169; Mreńca-Kolasińska, A., Chen, S.-C., and Liu, M.-H., npj 2D Materials and Applications **7** (2023) Article number: 64

Global vector potential

Since we wish $\mathbf{A}_n$ to take effect only in lead n, we may:

$$f_n(x,y) \to \zeta_n f_n(x,y)\ , \qquad \zeta_n = \frac{1}{\exp\dfrac{x_n^0 - x_n}{d} + 1}$$

The final gauge transformation can be achieved by

$$f(x,y) = \sum_{n=2}^{N} \zeta_n f_n(x,y)$$

$$f_n(x,y) = Bxy\sin^2\theta_n + \frac{1}{2}B(x^2 - y^2)\sin\theta_n\cos\theta_n$$

Global vector potential:

$$\mathbf{A} = \mathbf{A}_1 + \nabla f$$

---

[1] Baranger, H. U. and Stone, A. D., Physical Review B **40** (1989) 8169; Mreńca-Kolasińska, A., Chen, S.-C., and Liu, M.-H., npj 2D Materials and Applications **7** (2023) Article number: 64

Two examples

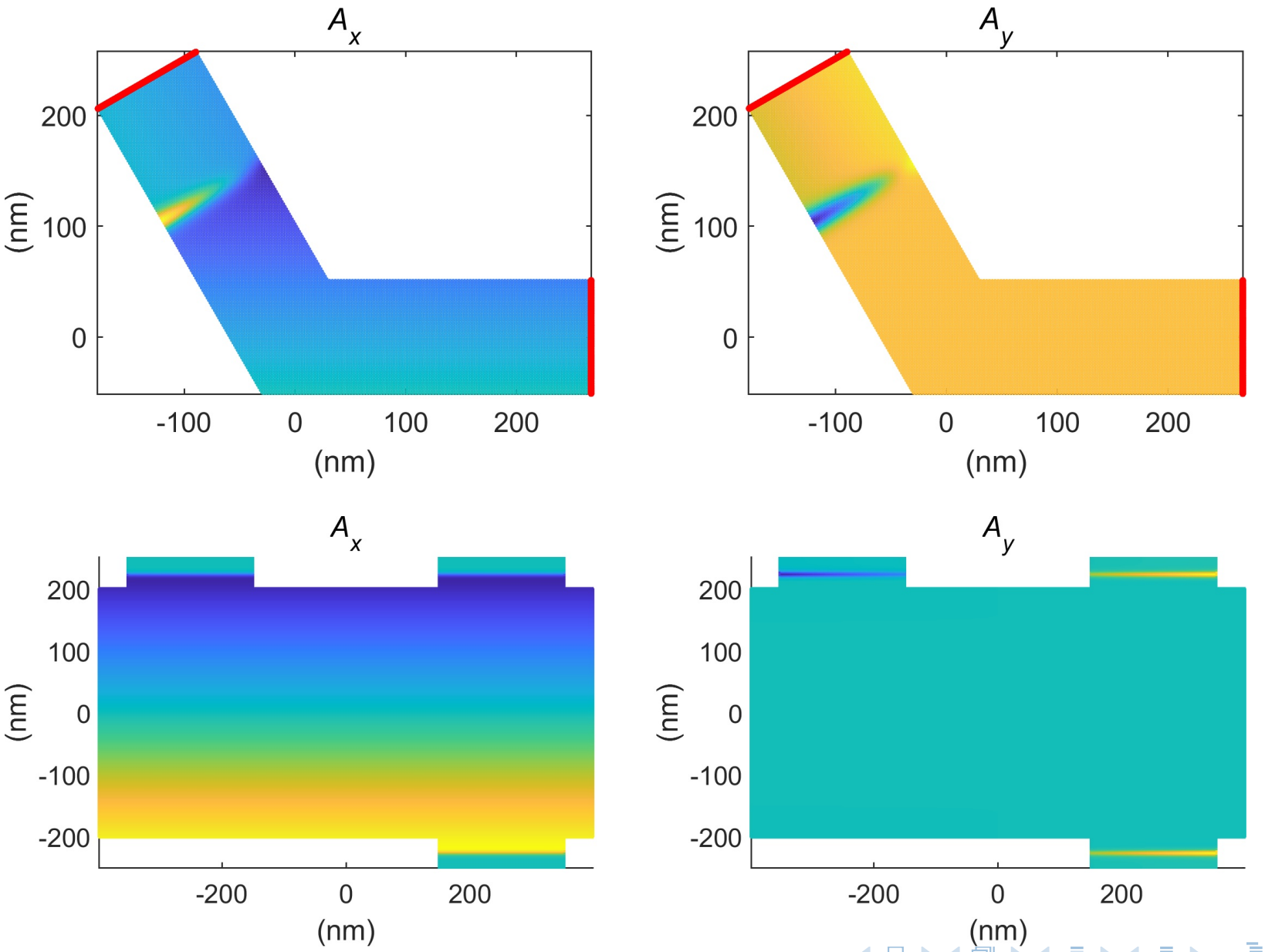

Semiclassical motion of Bloch electrons

Semiclassical equations of motion:[1]

$$\dot{\mathbf{r}} = \frac{1}{\hbar}\nabla_k E(\mathbf{k}) + \cancel{\text{anomalous velocity}}^{2}$$
$$\hbar\dot{\mathbf{k}} = -e\left(\mathbf{E} + \dot{\mathbf{r}} \times \mathbf{B}\right)$$

2D (x-y plane) subject to $\mathbf{E} = (E_x, E_y, 0)$ and $\mathbf{B} = (0, 0, B)$:

$$\dot{x} = \frac{1}{\hbar}\frac{\partial E(k_x, k_y)}{\partial k_x} \qquad \dot{k}_x = -\frac{e}{\hbar}\left(E_x + B_z\dot{y}\right)$$
$$\dot{y} = \frac{1}{\hbar}\frac{\partial E(k_x, k_y)}{\partial k_y} \qquad \dot{k}_y = -\frac{e}{\hbar}\left(E_y - B_z\dot{x}\right)$$

Coupled ordinary differential equations (ODEs).

---

[1] Ashcroft, N. W. and Mermin, N. D., *Solid State Physics*, New York: Holt, Rinehart and Winston, 1976

[2] Chang, M.-C. and Niu, Q., Phys. Rev. Lett. **75** (1995) 1348

Part II

Applications

- 2DEG & MoS_2
- Graphene
- Bilayer graphene
- Lieb lattice

1

2DEG & MoS_2

- Test calculations for QPC
- MoS_2 superlattice

Discretization by finite-difference approximation

$$E(k) = \frac{\hbar^2 k^2}{2m^*}$$

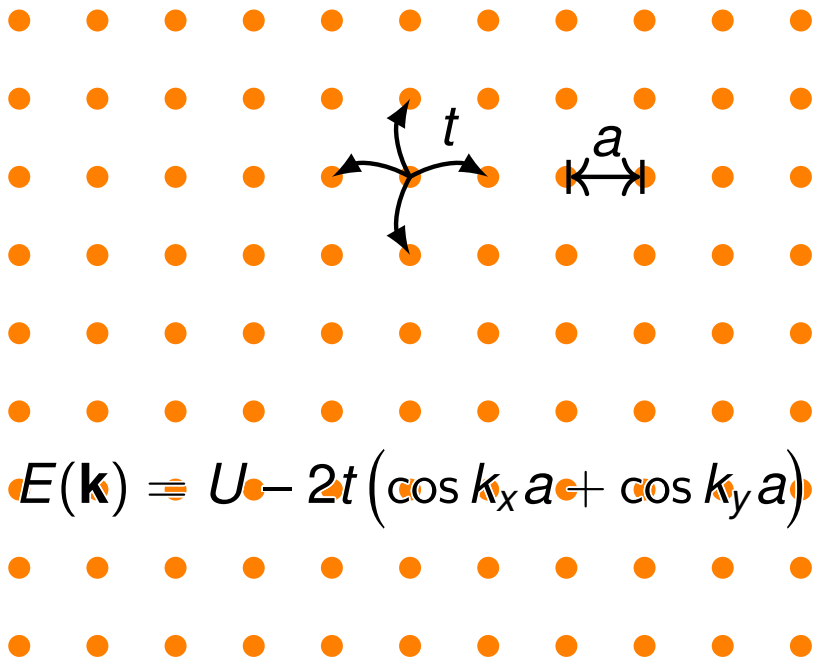

The approximation approaches exact when:

$$U = 4t\,, \quad t = \frac{\hbar^2}{2m^* a^2}\,, \quad |\mathbf{k}|a \ll 1$$

Datta, S., *Electronic Transport in Mesoscopic Systems* (1995)

Finding a good lattice spacing

Considering $m^* = 0.067 m_0$ for GaAs:

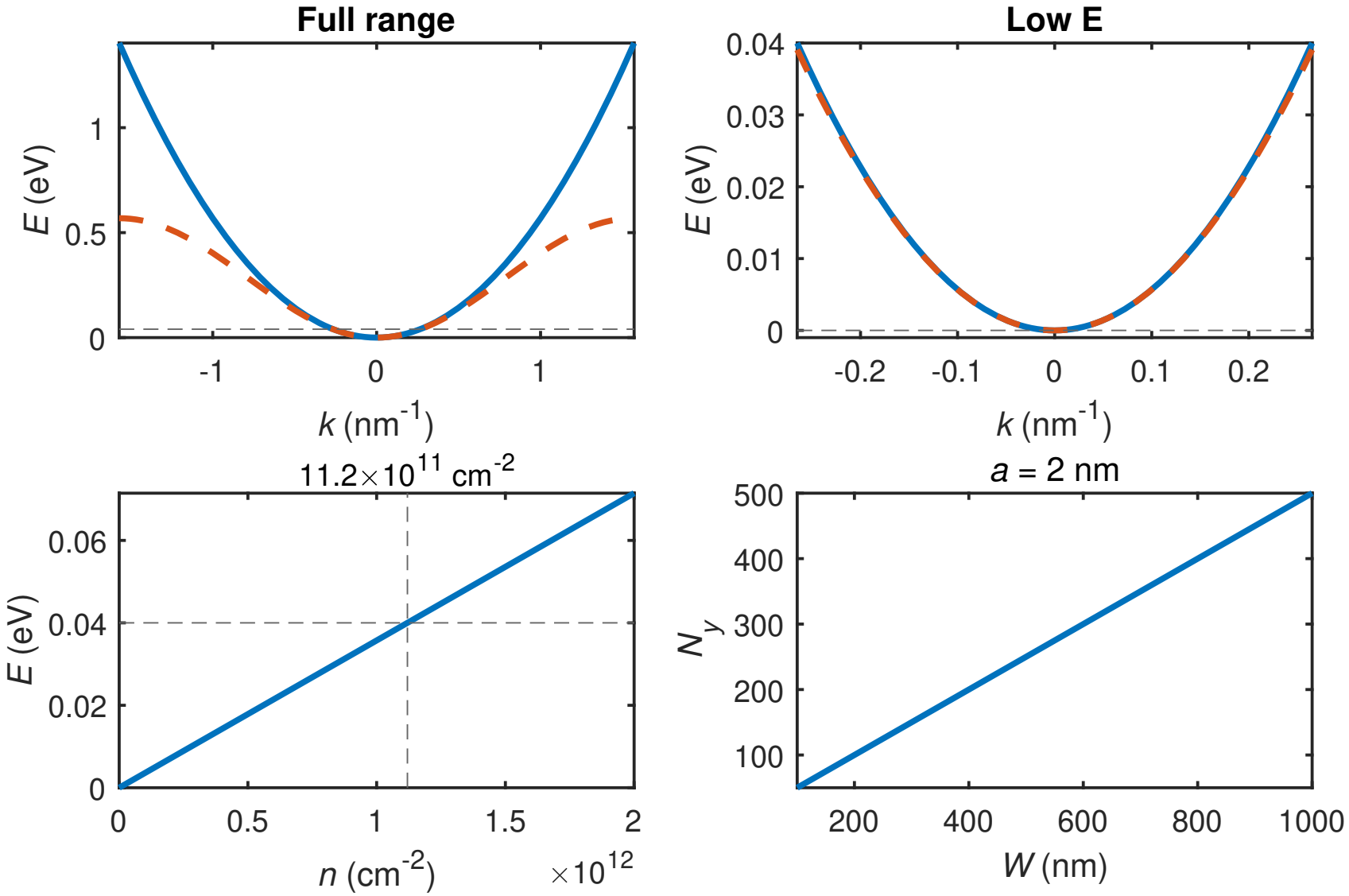

Finding a good lattice spacing

Considering $m^* = 0.067 m_0$ for GaAs:

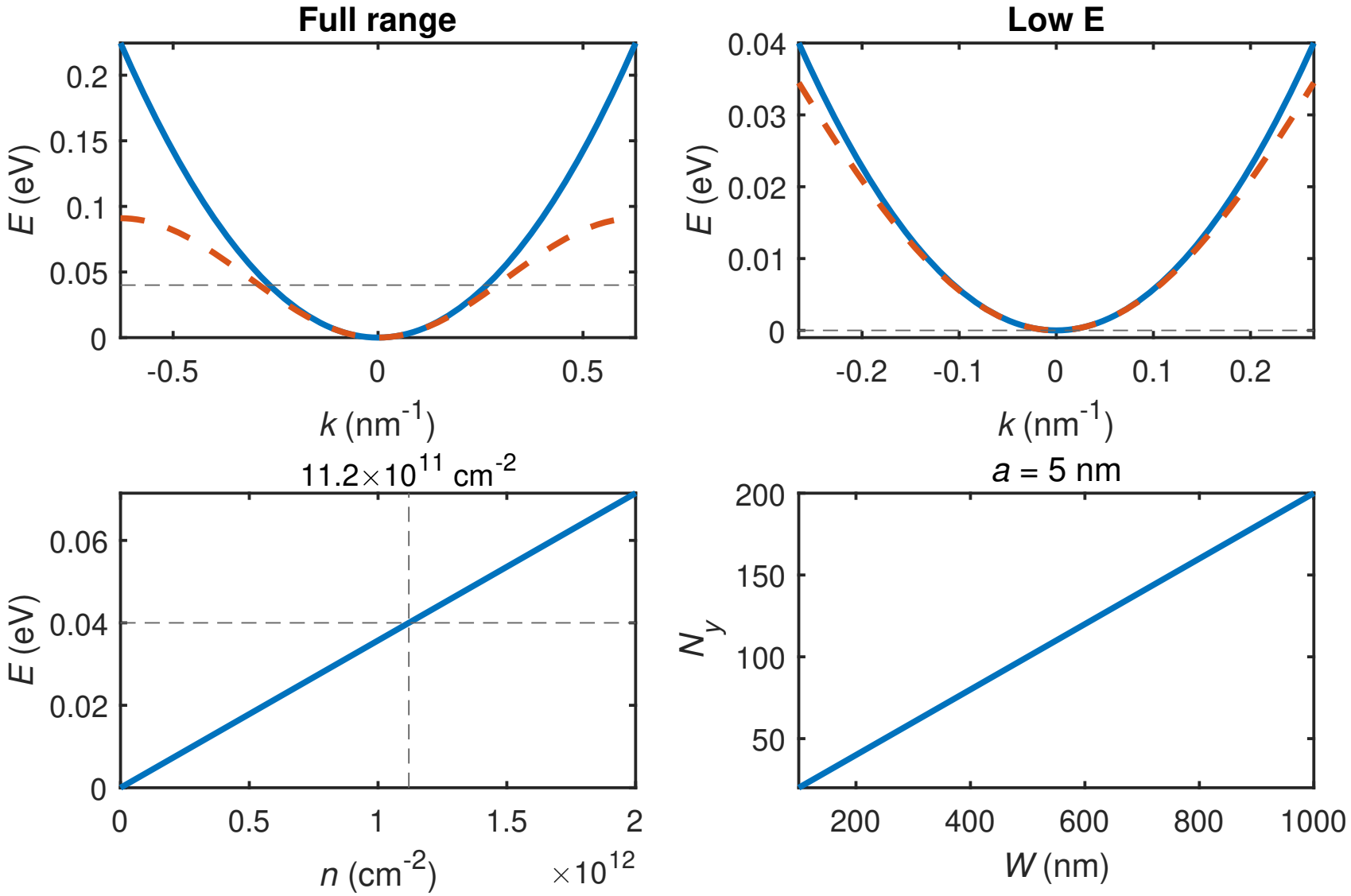

Revisiting an old experiment

VOLUME 60, NUMBER 9 PHYSICAL REVIEW LETTERS 29 FEBRUARY 1988

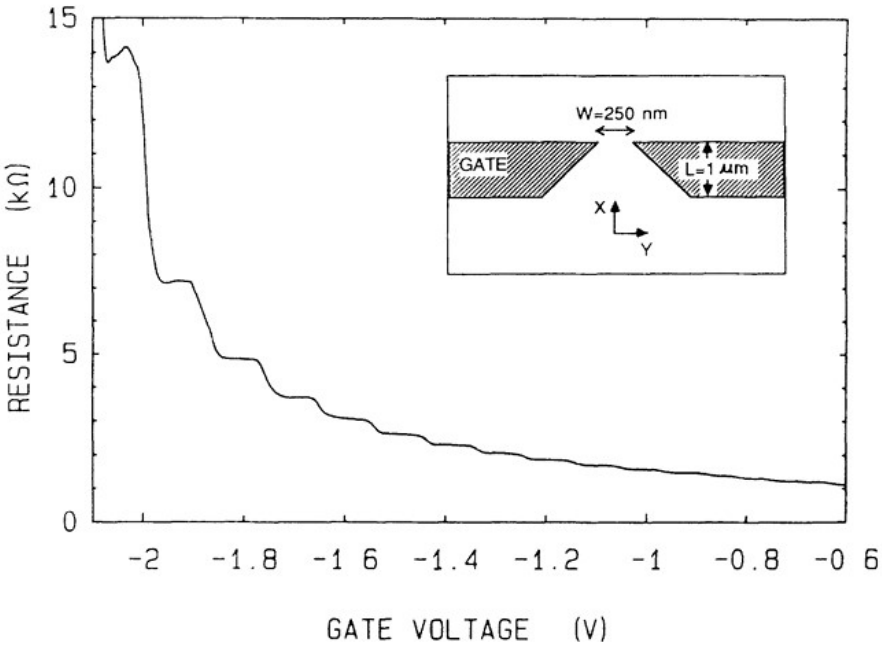

FIG. 1. Point-contact resistance as a function of gate voltage at 0.6 K. Inset: Point-contact layout.

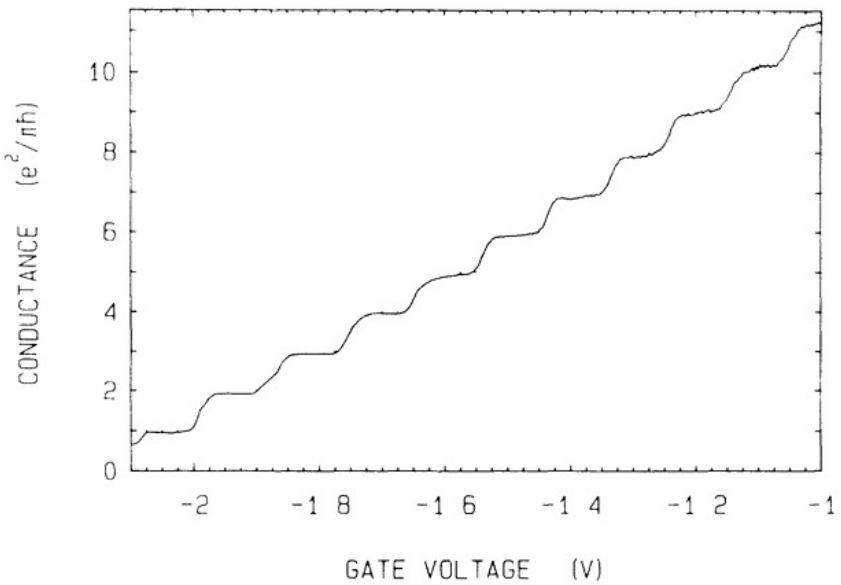

FIG. 2. Point-contact conductance as a function of gate voltage, obtained from the data of Fig. 1 after subtraction of the lead resistance. The conductance shows plateaus at multiples of $e^2/\pi\hbar$.

van Wees, B. J. et al., Physical Review Letters **60** (1988) 848

Revisiting an old experiment

VOLUME 60, NUMBER 9 PHYSICAL REVIEW LETTERS 29 FEBRUARY 1988

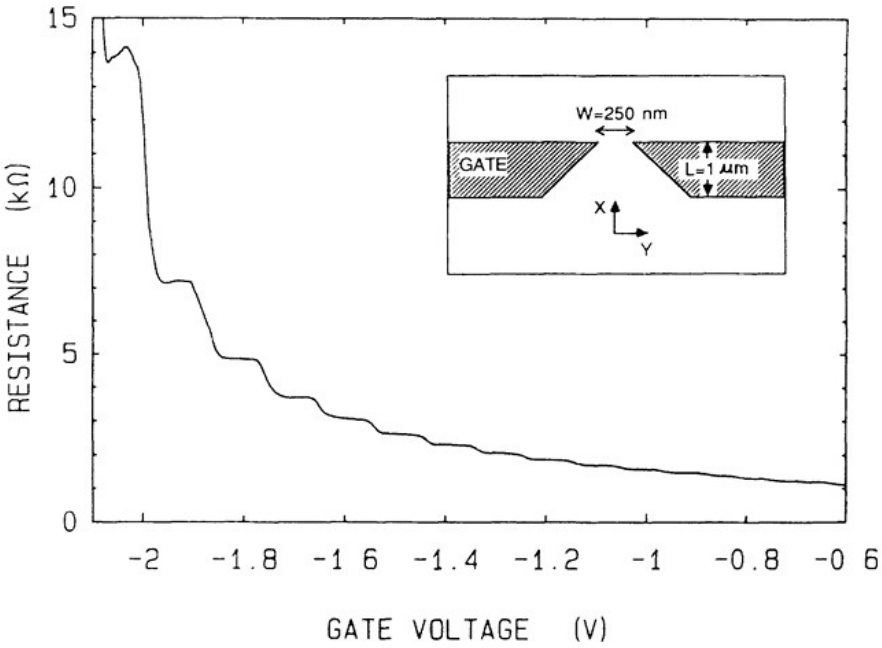

FIG. 1. Point-contact resistance as a function of gate voltage at 0.6 K. Inset: Point-contact layout.

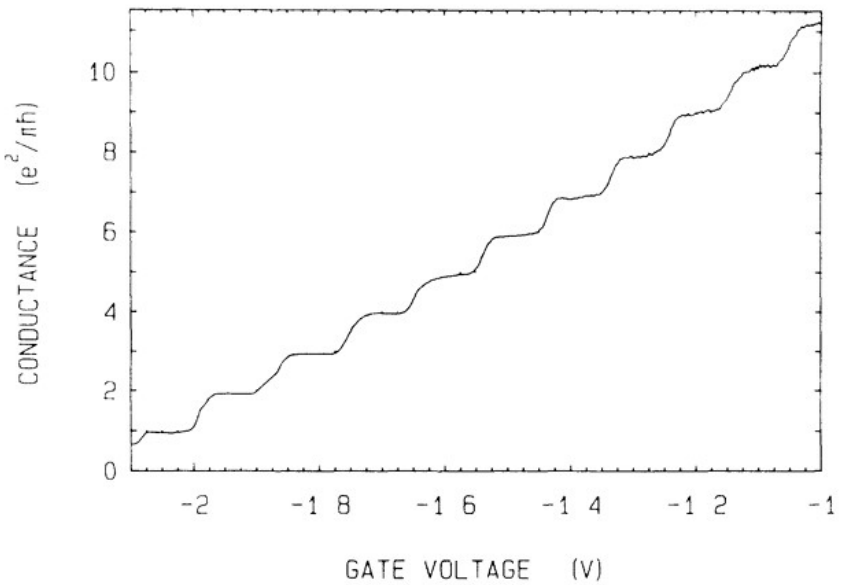

FIG. 2. Point-contact conductance as a function of gate voltage, obtained from the data of Fig. 1 after subtraction of the lead resistance. The conductance shows plateaus at multiples of $e^2/\pi\hbar$.

Let's try with:

$$m^* = 0.067 m_0 \,, \quad a = 5\,\text{nm} \,, \quad t = \frac{\hbar^2}{2m^* a^2} \approx 22.74\,\text{meV}$$

van Wees, B. J. et al., Physical Review Letters **60** (1988) 848

Quantized conductance plateaus

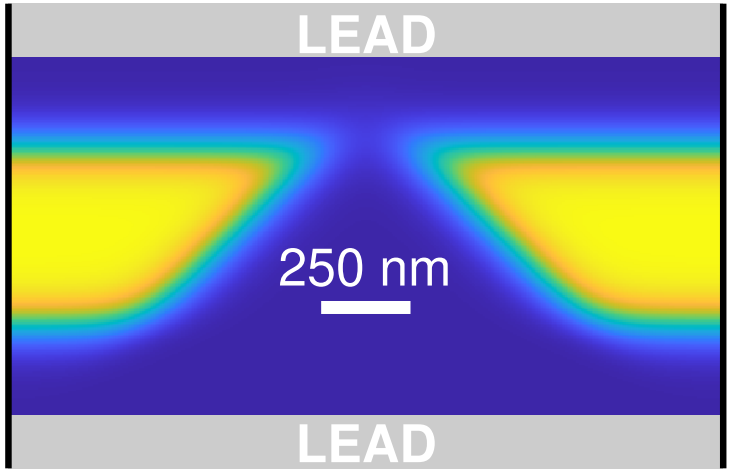

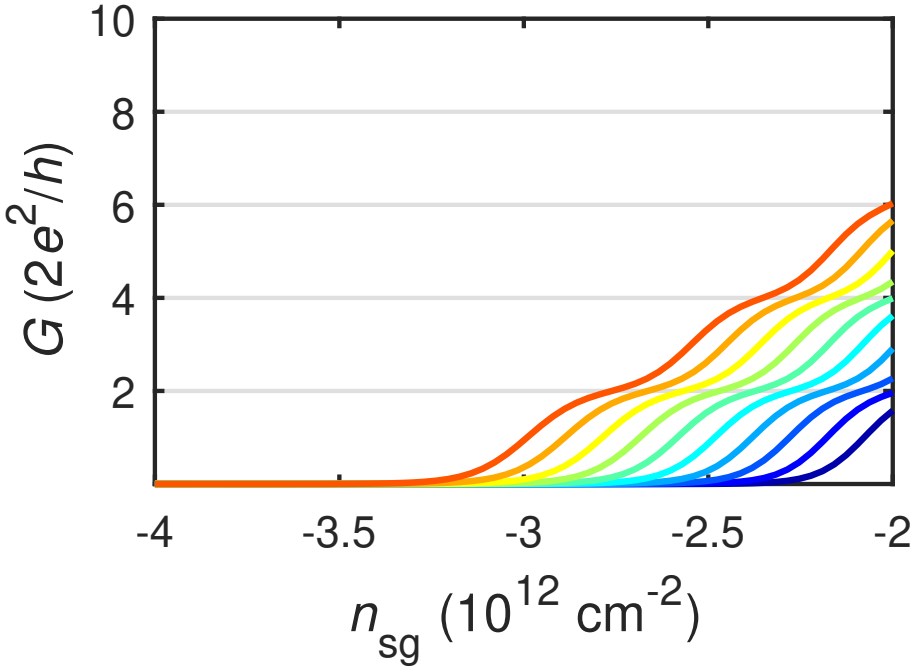

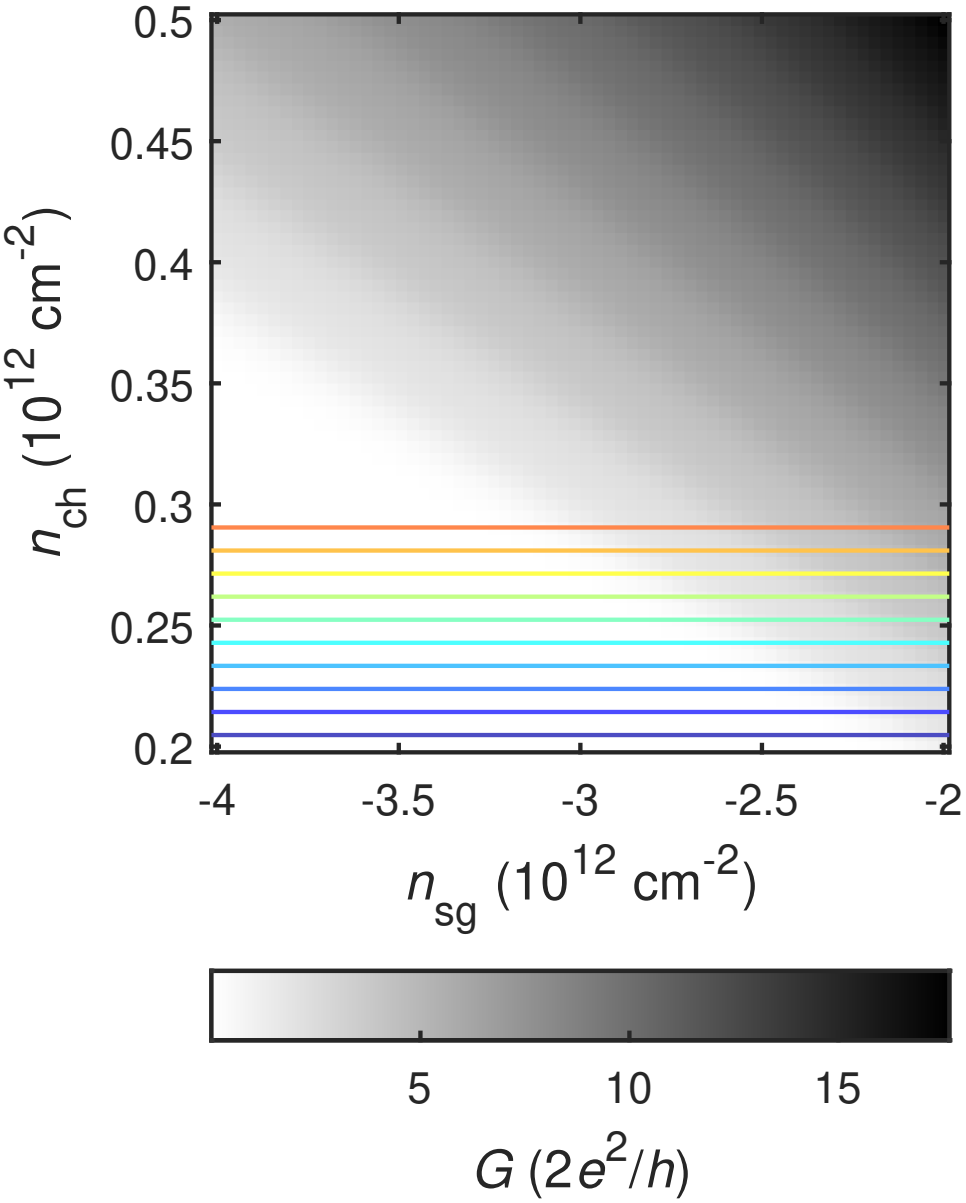

Quantized conductance plateaus

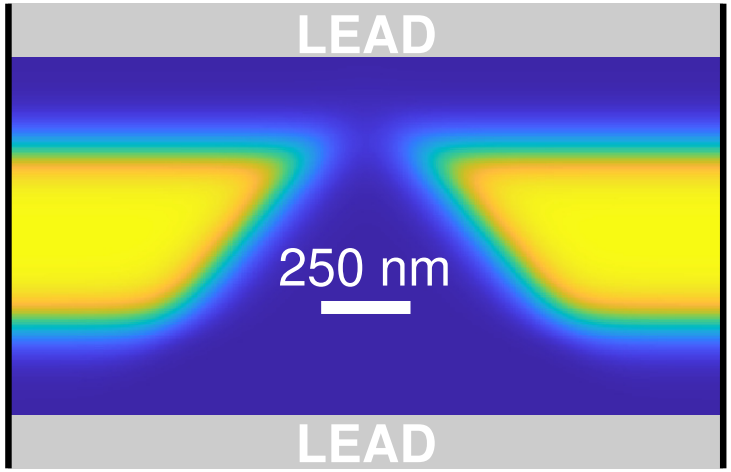

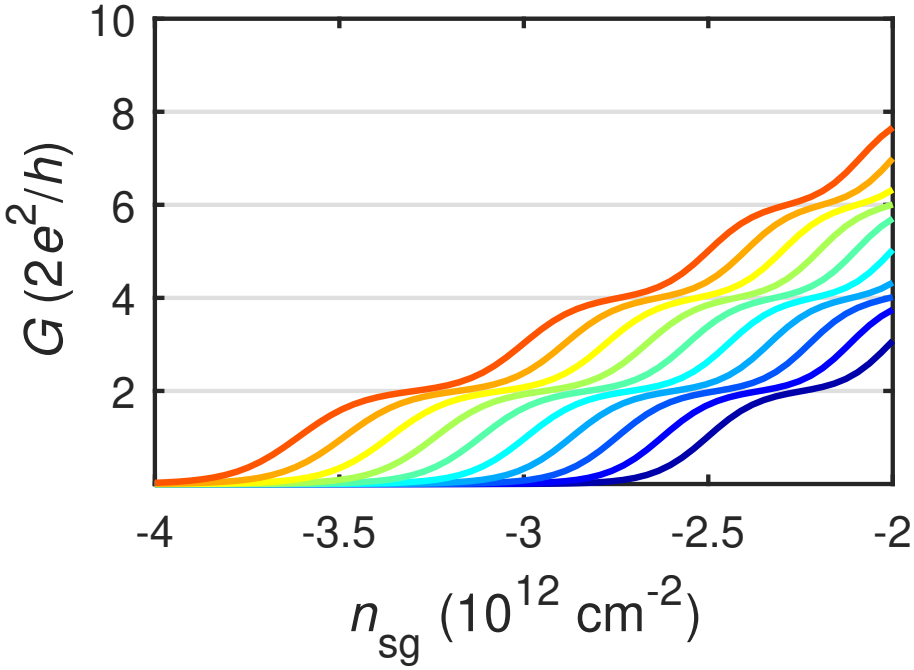

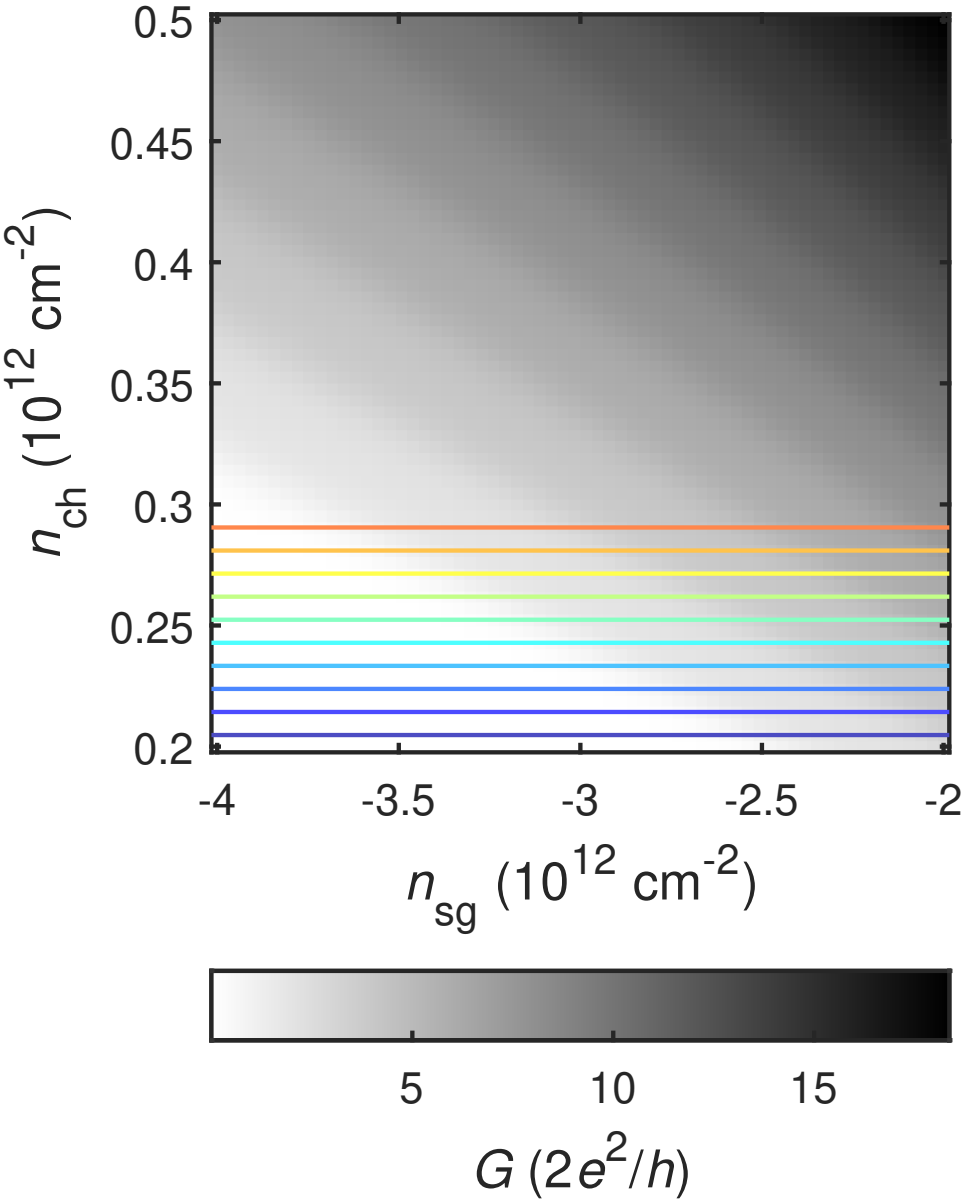

Quantized conductance plateaus

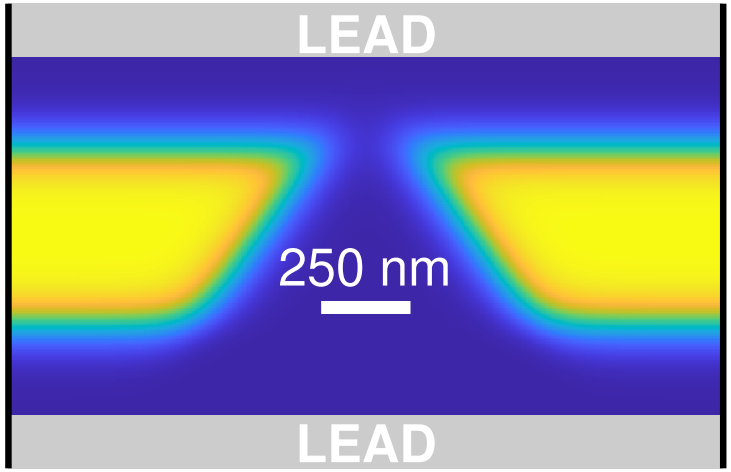

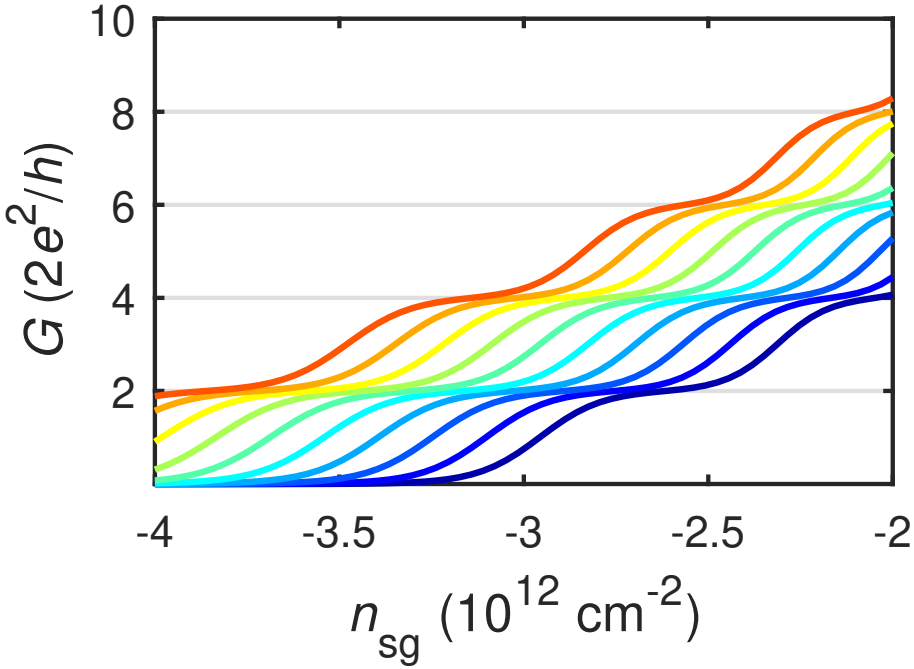

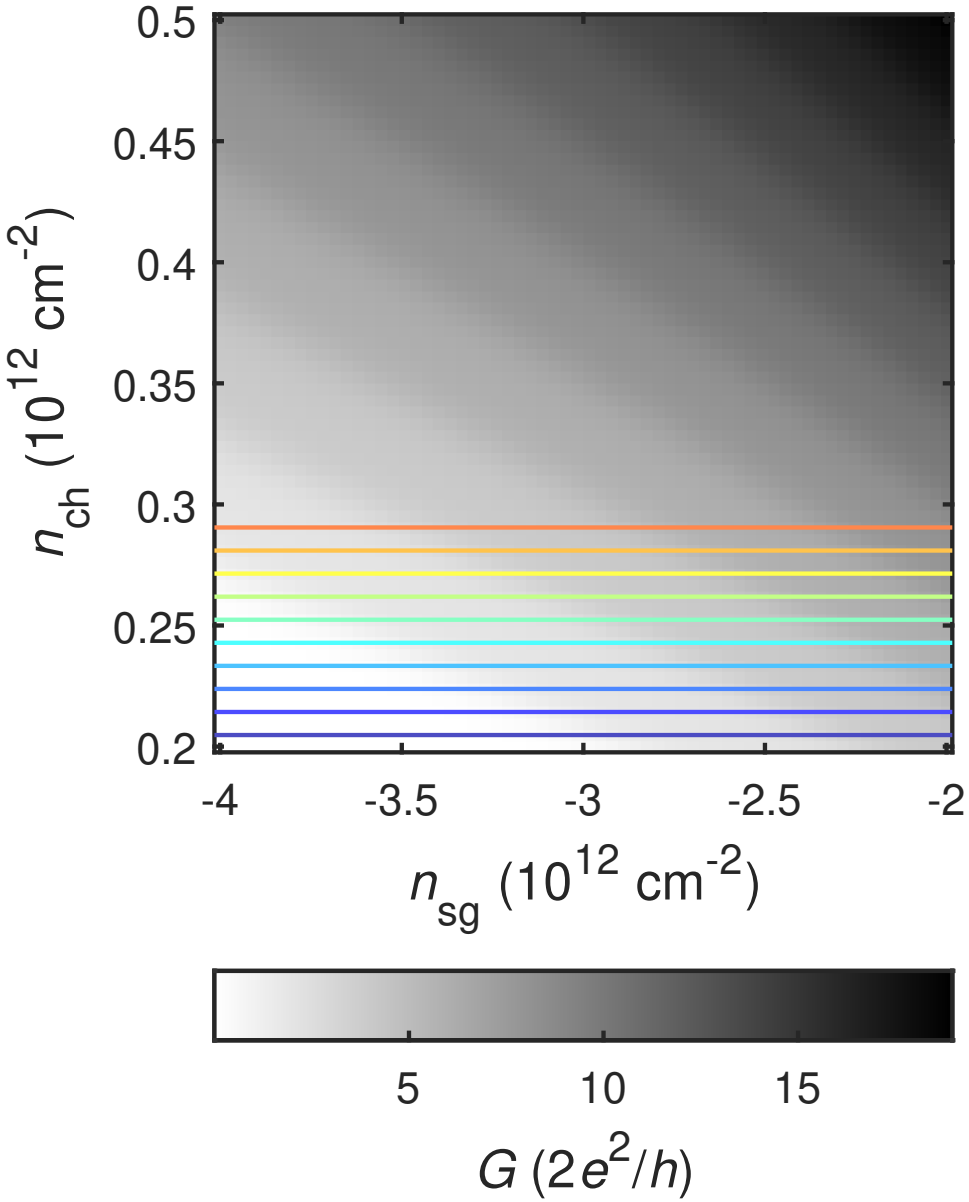

Quantized conductance plateaus

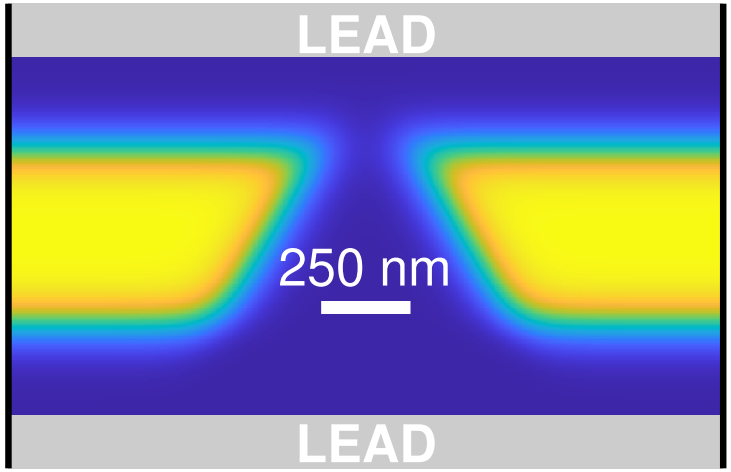

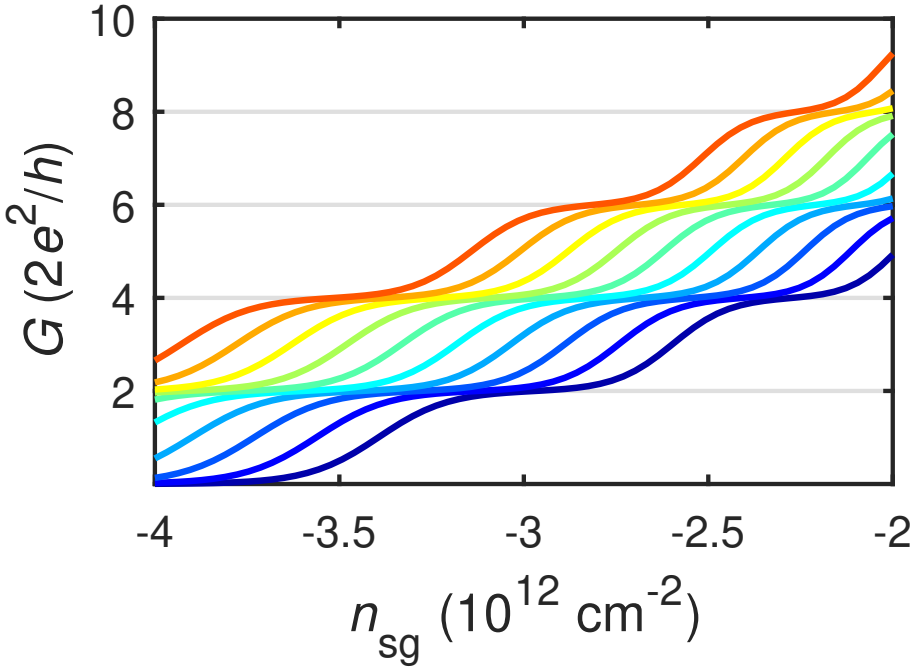

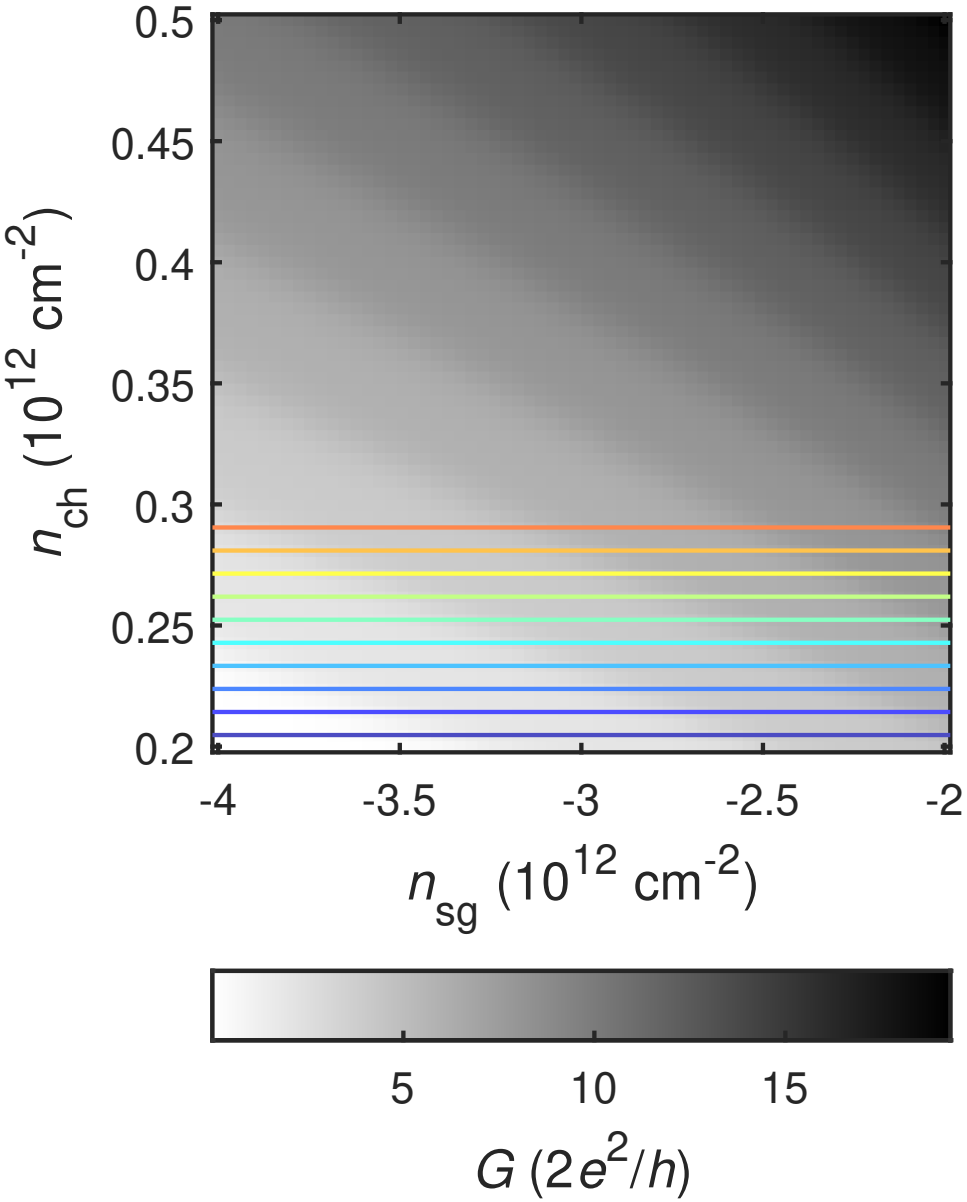

Quantized conductance plateaus

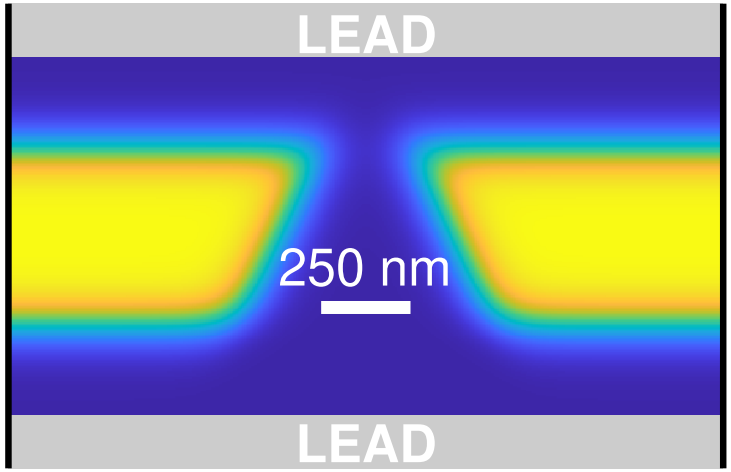

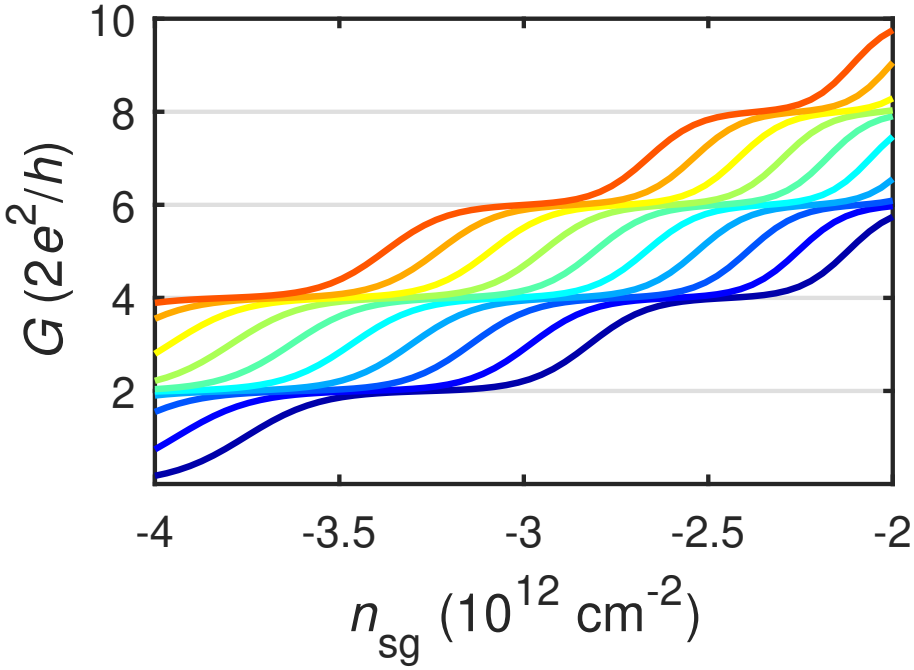

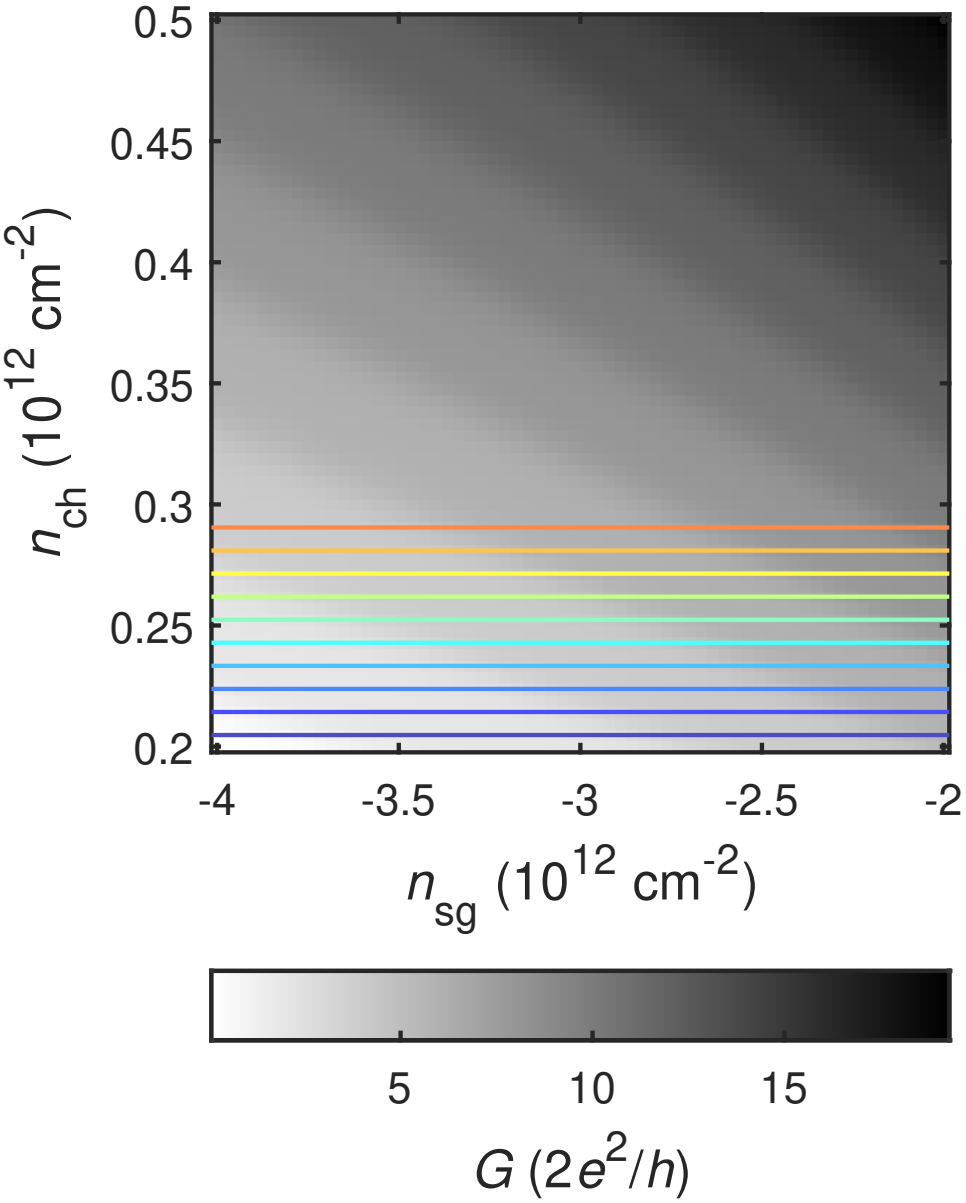

Quantized conductance plateaus

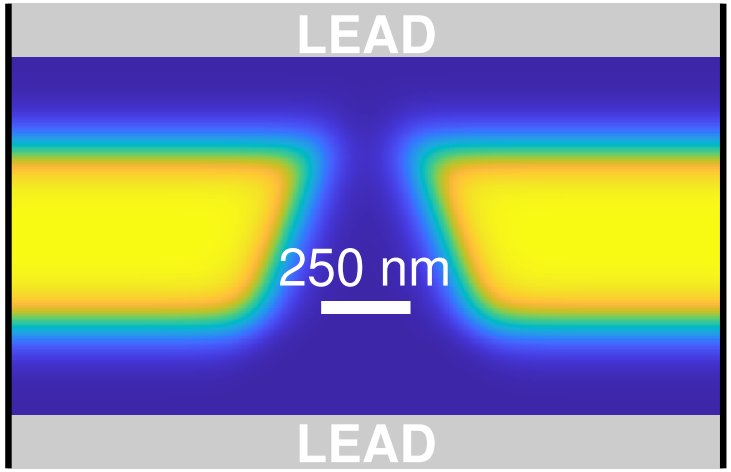

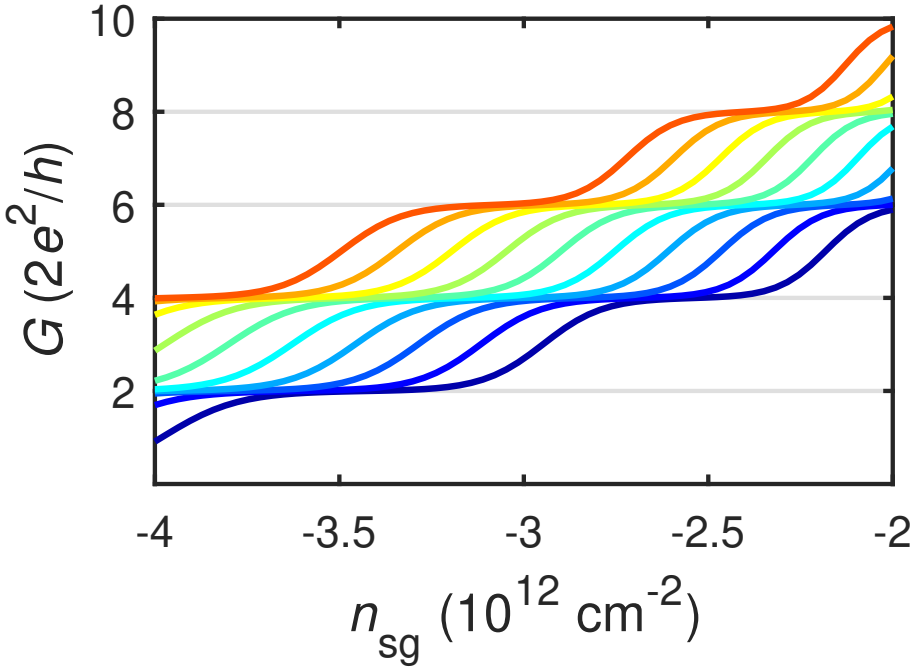

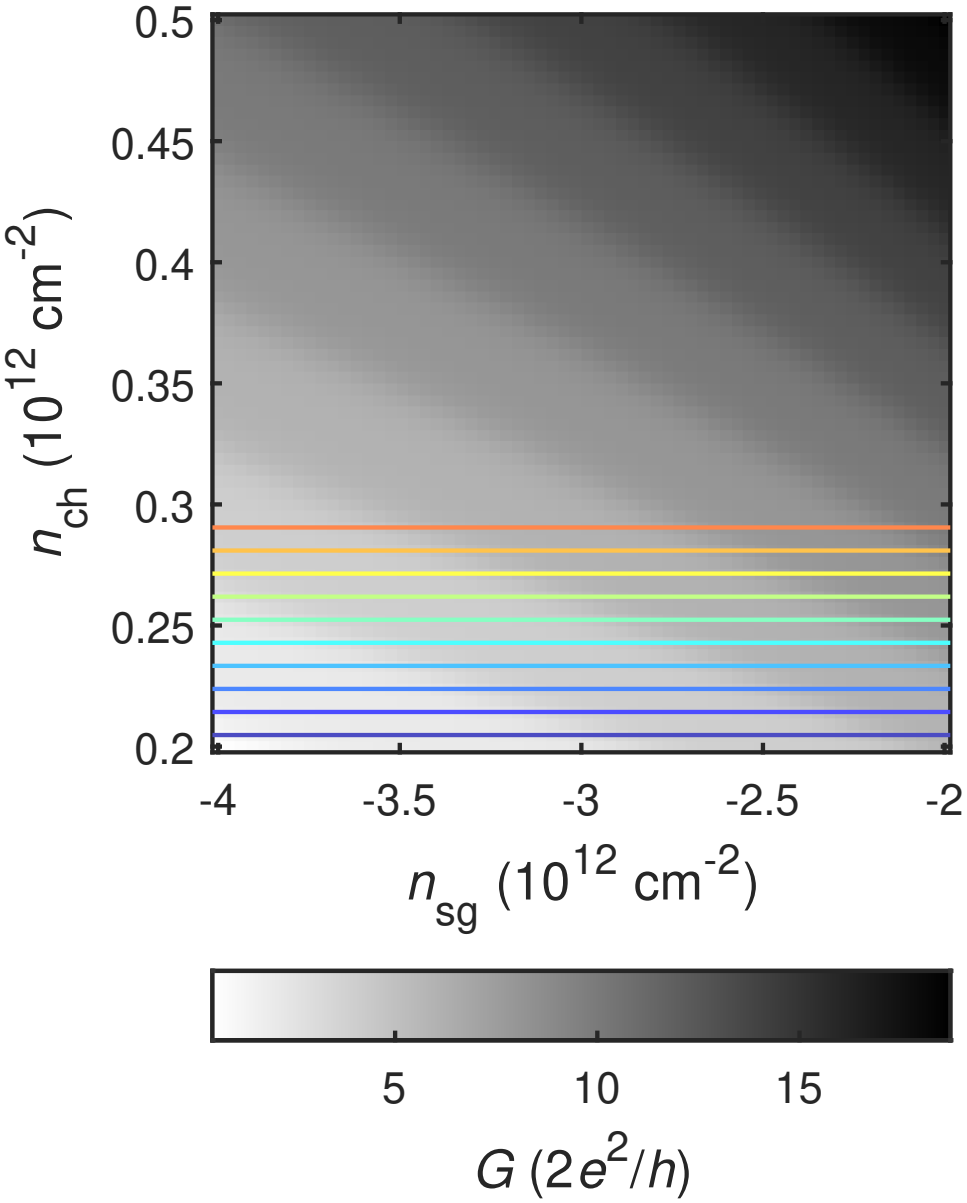

Quantized conductance plateaus

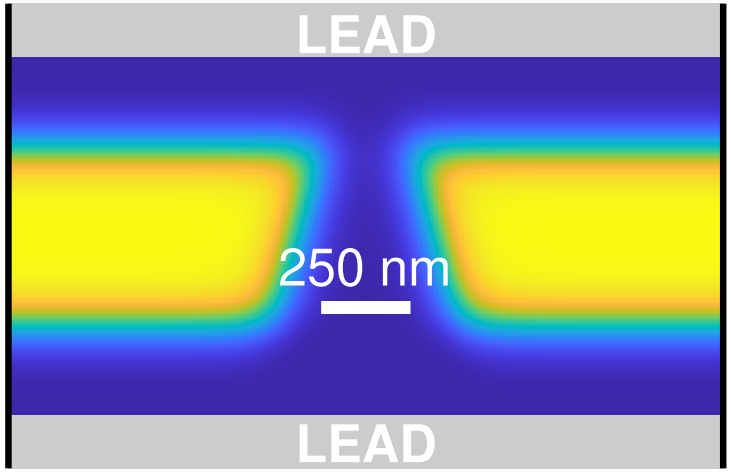

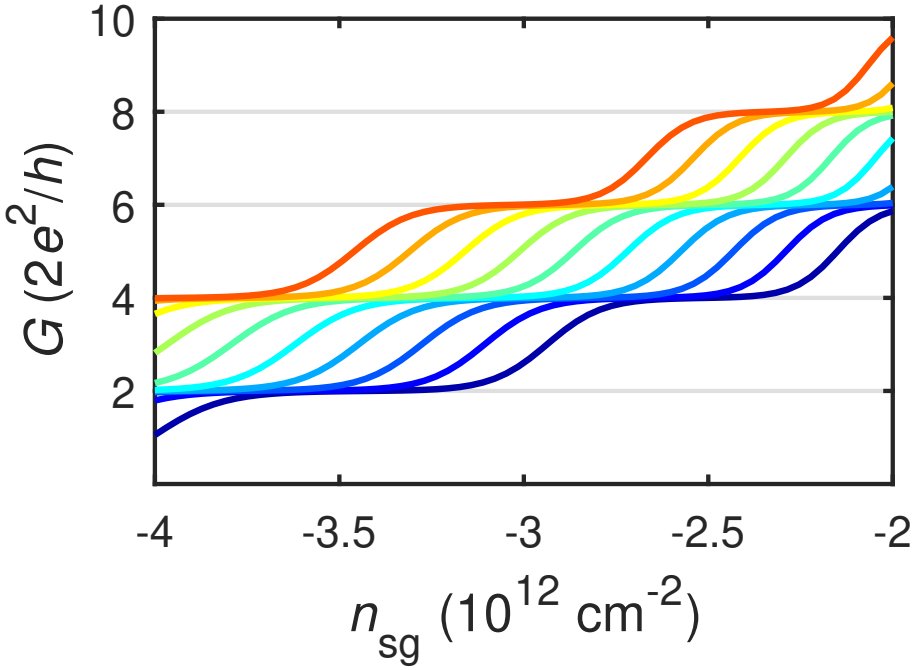

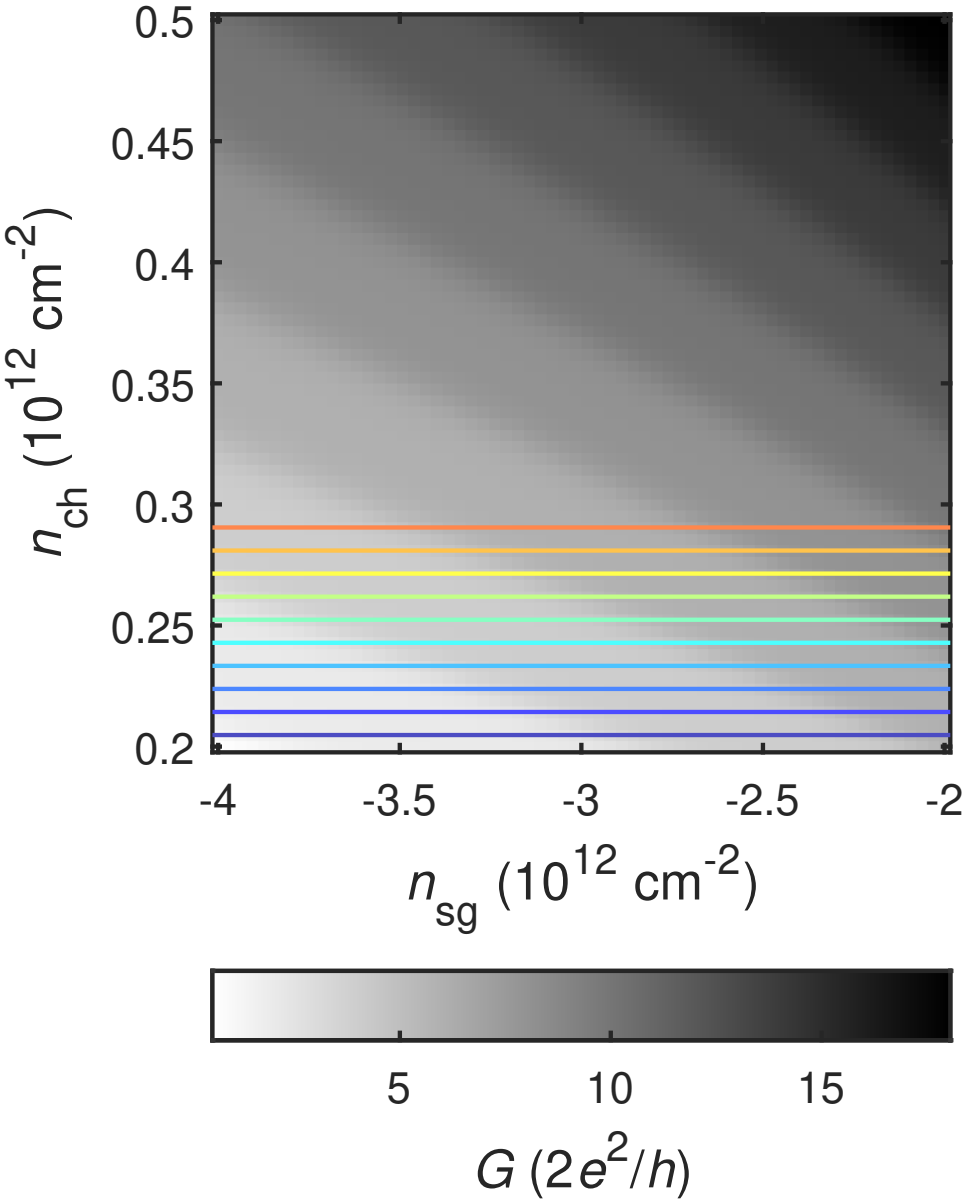

Quantized conductance plateaus

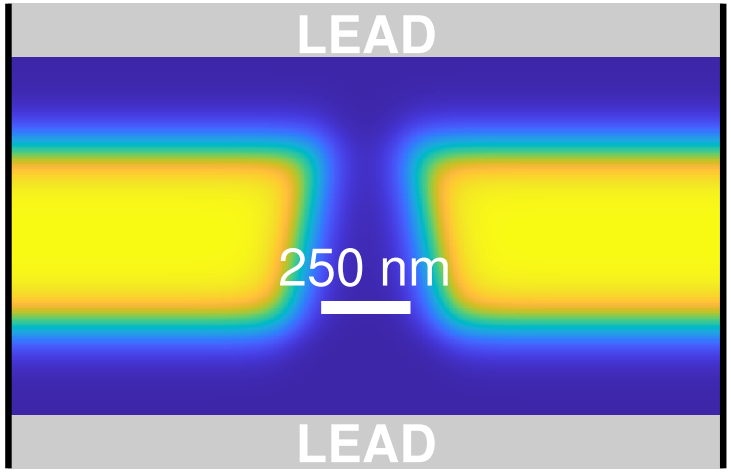

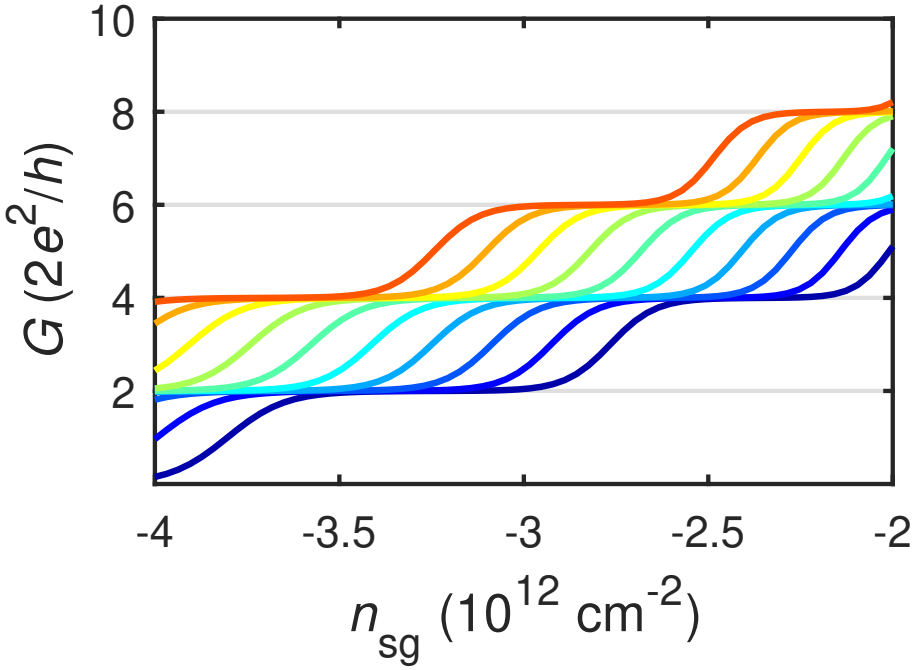

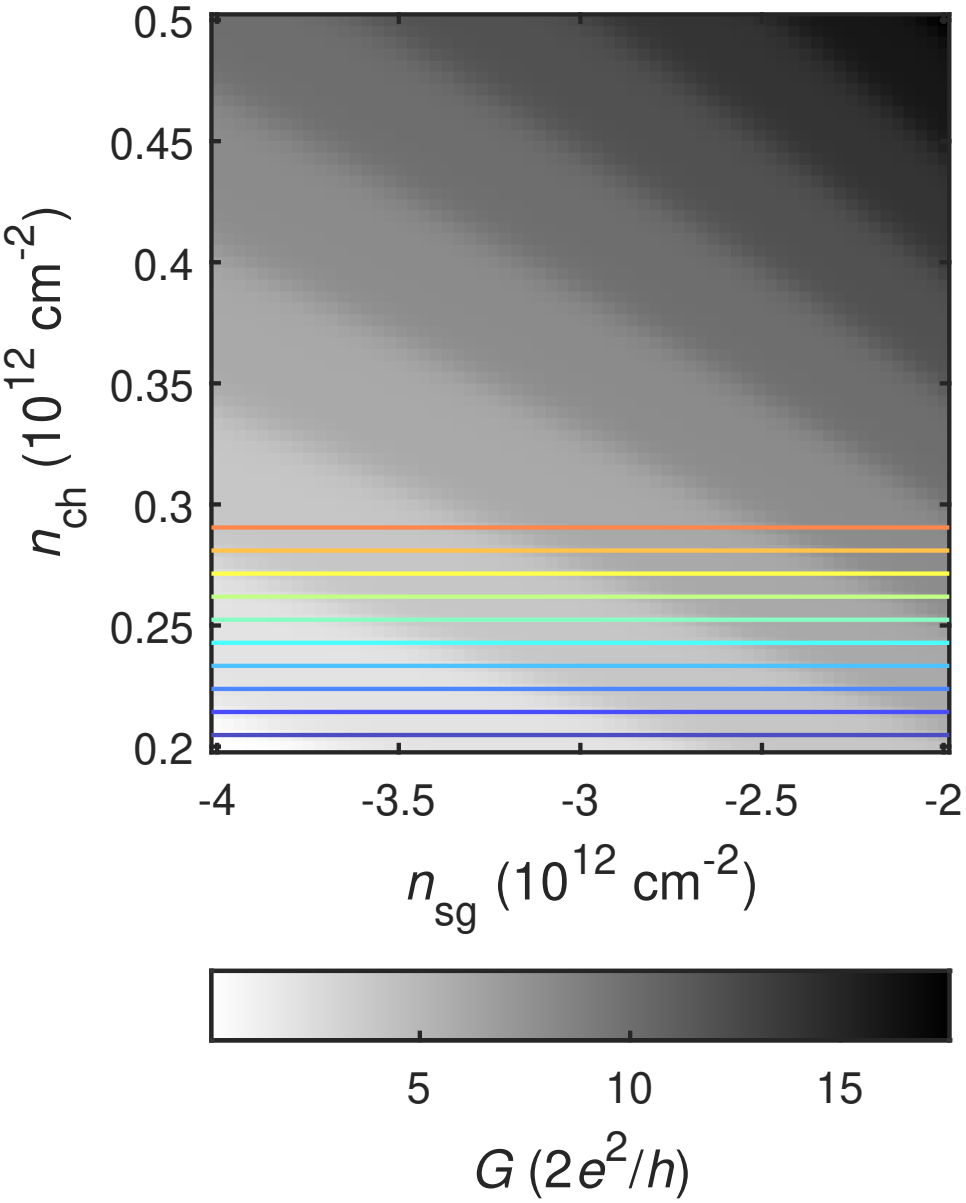

Quantized conductance plateaus

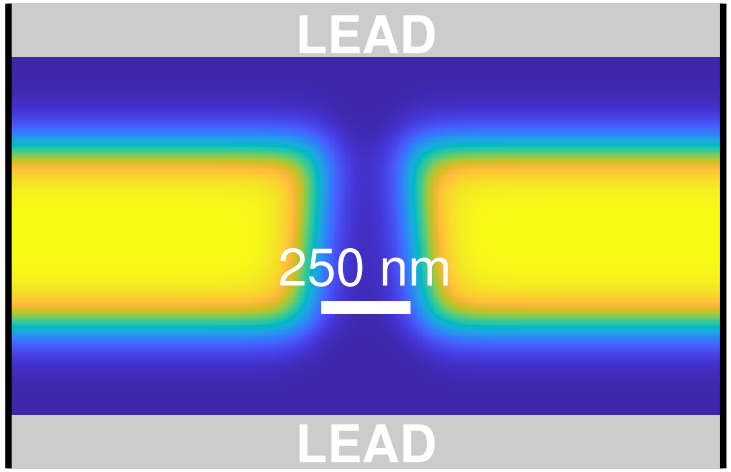

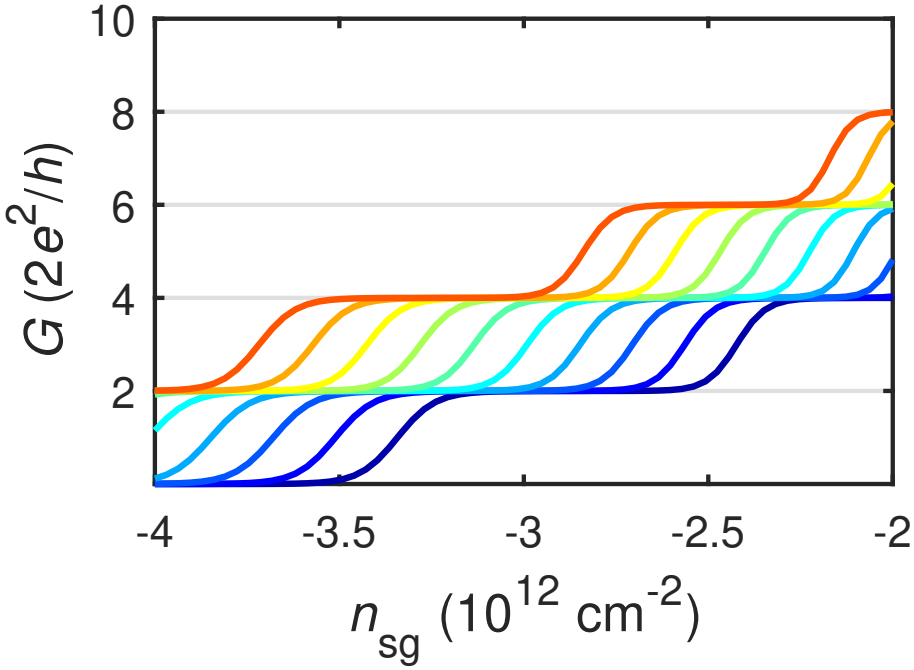

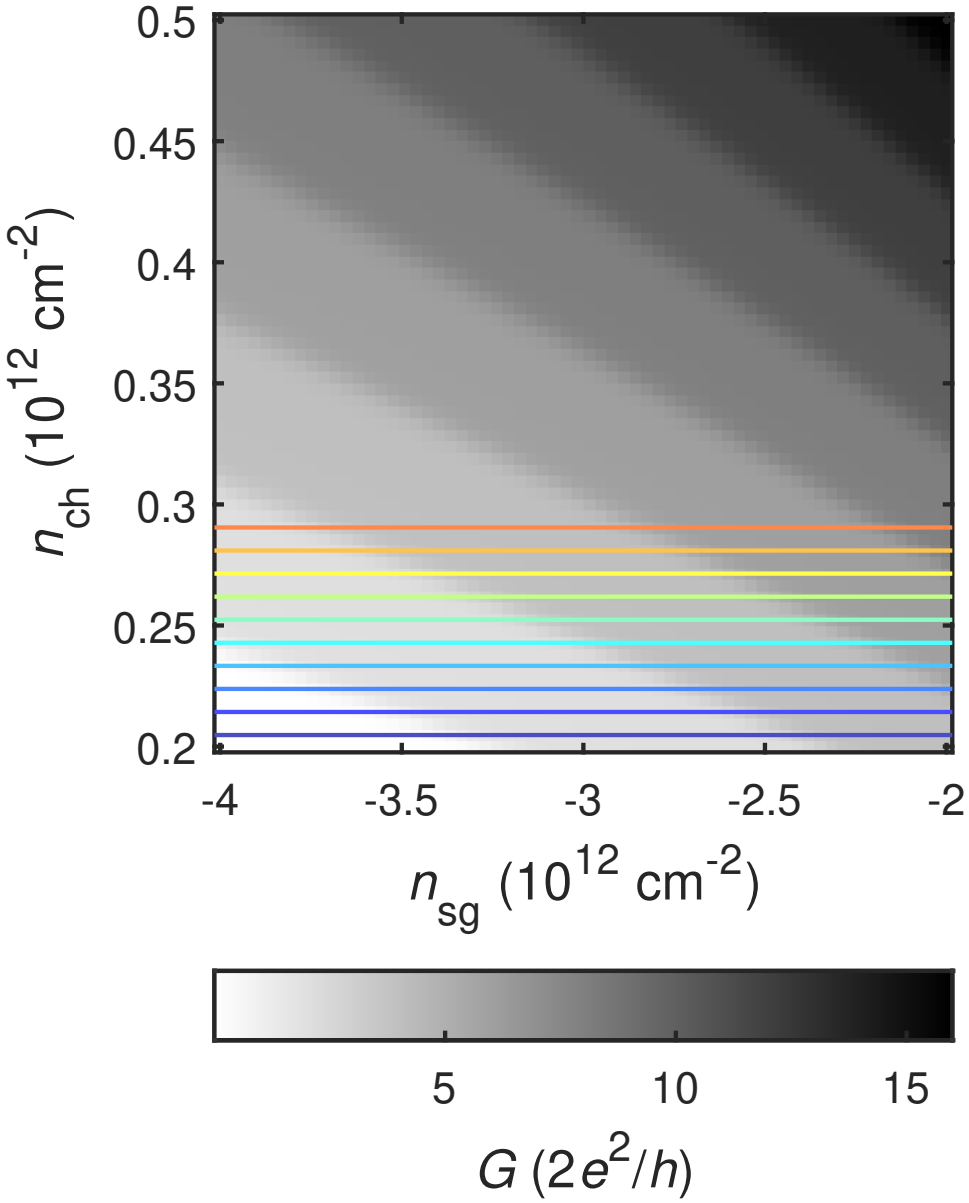

Quantized conductance plateaus

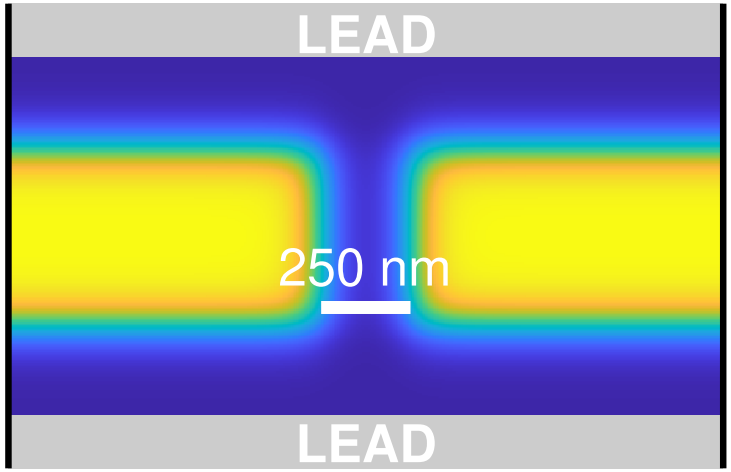

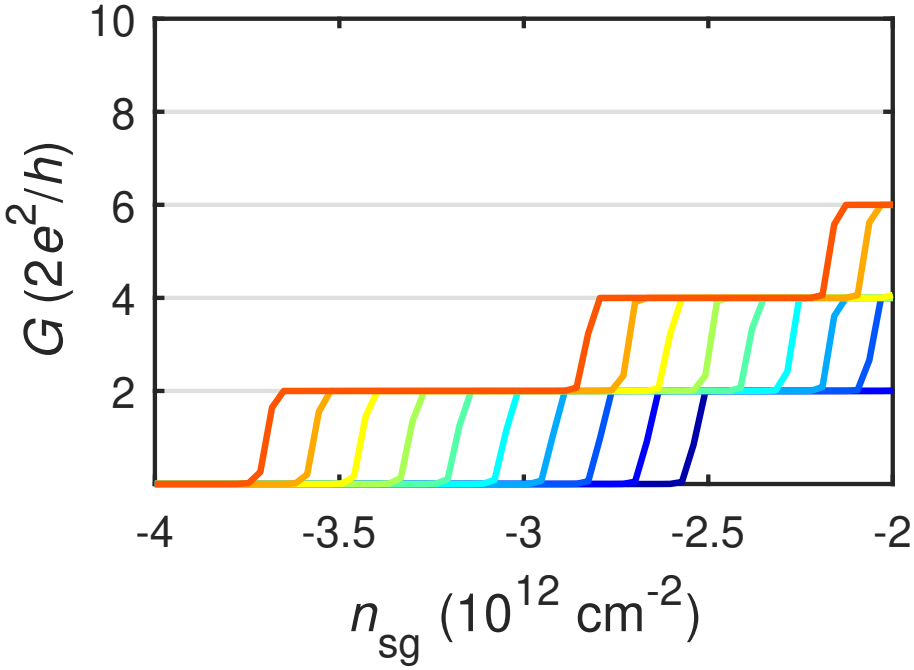

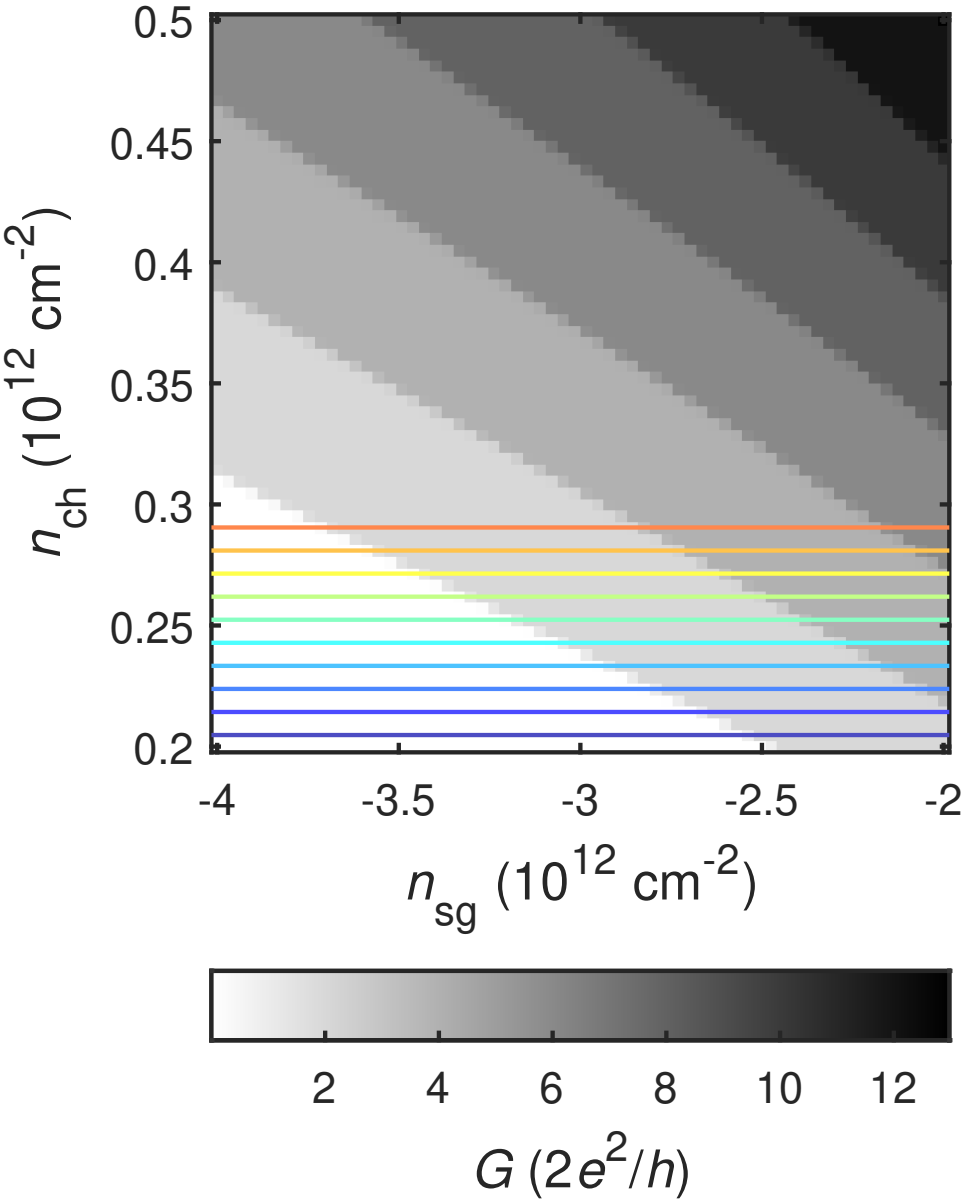

Imaging local current & charge densities

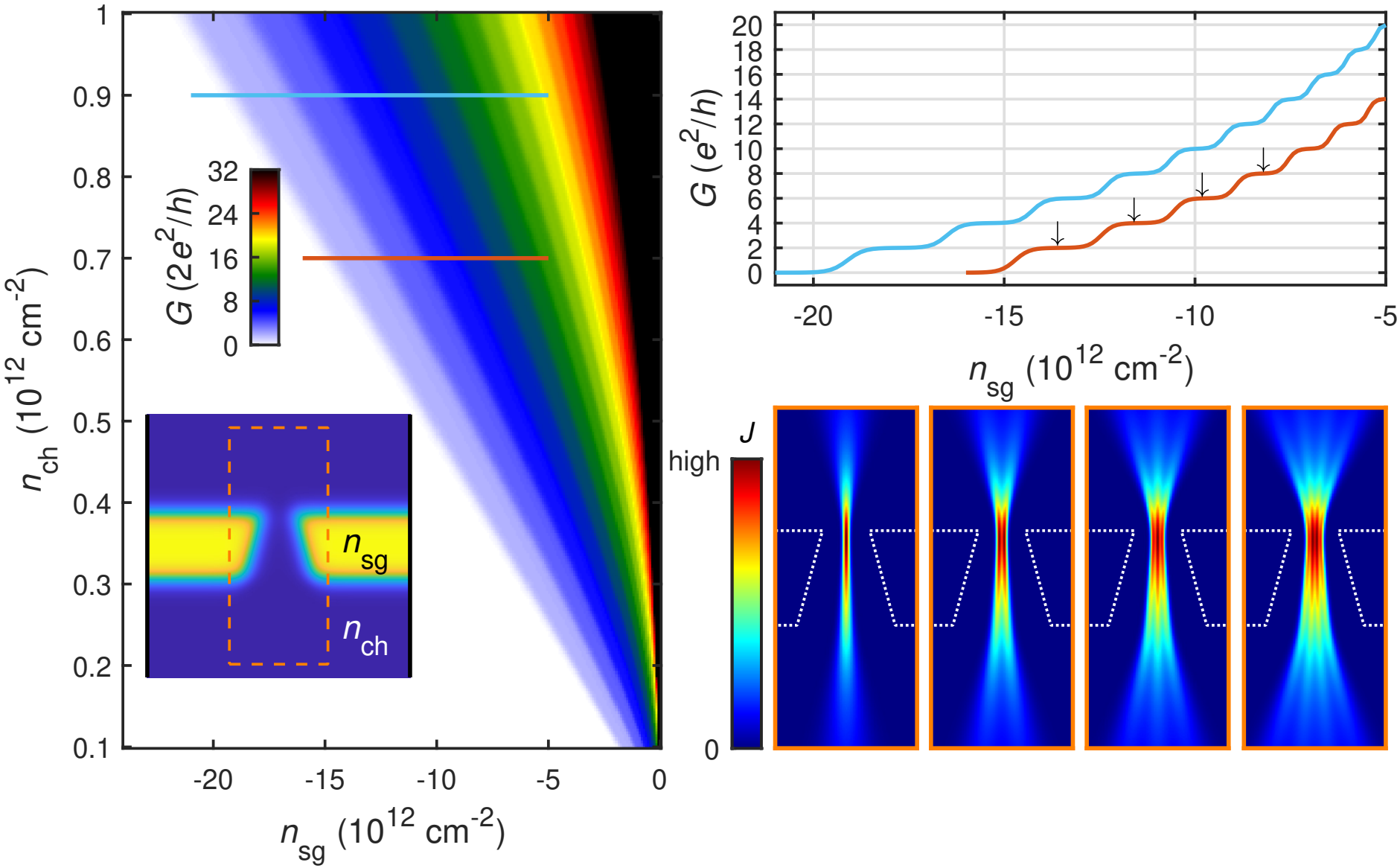

Imaging local current & charge densities

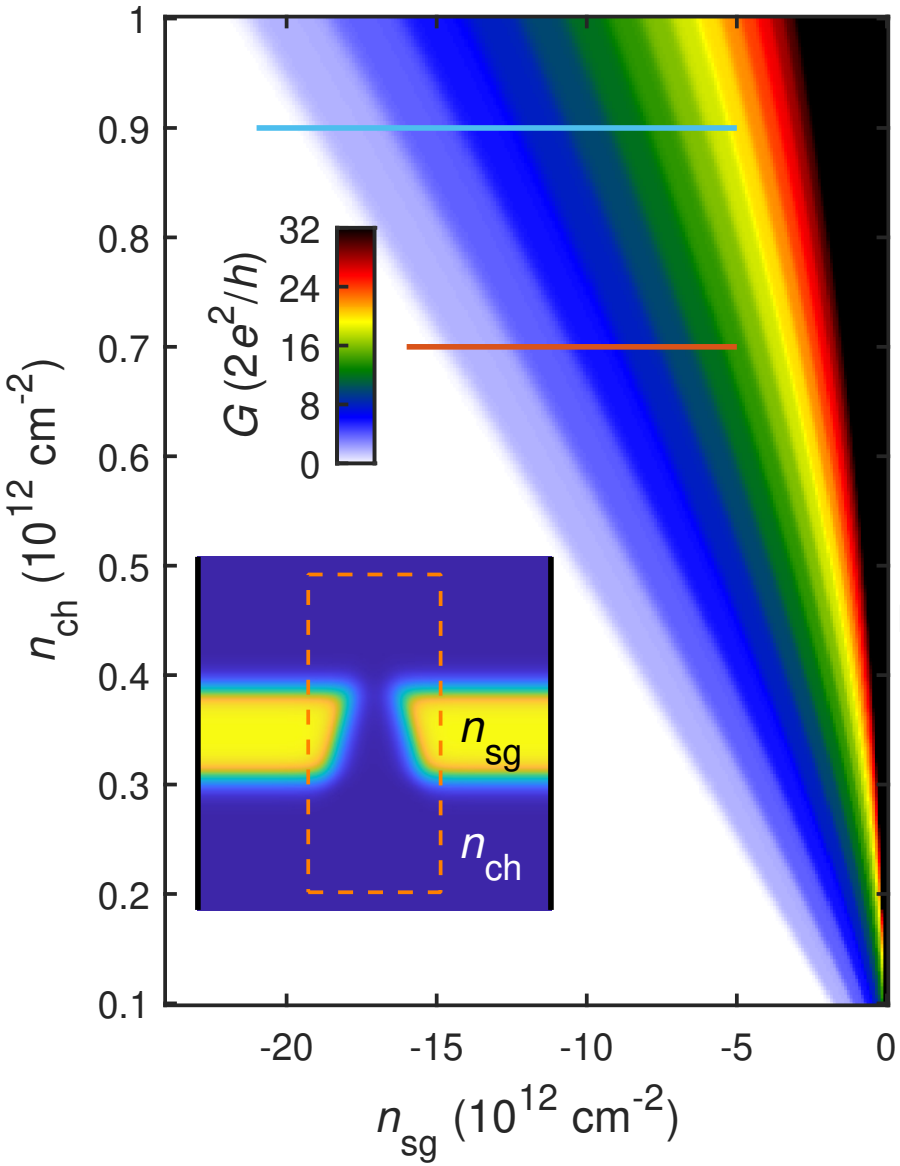

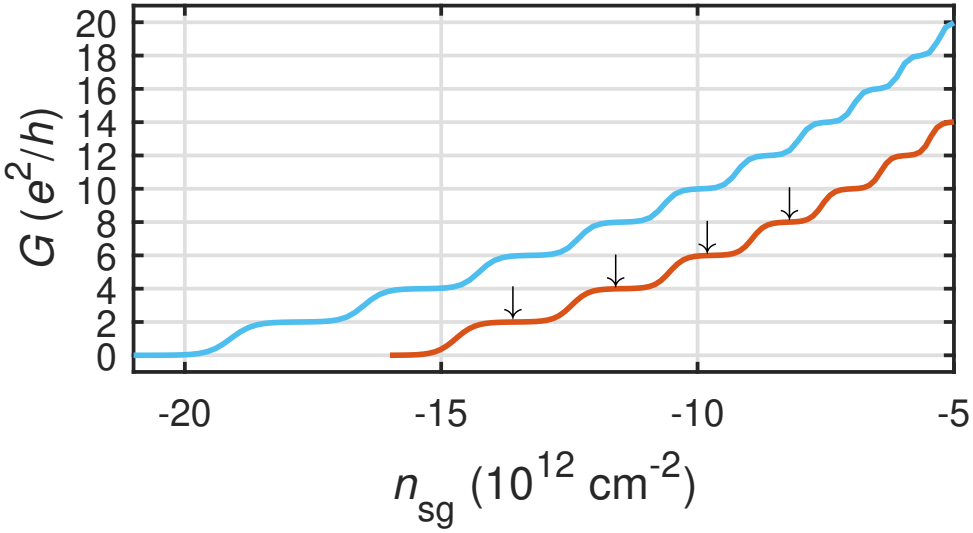

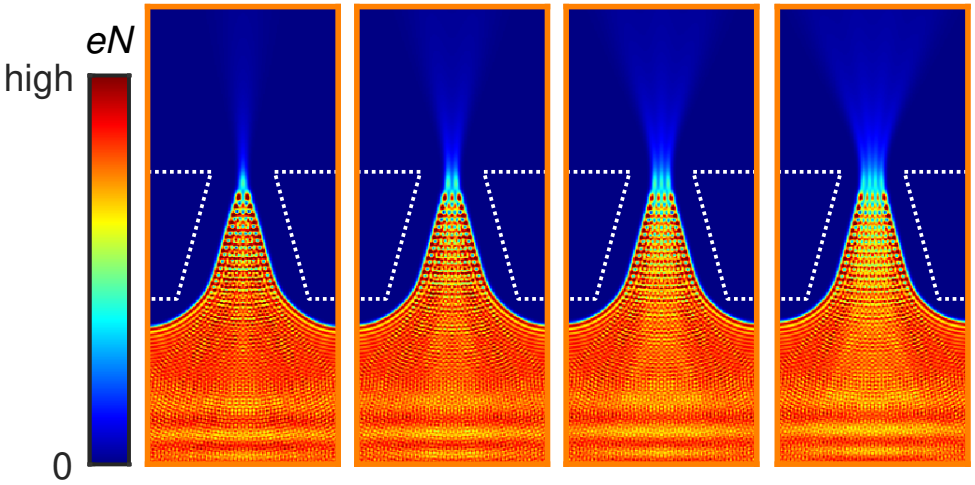

Two-band effective mass model for MoS_2

$$H = \sum_{\langle i,j \rangle} t c_i^\dagger c_j + \sum_n U_i c_i^\dagger c_i$$

$$t = \begin{pmatrix} t_e & 0 \\ 0 & t_h \end{pmatrix}, \quad t_e = -\frac{\hbar^2}{2m_e^* a^2}, \quad t_h = \frac{\hbar^2}{2m_h^* a^2}$$

$$U_i = \begin{pmatrix} U_{i,e} & 0 \\ 0 & U_{i,h} \end{pmatrix}$$

$$U_{i,e} = -4t_e + V(\mathbf{r}_i)$$

$$U_{i,h} = -4t_h - E_g + V(\mathbf{r}_i)$$

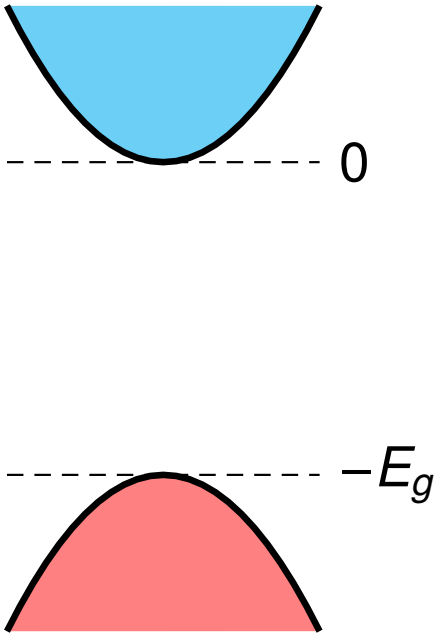

Using effective masses[a] $m_e^* = 0.4625$, $m_h^* = 0.5659$ and adopting $a = 2\,\text{nm}$, hopping parameters are:

$$t_e = -0.0206\,\text{eV}, \quad t_h = 0.0168\,\text{eV}$$

[a] Fang, S. et al., Phys. Rev. B **92** (2015) 205108

Twisted bilayer MoS_2

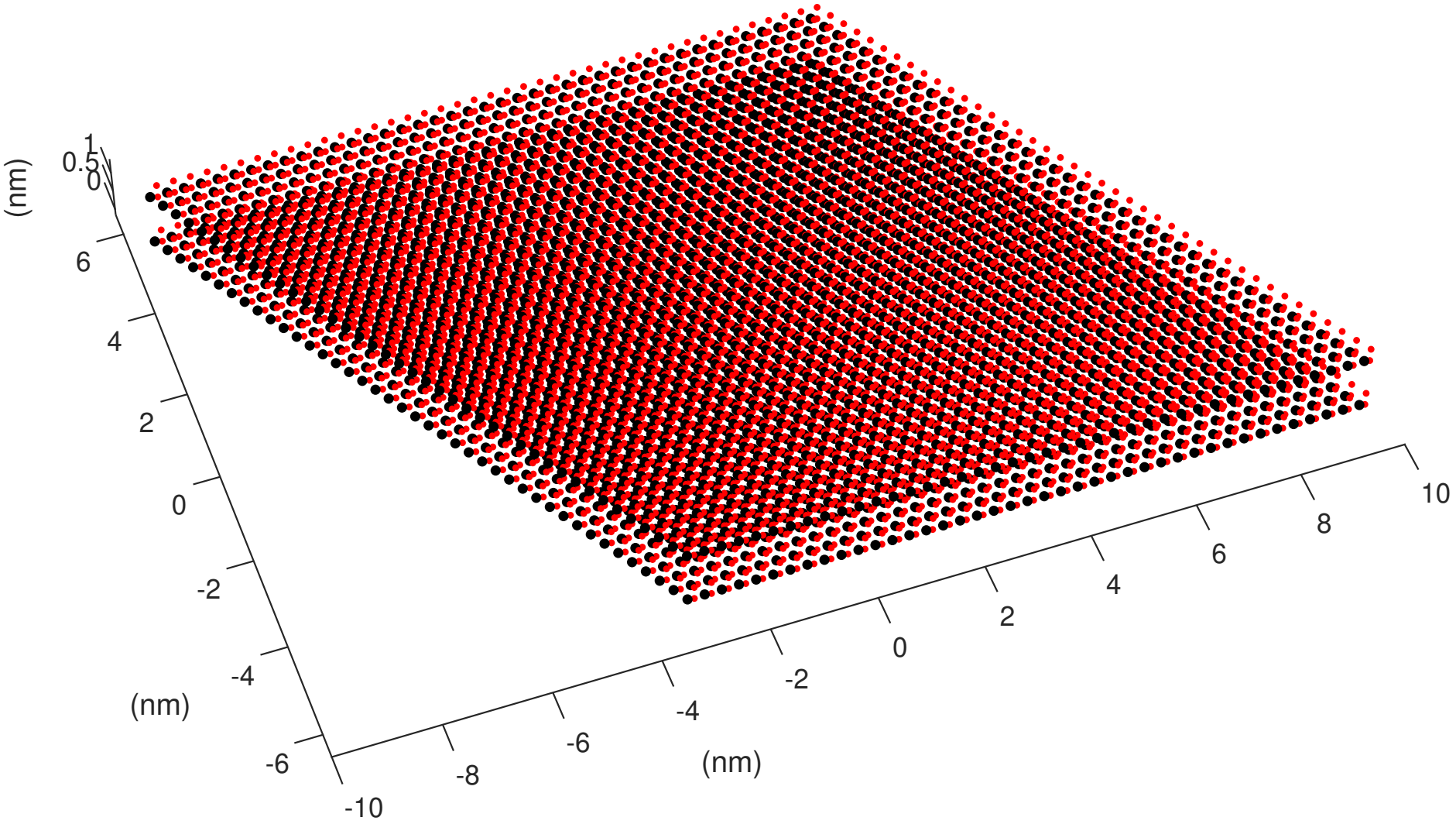

Twisted bilayer MoS_2

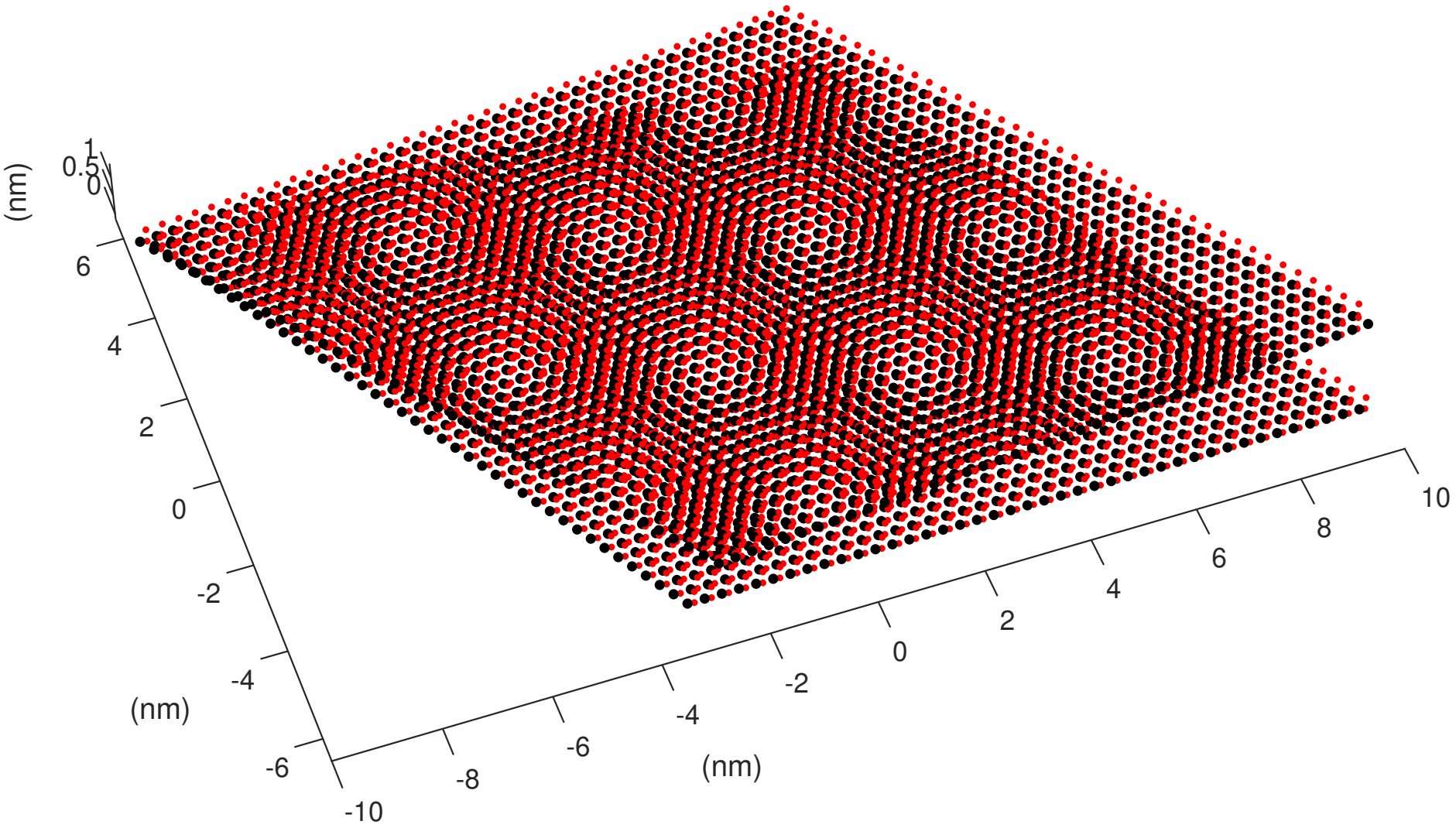

Model periodic potential[1]

$$V(\mathbf{r}) = \gamma \sum_{j=1}^{3} \cos(\mathbf{G}_j \cdot \mathbf{r})$$

$$\mathbf{G}_j = \frac{4\pi}{\sqrt{3}R_m}\left[\sin\left(j\frac{2\pi}{3}\right), -\cos\left(j\frac{2\pi}{3}\right)\right]$$

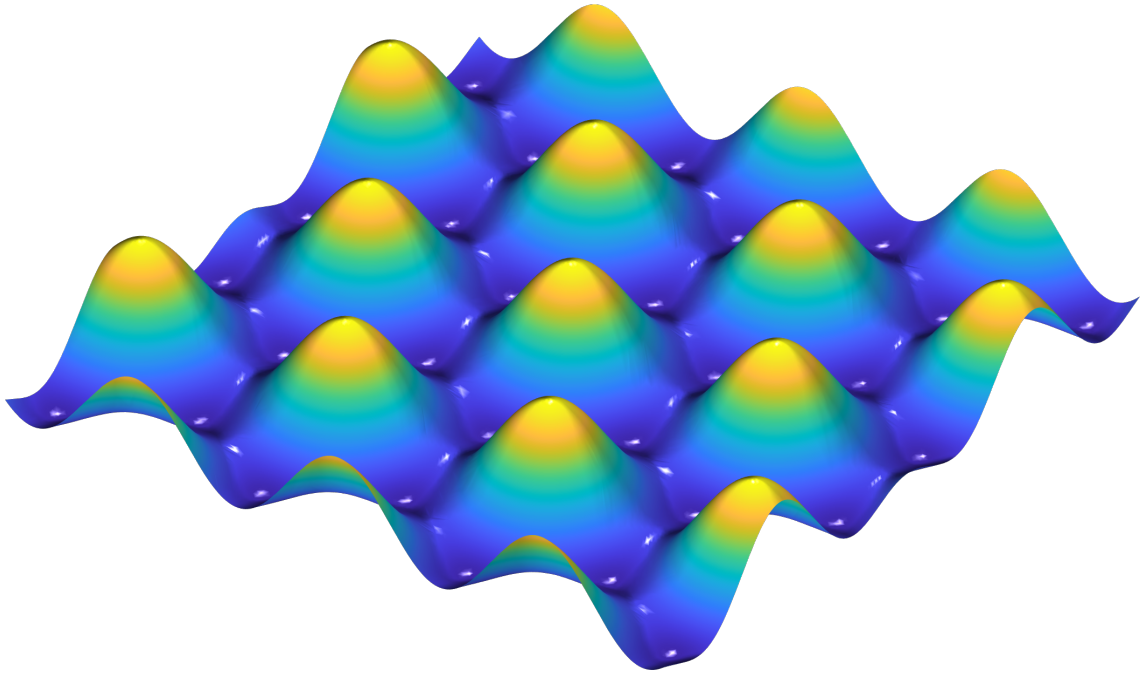

[1] Same form used in, e.g., Kraft, R. et al., Phys. Rev. Lett. **125** (2020) 217701.

A two-terminal MoS_2 superlattice device

A. Garcia-Ruiz and M.-H. Liu, arXiv:2401.10436

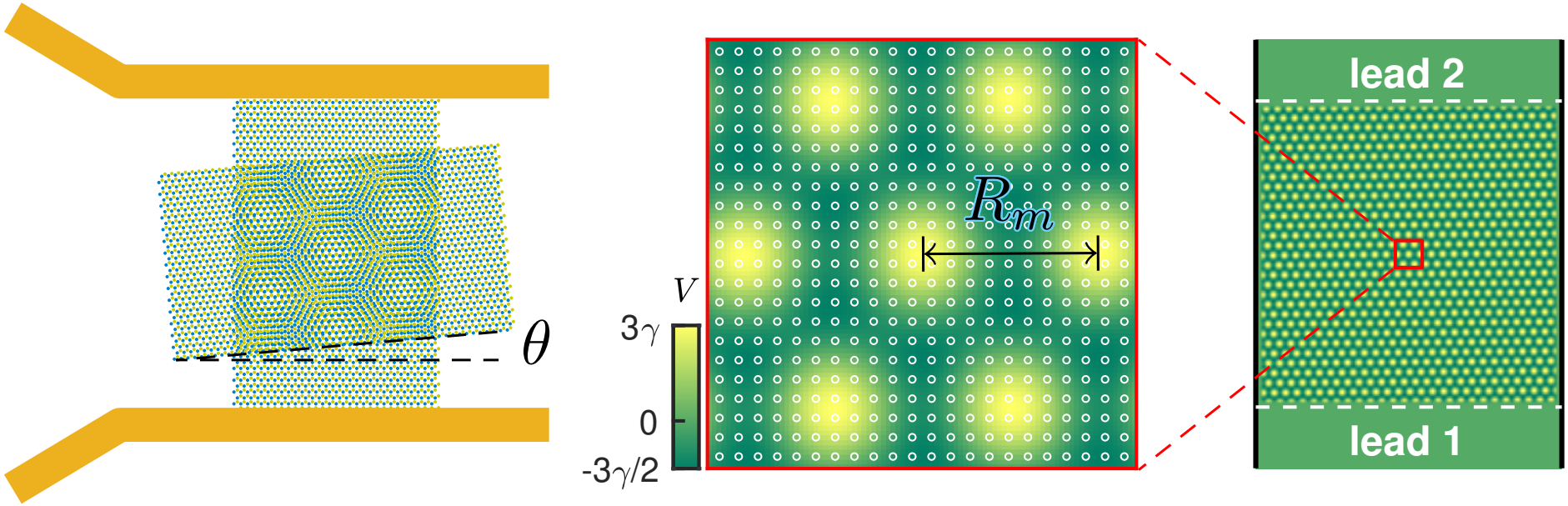

We consider $\theta \approx 1^\circ \implies R_m \approx 18.47\,\text{nm}$

A two-terminal MoS_2 superlattice device

A. Garcia-Ruiz and M.-H. Liu, arXiv:2401.10436

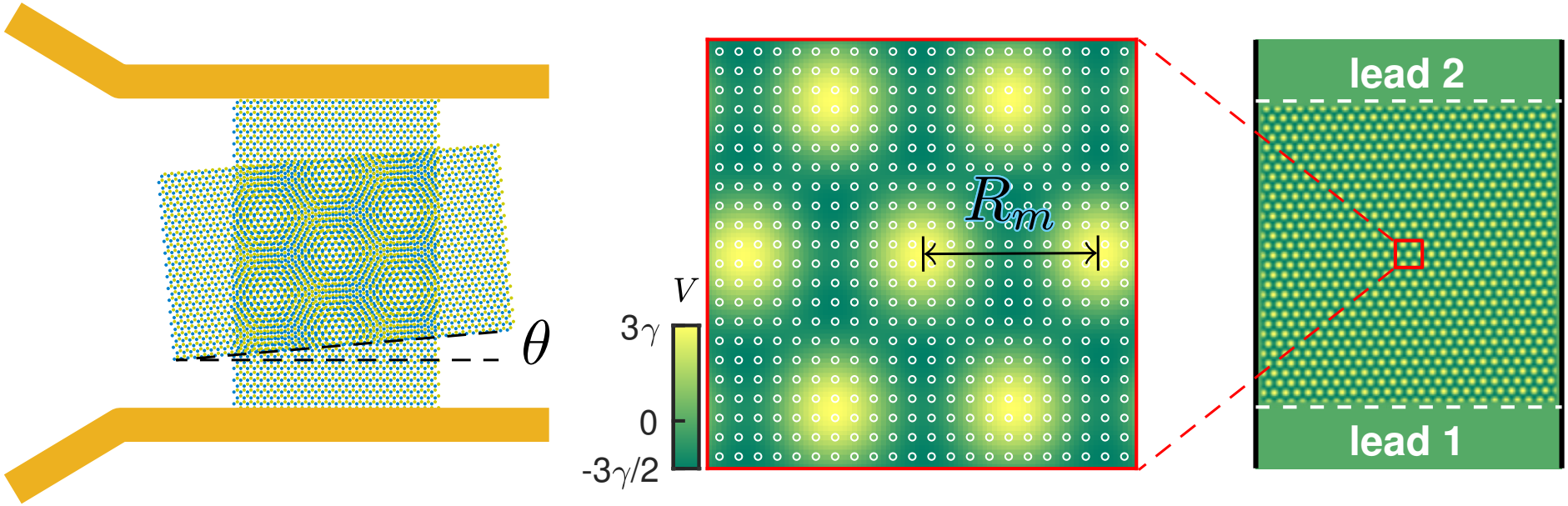

We consider $\theta \approx 1^\circ \implies R_m \approx 18.47\,\text{nm}$

What about γ?

Test calculations: Coupling strength dependence

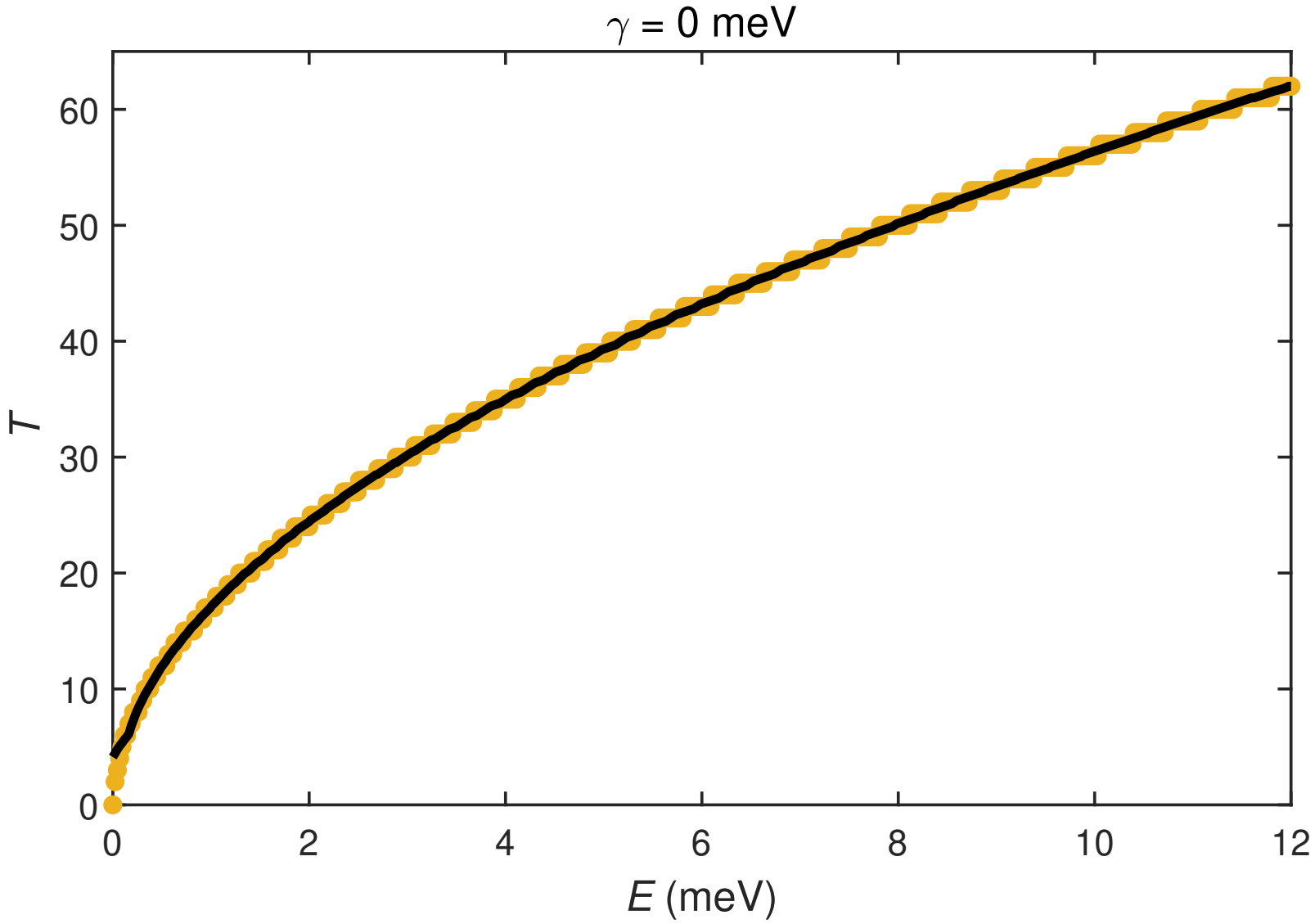

Test calculations: Coupling strength dependence

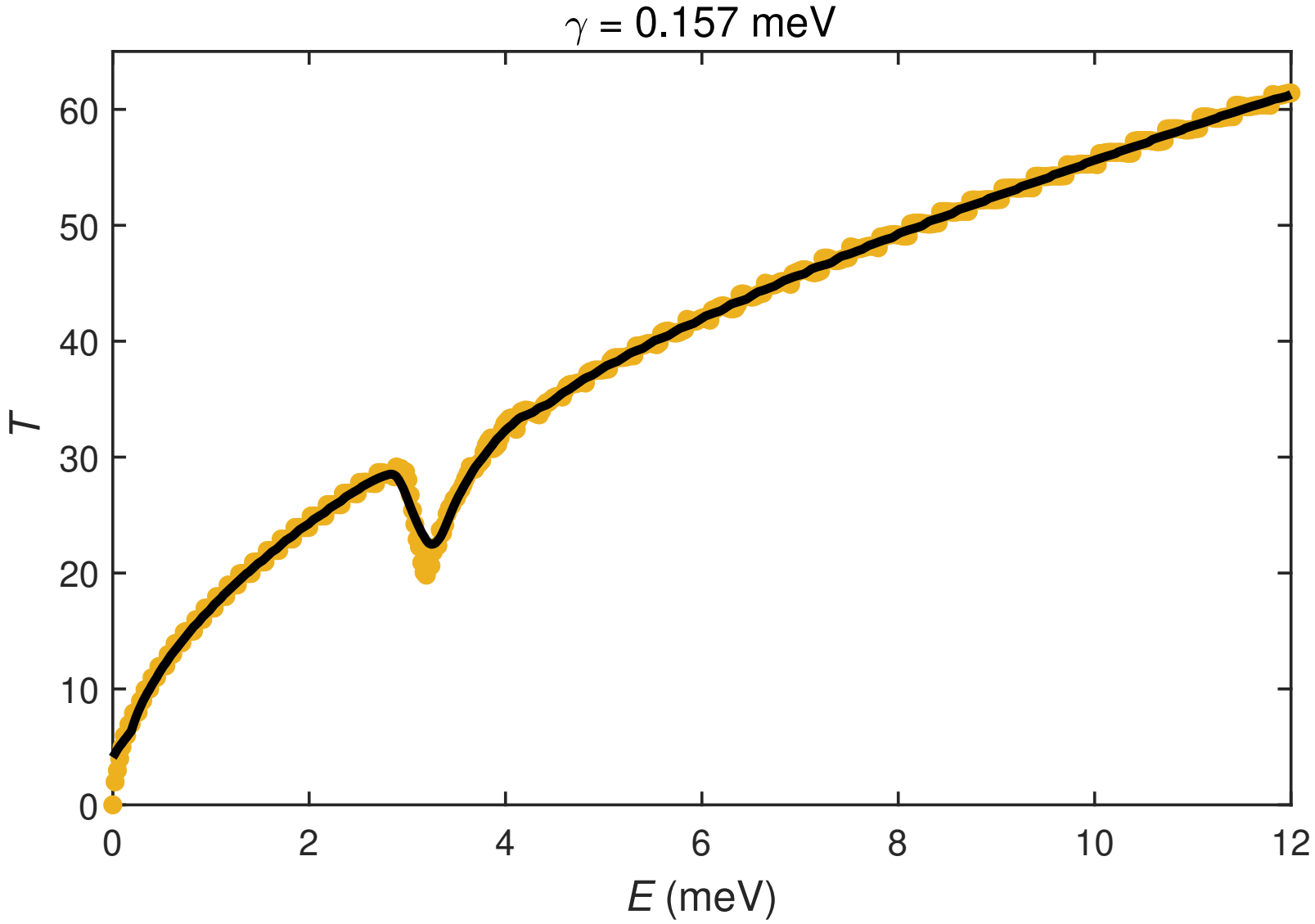

Test calculations: Coupling strength dependence

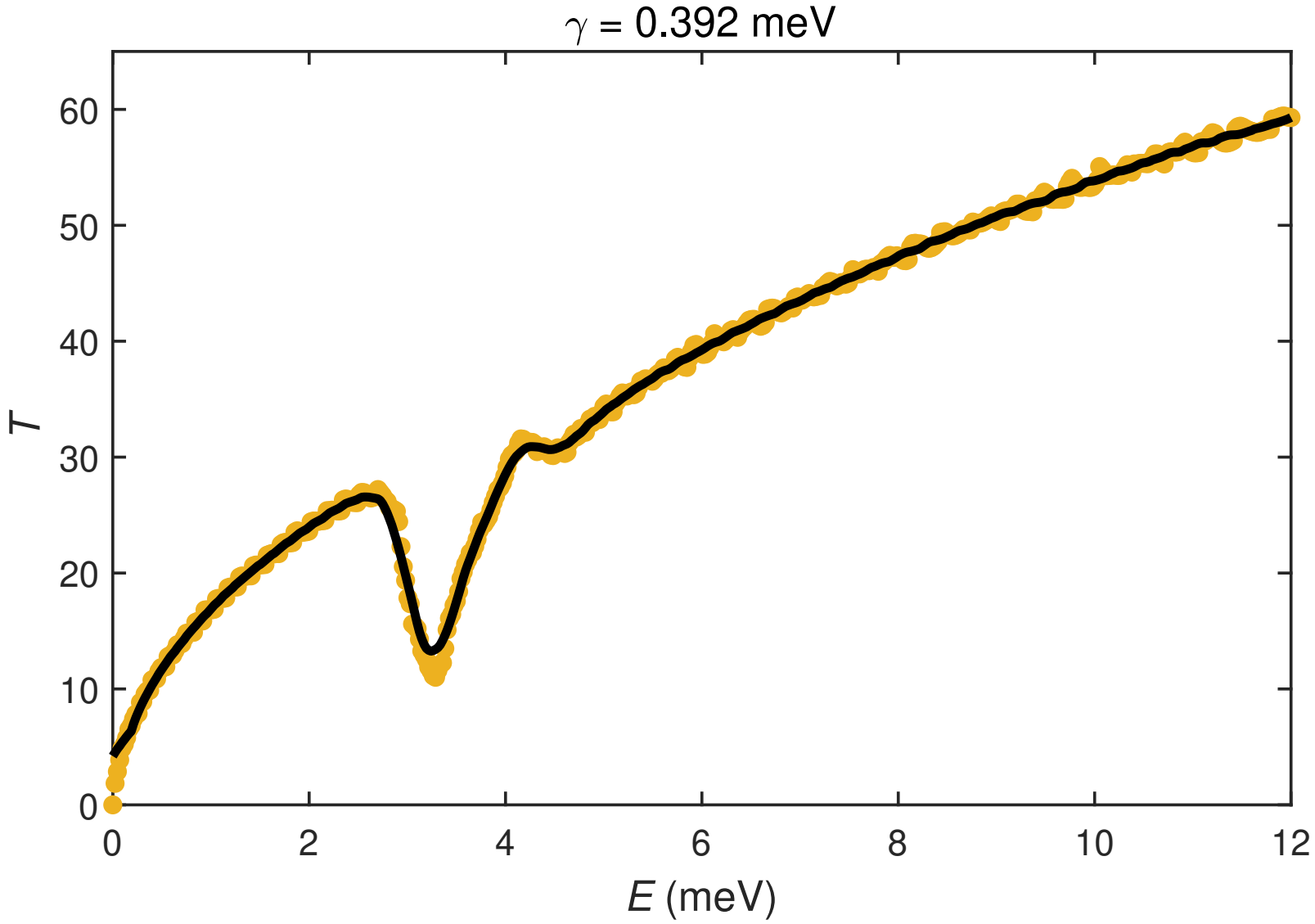

Test calculations: Coupling strength dependence

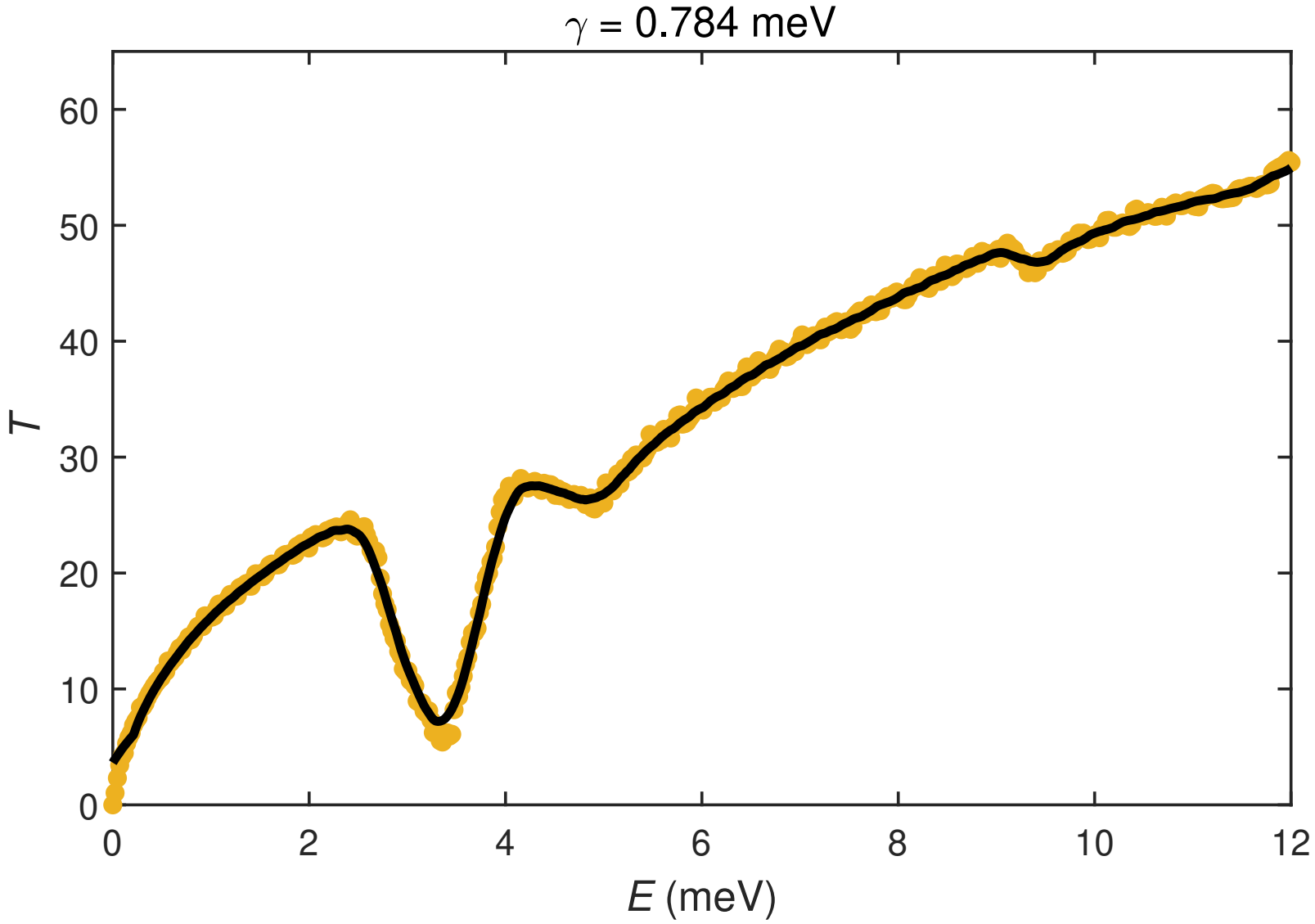

Test calculations: Coupling strength dependence

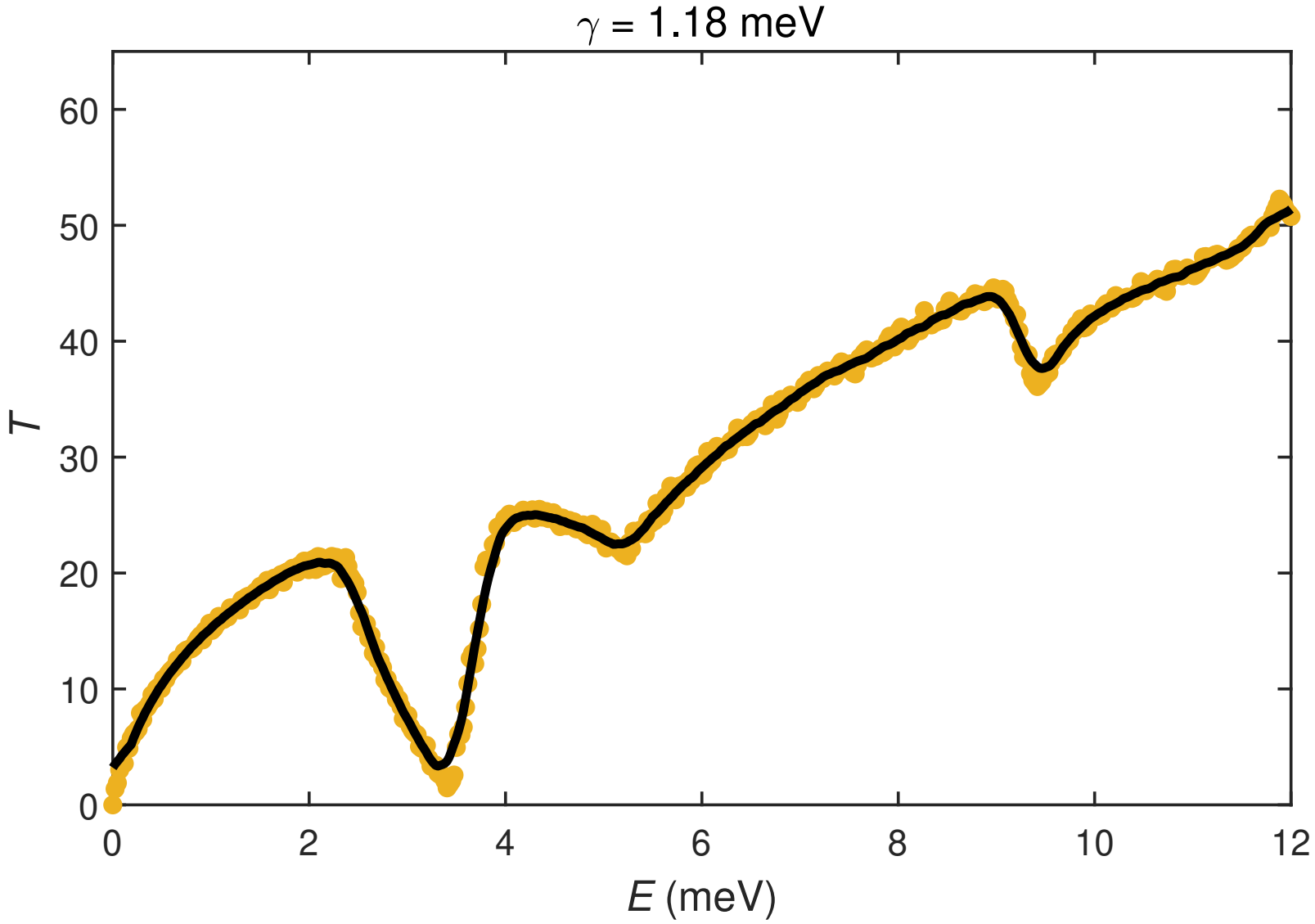

Test calculations: Coupling strength dependence

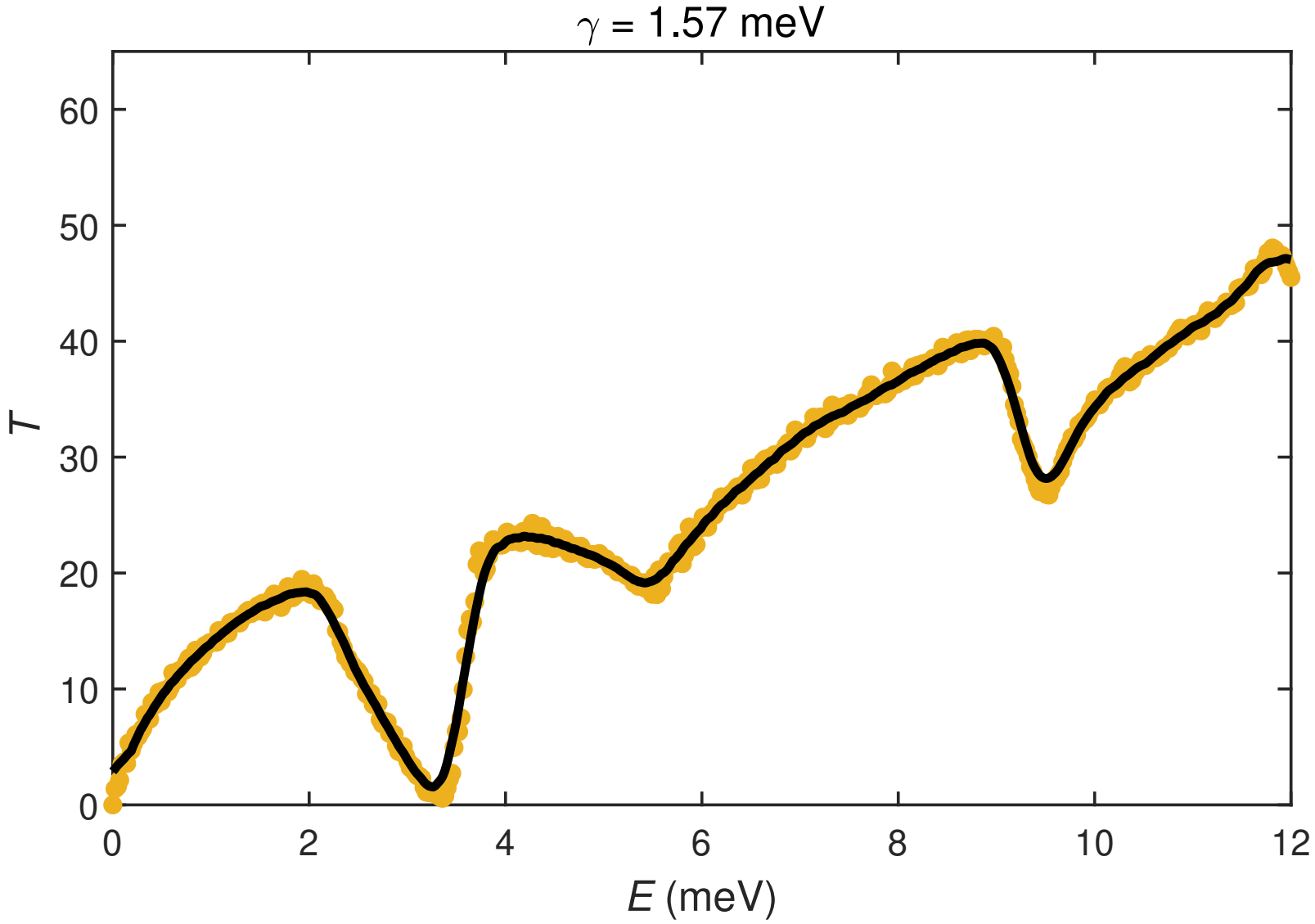

Comparison with continuum model

A. Garcia-Ruiz and M.-H. Liu, arXiv:2401.10436

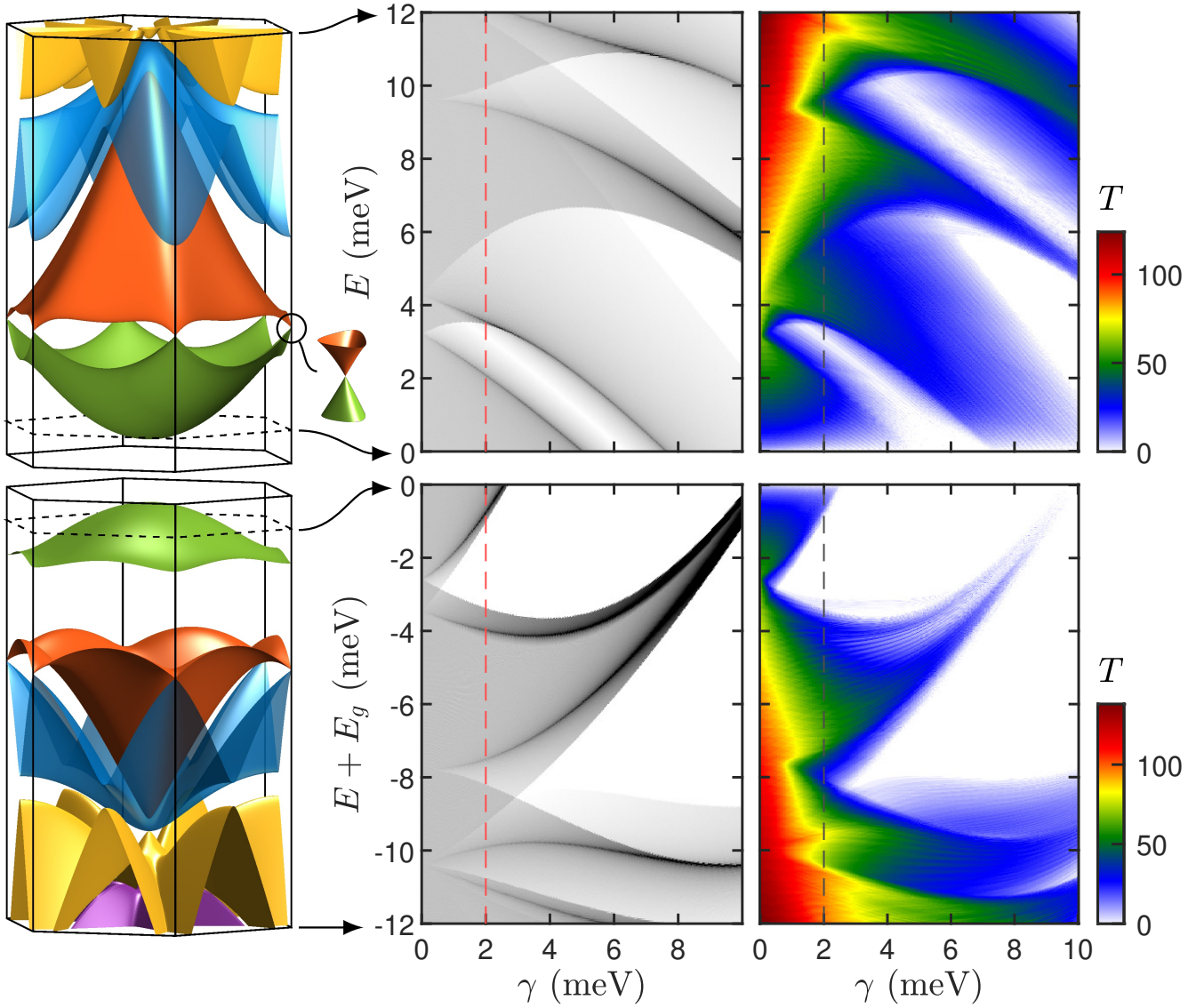

Magnetotransport: Emerging Hofstadter's butterfly

A. Garcia-Ruiz and M.-H. Liu, arXiv:2401.10436

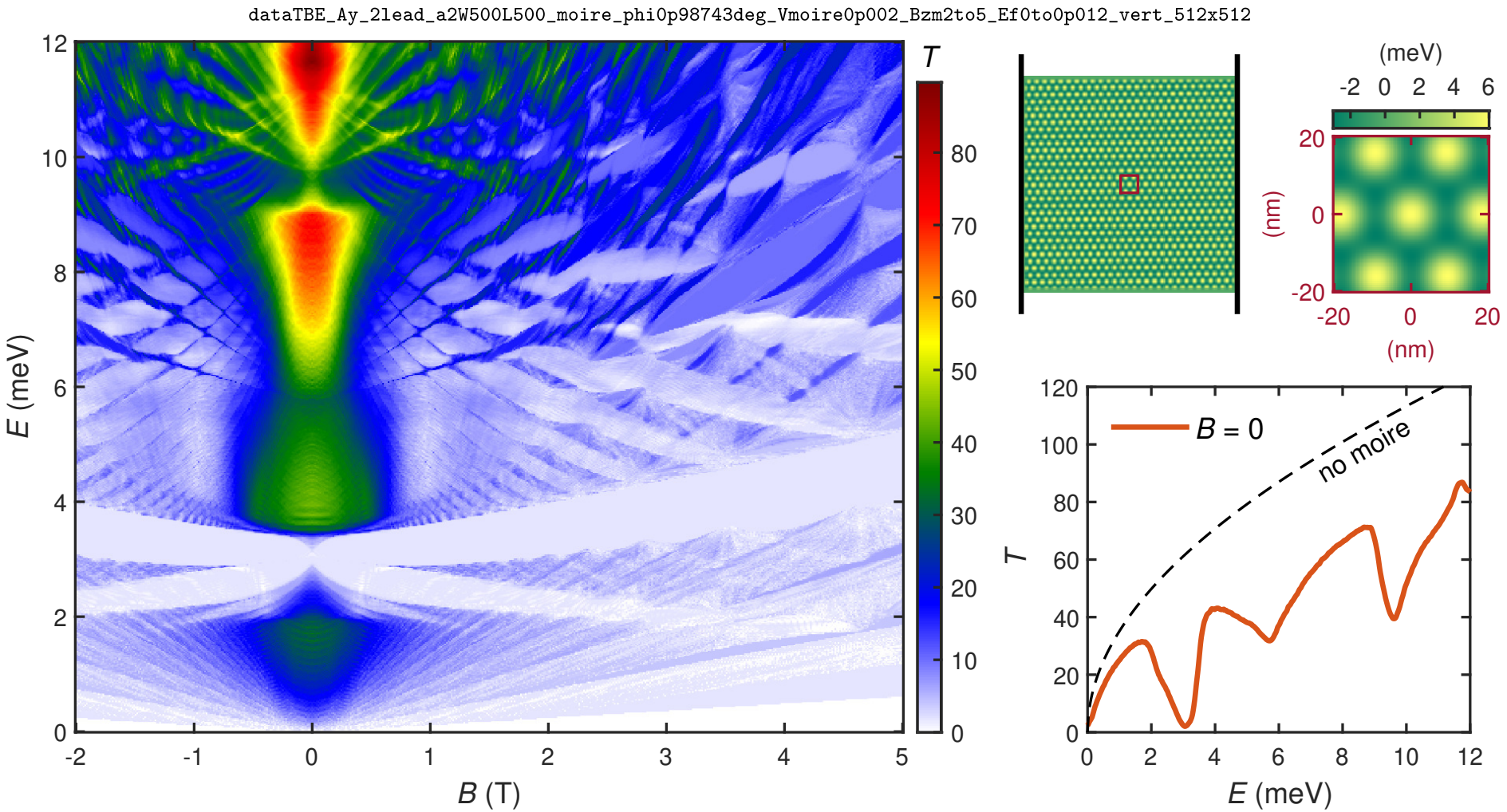

Magnetotransport: Emerging Hofstadter's butterfly

A. Garcia-Ruiz and M.-H. Liu, arXiv:2401.10436

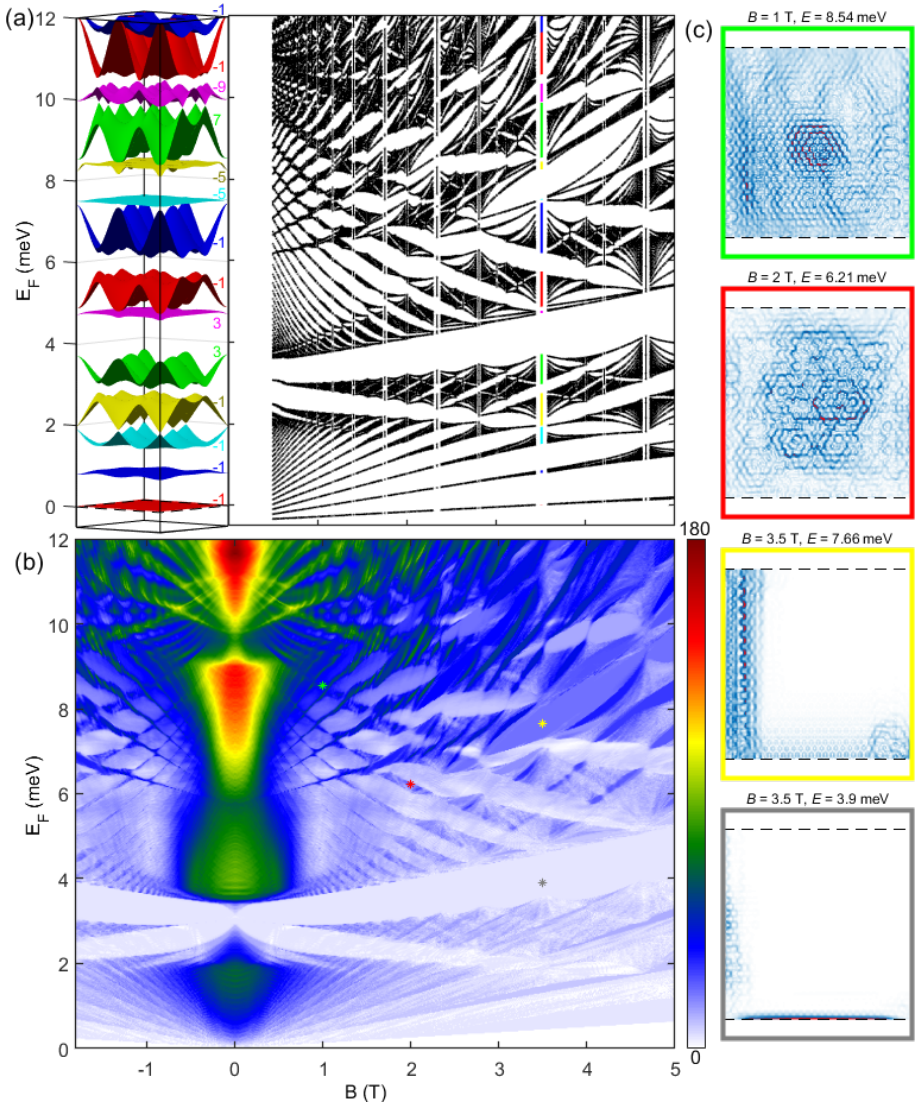

Magnetotransport: Emerging Hofstadter's butterfly

A. Garcia-Ruiz and M.-H. Liu, arXiv:2401.10436

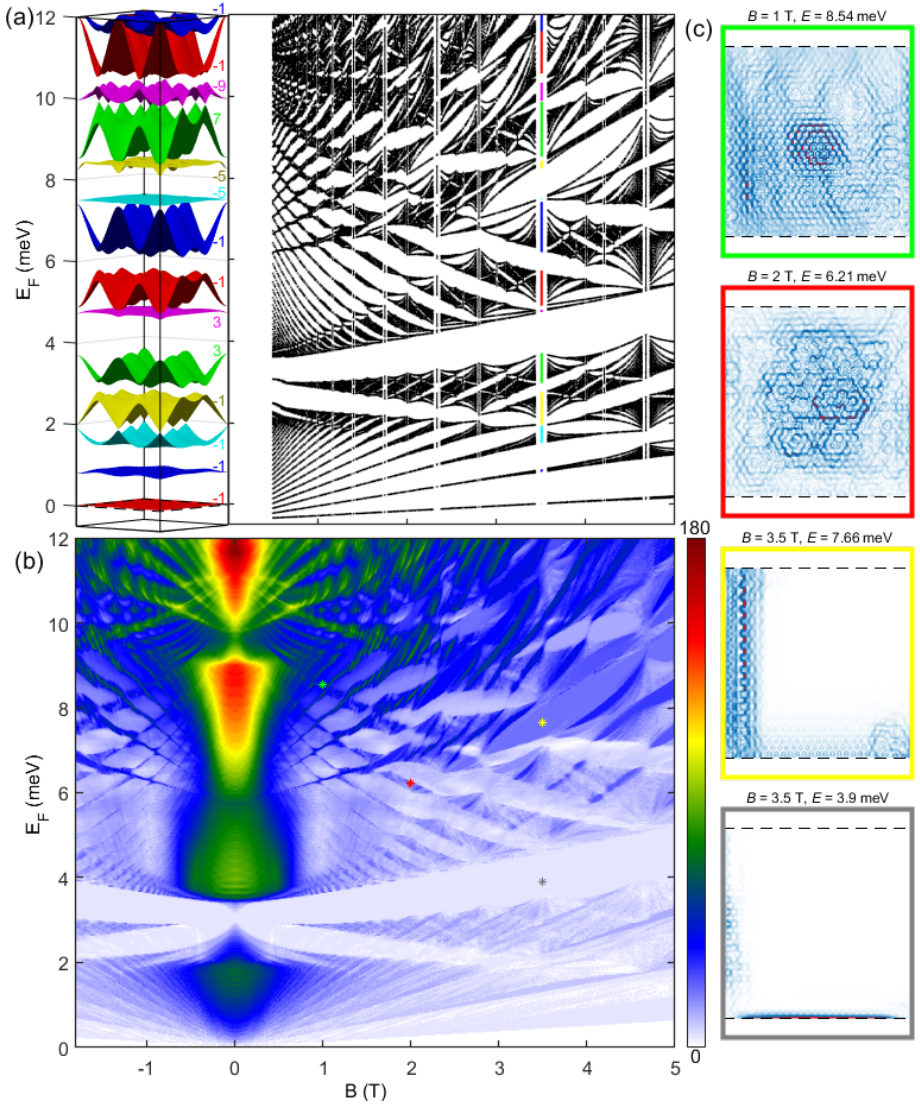

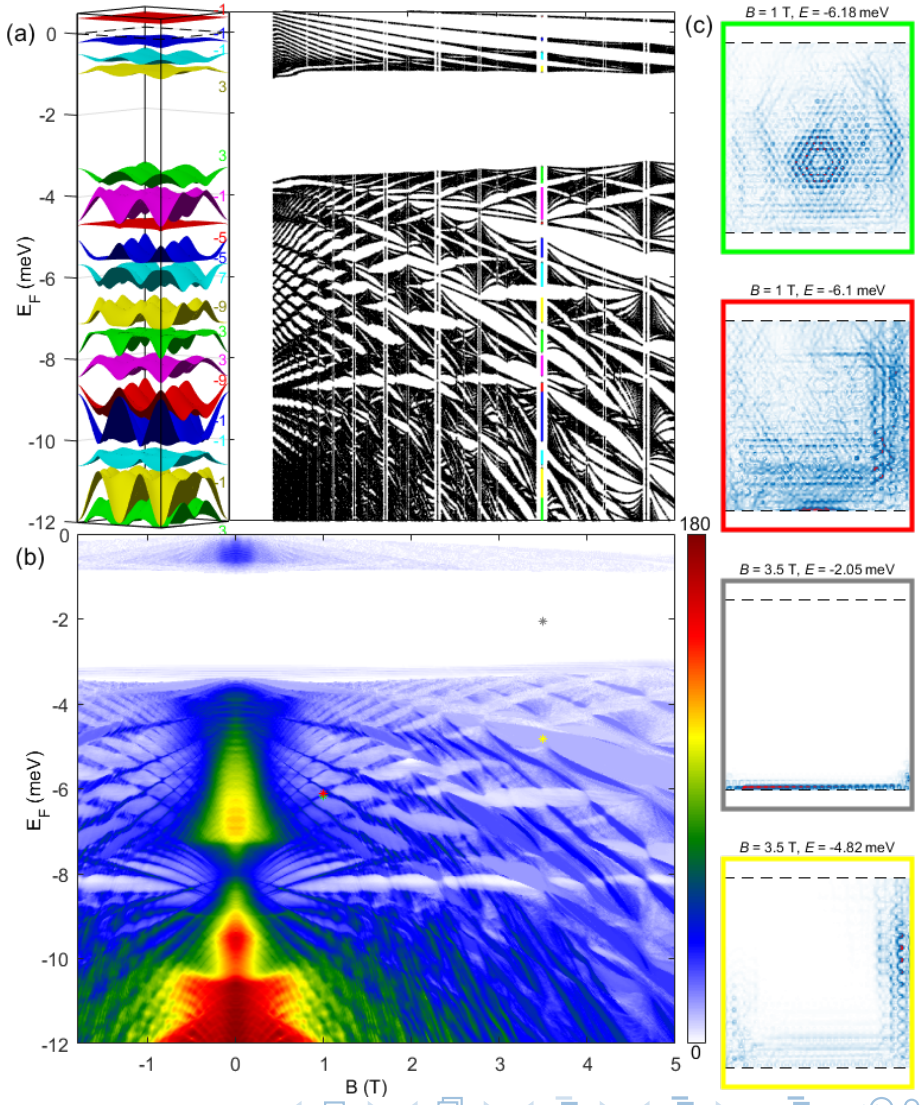

2

Graphene

- Test calculations
- Transverse magnetic focusing
- Spin-dependent transverse magnetic focusing
- Graphene/hBN moiré superlattice

Scalable tight-binding model for (low E) graphene[1]

Basic idea:

$$E(k) = \pm\hbar v_F k \,, \qquad \hbar v_F = \frac{3}{2} t_0 a_0 = \frac{3}{2}\frac{t_0}{s_f} s_f a_0$$

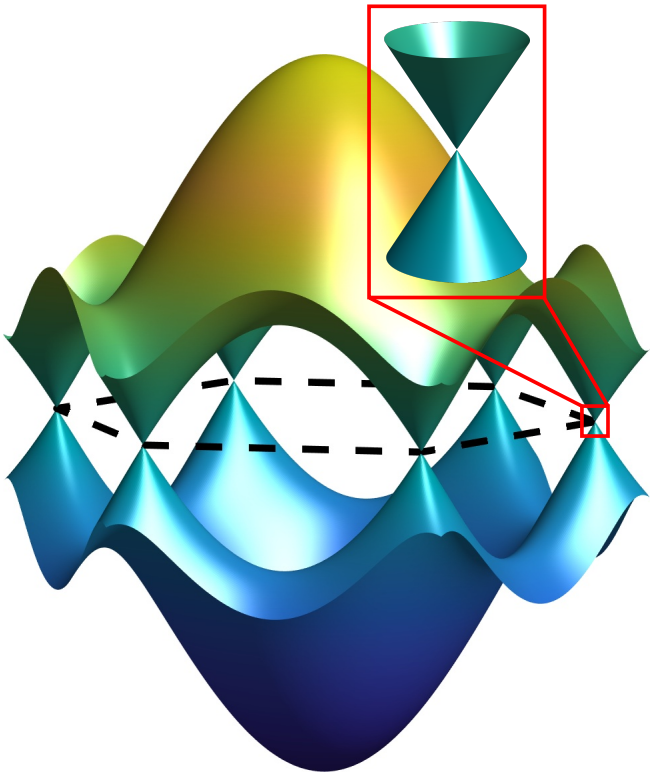

[1] Liu, M.-H. et al., Phys. Rev. Lett. **114** (2015) 036601

Scalable tight-binding model for (low E) graphene[1]

Basic idea:

$$E(k) = \pm\hbar v_F k\ , \qquad \hbar v_F = \frac{3}{2} t_0 a_0 = \frac{3}{2}\frac{t_0}{s_f} s_f a_0$$

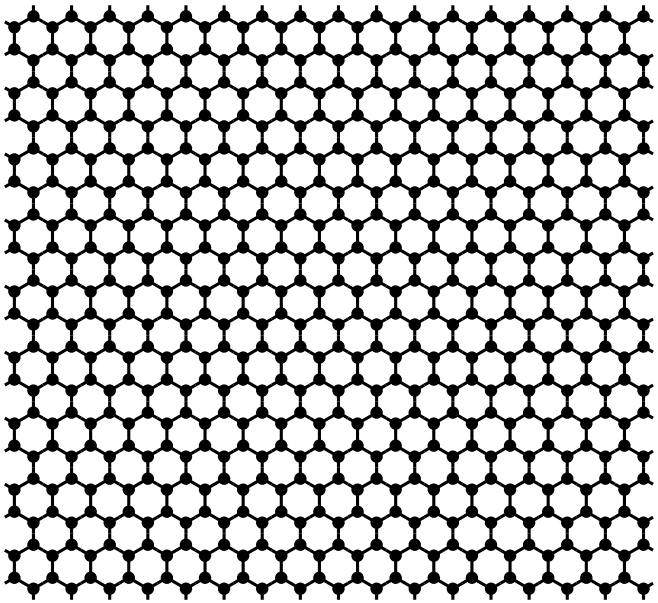

$$\xrightarrow[a = s_f a_0,\ t = \frac{t_0}{s_f}]{\lambda_F,\, l_B \gg a}$$

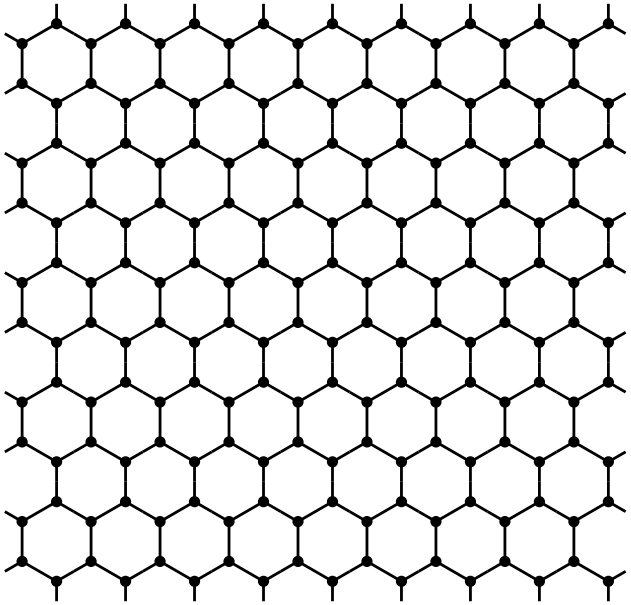

[1] Liu, M.-H. et al., Phys. Rev. Lett. **114** (2015) 036601

Scalable tight-binding model for (low E) graphene[1]

Basic idea:

$$E(k) = \pm\hbar v_F k\ , \qquad \hbar v_F = \frac{3}{2} t_0 a_0 = \frac{3}{2}\frac{t_0}{s_f} s_f a_0$$

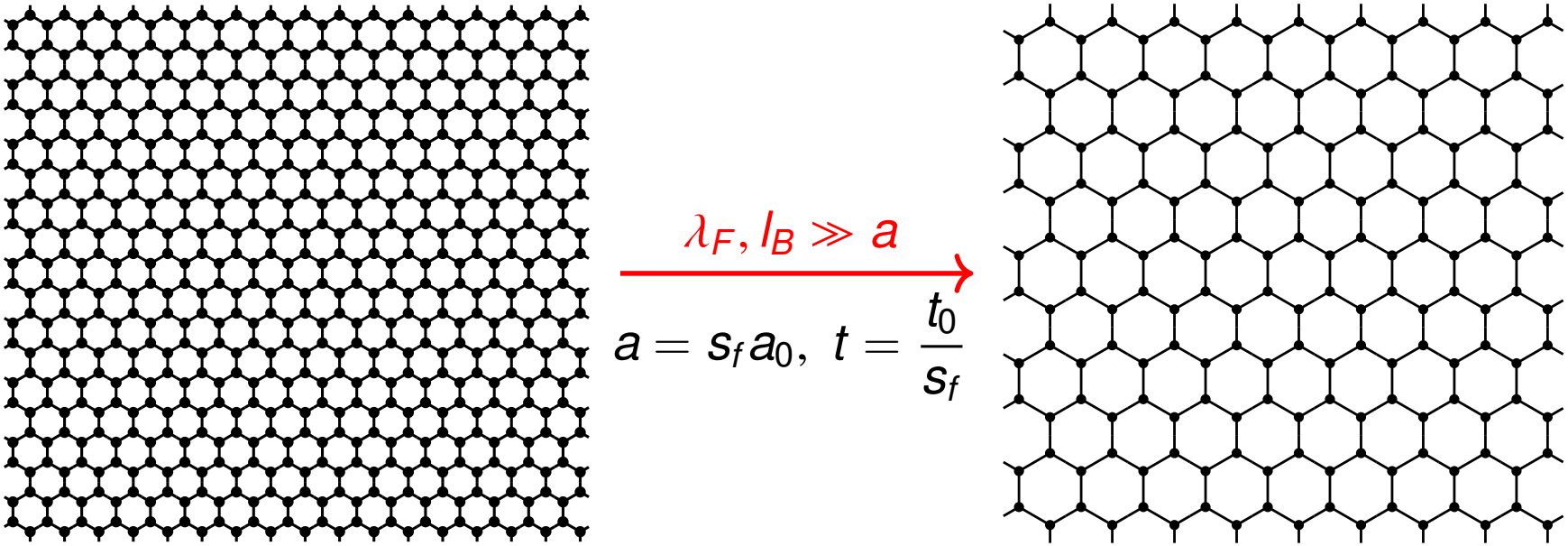

Example:

$$1\,\mu\text{m}^2 : 3.8 \times 10^7 \text{ C atoms} \xrightarrow{s_f = 20} 9.5 \times 10^4 \text{ lattice sites}$$

[1] Liu, M.-H. et al., Phys. Rev. Lett. **114** (2015) 036601

Electron wave and quantum optics in graphene

A review

Journal of Physics: Condensed Matter

ACCEPTED MANUSCRIPT • OPEN ACCESS

Electron wave and quantum optics in graphene

To cite this article before publication: Himadri Chakraborti *et al* 2024 *J. Phys.: Condens. Matter* in press https://doi.org/10.1088/1361-648X/ad46bc

Topical Review

Electron wave and quantum optics in graphene

Himadri Chakraborti[1], Cosimo Gorini[1], Angelika Knothe[2,‡], Ming-Hao Liu[3], Péter Makk[4,5,§], François D. Parmentier[1], David Perconte[6], Klaus Richter[2], Preden Roulleau[1,‖], Benjamin Sacépé[6], Christian Schönenberger[7], Wenmin Yang[6]

[1]Université Paris-Saclay, CEA, CNRS, SPEC, 91191, Gif-sur-Yvette, France
[2]Institut für Theoretische Physik, Universität Regensburg, D-93040 Regensburg, Germany
[3]Department of Physics and Center for Quantum Frontiers of Research and Technology (QFort), National Cheng Kung University, Tainan 70101, Taiwan
[4]Department of Physics, Institute of Physics, Budapest University of Technology and Economics, Müegyetem rkp. 3., H-1111 Budapest, Hungary
[5]MTA-BME Correlated van der Waals Structures Momentum Research Group, Müegyetem rkp. 3., H-1111 Budapest, Hungary
[6]Université Grenoble Alpes, CNRS, Grenoble INP, Institut Néel, 38000 Grenoble, France
[7]Nanoelectronics Group, Department of Physics, University of Basel, Basel, Switzerland

Abstract. In the last decade, graphene has become an exciting platform for electron optical experiments, in some aspects superior to conventional two-dimensional electron gases (2DEGs). A major advantage, besides the ultra-large mobilities, is the fine control over the electrostatics, which gives the possibility of realising gap-less and compact p-n interfaces with high precision. The latter host non-trivial states, *e.g.* , snake states in moderate magnetic fields, and serve as building blocks of complex electron interferometers. Thanks to the Dirac spectrum and its non-trivial Berry phase, the internal (valley and sublattice) degrees of freedom, and the possibility to tailor the band structure using proximity effects, such interferometers open up a completely new playground based on novel device architectures. In this review, we introduce the theoretical background of graphene electron optics, fabrication methods used to realise electron-optical devices, and techniques for corresponding numerical simulations. Based on this, we give a comprehensive review of ballistic transport experiments and simple building blocks of electron optical devices both in single and bilayer graphene, highlighting the novel physics that is brought in compared to conventional 2DEGs. After describing the different magnetic field regimes in graphene p-n junctions and nanostructures, we conclude by discussing the state of the art in graphene-based Mach-Zender and Fabry-Perot interferometers.

‡ angelika.knothe@physik.uni-regensburg.de
§ makk.peter@ttk.bme.hu
‖ preden.roulleau@cea.fr

Chakraborti, H. et al., Journal of Physics: Condensed Matter (2024)

Quantum Hall edge current in angled ribbons

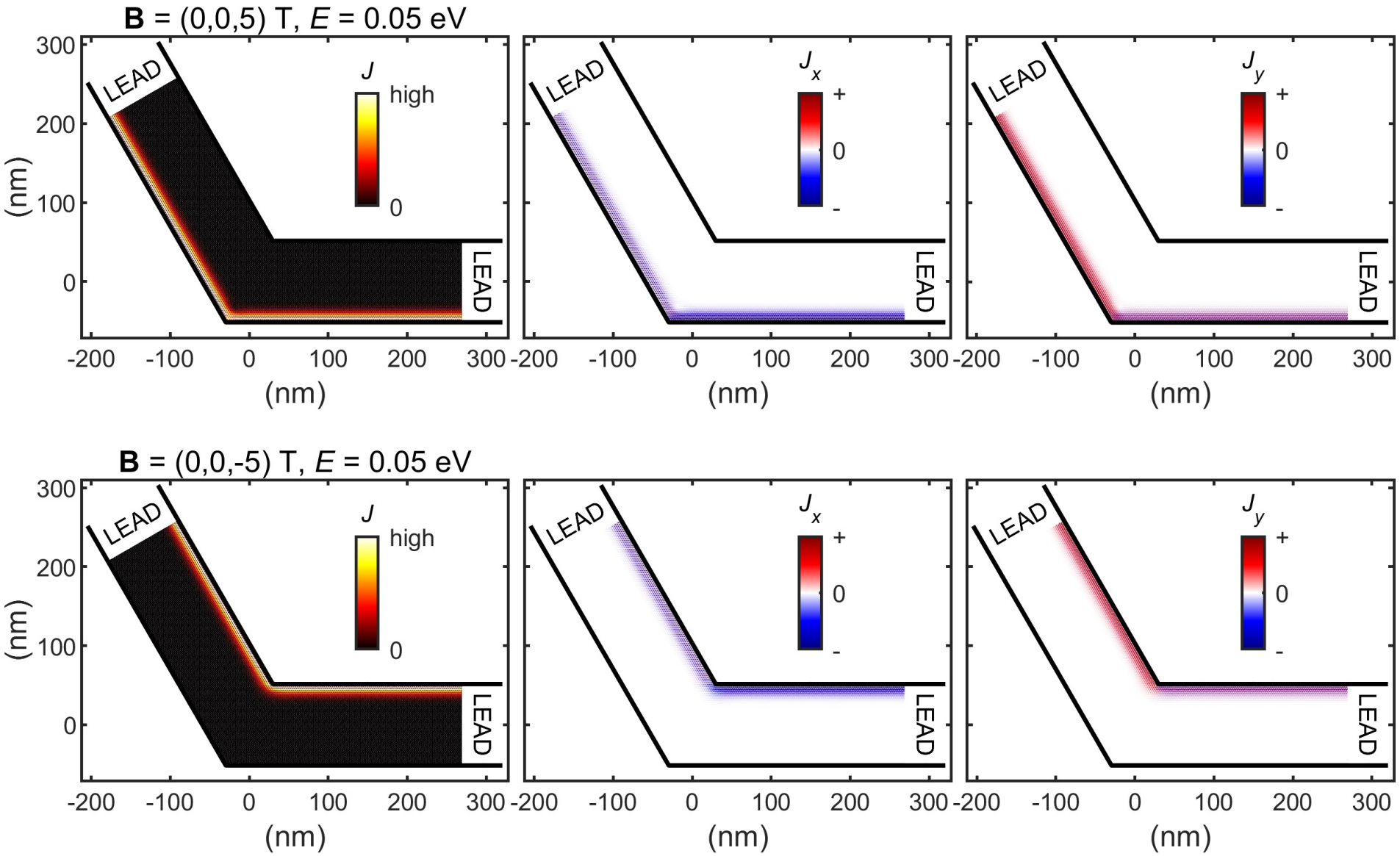

Quantum Hall edge current in angled ribbons

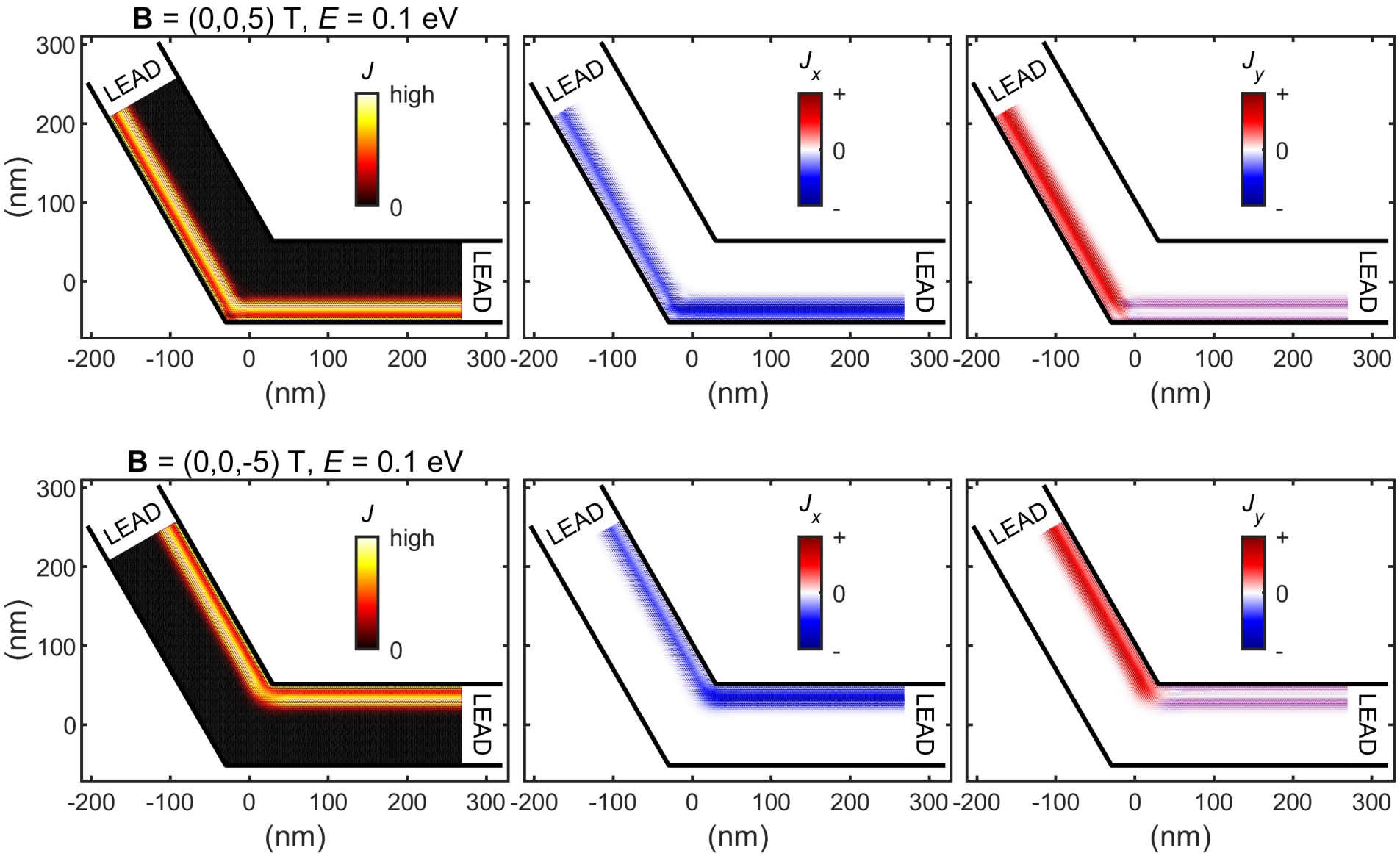

Quantum Hall edge current in angled ribbons

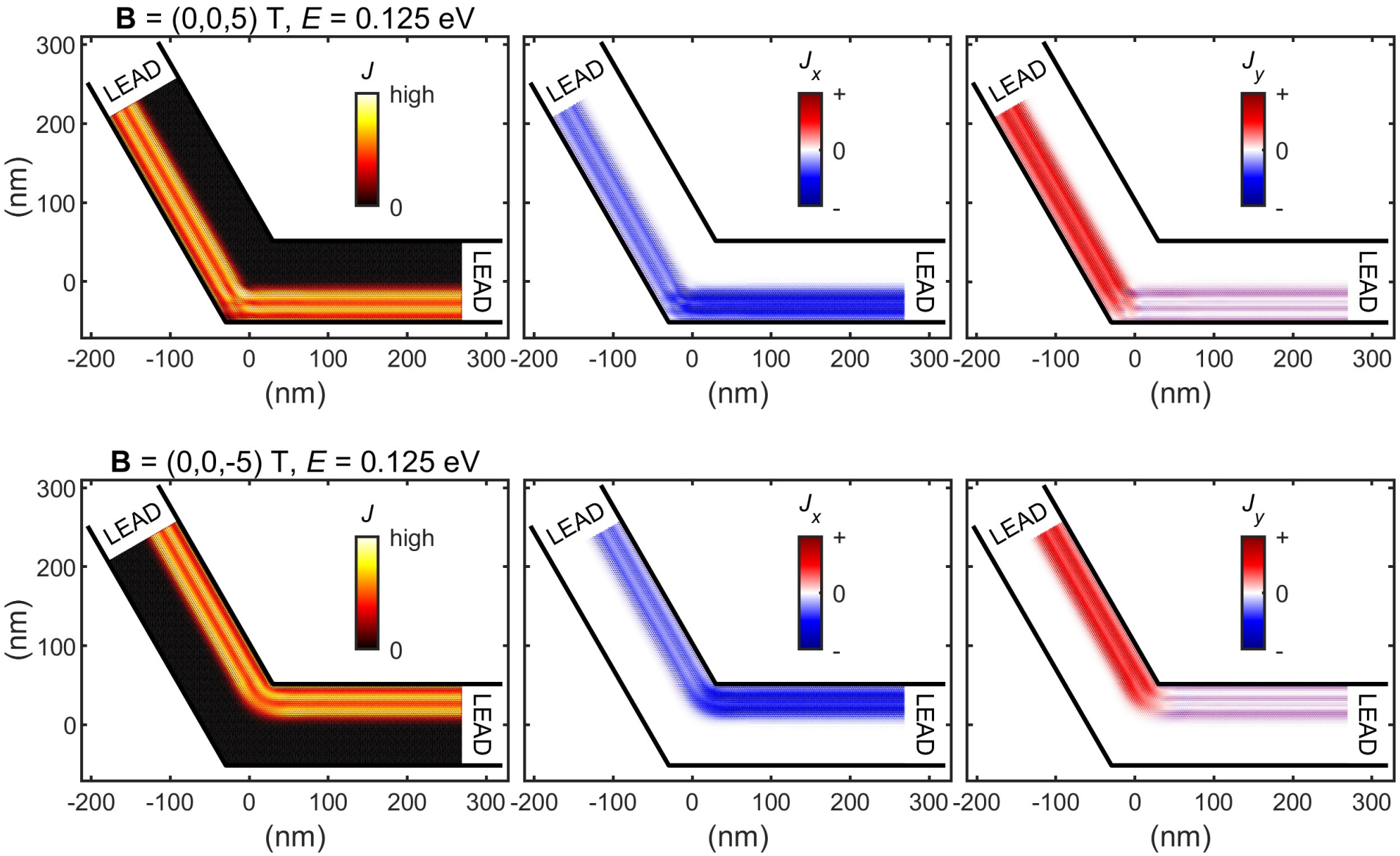

Quantum Hall edge current in angled ribbons

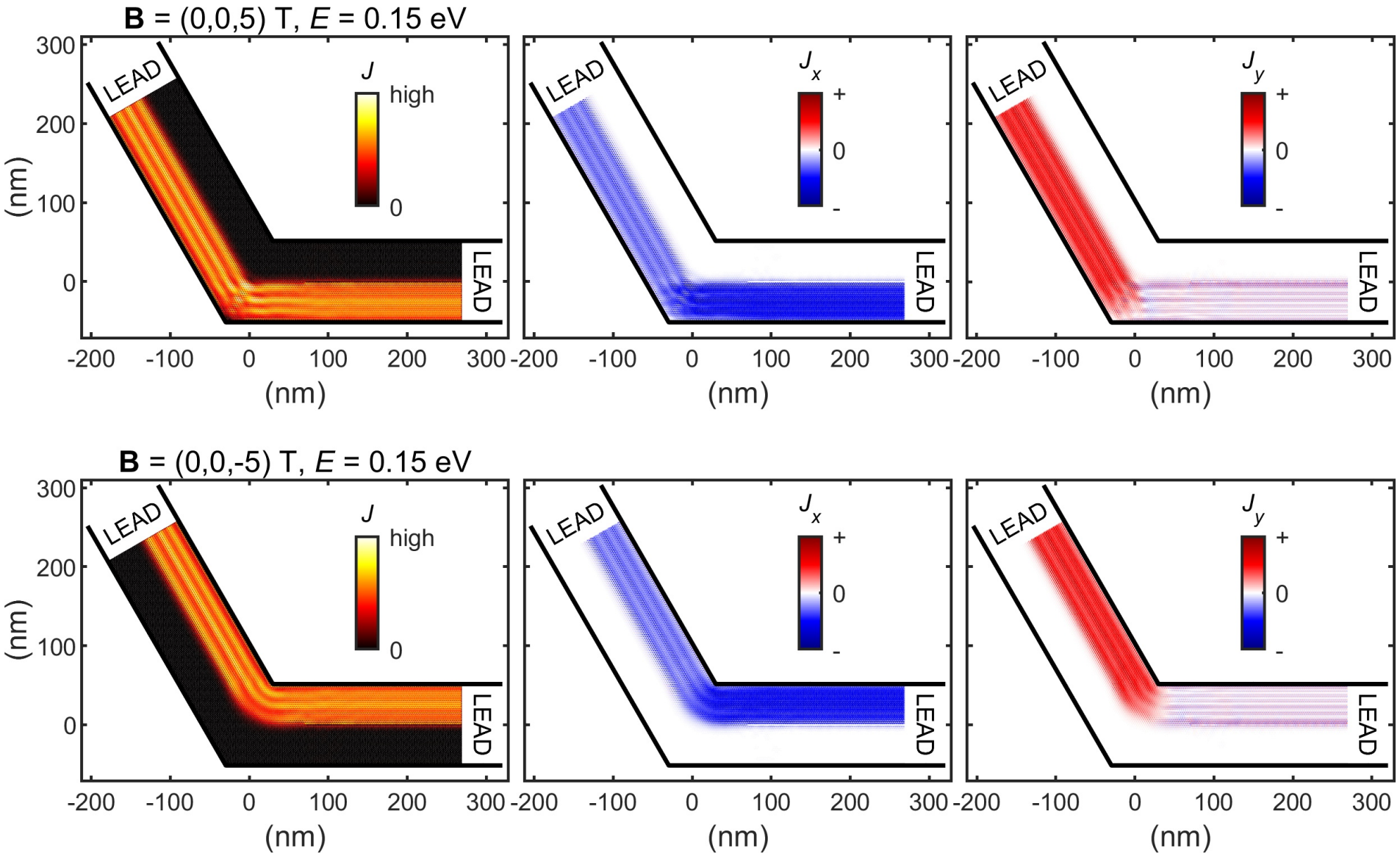

Transverse magnetic focusing (TMF)

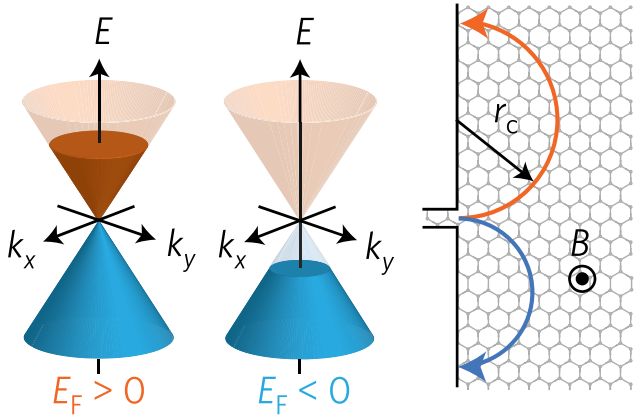

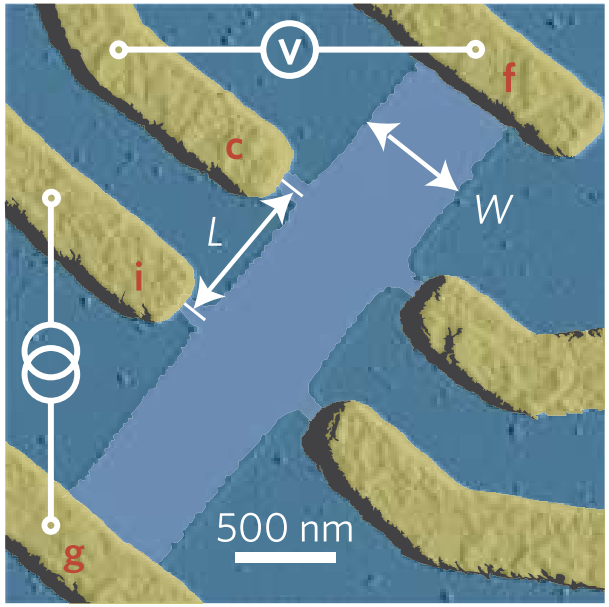

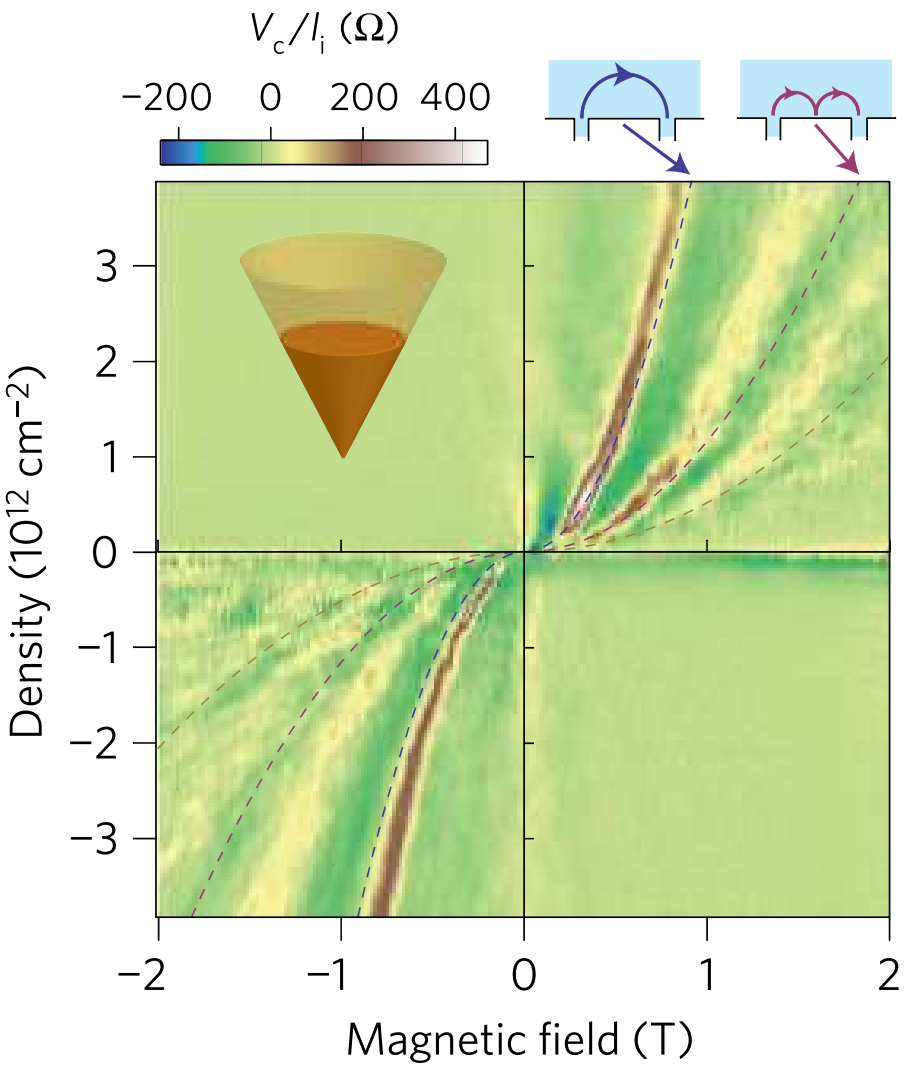

Taychatanapat, T., Watanabe, K., Taniguchi, T., and Jarillo-Herrero, P., Nat. Phys. **9** (2013) 225

Semiclassical trajectory simulation for TMF

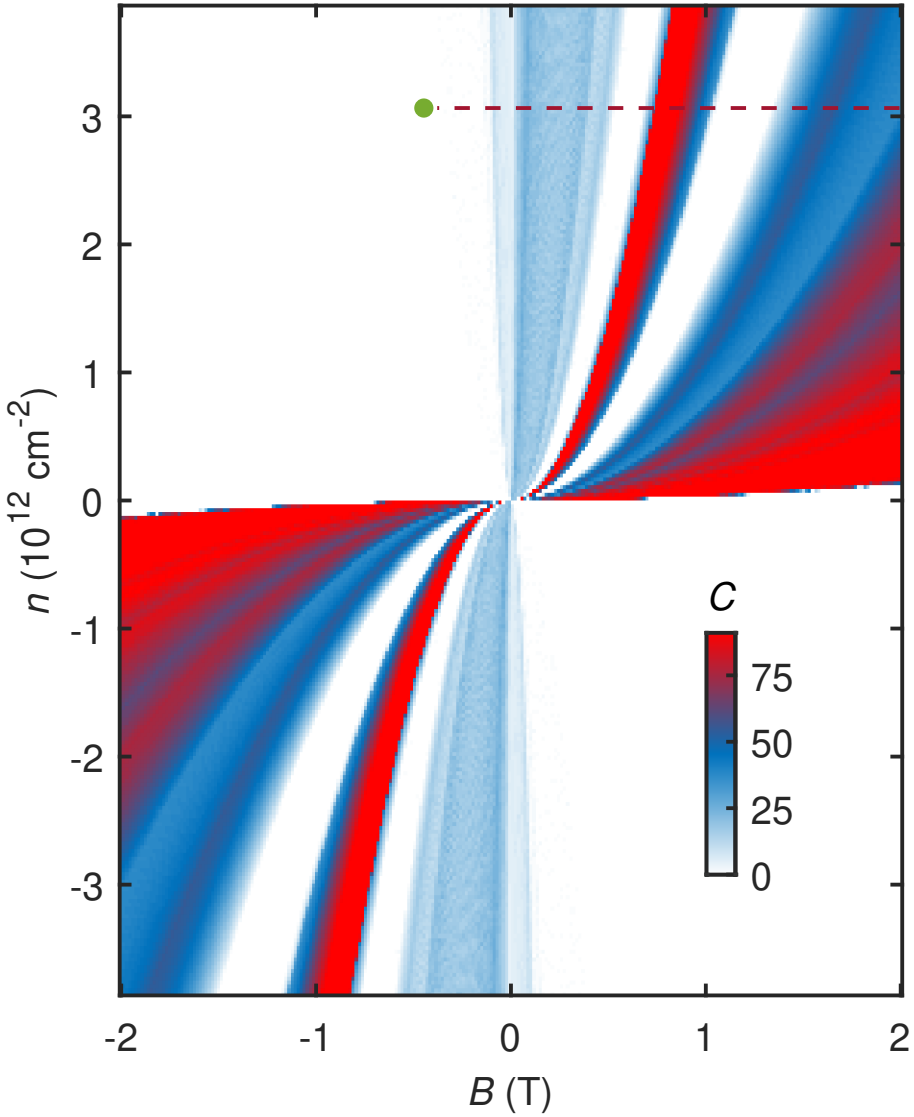

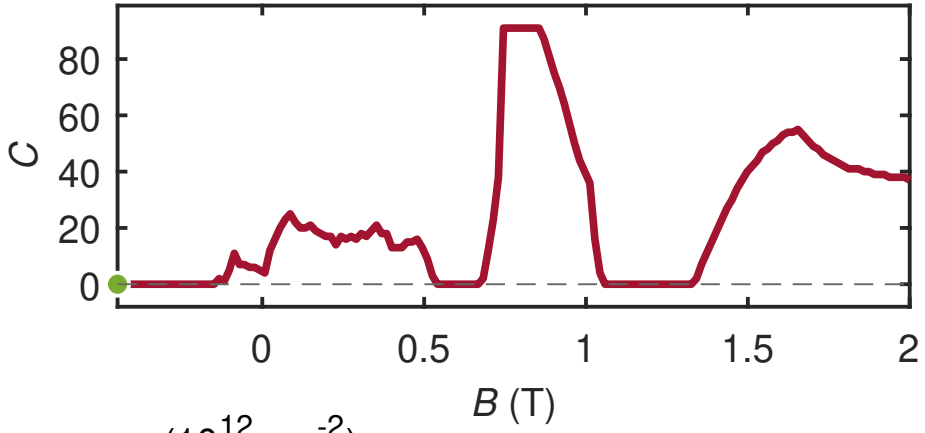

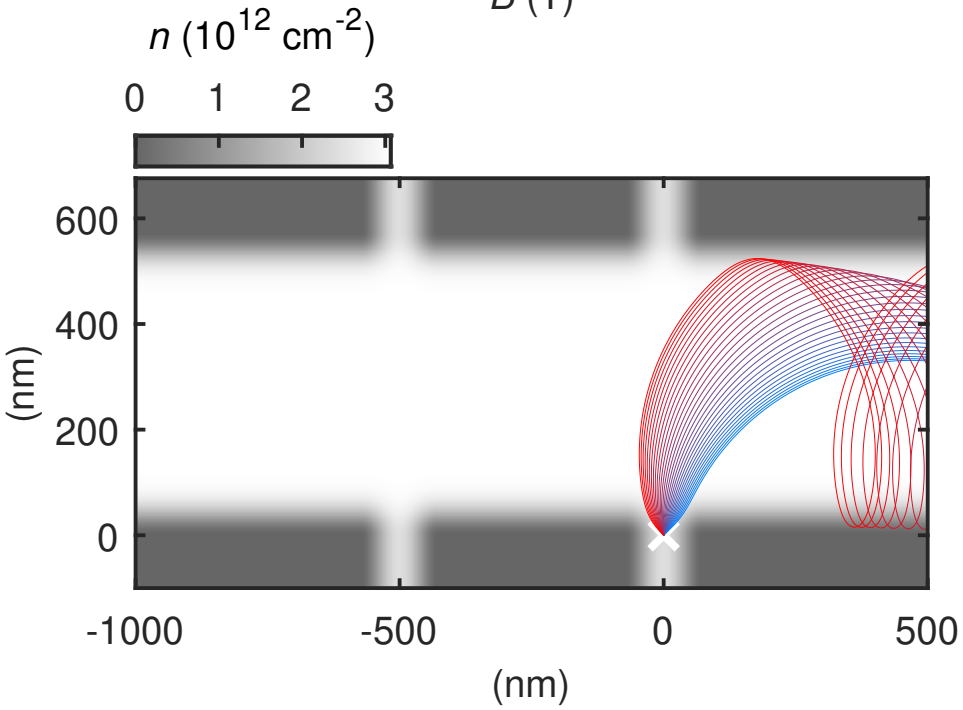

Semiclassical trajectory simulation for TMF

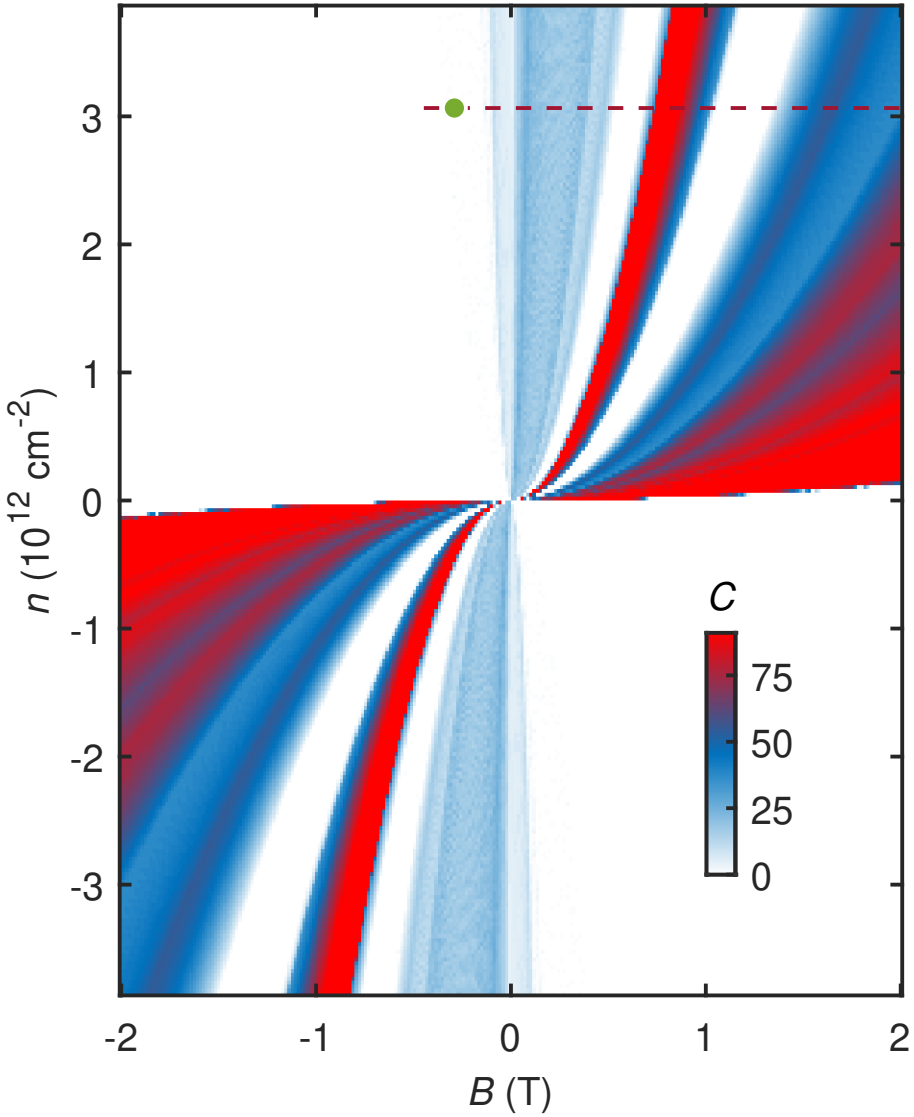

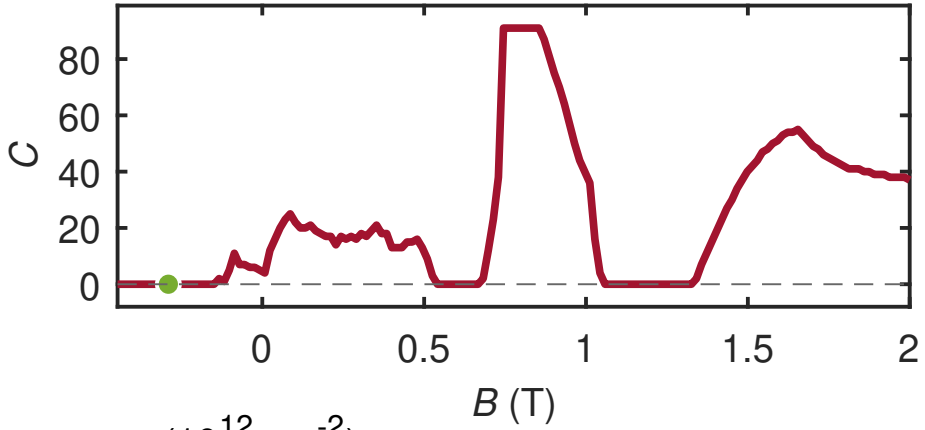

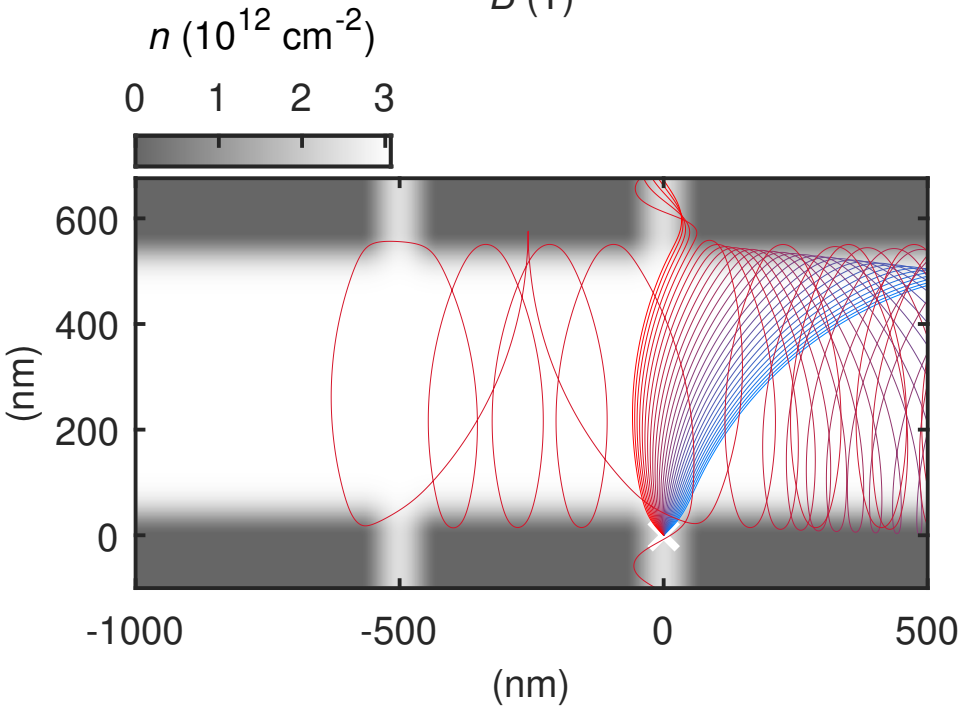

Semiclassical trajectory simulation for TMF

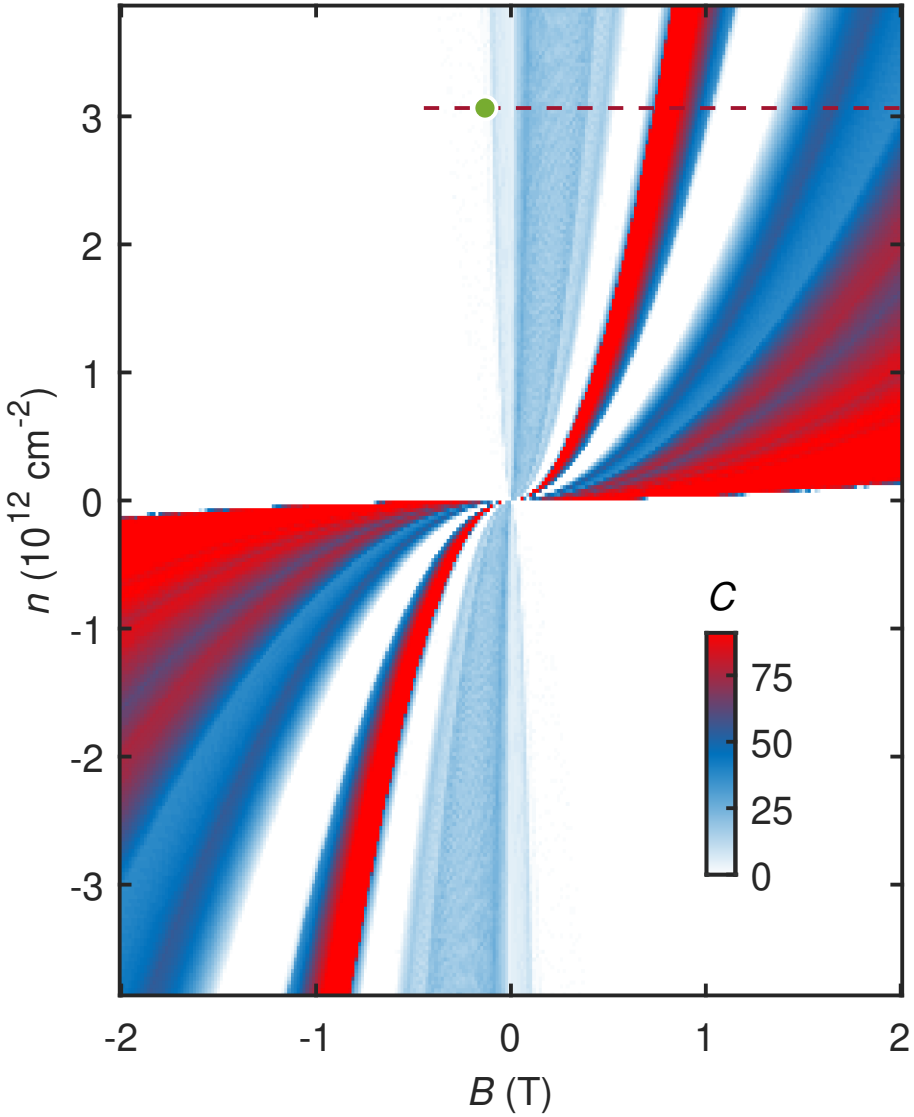

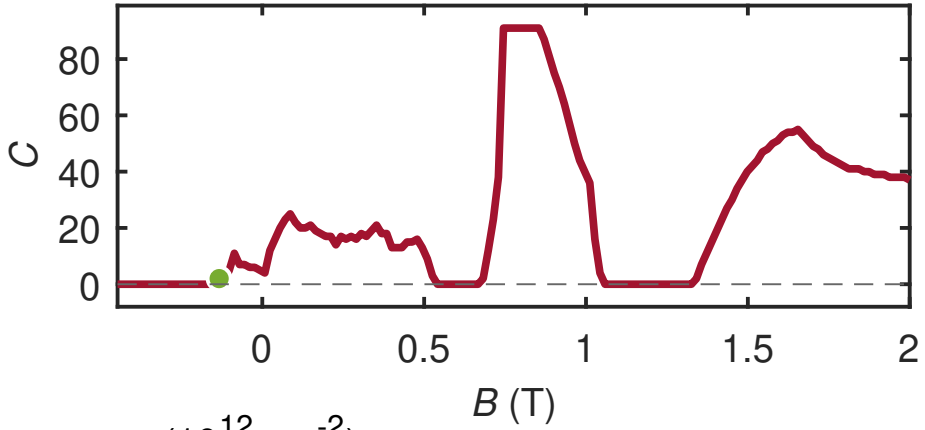

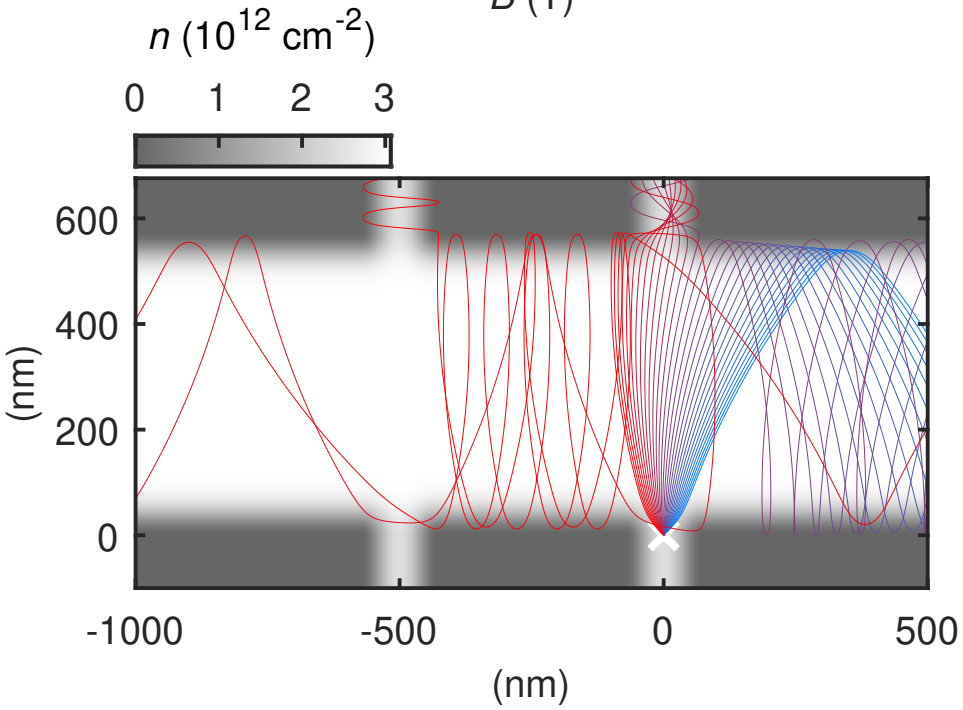

Semiclassical trajectory simulation for TMF

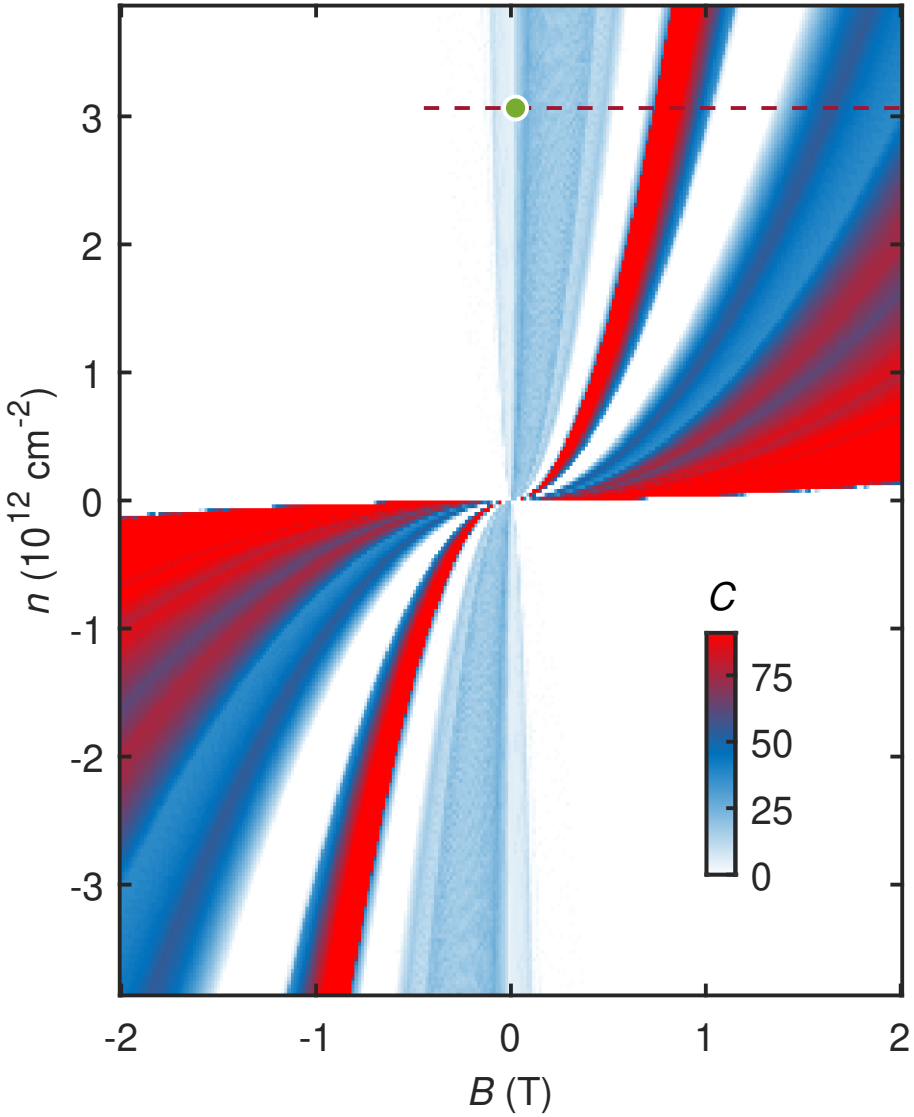

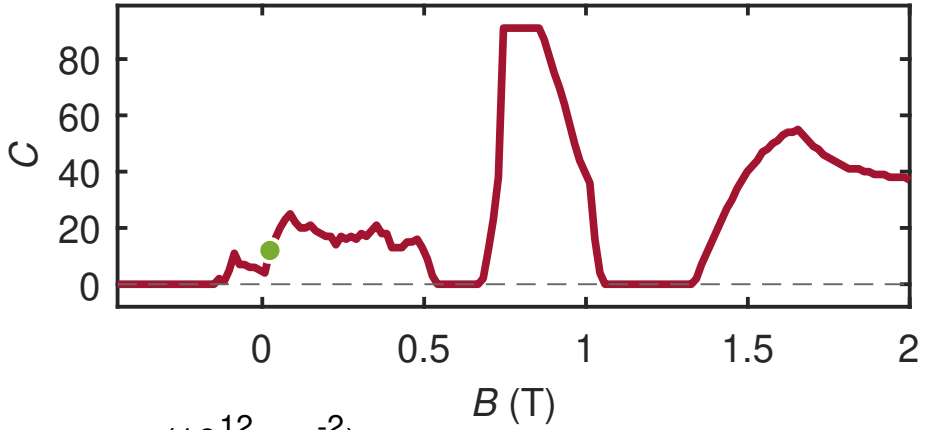

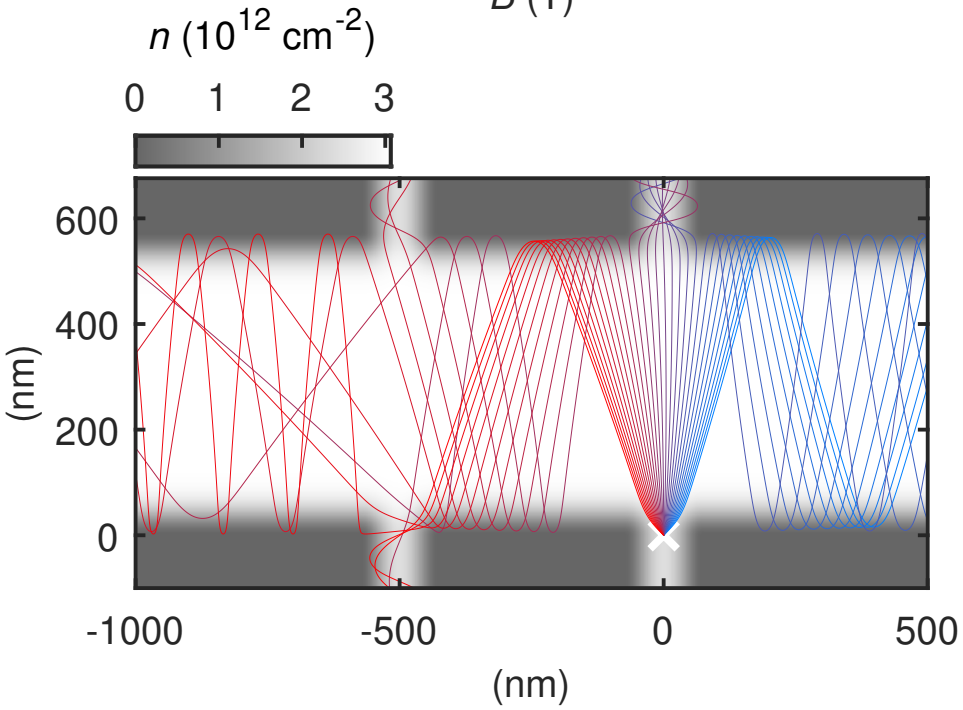

Semiclassical trajectory simulation for TMF

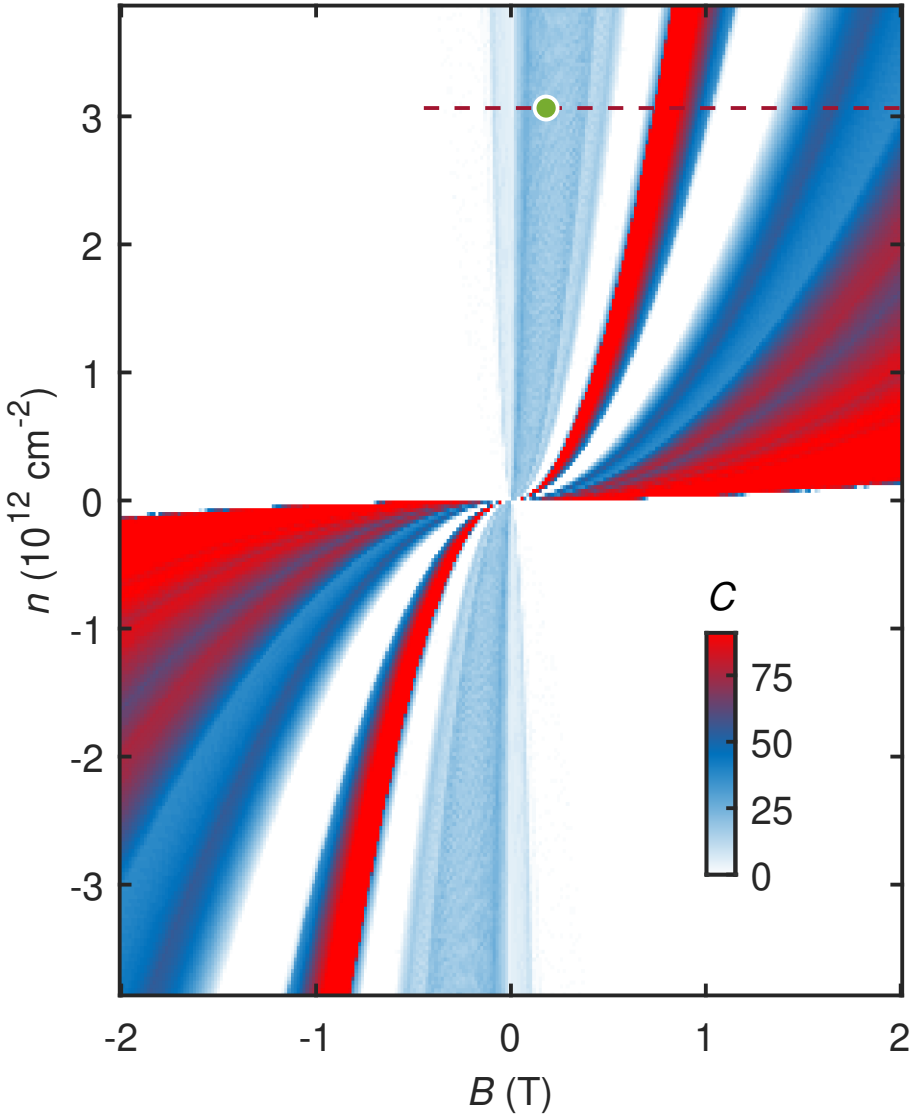

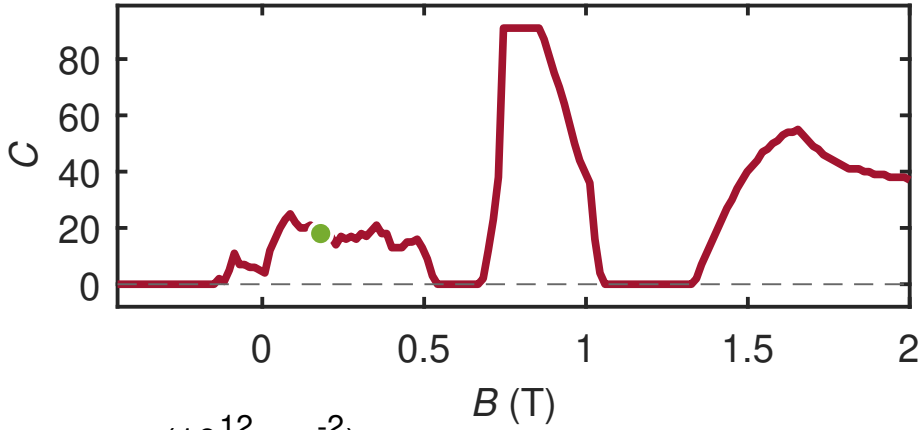

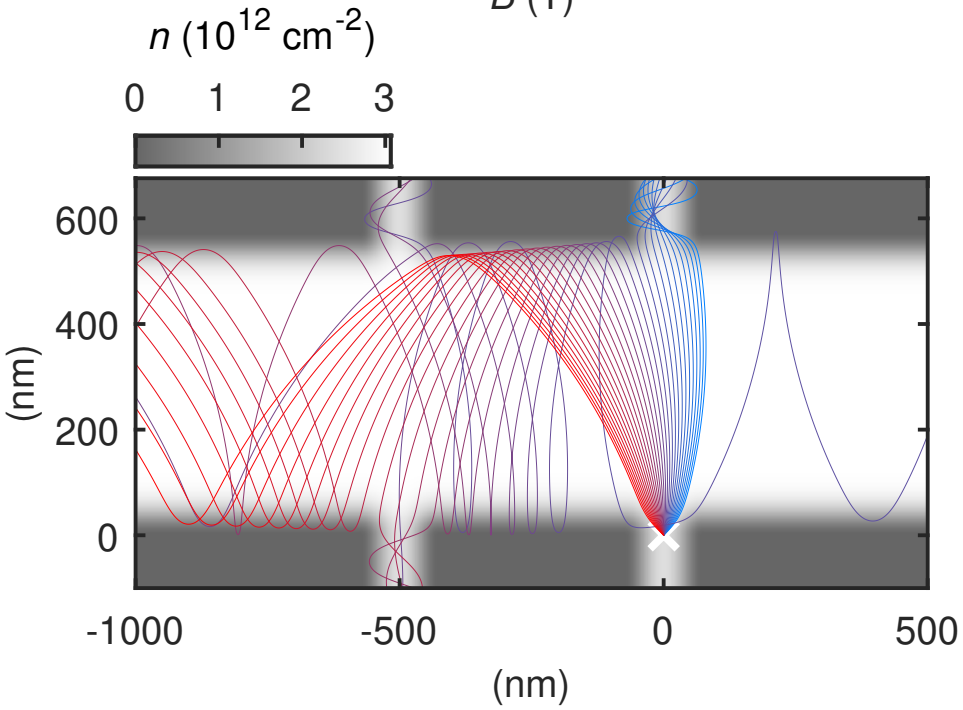

Semiclassical trajectory simulation for TMF

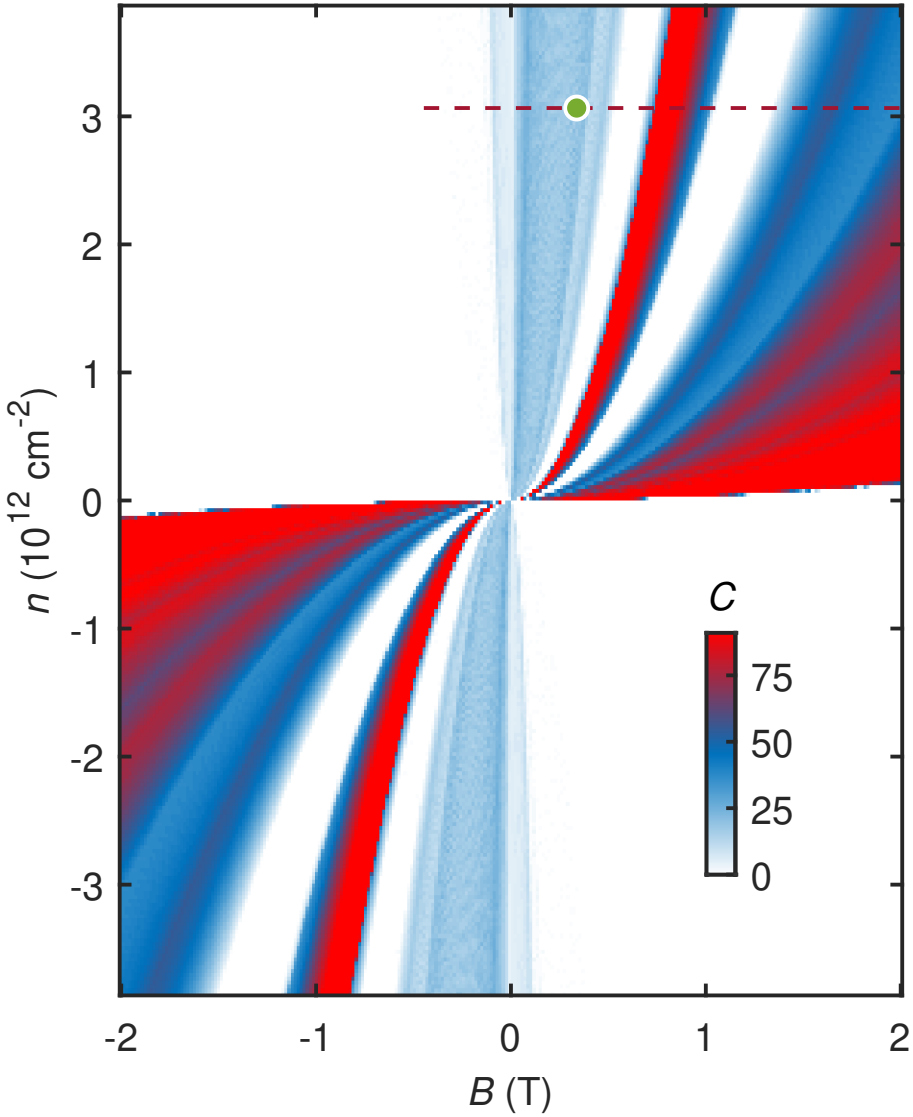

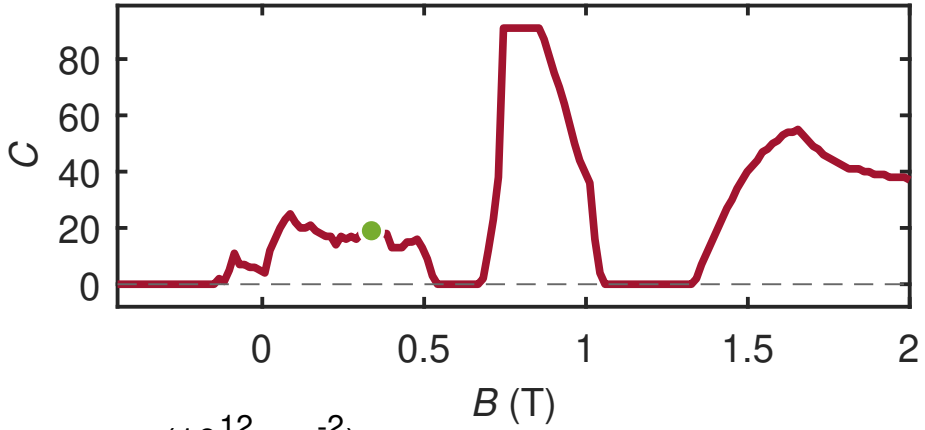

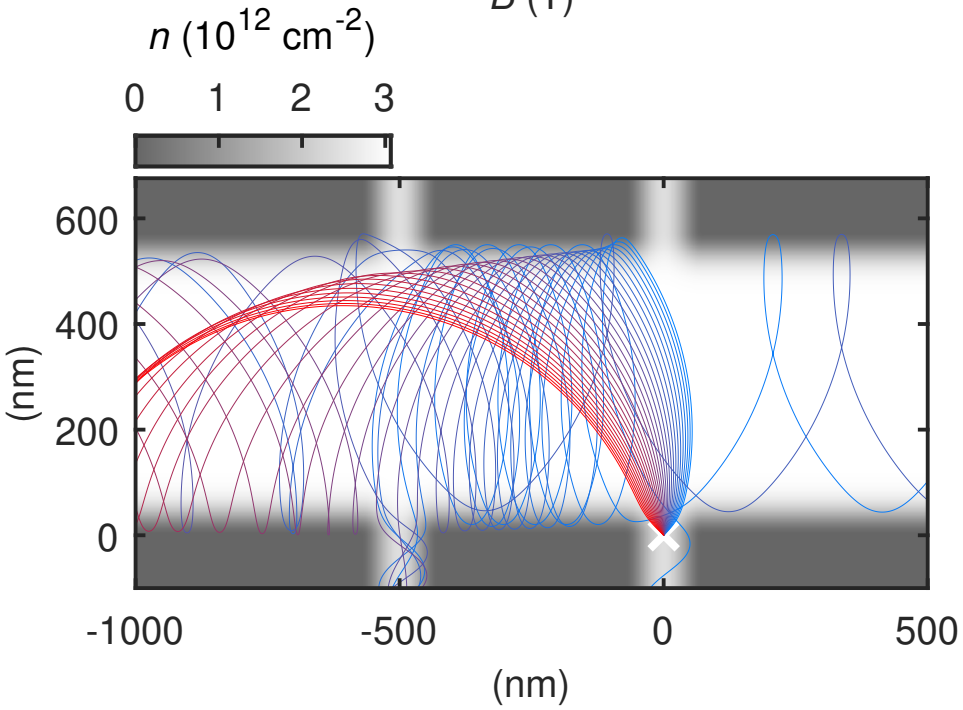

Semiclassical trajectory simulation for TMF

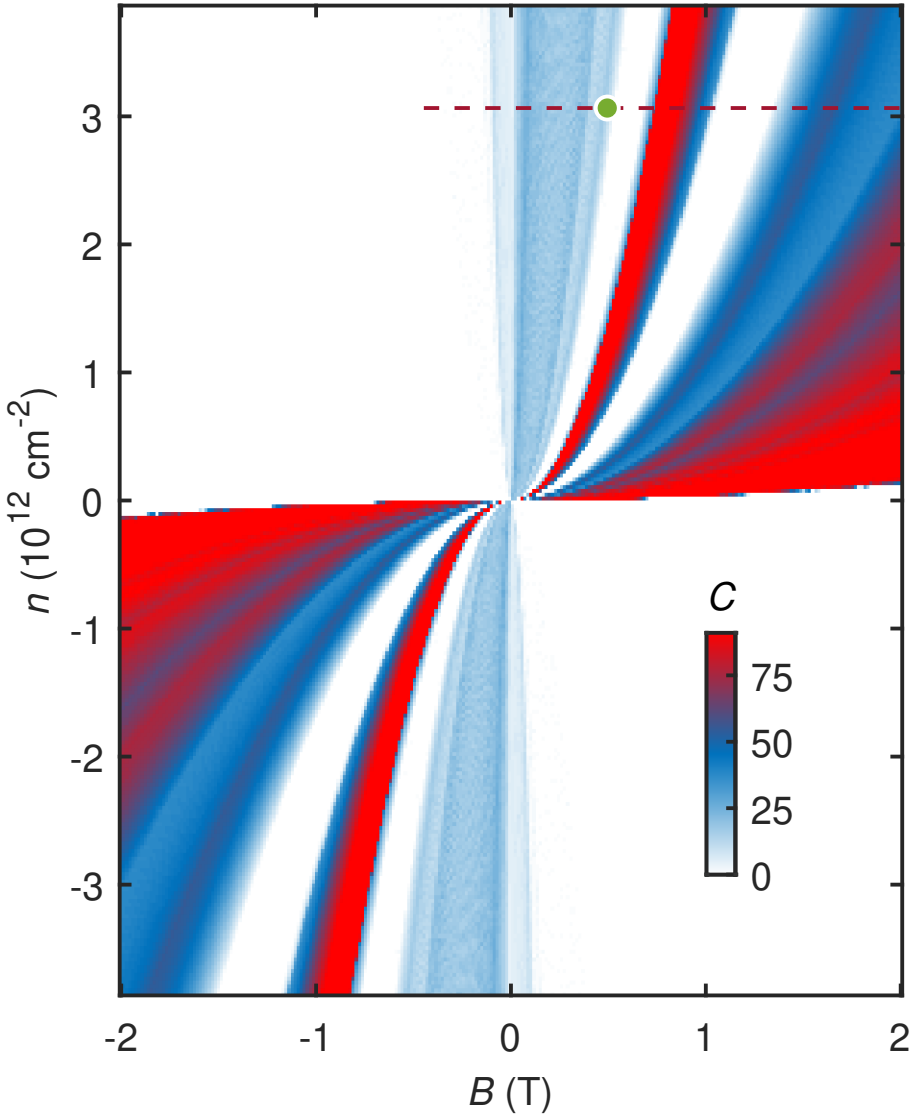

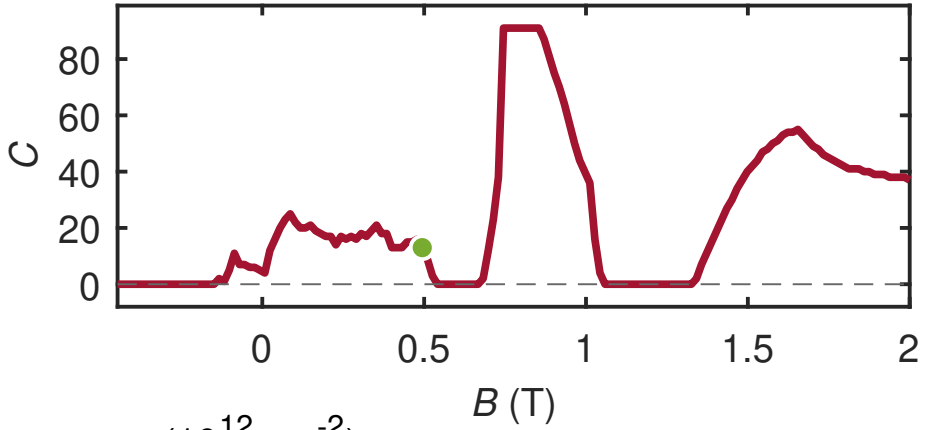

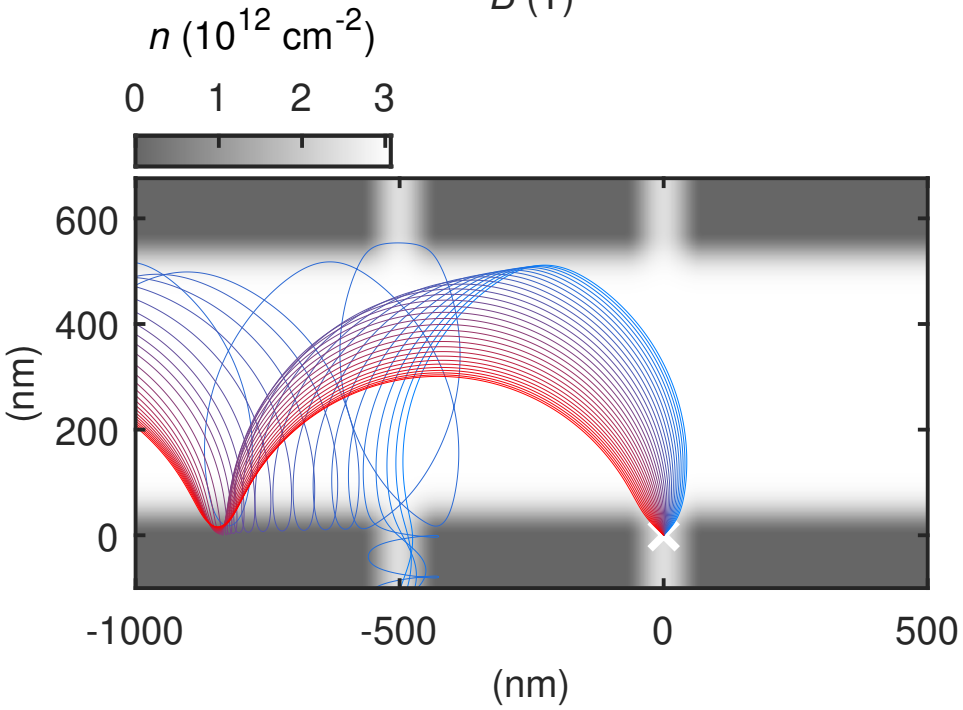

Semiclassical trajectory simulation for TMF

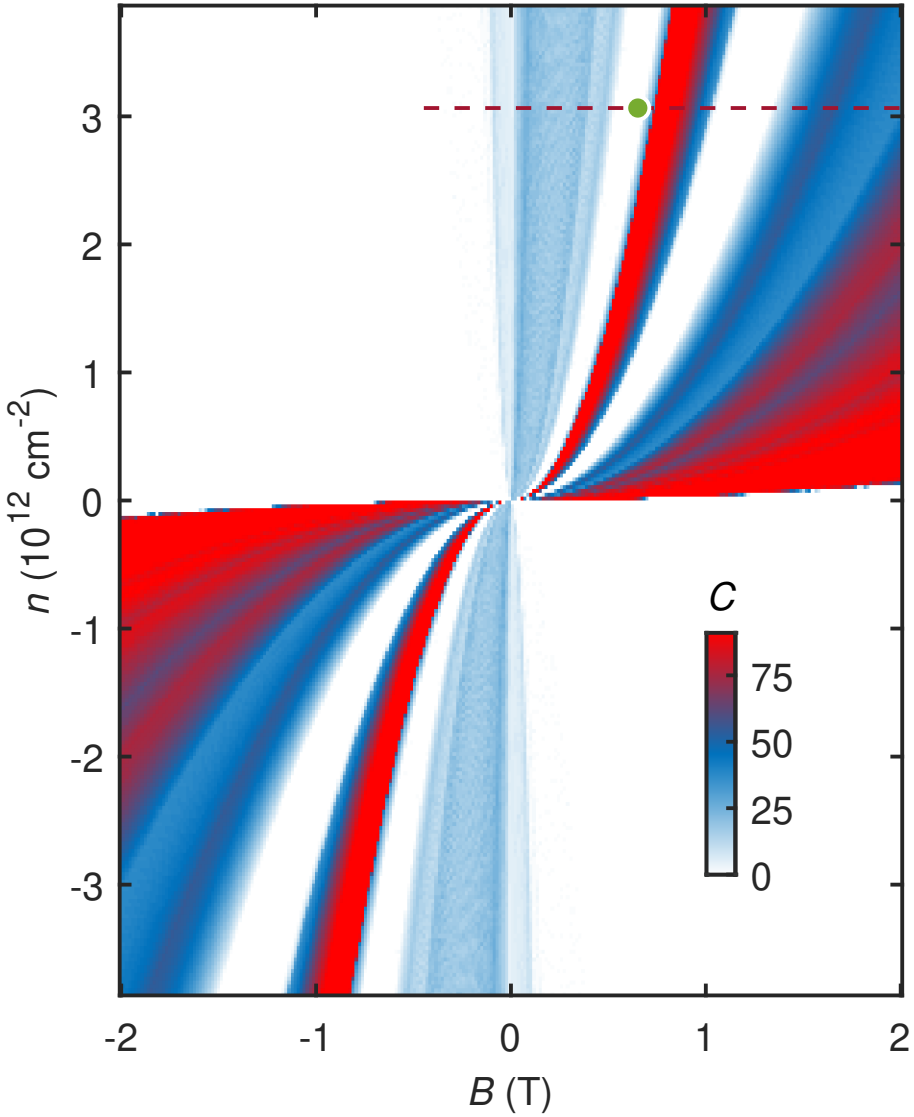

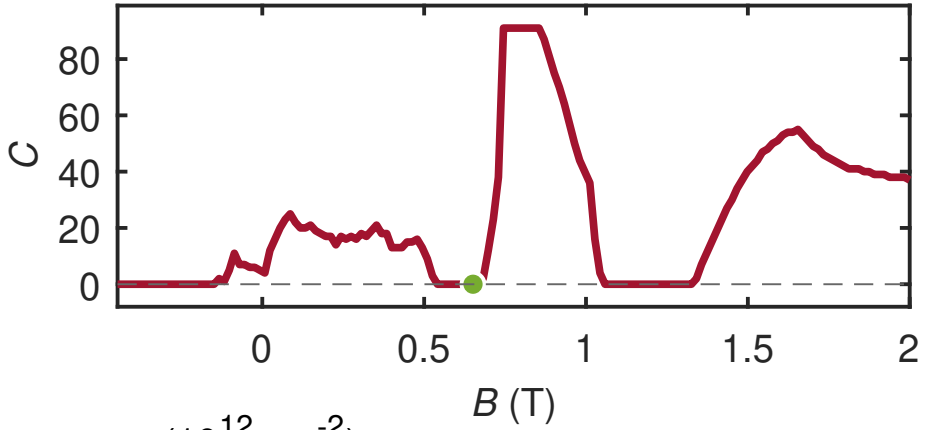

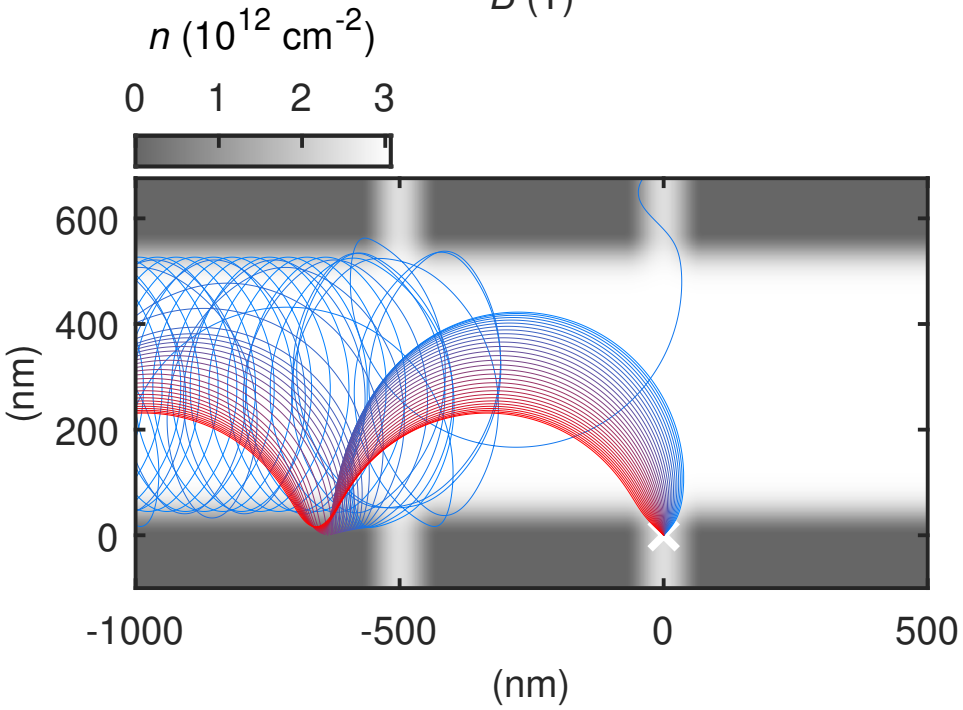

Semiclassical trajectory simulation for TMF

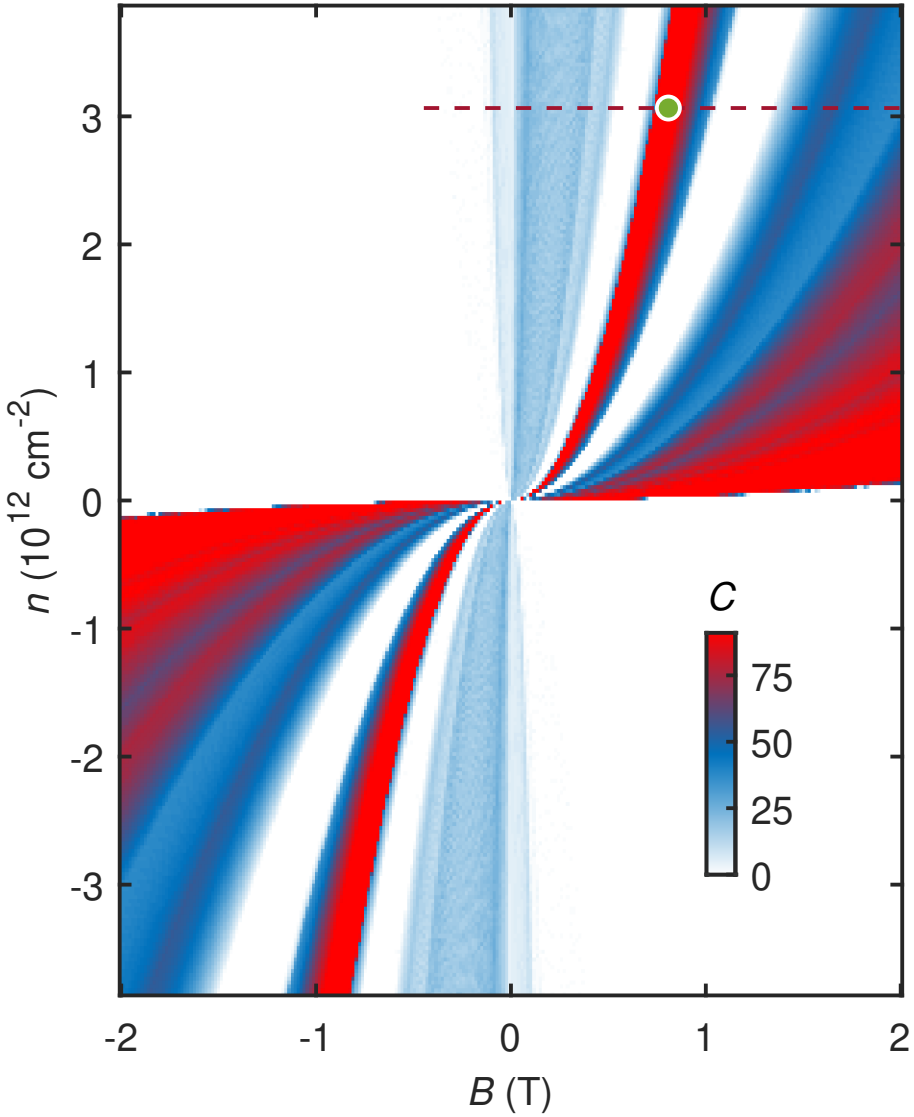

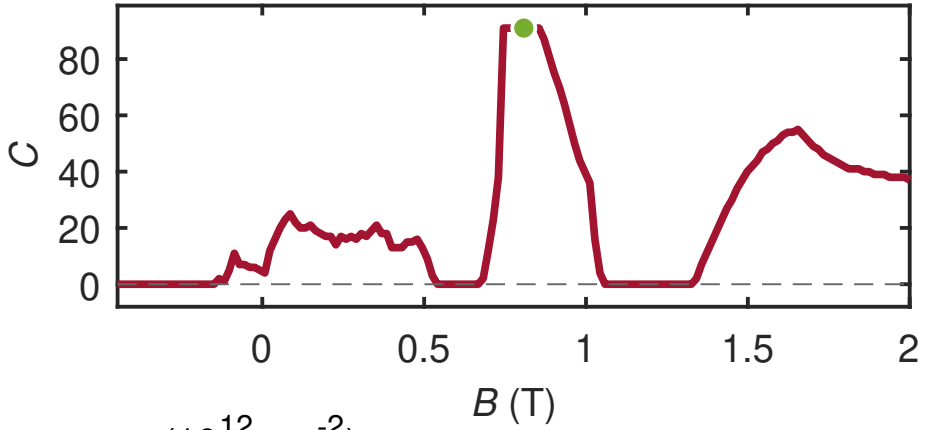

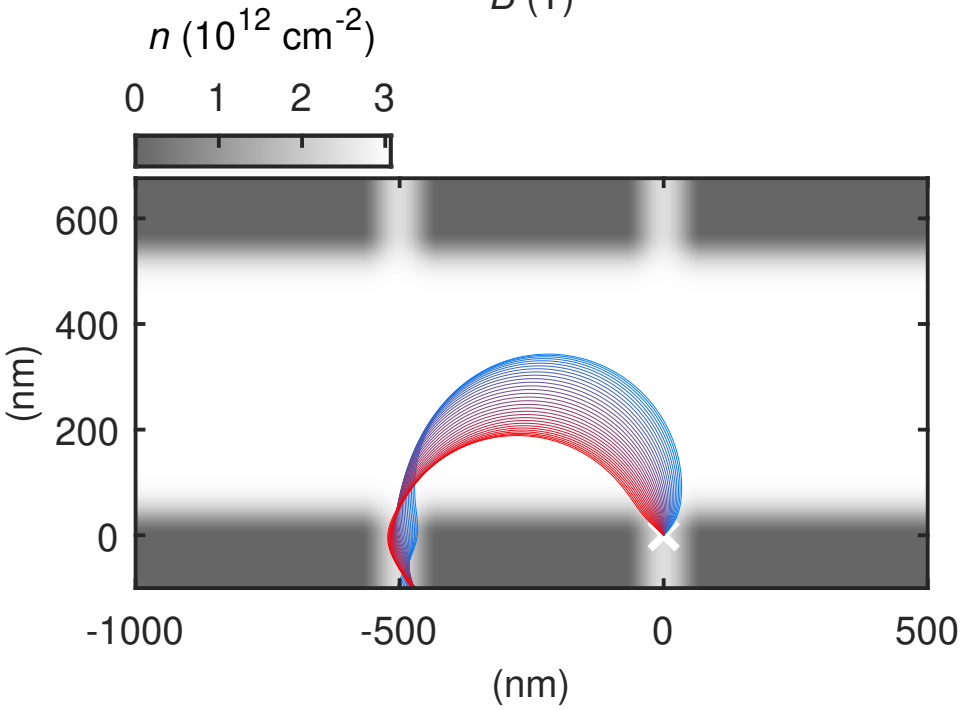

Semiclassical trajectory simulation for TMF

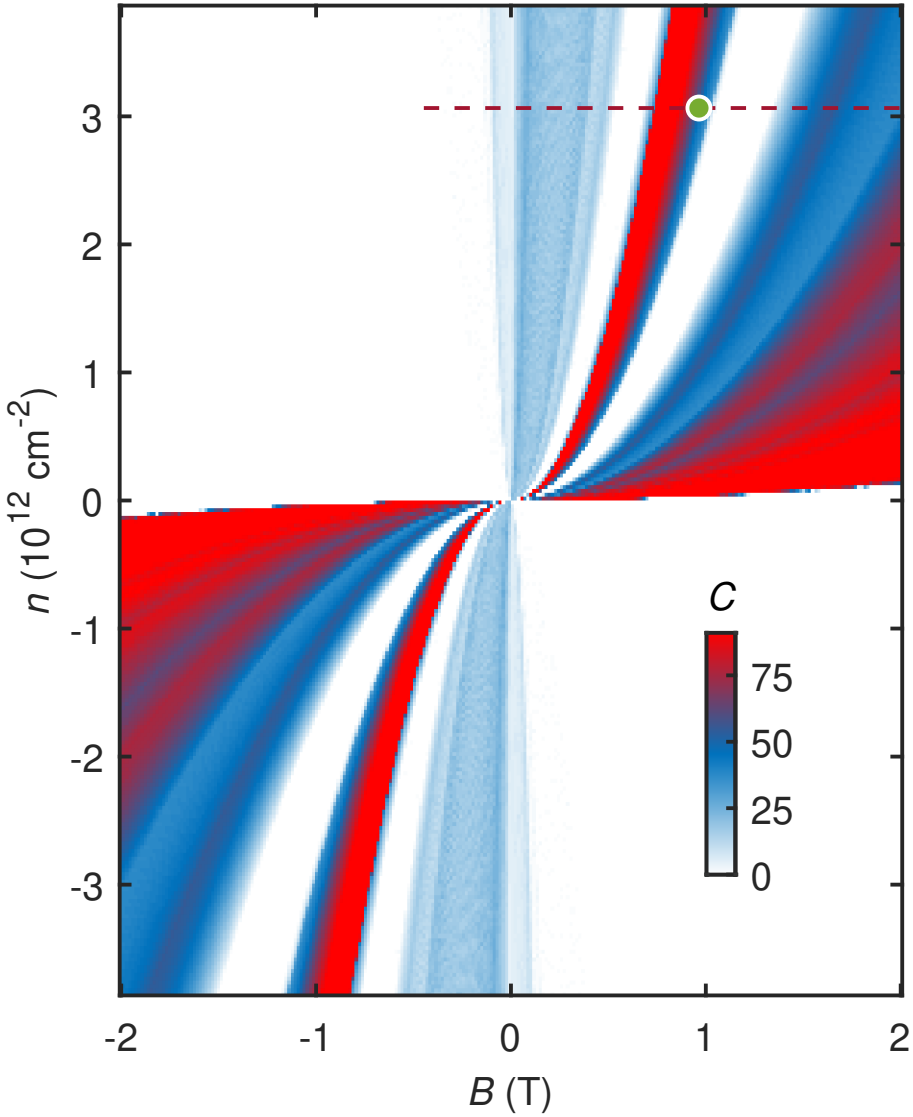

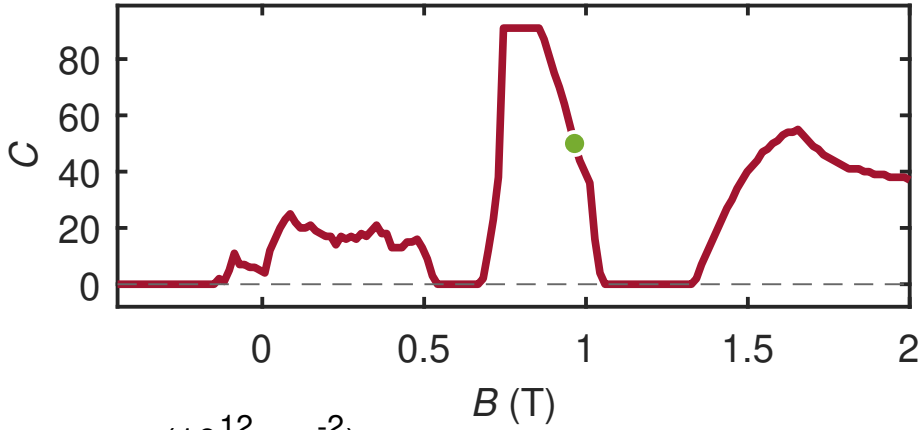

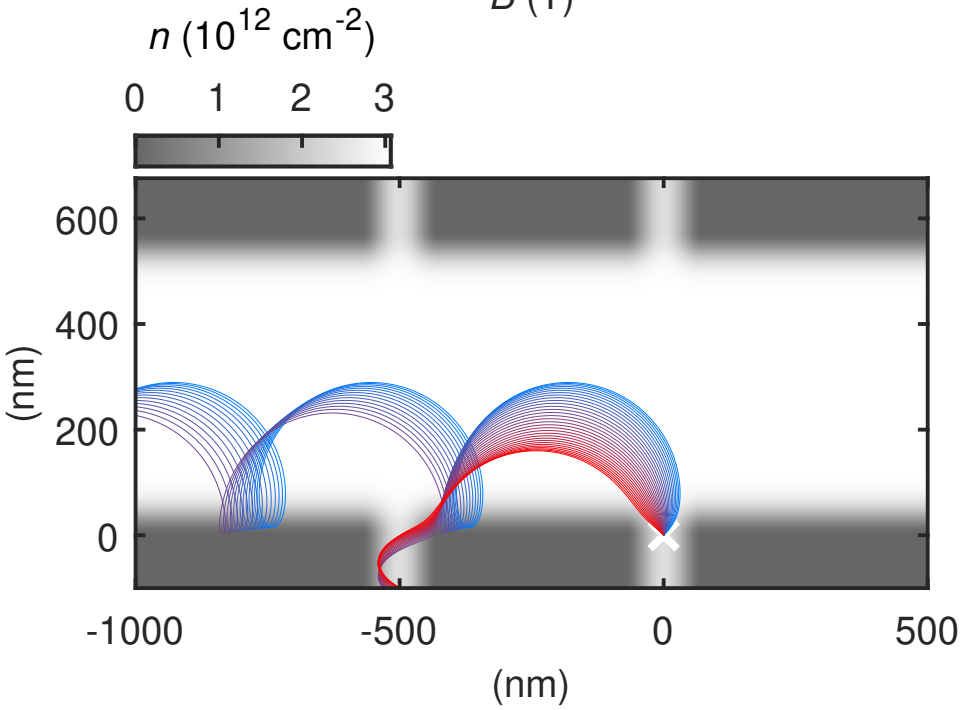

Semiclassical trajectory simulation for TMF

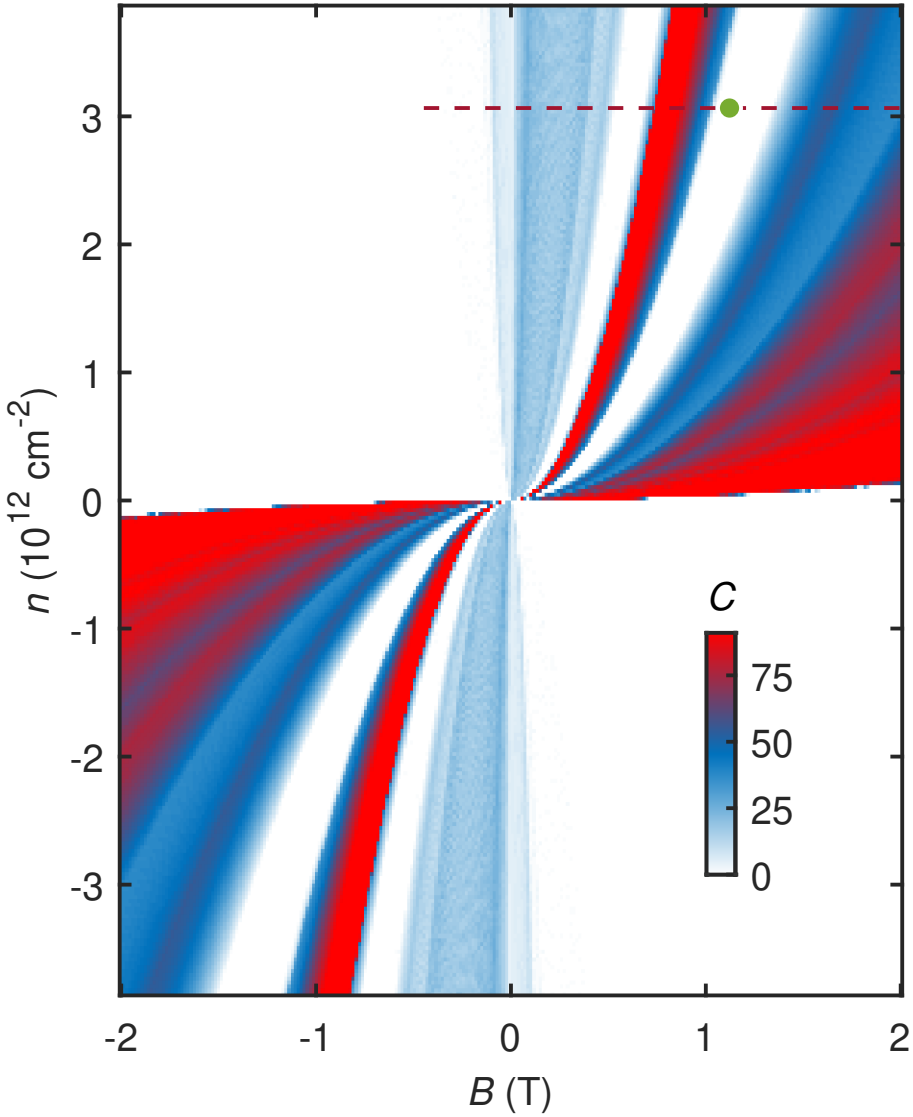

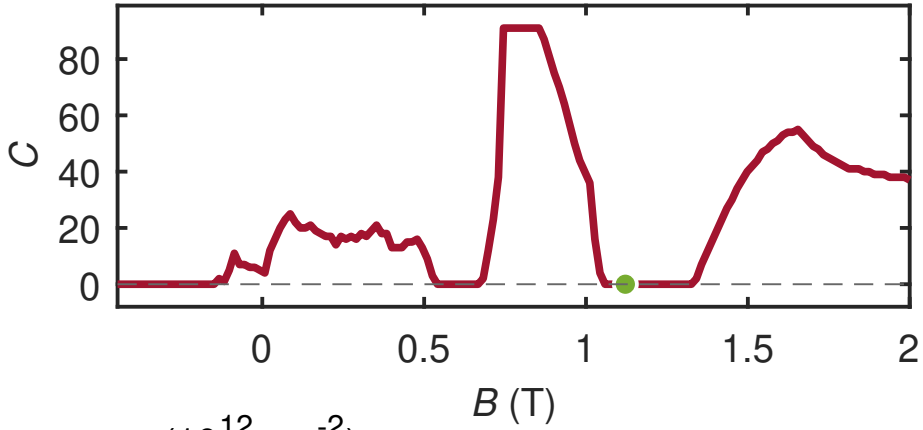

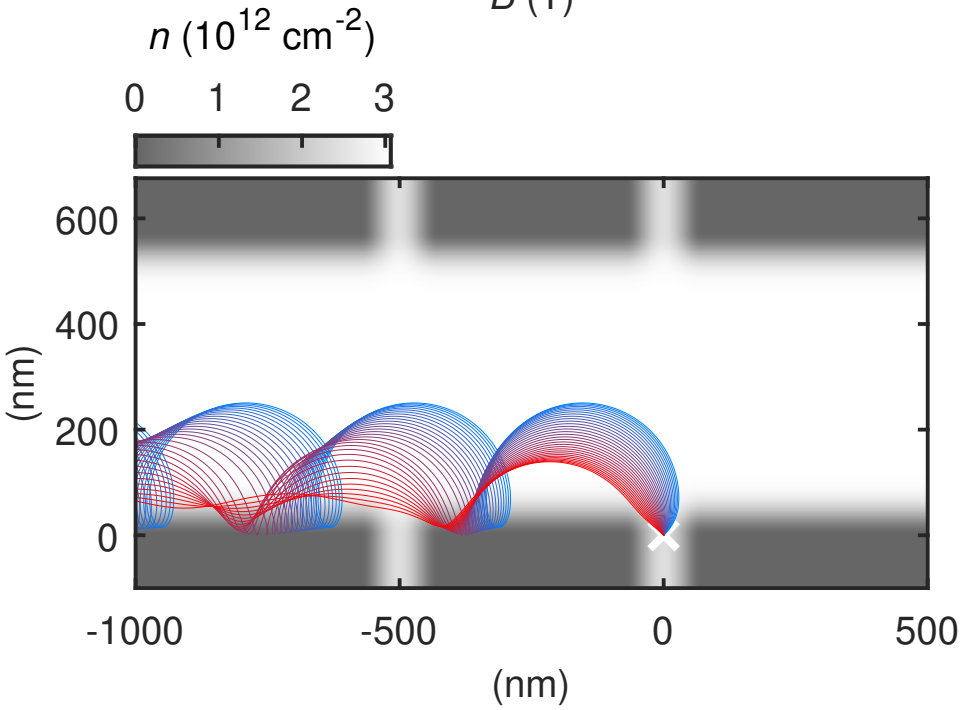

Semiclassical trajectory simulation for TMF

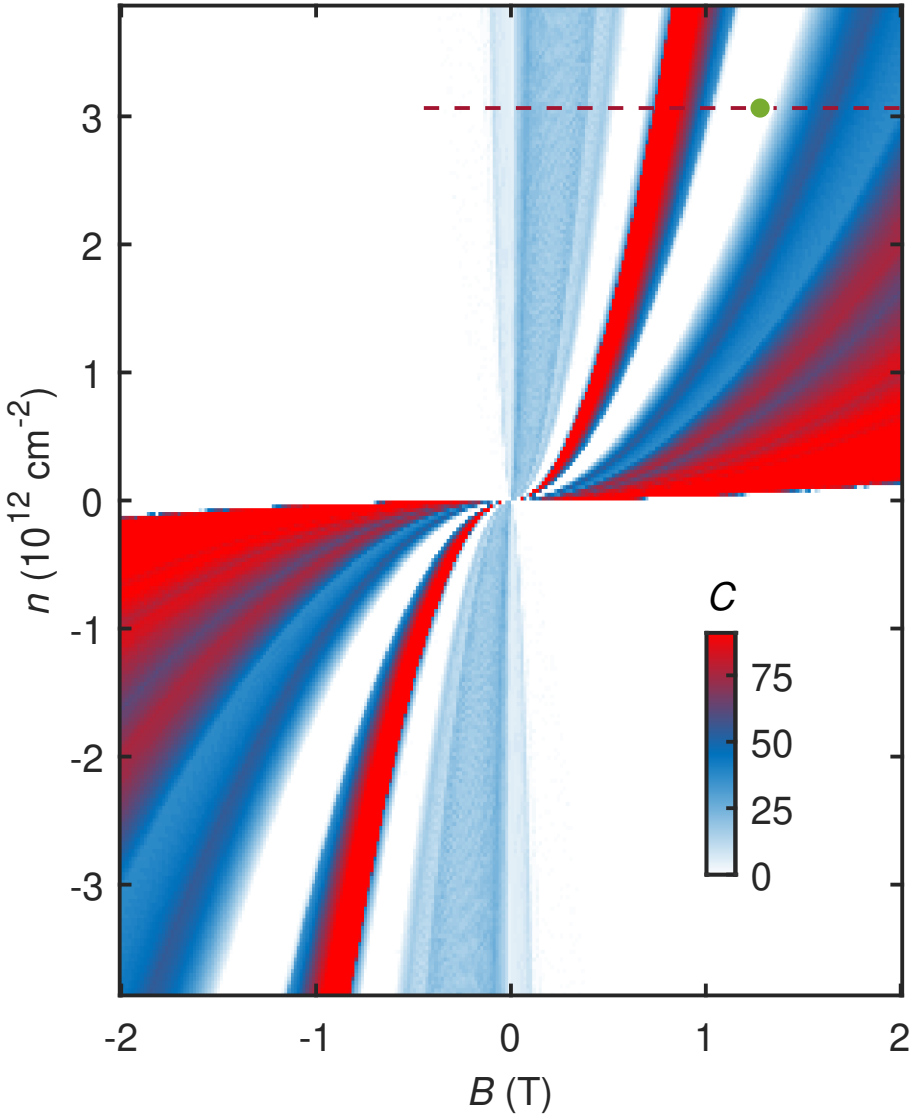

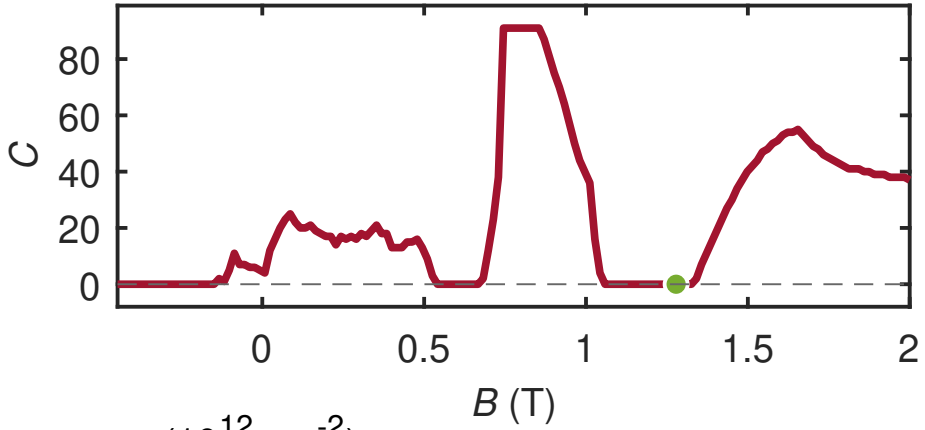

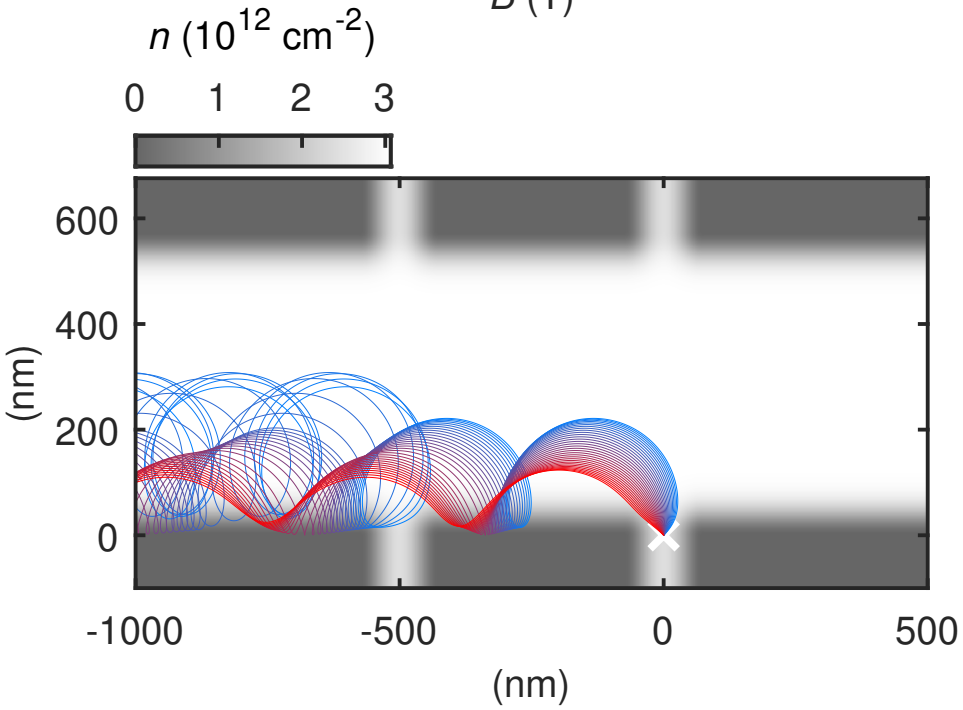

Semiclassical trajectory simulation for TMF

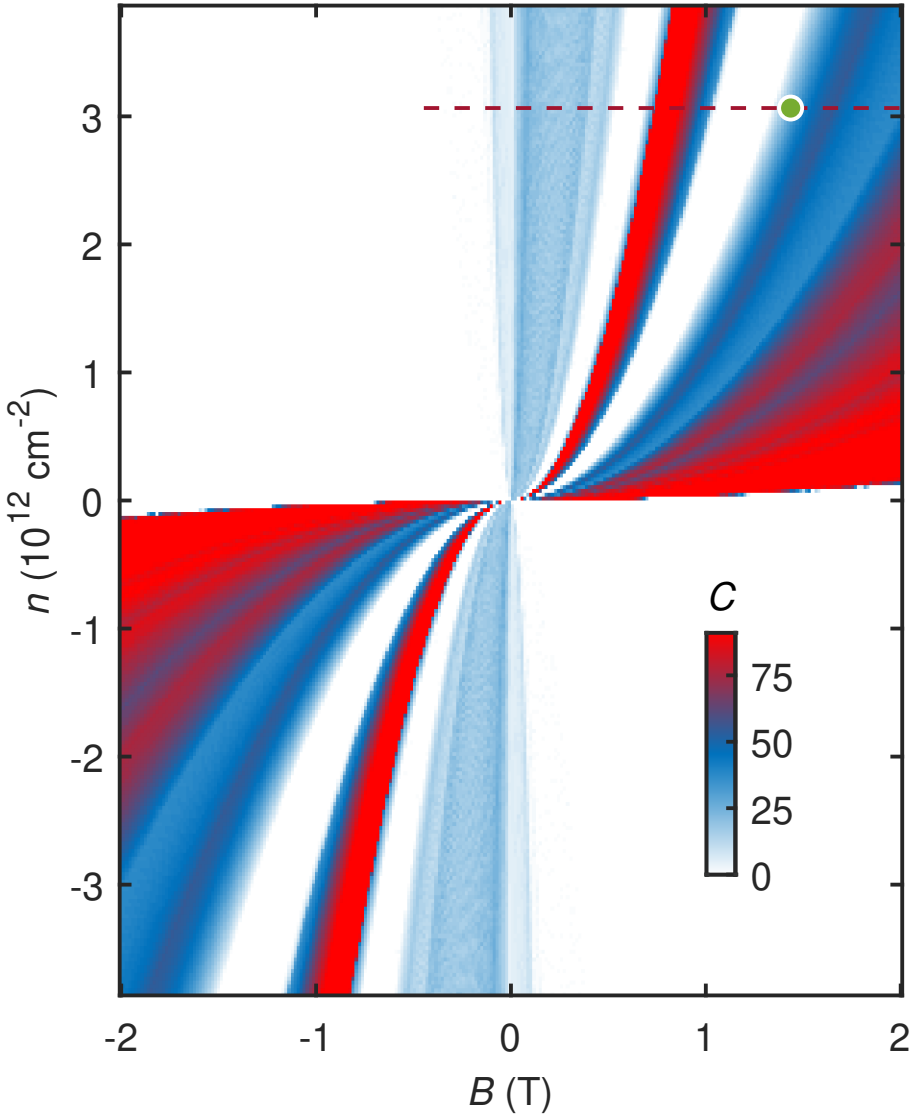

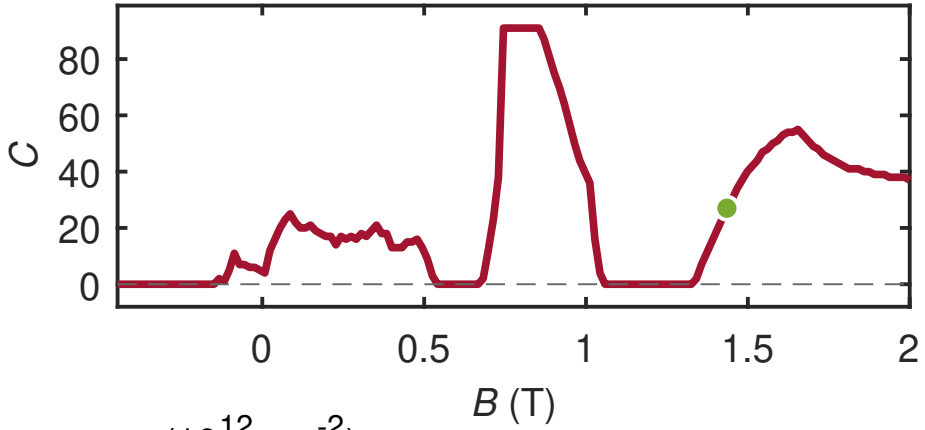

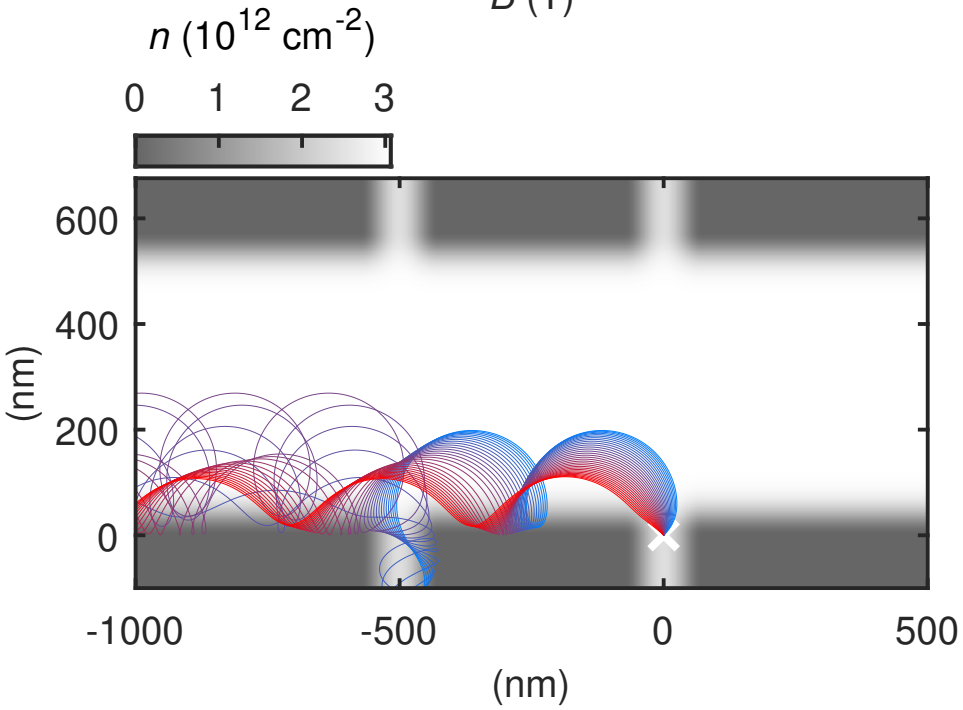

Semiclassical trajectory simulation for TMF

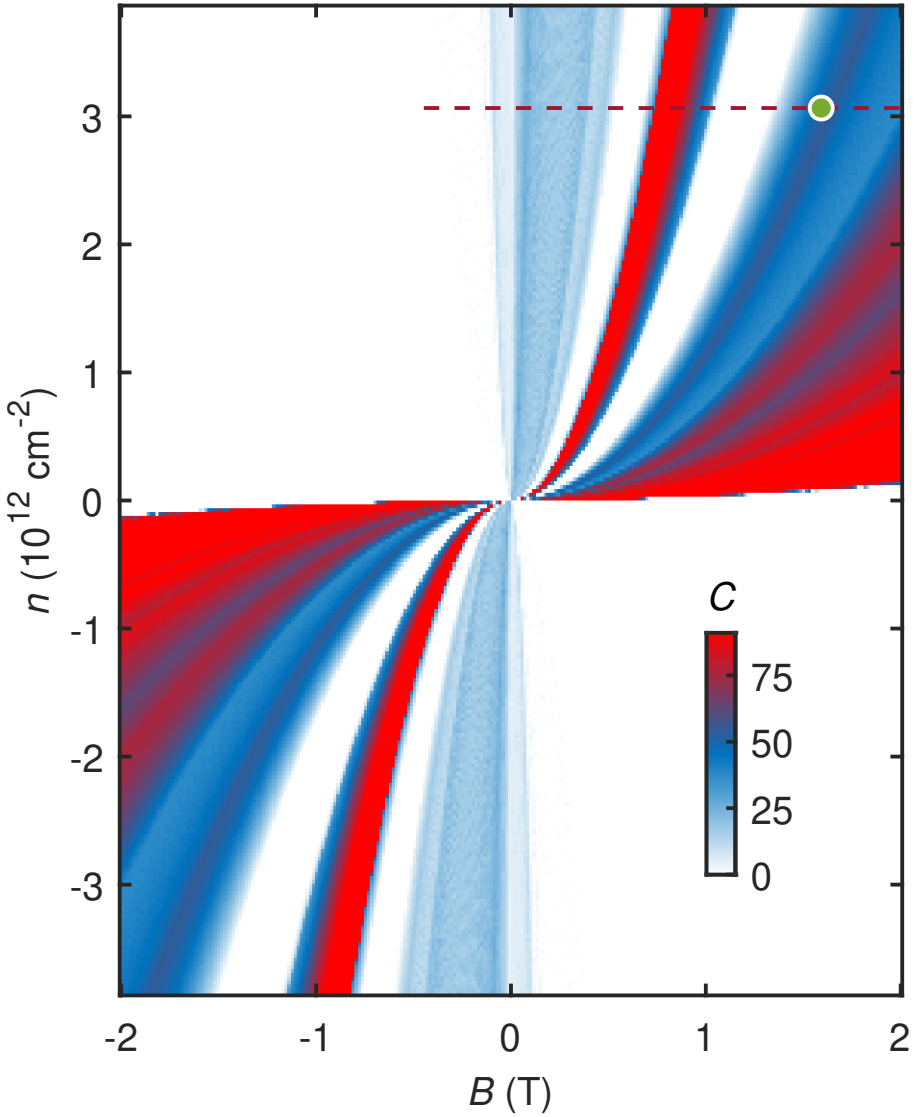

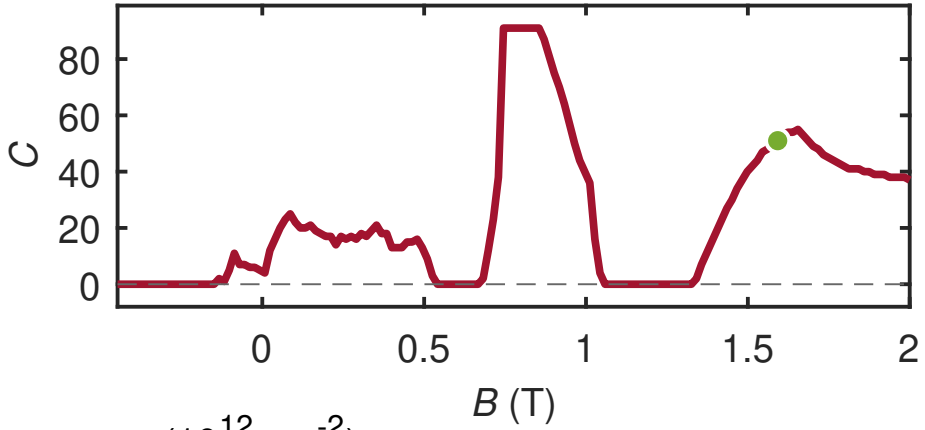

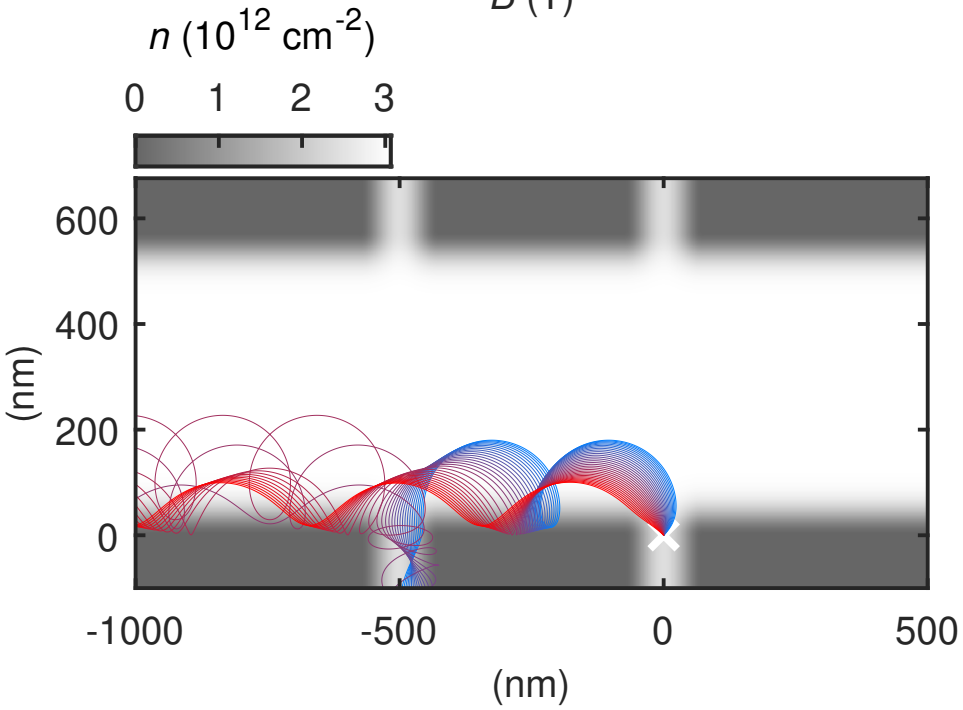

Semiclassical trajectory simulation for TMF

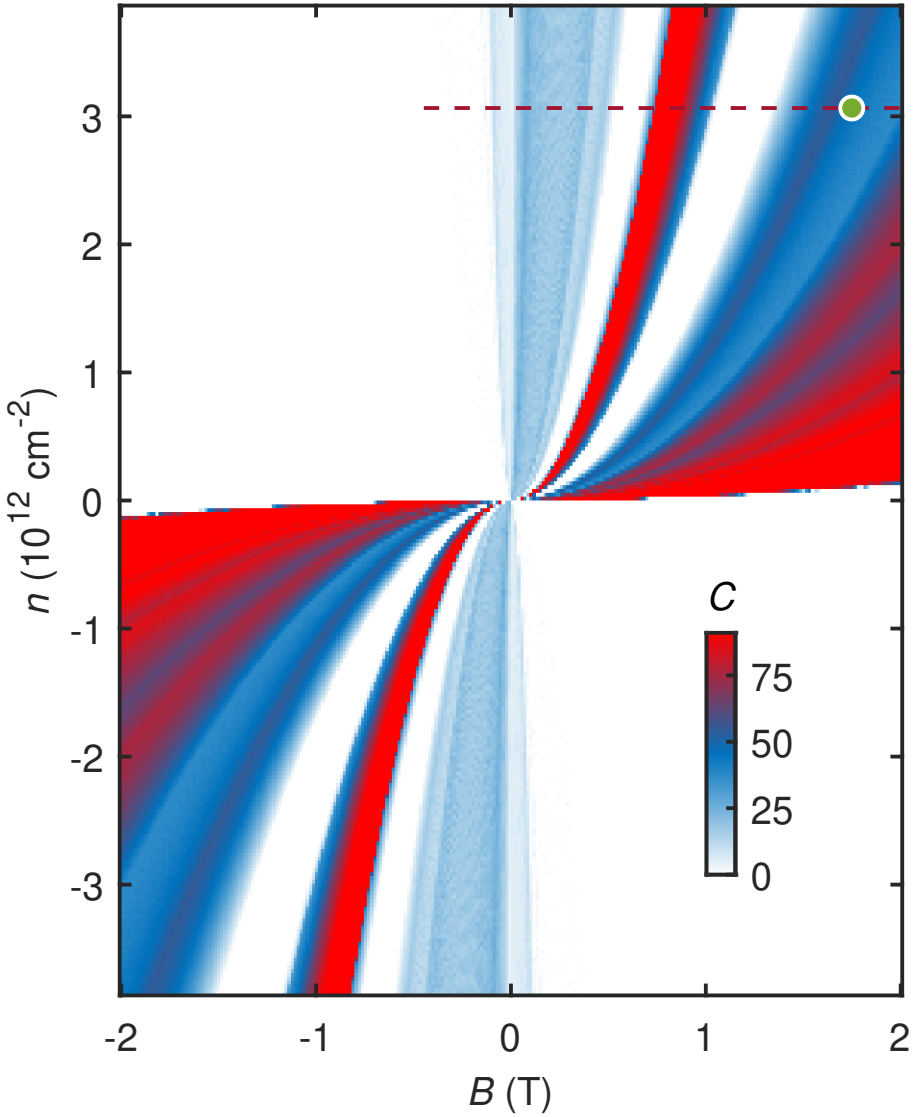

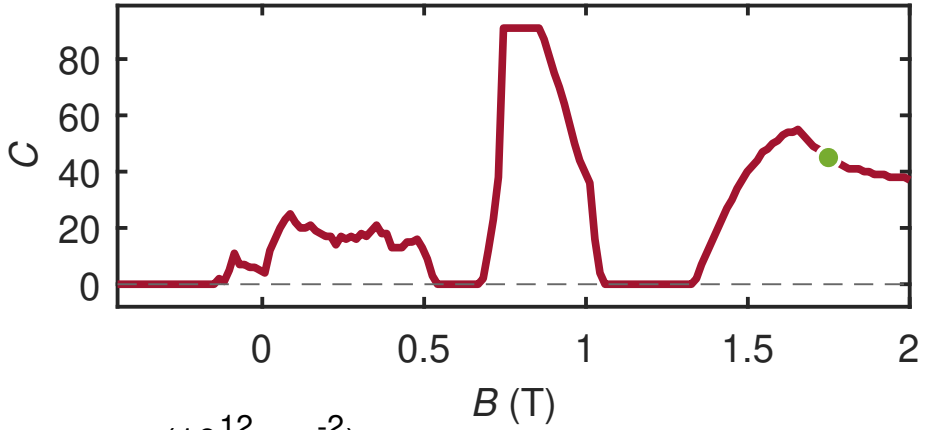

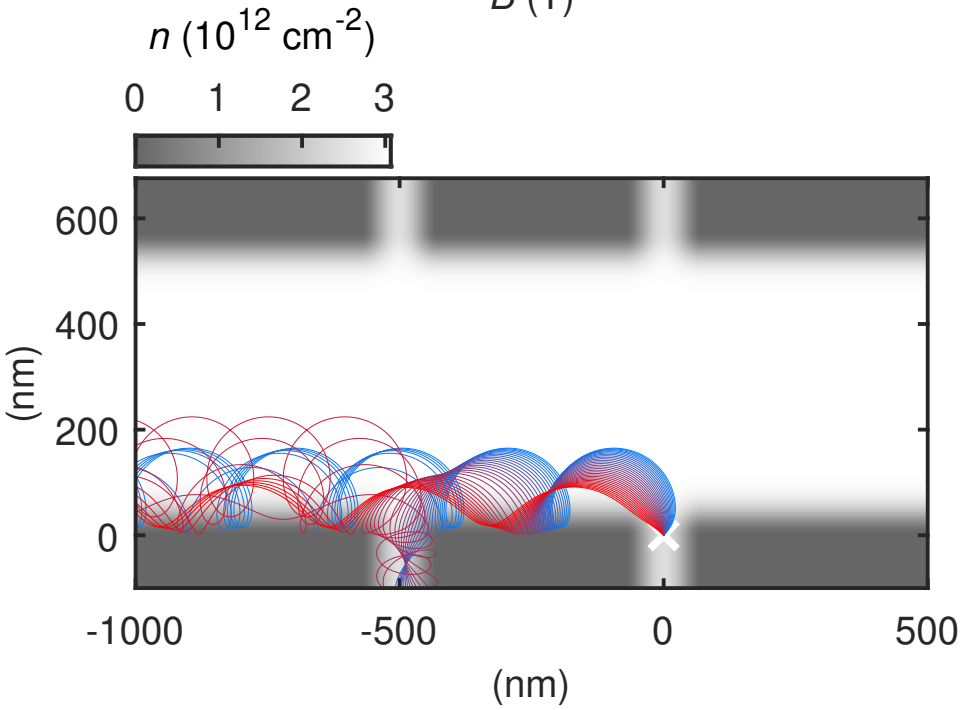

Quantum transport simulation for TMF

Mreńca-Kolasińska, A., Chen, S.-C., and Liu, M.-H., npj 2D Materials and Applications **7** (2023)
Article number: 64

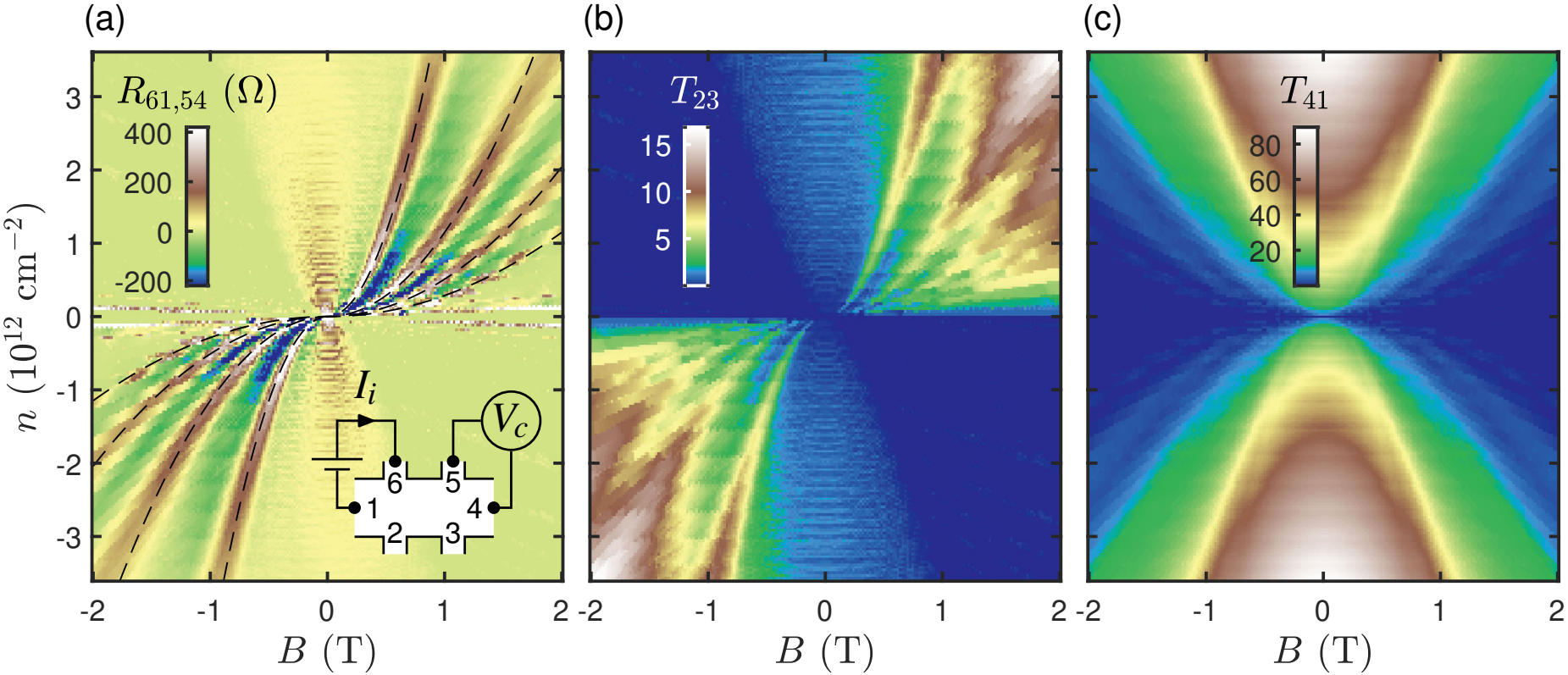

Quantum transport simulation for TMF

Mreńca-Kolasińska, A., Chen, S.-C., and Liu, M.-H., npj 2D Materials and Applications **7** (2023)
Article number: 64

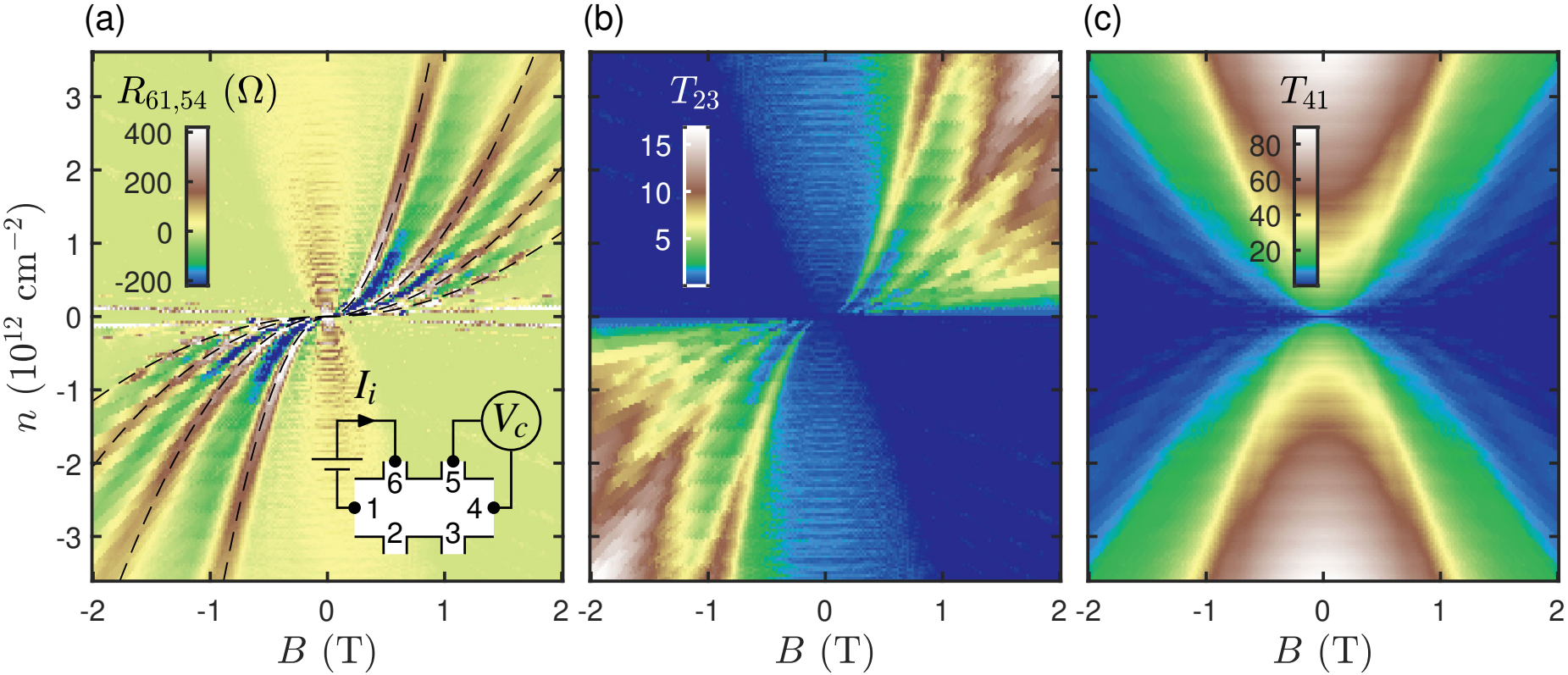

$6 \times 5 = 30$ transmission functions needed for $R_{61,54}$.

Spin-dependent TMF

Rao, Q. et al., Nature Communications **14** (2023)

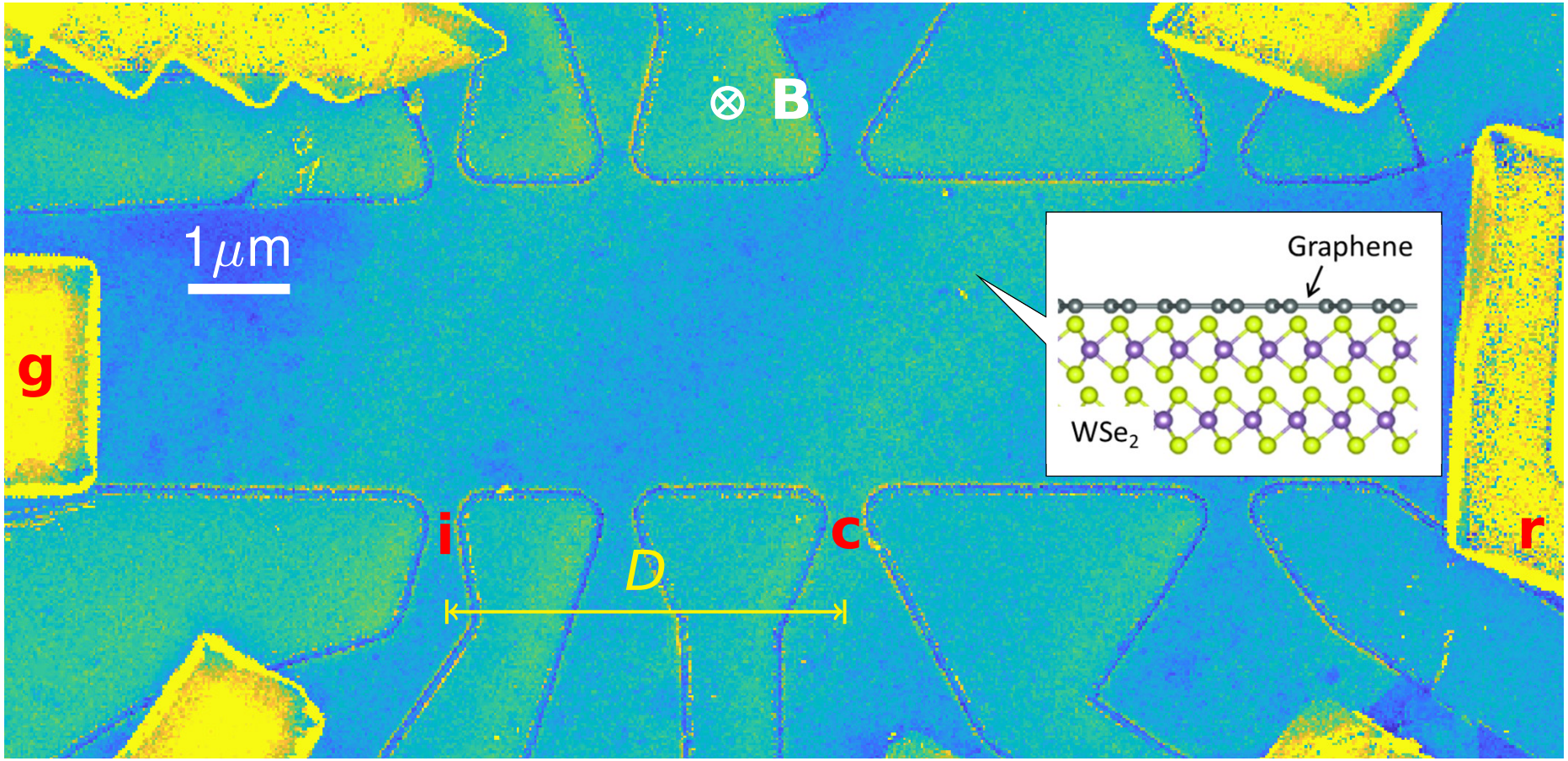

Spin-dependent TMF

Rao, Q. et al., Nature Communications **14** (2023)

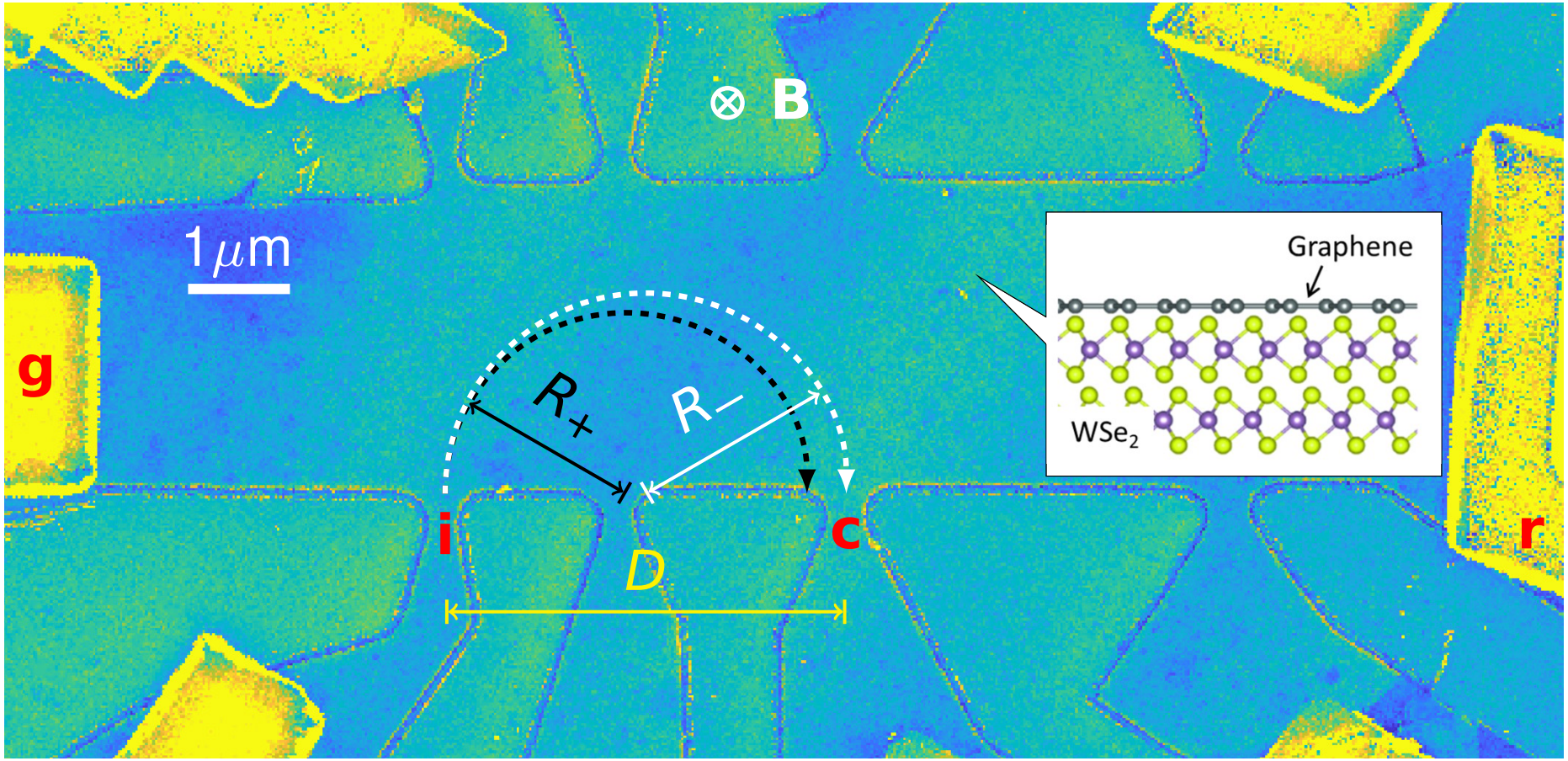

Spin-dependent TMF

Rao, Q. et al., Nature Communications **14** (2023)

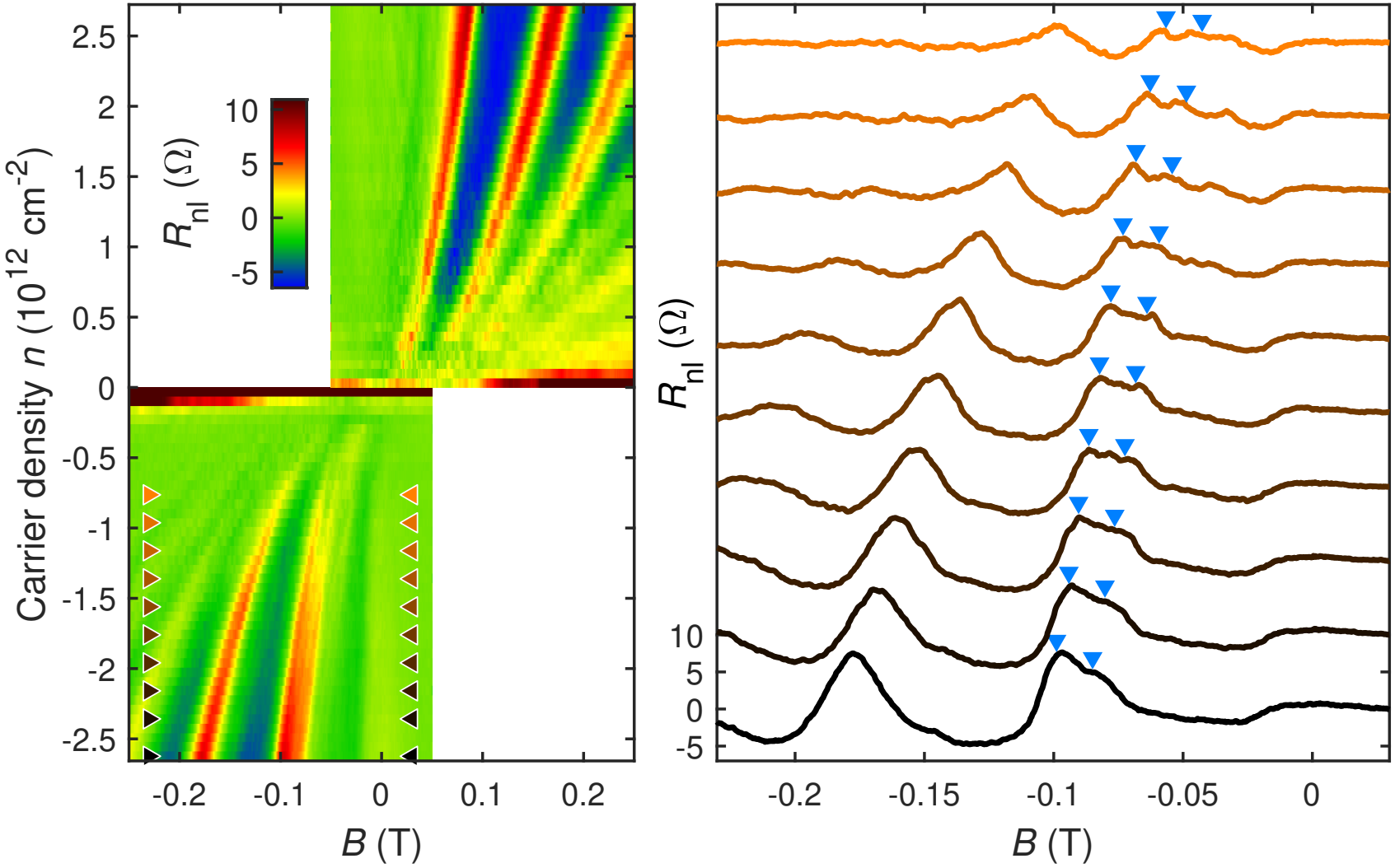

Proximity-induced SOC in graphene: Model[1]

$$\mathcal{H} = \sum_{\langle i,j\rangle,\sigma} t c^{\dagger}_{i\sigma} c_{j\sigma} \qquad \text{(nearest neighbor (nn) kinetic hopping)}$$

$$+ \sum_{i,\sigma} \xi_{o_i} \Delta c^{\dagger}_{i\sigma} c_{i\sigma} \qquad \text{(staggered onsite energy)}$$

$$+ \frac{2i}{3} \sum_{\langle i,j\rangle} \sum_{\sigma,\sigma'} c^{\dagger}_{i\sigma} c_{j\sigma} \left[\lambda_R \left(\hat{\mathbf{s}} \times \hat{\mathbf{d}}_{ij} \right)_z \right]_{\sigma\sigma'} \qquad \text{(nn Rashba hopping)}$$

$$+ \frac{i}{3\sqrt{3}} \sum_{\langle\langle i,j\rangle\rangle} \sum_{\sigma,\sigma'} c^{\dagger}_{i\sigma} c_{j\sigma} \left[\lambda_I^{o_i} \nu_{ij} \hat{s}_z \right]_{\sigma\sigma'} \qquad \text{(second nn valley-Zeeman hopping)}$$

$$+ \mathcal{H}_{\mathrm{PIA}} \qquad \text{(unimportant for low energy)}$$

[1] Gmitra, M., Kochan, D., Högl, P., and Fabian, J., Phys. Rev. B **93** (2016) 155104

Low-energy bands of graphene on TMDC

- By:
  - Dropping PIA term
  - Setting $\lambda_I^A = -\lambda_I^B = \lambda$ for simplicity

  the low-energy dispersion is given by:

$$E_{\mu,\nu}(k) = \mu\sqrt{\left(\Delta^2 + \lambda^2 + 2\lambda_R^2 + \hbar^2 v_F^2 k^2\right) + 2\nu\sqrt{\left(\lambda_R^2 - \lambda\Delta\right)^2 + \left(\lambda^2 + \lambda_R^2\right)\hbar^2 v_F^2 k^2}}$$

$$\mu, \nu = \pm 1$$

- Δ will also be put to zero for simplicity
- Consistent with Zubair, M., Vasilopoulos, P., and Tahir, M., Phys. Rev. B **101** (2020)
- Following the literature:

$$\lambda \equiv \lambda_{\rm so} \cos\theta_{\rm so} \qquad \text{(valley-Zeeman)}$$

$$\lambda_R \equiv \lambda_{\rm so} \sin\theta_{\rm so} \qquad \text{(Rashba)}$$

Low-energy bands of graphene on TMDC (cont.)

- Examples:

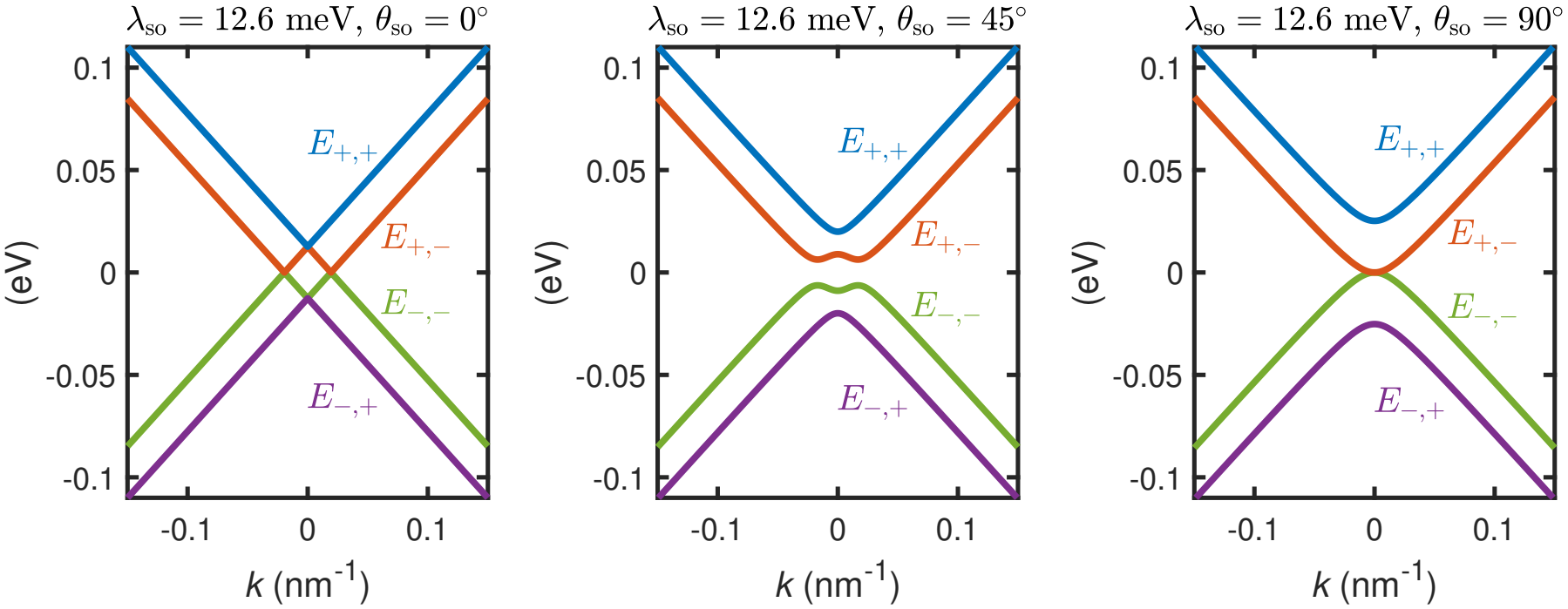

purely valley Zeeman | equal strengths | purely Rashba

Quantum transport simulations

Rao, Q. et al., Nature Communications **14** (2023)

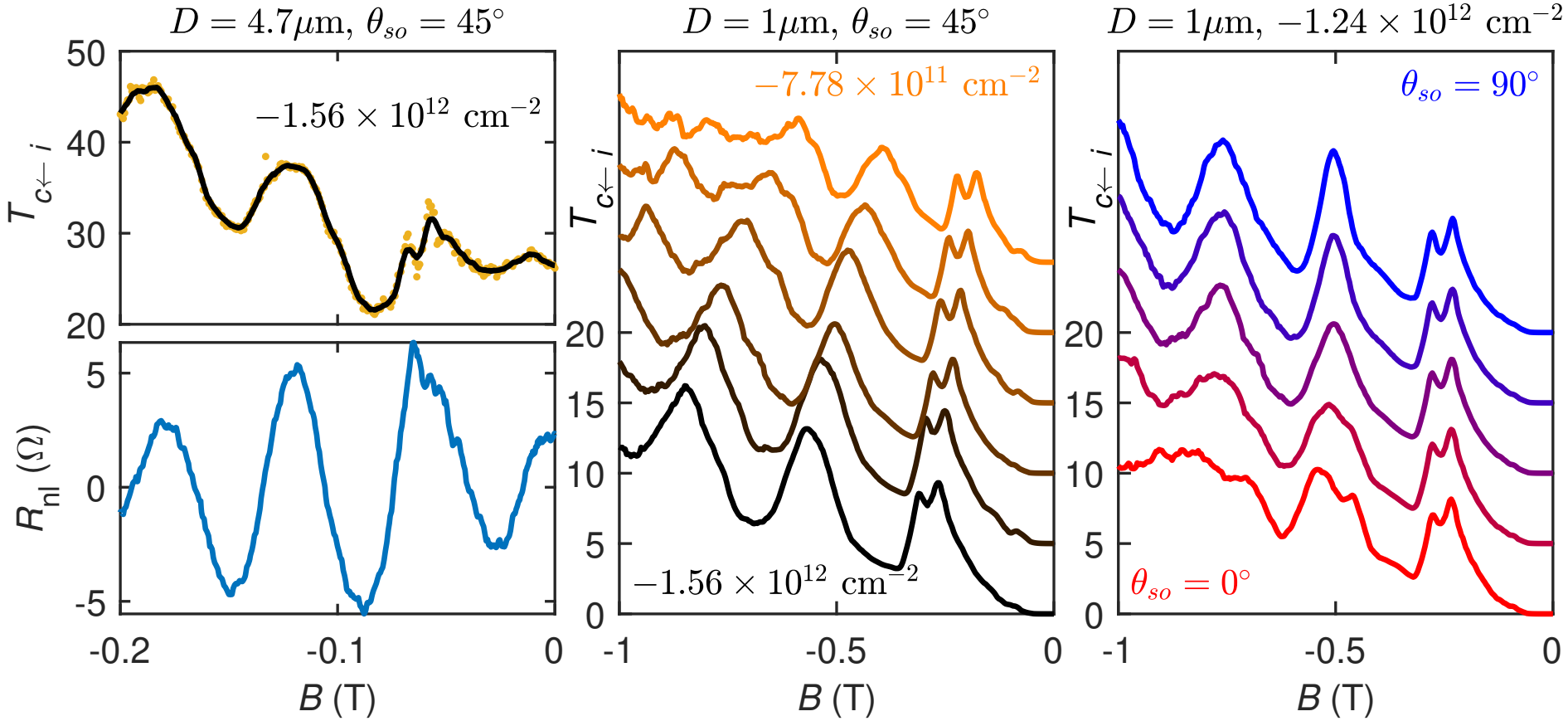

- Even though scaled, still too heavy!
- Smaller device simulated instead, but similar features obtained.

Why second peaks don't split?

For purely Rashba:

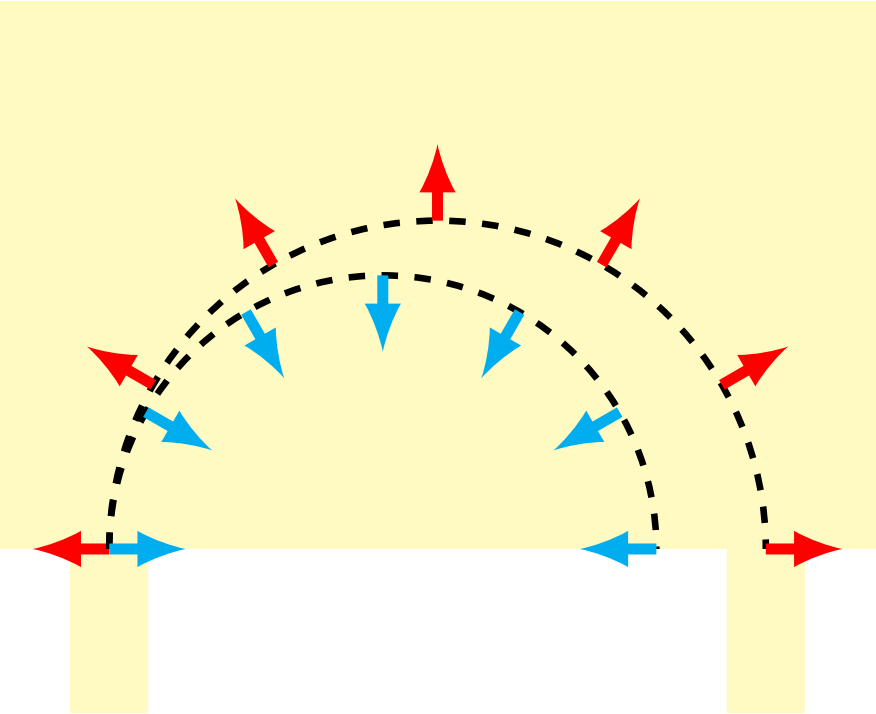

First peak

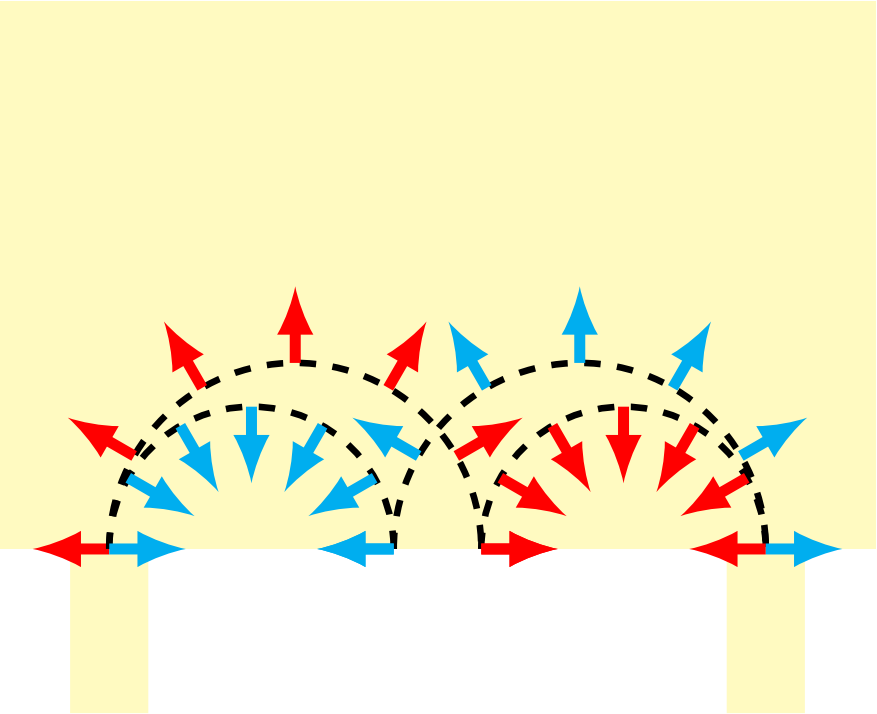

Second peak

Why second peaks don't split?

For purely Rashba:

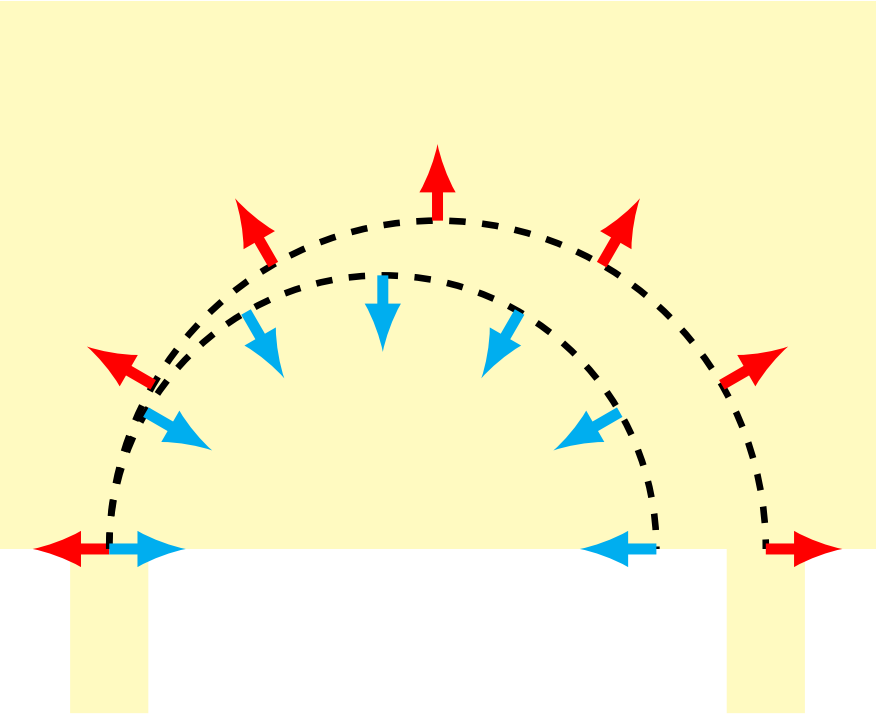

First peak

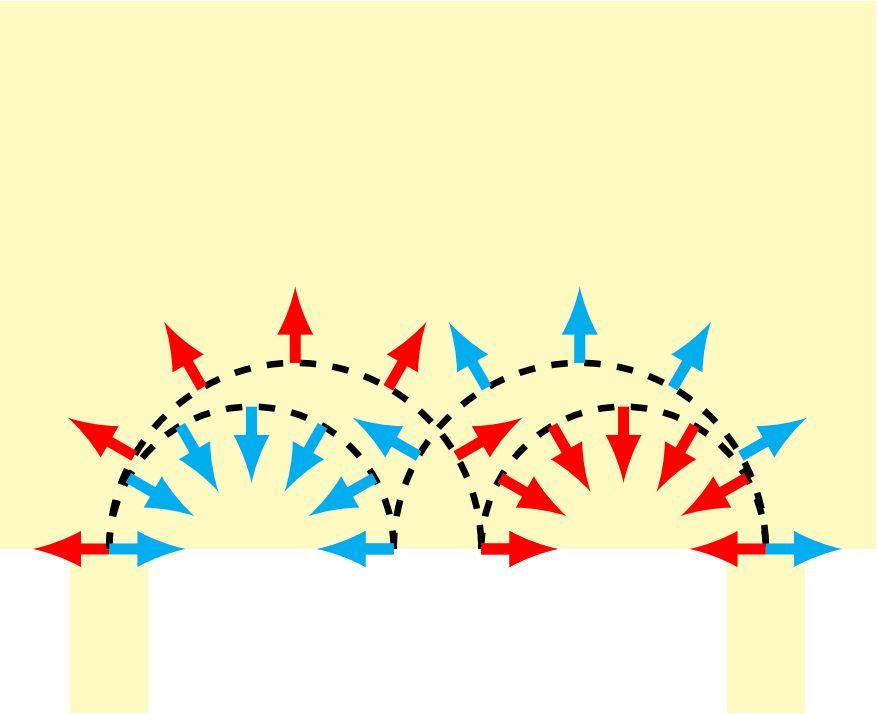

Second peak

- For valley Zeeman, staying in the same circle allowed.
- Therefore, Rashba SOC could be dominating.

Graphene/hBN moiré pattern

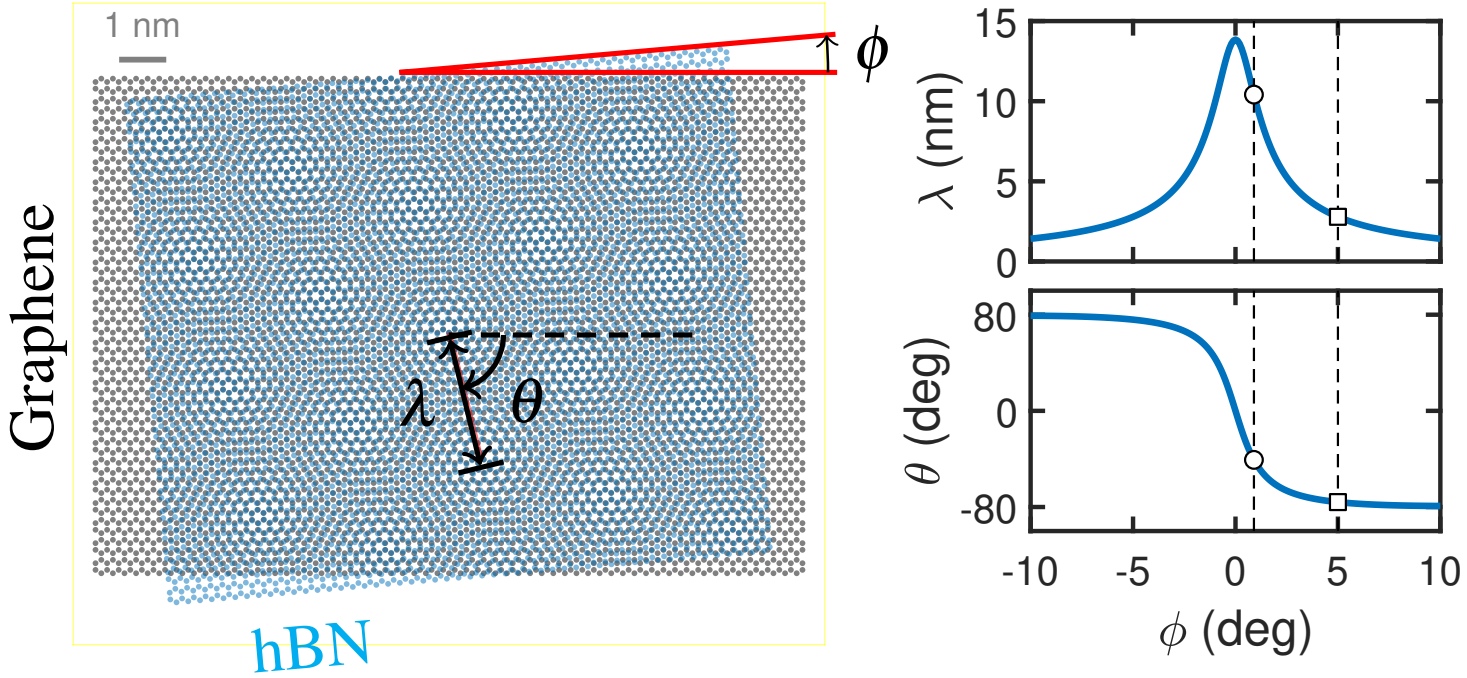

$$\lambda = \frac{1+\epsilon}{\sqrt{\epsilon^2 + 2(1+\epsilon)(1-\cos\phi)}}\, a\,, \qquad \theta = \arctan\frac{-\sin\phi}{1+\epsilon-\cos\phi}$$

$\epsilon \approx 1.81\%$ (lattice mismatch)

Yankowitz, M. et al., Nat. Phys. **8** (2012) 382; Moon, P. and Koshino, M., Phys. Rev. B **90** (2014) 155406

Graphene/hBN moiré model superlattice potential

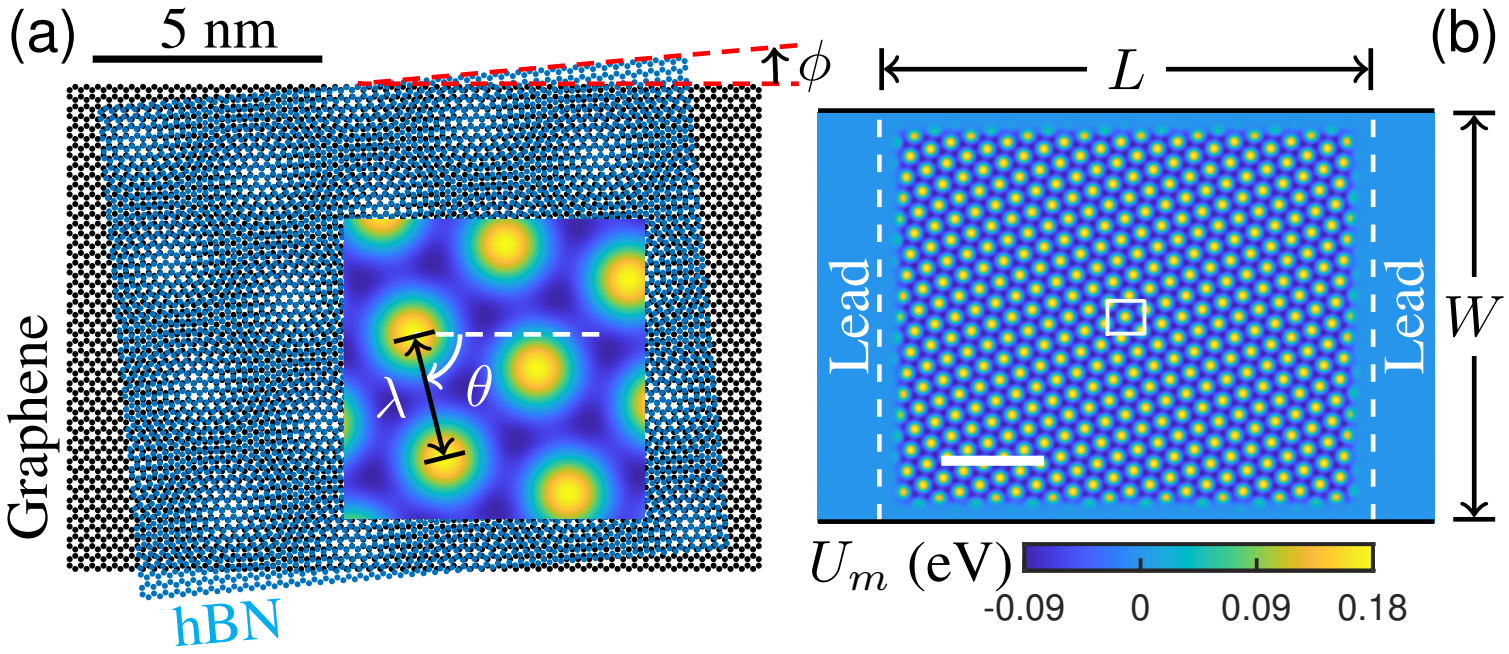

Following Yankowitz, M. et al., Nat. Phys. **8** (2012) 382:

$$U_{\text{moire}}(\mathbf{r}) = V \sum_{j=1,2,3} \cos\left(\mathbf{G}_j \cdot \mathbf{r}\right) , \quad V = 0.06\,\text{eV}$$

More advanced models: Kindermann, M., Uchoa, B., and Miller, D. L., Phys. Rev. B **86** (2012) 115415; Wallbank, J. R., Patel, A. A., Mucha-Kruczyński, M., Geim, A. K., and Fal'ko, V. I., Phys. Rev. B **87** (2013) 245408; Moon, P. and Koshino, M., Phys. Rev. B **90** (2014) 155406

Transport experiment vs transport simulation

Chen, S.-C., Kraft, R., Danneau, R., Richter, K., and Liu, M.-H., Commun. Phys. **3** (2020) 71

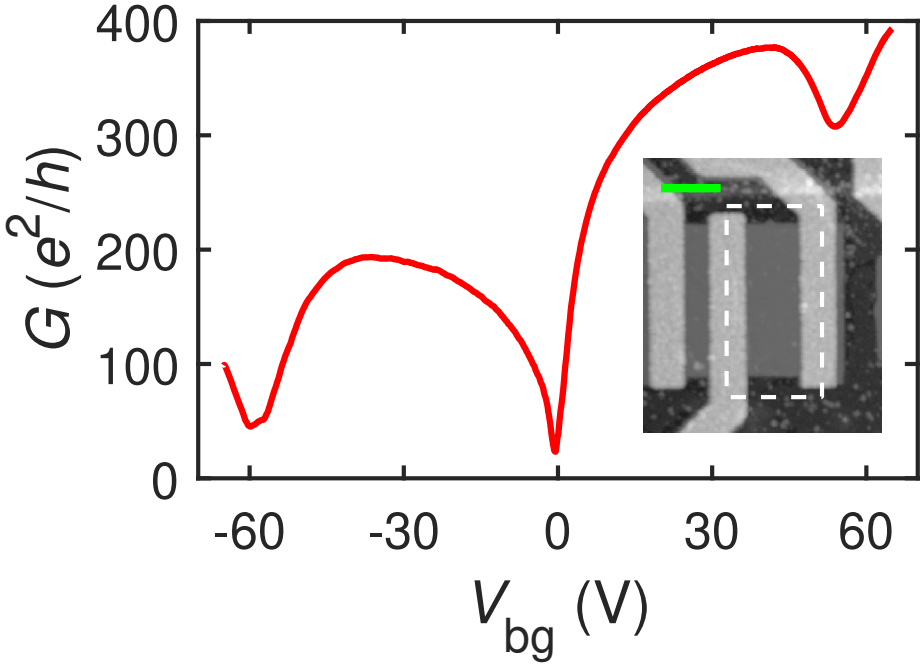

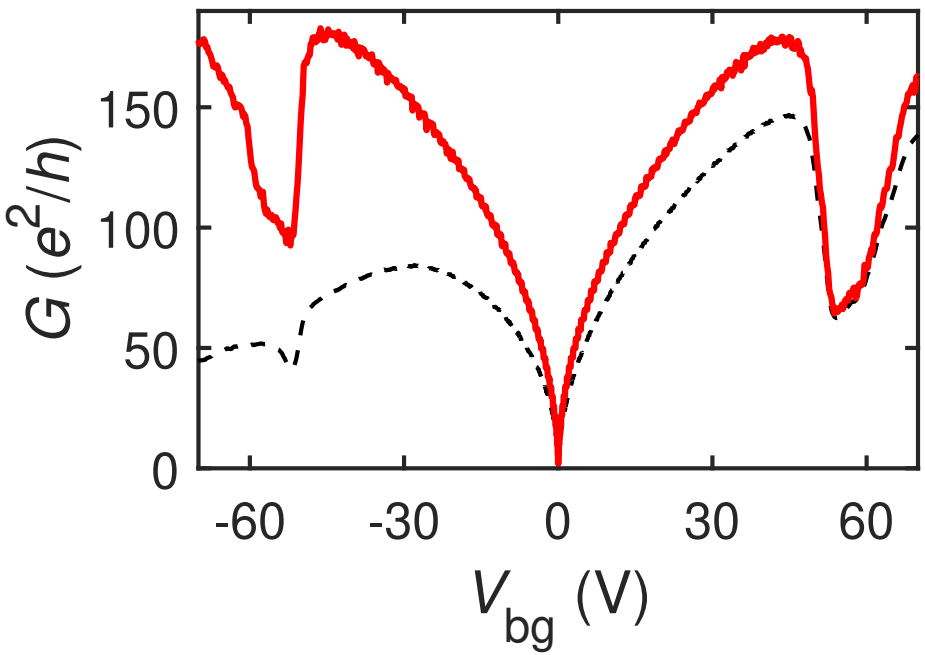

Simulation:

$$\phi = 0.9^\circ\,, \quad L = W = 500\,\text{nm}$$

$$G(E) = \frac{2e^2}{h}T(E)\,, \quad V_{\text{bg}} = \frac{e}{\pi C}\left(\frac{E}{\hbar v_F}\right)^2 \text{sgn}(E)$$

Tight-binding transport vs continuum model

Chen, S.-C., Kraft, R., Danneau, R., Richter, K., and Liu, M.-H., Commun. Phys. **3** (2020) 71

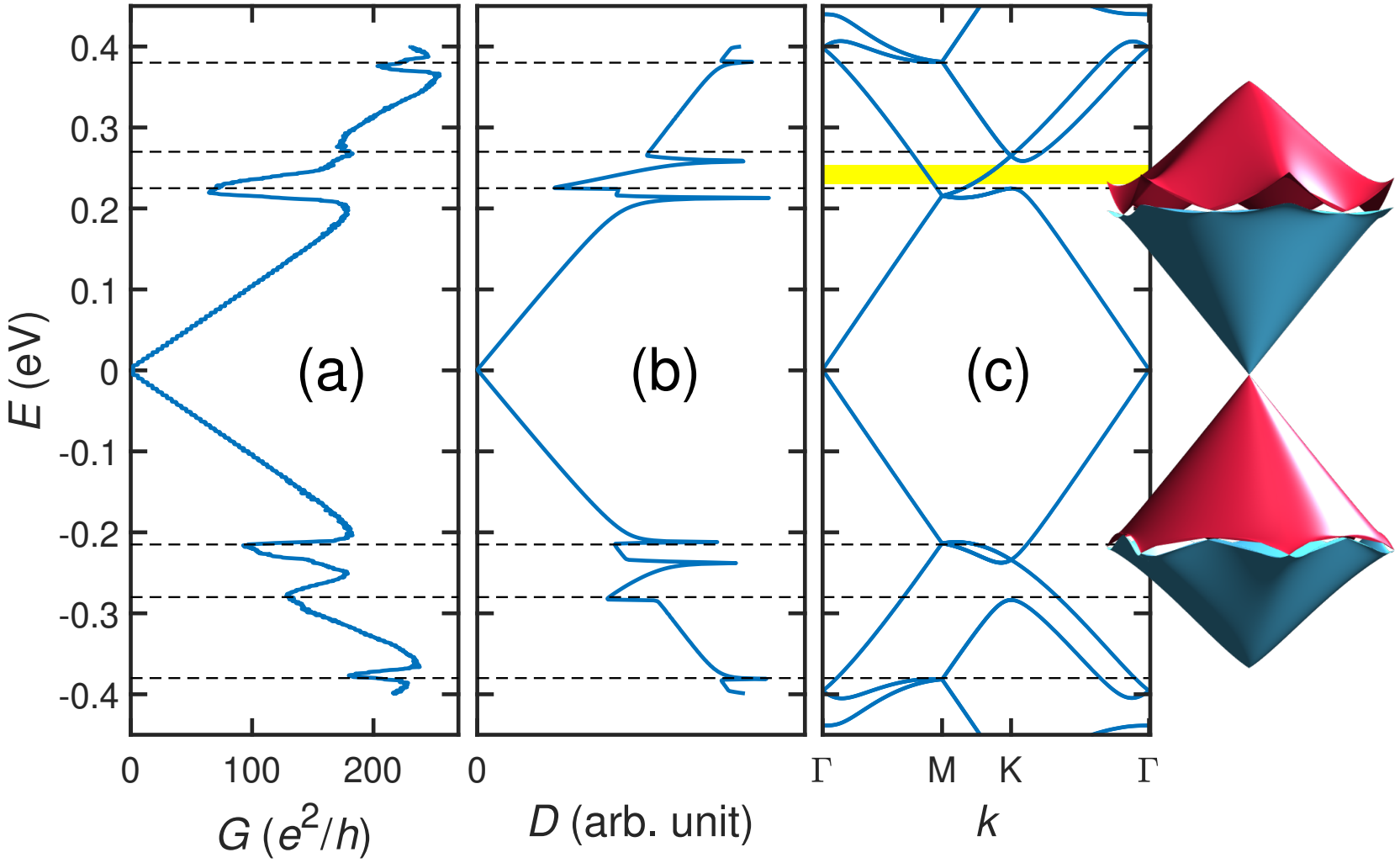

Moiré + *pnp*

Kraft, R. et al., Phys. Rev. Lett. **125** (2020) 217701

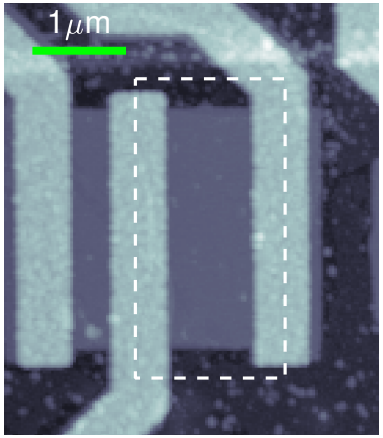

Moiré + *pnp*

Kraft, R. et al., Phys. Rev. Lett. **125** (2020) 217701

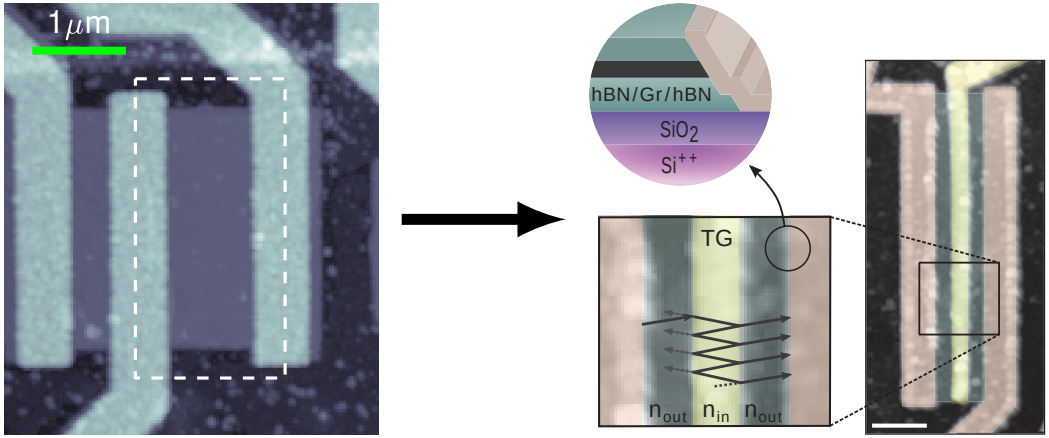

Moiré + *pnp*

Kraft, R. et al., Phys. Rev. Lett. **125** (2020) 217701

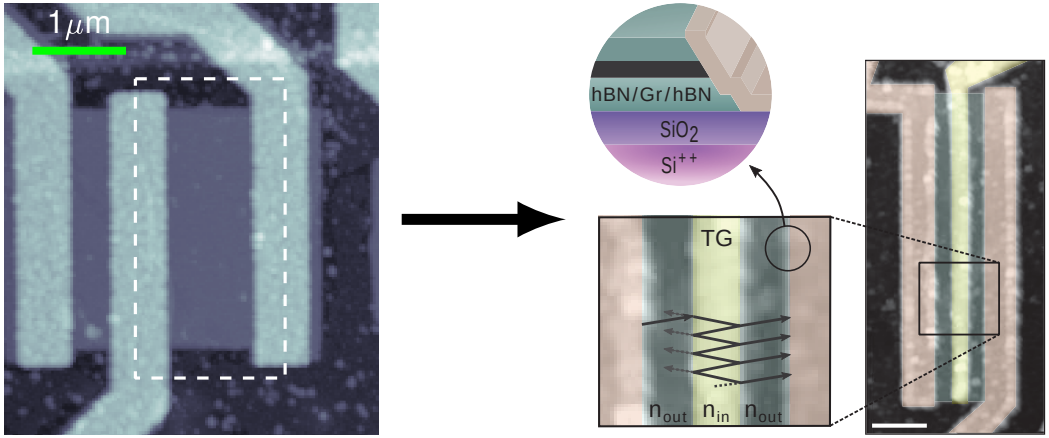

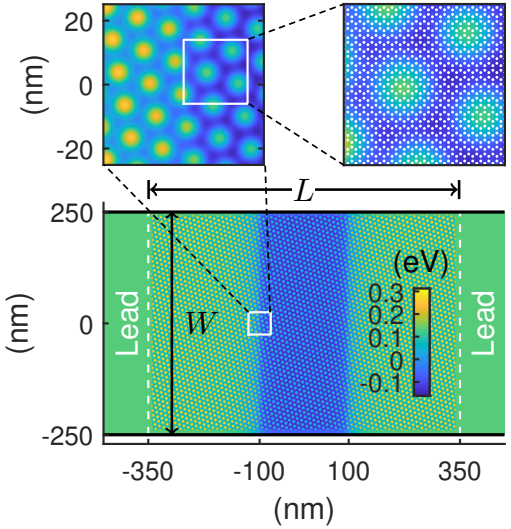

Moiré + *pnp*

Kraft, R. et al., Phys. Rev. Lett. **125** (2020) 217701

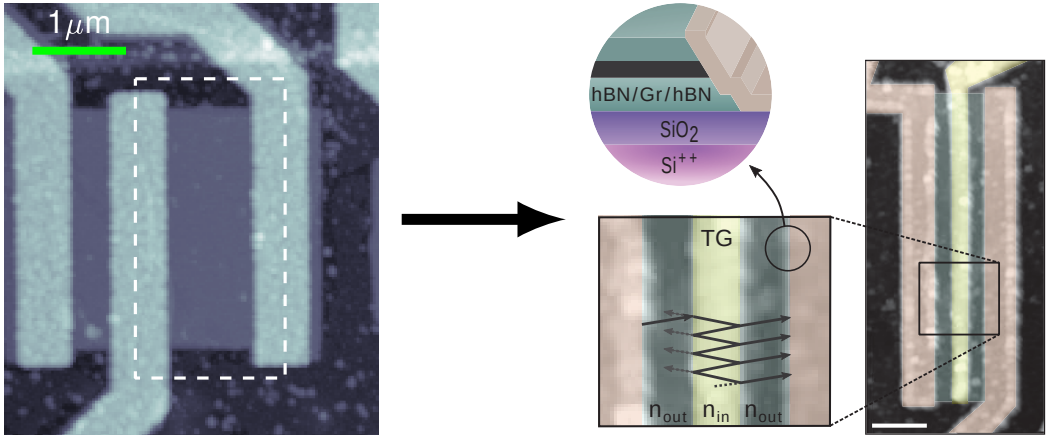

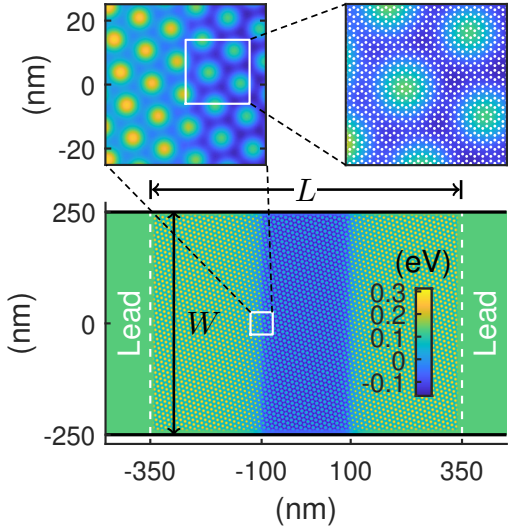

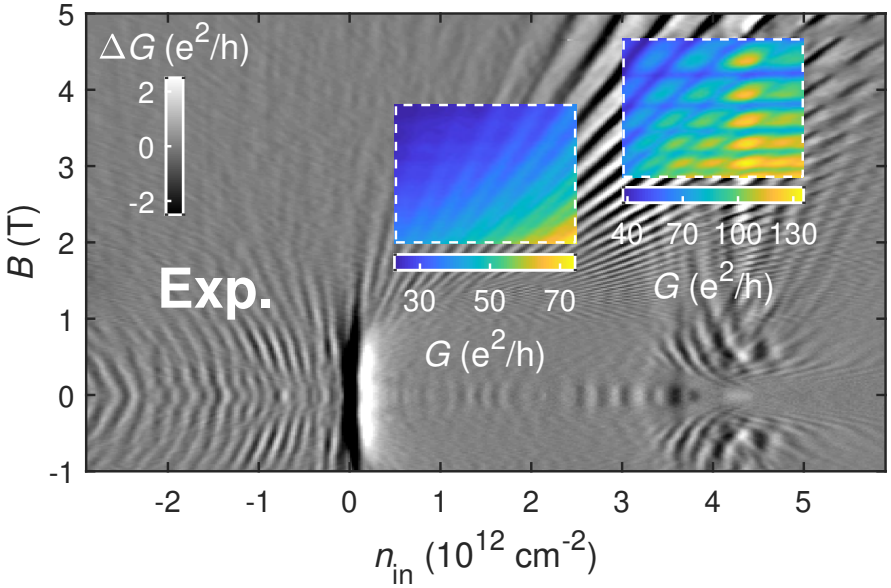

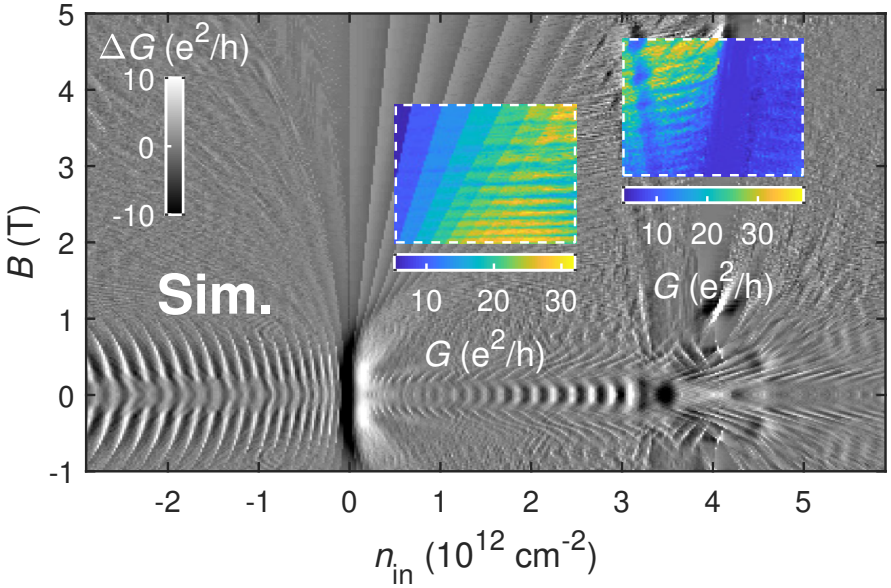

Fabry-Pérot interference

Kraft, R. et al., Phys. Rev. Lett. **125** (2020) 217701

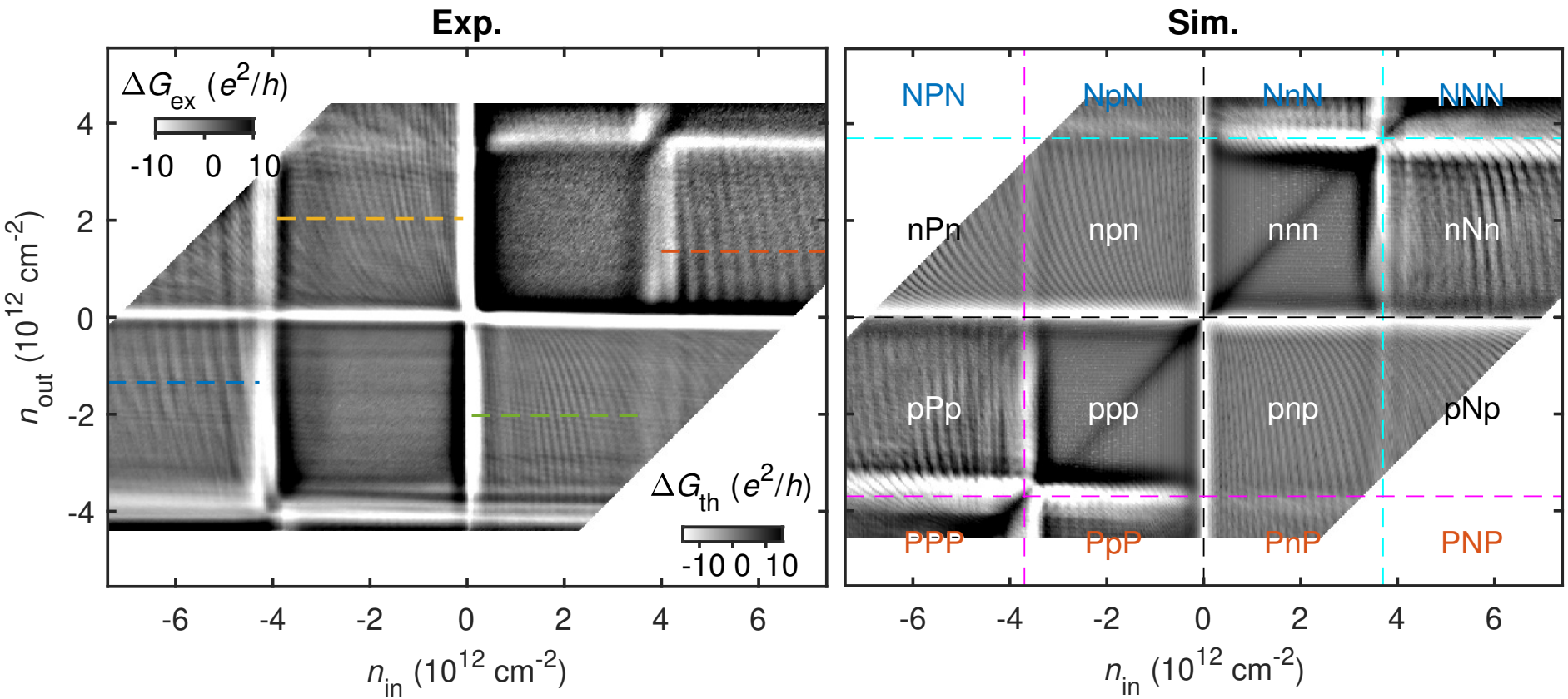

Fabry-Pérot interference

Kraft, R. et al., Phys. Rev. Lett. **125** (2020) 217701

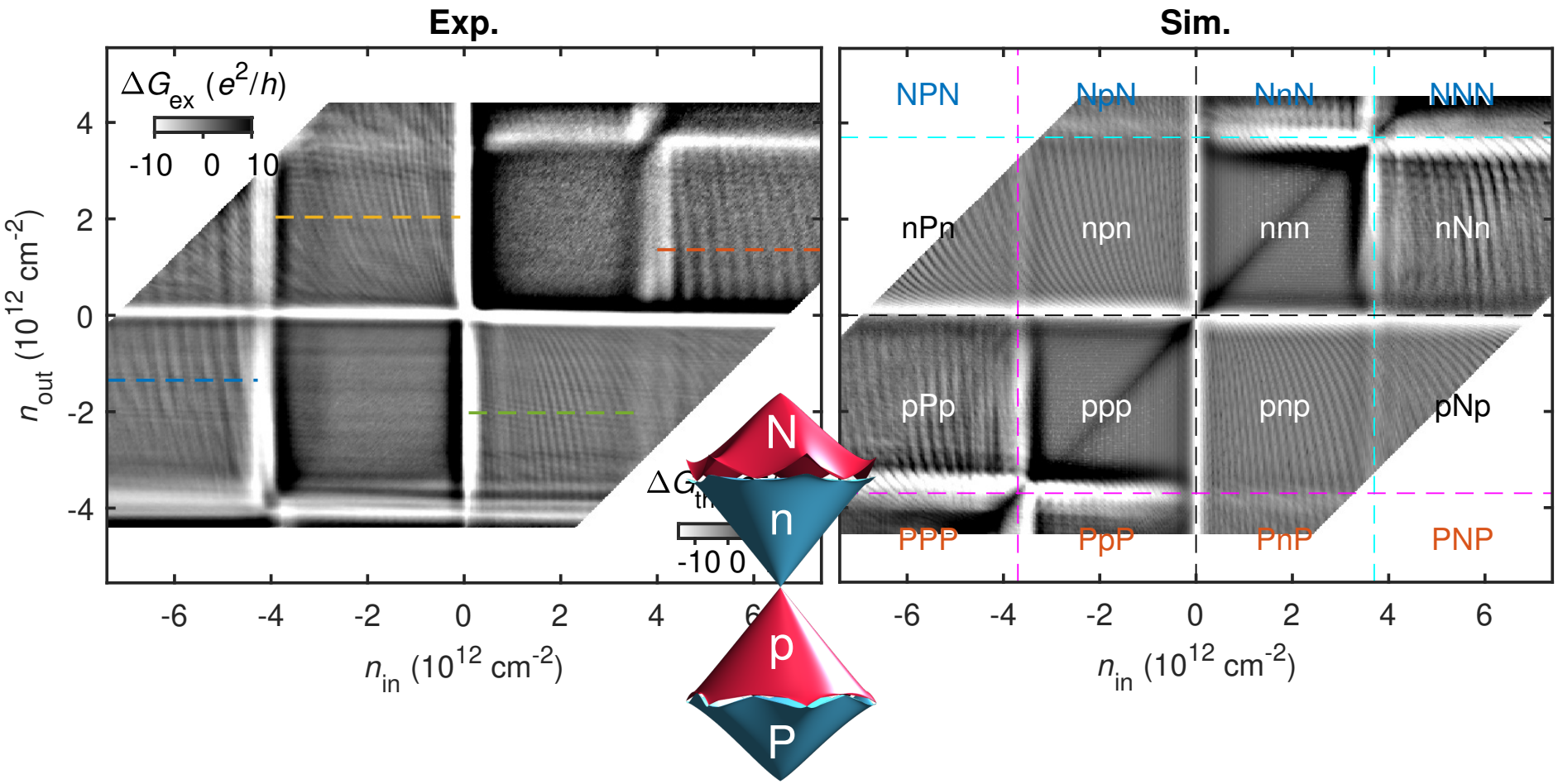

3

Bilayer graphene

- Effective 4-band square lattice model

The model

Chen, S.-C., Mreńca-Kolasińska, A., and Liu, M.-H., (2024) arXiv:2403.03155

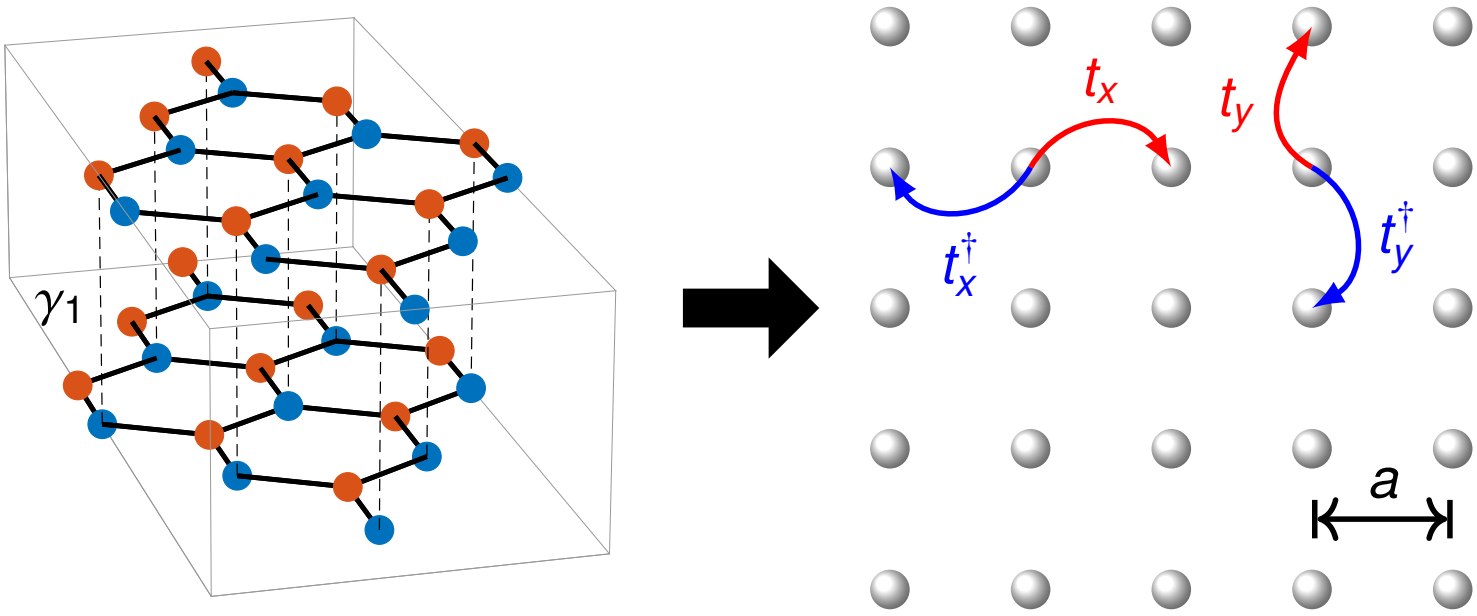

Hopping and onsite-energy matrices:

$$t_x = \frac{\hbar v_F}{2a}\begin{pmatrix} 0 & -i & 0 & 0 \\ -i & 0 & 0 & 0 \\ 0 & 0 & 0 & -i \\ 0 & 0 & -i & 0 \end{pmatrix}, \quad t_y = \frac{\hbar v_F}{2a}\begin{pmatrix} 0 & 1 & 0 & 0 \\ -1 & 0 & 0 & 0 \\ 0 & 0 & 0 & -1 \\ 0 & 0 & 1 & 0 \end{pmatrix}, \quad \mathbb{U}_n = \begin{pmatrix} V_n + \frac{U_n}{2} & 0 & \gamma_1 & 0 \\ 0 & V_n + \frac{U_n}{2} & 0 & 0 \\ \gamma_1 & 0 & V_n - \frac{U_n}{2} & 0 \\ 0 & 0 & 0 & V_n - \frac{U_n}{2} \end{pmatrix}$$

The model

Chen, S.-C., Mreńca-Kolasińska, A., and Liu, M.-H., (2024) arXiv:2403.03155

Hopping and onsite-energy matrices:

$$t_x = \frac{\hbar v_F}{2a}\begin{pmatrix} 0 & -i & 0 & 0 \\ -i & 0 & 0 & 0 \\ 0 & 0 & 0 & -i \\ 0 & 0 & -i & 0 \end{pmatrix}, \quad t_y = \frac{\hbar v_F}{2a}\begin{pmatrix} 0 & 1 & 0 & 0 \\ -1 & 0 & 0 & 0 \\ 0 & 0 & 0 & -1 \\ 0 & 0 & 1 & 0 \end{pmatrix}, \quad \mathbb{U}_n = \begin{pmatrix} V_n + \frac{U_n}{2} & 0 & \gamma_1 & 0 \\ 0 & V_n + \frac{U_n}{2} & 0 & 0 \\ \gamma_1 & 0 & V_n - \frac{U_n}{2} & 0 \\ 0 & 0 & 0 & V_n - \frac{U_n}{2} \end{pmatrix}$$

Effective tight-binding Hamiltonian on a square lattice:

$$\mathcal{H} = \sum_n c_n^\dagger \mathbb{U}_n c_n + \sum_{\langle m,n \rangle} c_m^\dagger \mathbb{T}_{m \leftarrow n} c_n$$

$$\mathbb{T}_{m \leftarrow n} = \begin{cases} t_x\,, & \text{nearest-neighbor} \rightarrow \text{hopping} \\ t_x^\dagger\,, & \text{nearest-neighbor} \leftarrow \text{hopping} \\ t_y\,, & \text{nearest-neighbor} \uparrow \text{hopping} \\ t_y^\dagger\,, & \text{nearest-neighbor} \downarrow \text{hopping} \\ 0\,, & \text{else} \end{cases}$$

Bulk band structure

For an infinitely extending lattice with translation invariance ($U_n = U$, $V_n = 0$), it can be shown:

$$E(k_x, k_y) = \pm\sqrt{t^2(\sin^2 k_x a + \sin^2 k_y a) + \frac{U^2}{4} + \frac{\gamma_1^2}{2} \pm \frac{1}{2}\sqrt{\gamma_1^4 + 4t^2(\sin^2 k_x a + \sin^2 k_y a)(U^2 + \gamma_1^2)}}$$

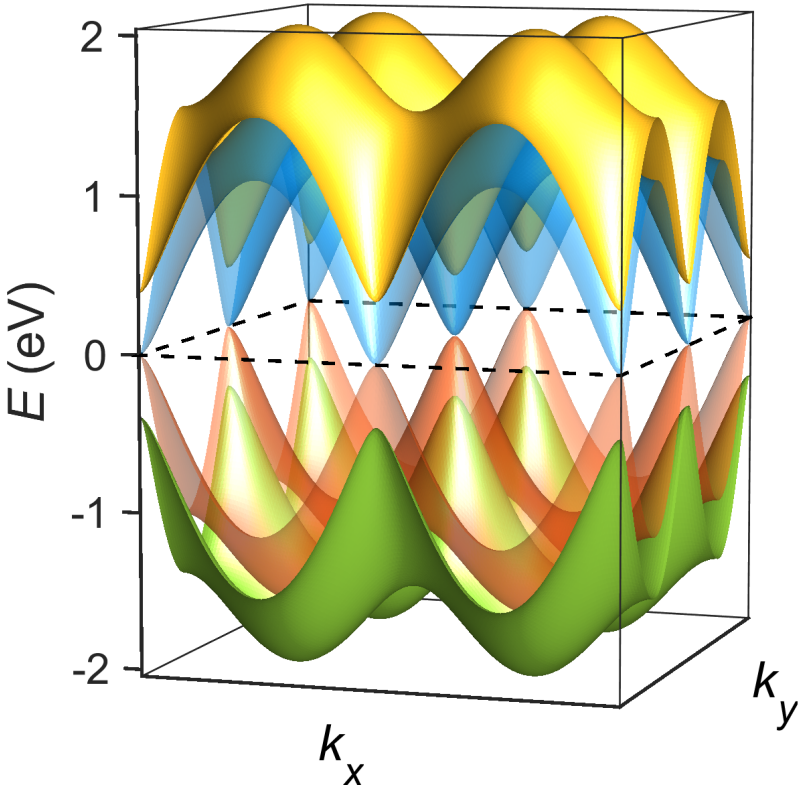

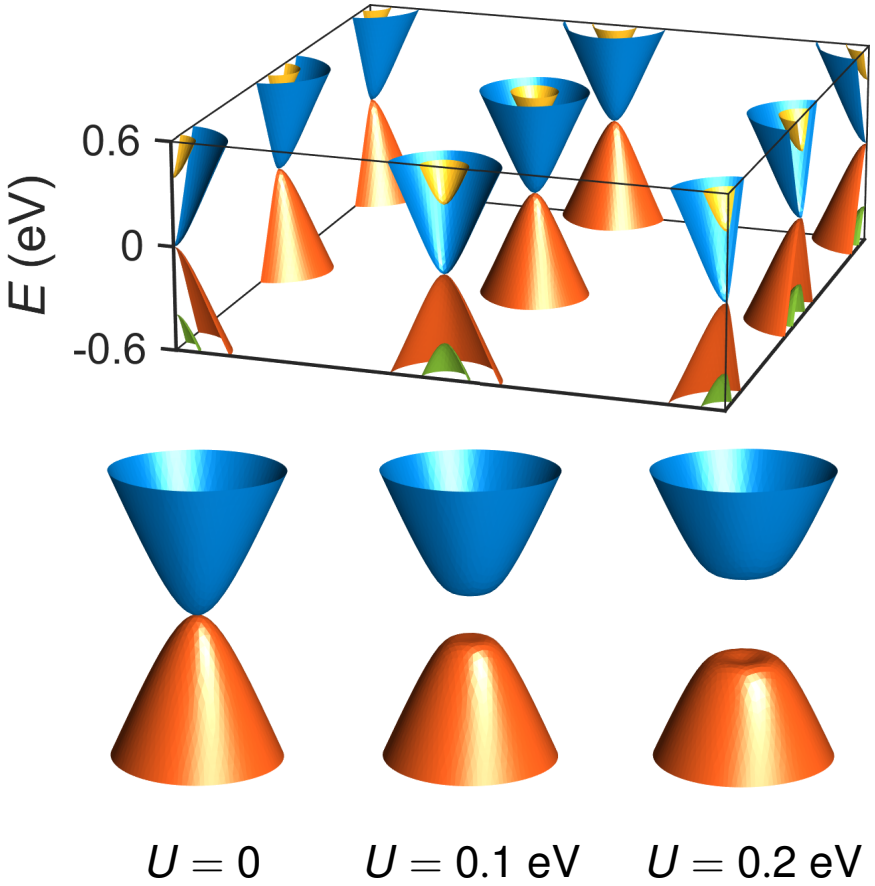

Bulk band structure

For an infinitely extending lattice with translation invariance ($U_n = U$, $V_n = 0$), it can be shown:

$$E(k_x, k_y) = \pm\sqrt{t^2(\sin^2 k_x a + \sin^2 k_y a) + \frac{U^2}{4} + \frac{\gamma_1^2}{2} \pm \frac{1}{2}\sqrt{\gamma_1^4 + 4t^2(\sin^2 k_x a + \sin^2 k_y a)(U^2 + \gamma_1^2)}}$$

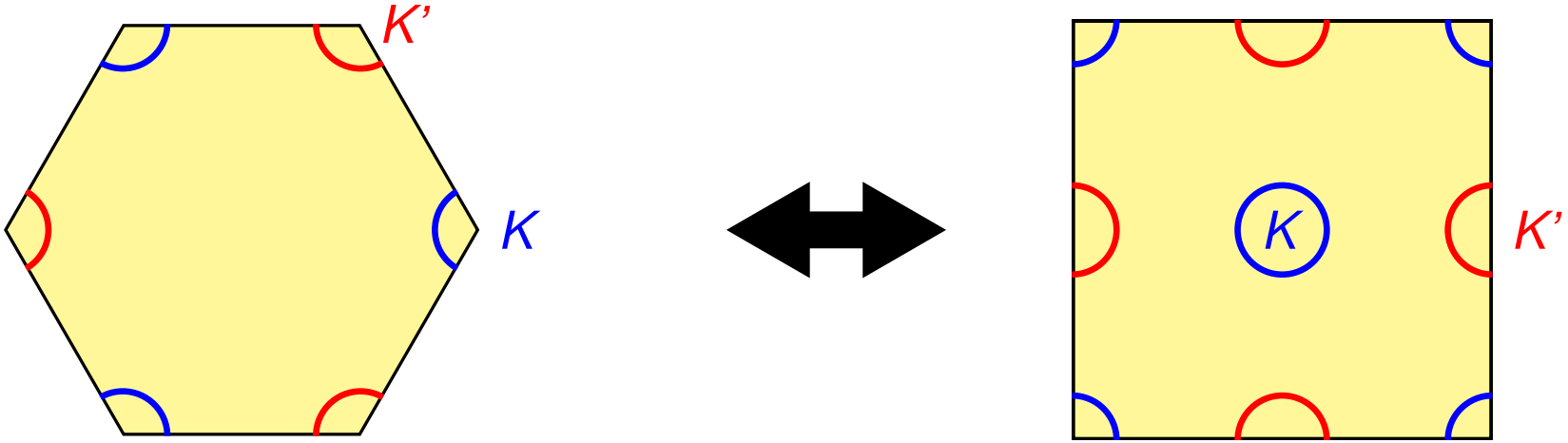

Bulk band structure

For an infinitely extending lattice with translation invariance ($U_n = U$, $V_n = 0$), it can be shown:

$$E(k_x, k_y) = \pm\sqrt{t^2(\sin^2 k_x a + \sin^2 k_y a) + \frac{U^2}{4} + \frac{\gamma_1^2}{2} \pm \frac{1}{2}\sqrt{\gamma_1^4 + 4t^2(\sin^2 k_x a + \sin^2 k_y a)(U^2 + \gamma_1^2)}}$$

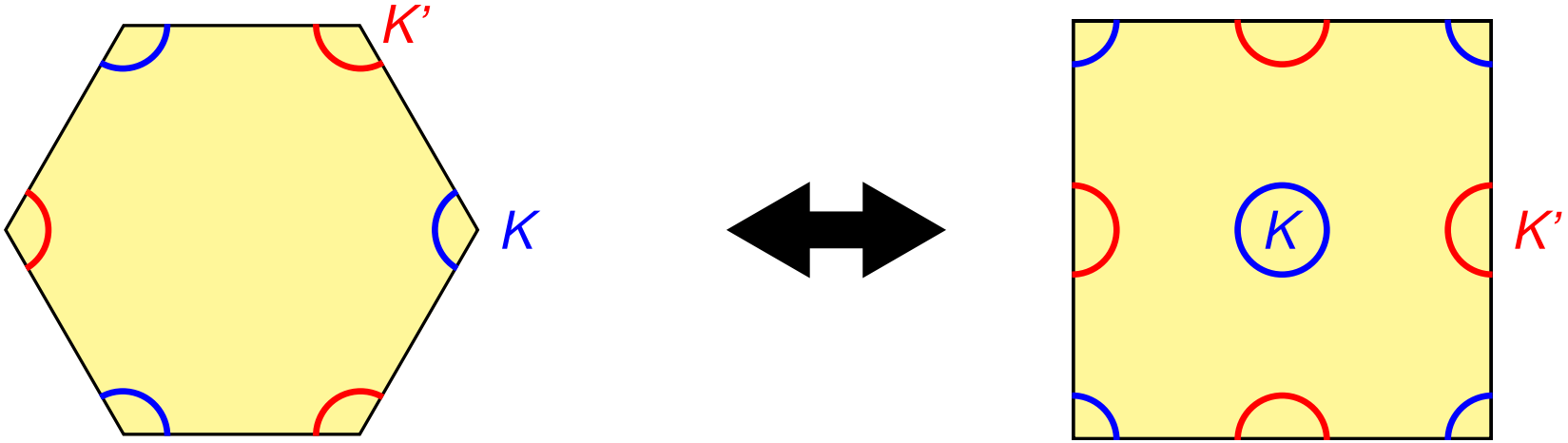

From atomistic tight-binding model[1]:

$$E(k) = \pm\sqrt{\frac{\gamma_1^2}{2} + \frac{U^2}{4} + (\hbar v_F k)^2 \pm \sqrt{\frac{\gamma_1^4}{4} + (\gamma_1^2 + U^2)(\hbar v_F k)^2}}$$

[1] McCann, E. and Koshino, M., Rep. Prog. Phys. **76** (2013) 056503

Comparison of band structures

Effective model vs atomistic tight-binding model

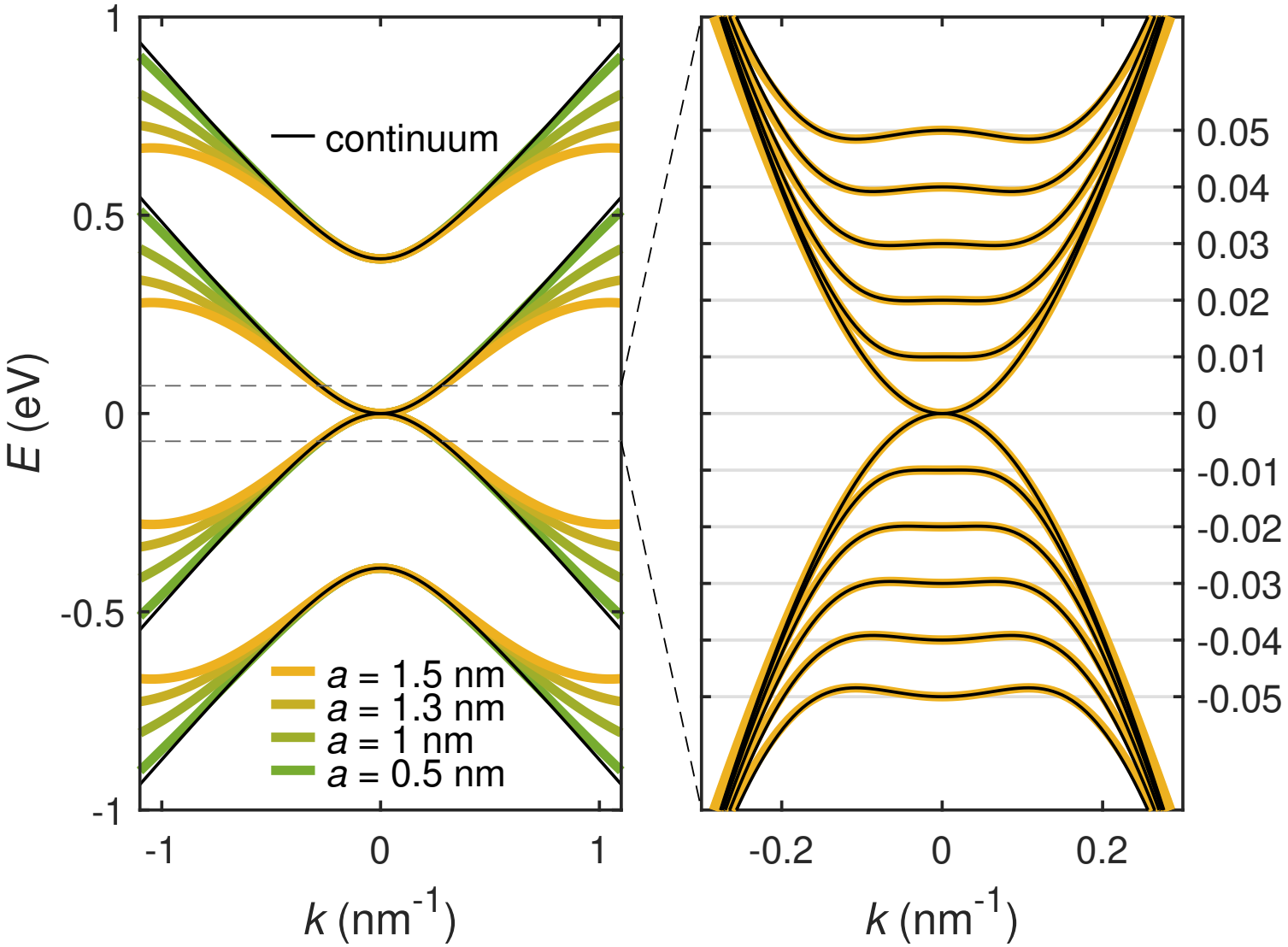

Ribbon band structures & magnetotransport

Chen, S.-C., Mreńca-Kolasińska, A., and Liu, M.-H., (2024) arXiv:2403.03155

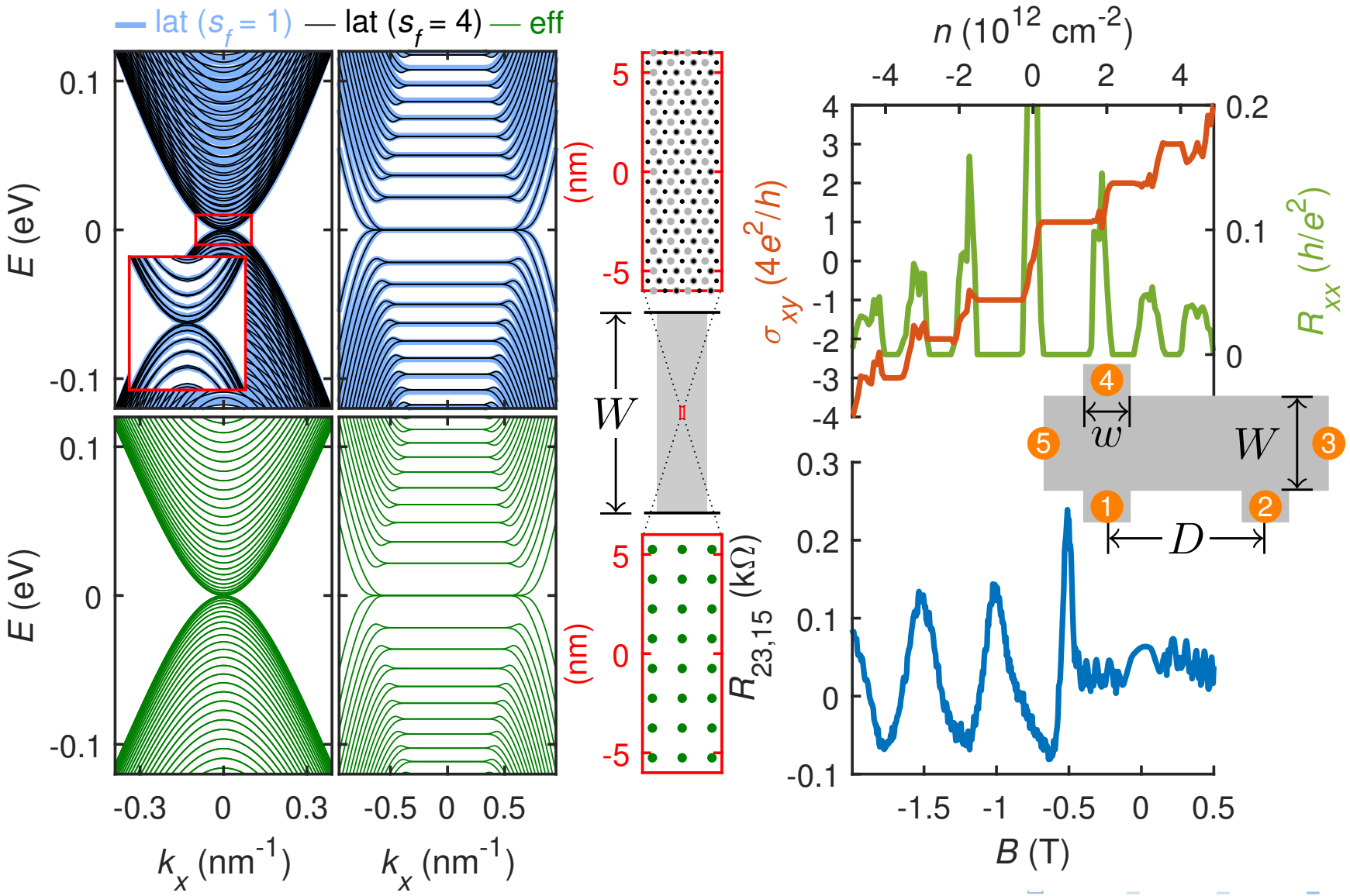

Revisiting the recent AB experiment[1]

Chen, S.-C., Mreńca-Kolasińska, A., and Liu, M.-H., (2024) arXiv:2403.03155

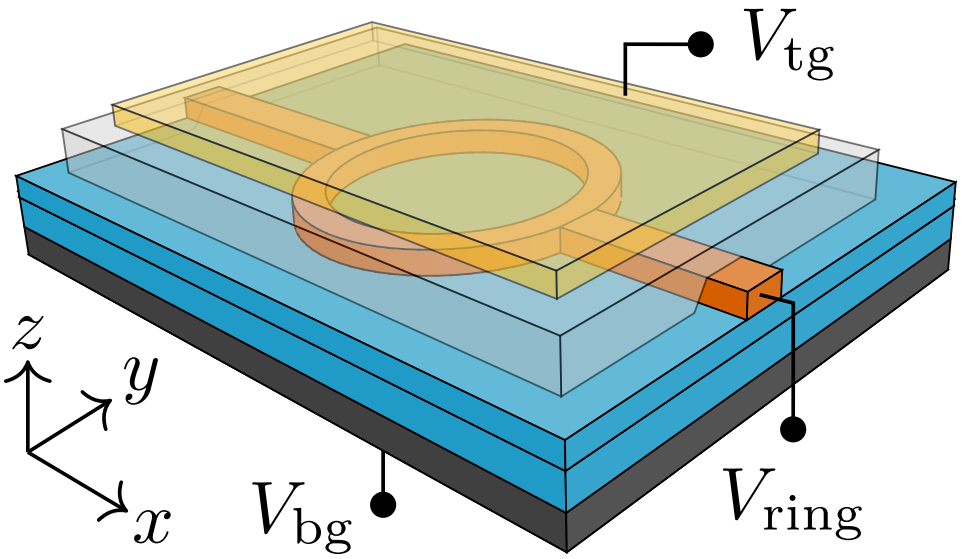

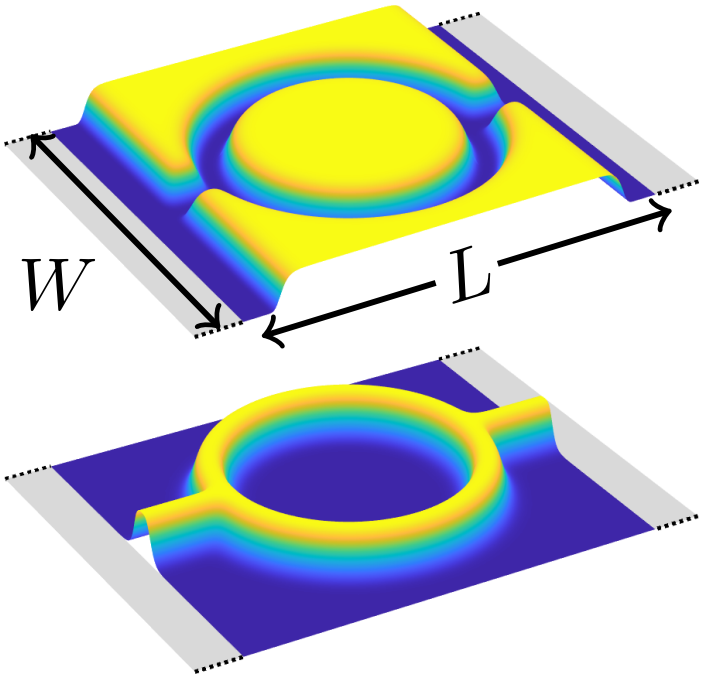

$L \approx 1.8\,\mu\text{m}\,, \quad W \approx 1.6\,\mu\text{m}$

[1] Iwakiri, S. et al., Nano Letters **22** (2022) 6292

Revisiting the recent AB experiment[1]

Chen, S.-C., Mreńca-Kolasińska, A., and Liu, M.-H., (2024) arXiv:2403.03155

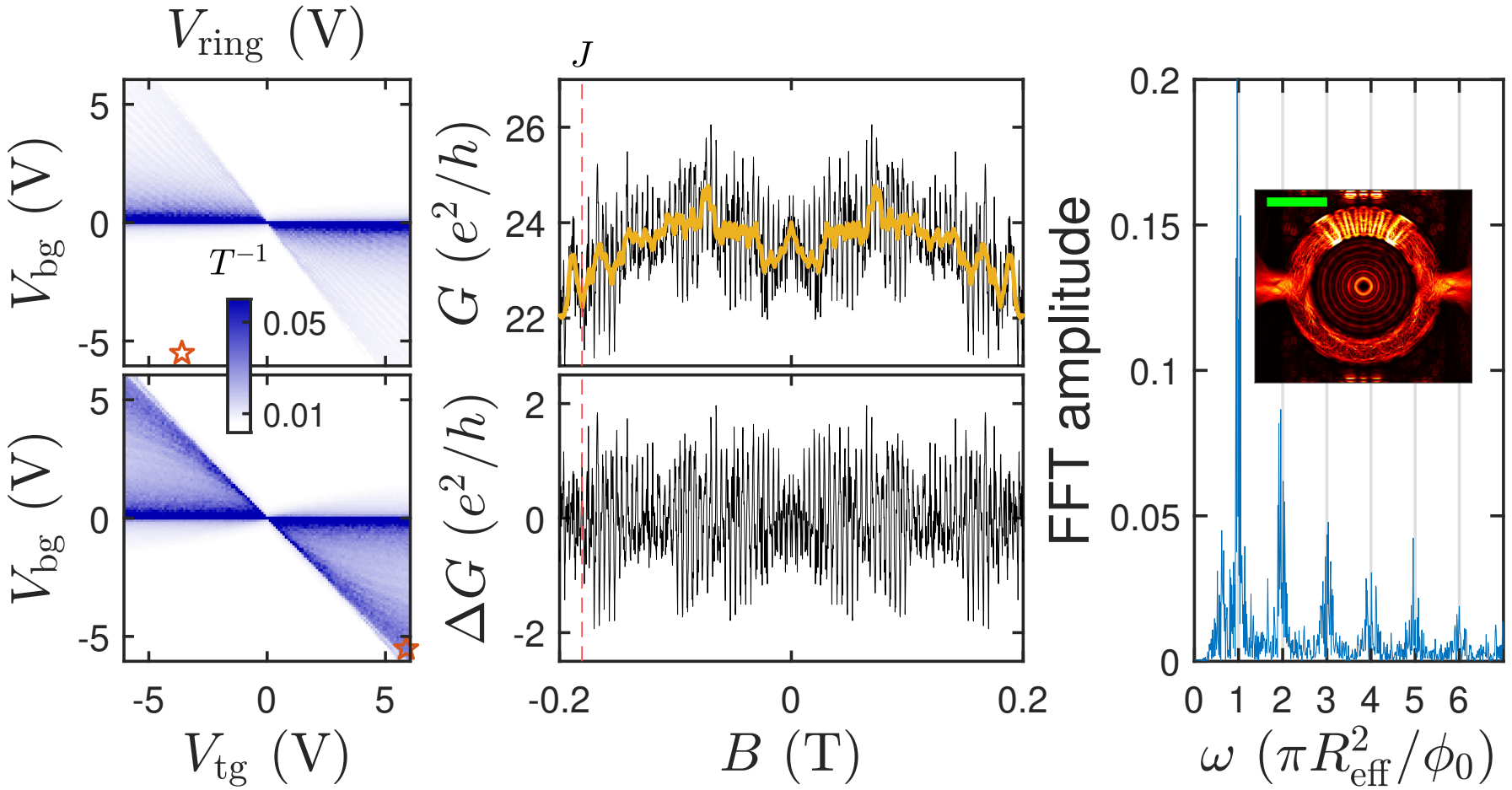

[1] Iwakiri, S. et al., Nano Letters **22** (2022) 6292

Revisiting the recent AB experiment[1]

Chen, S.-C., Mreńca-Kolasińska, A., and Liu, M.-H., (2024) arXiv:2403.03155

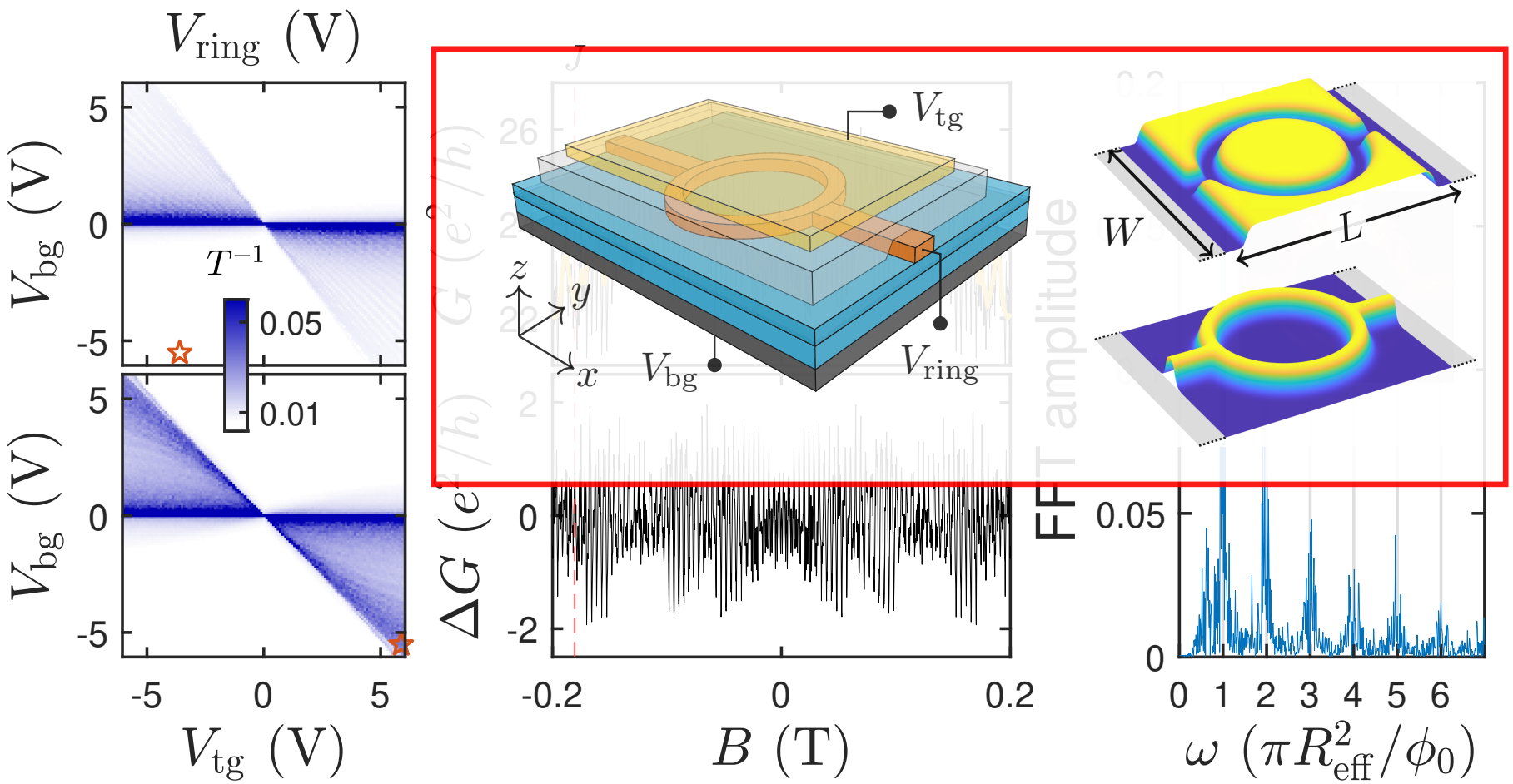

[1] Iwakiri, S. et al., Nano Letters **22** (2022) 6292

Revisiting the recent AB experiment[1]

Chen, S.-C., Mreńca-Kolasińska, A., and Liu, M.-H., (2024) arXiv:2403.03155

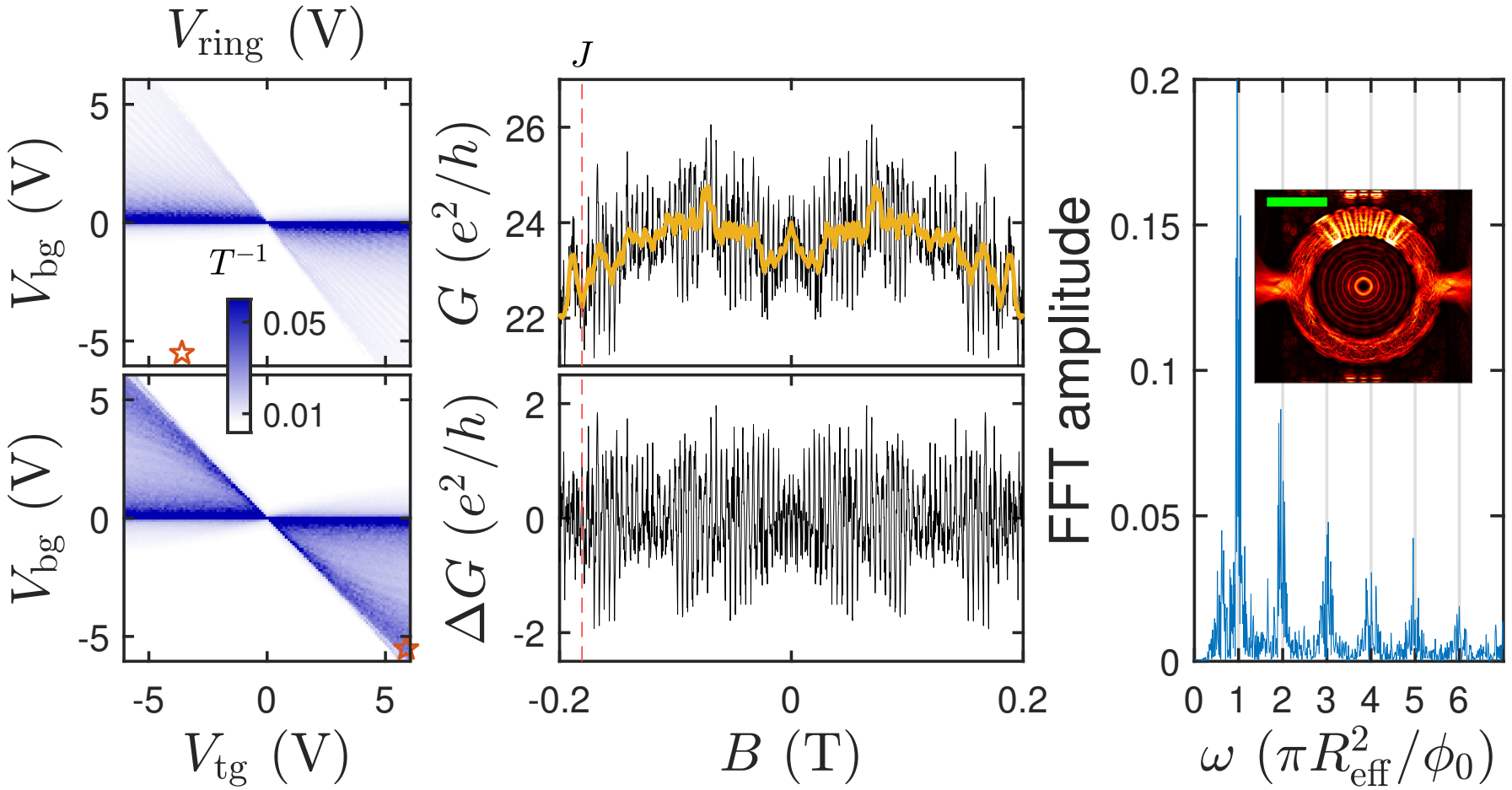

[1] Iwakiri, S. et al., Nano Letters **22** (2022) 6292

4

Lieb lattice

Lieb lattice

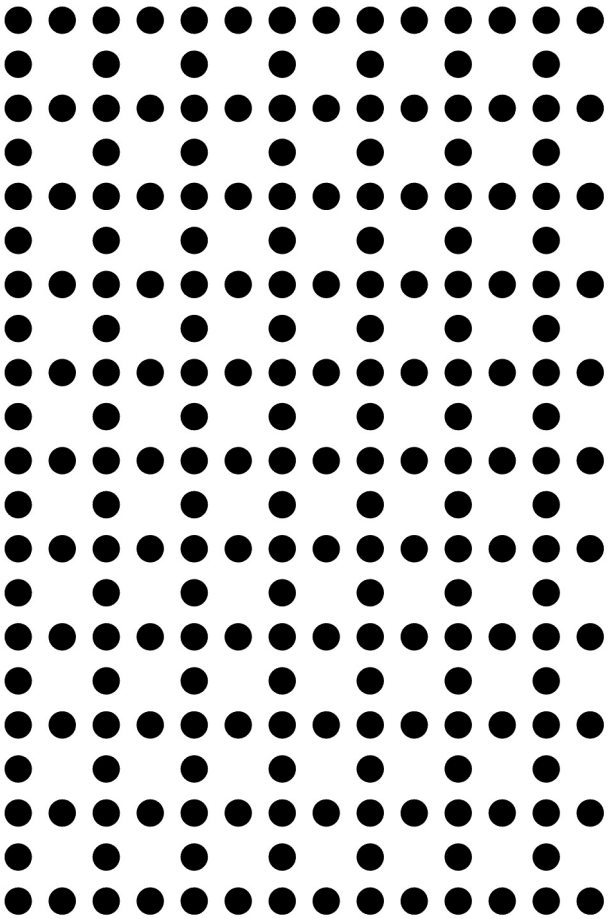

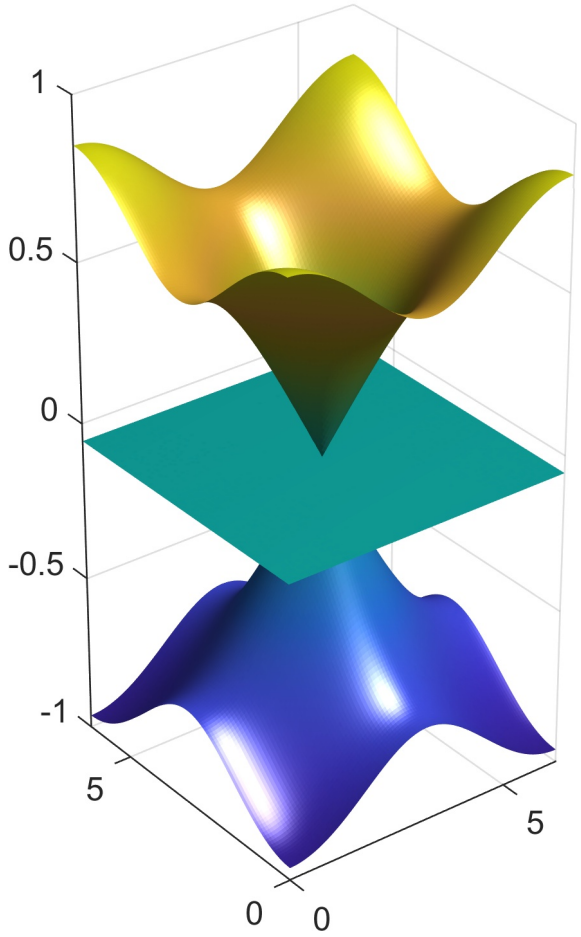

Nearest neighbor hoppings only.

Lieb lattice

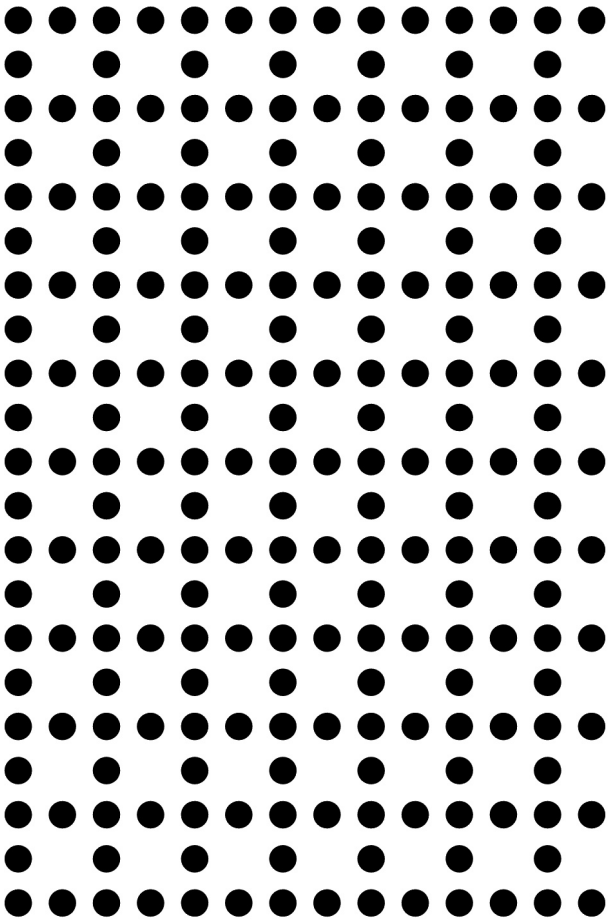

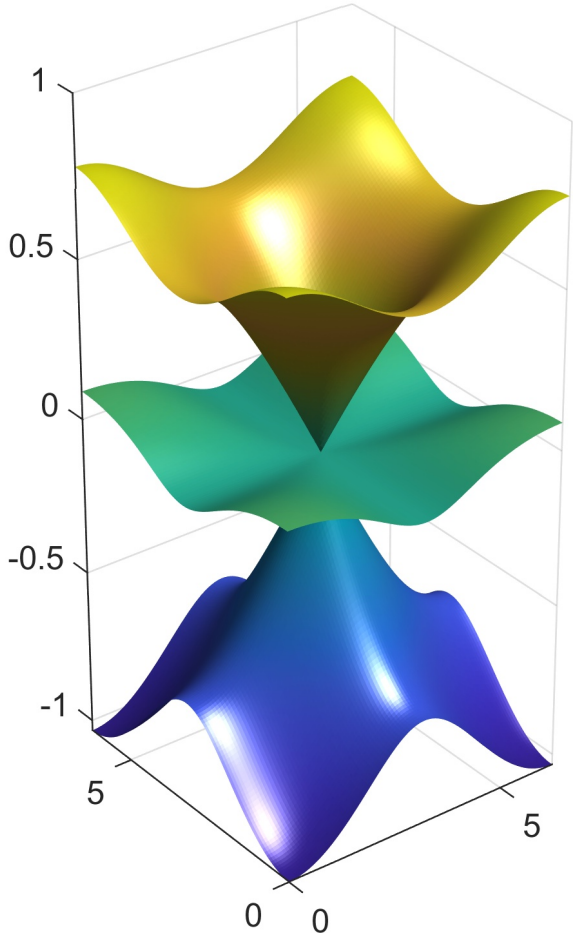

Up to second nearest neighbor hoppings.

Transmission across *pn* junctions

Kleing tunneling in graphene vs super-Klein tunneling in Lieb lattice

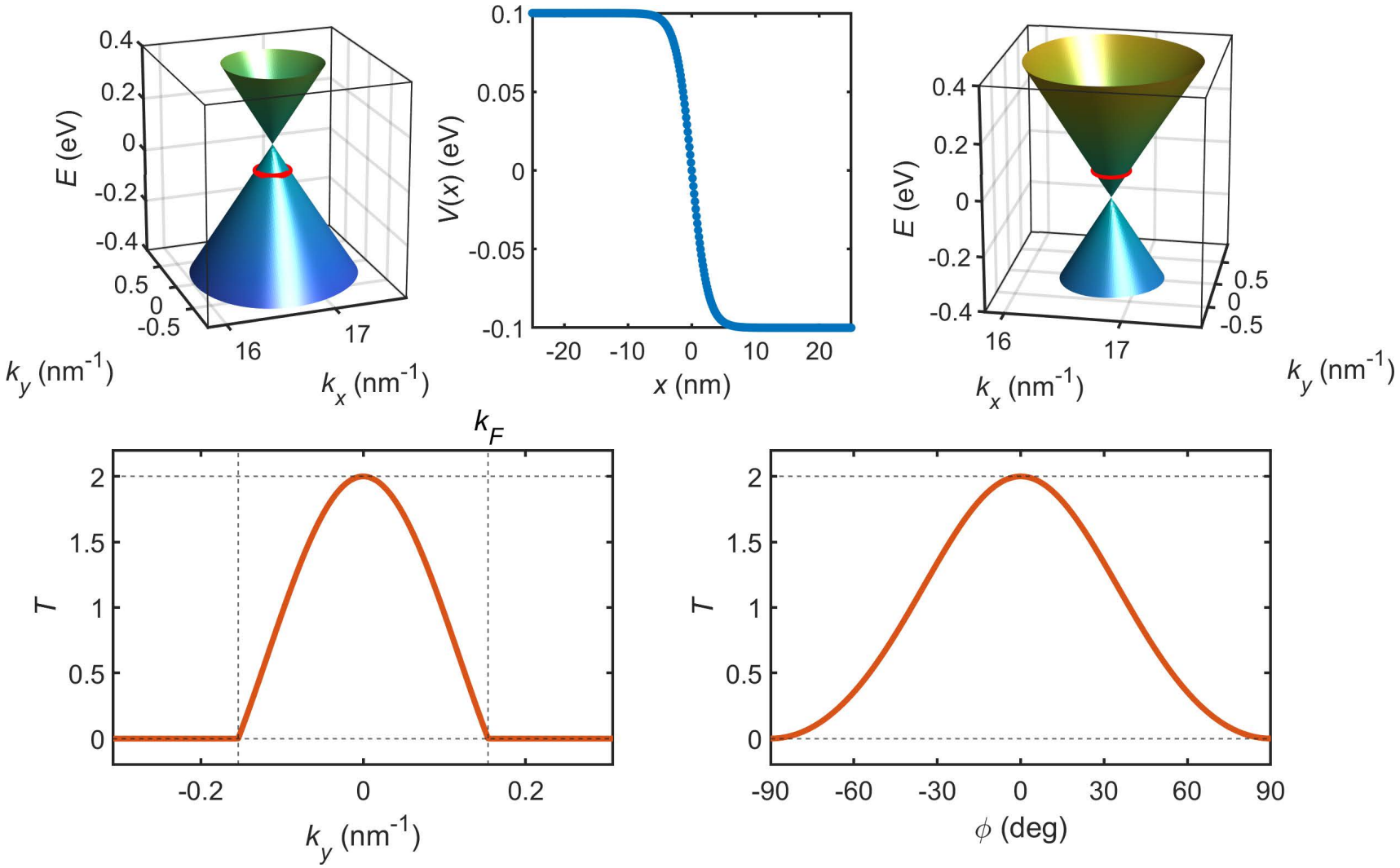

Transmission across *pn* junctions

Kleing tunneling in graphene vs super-Klein tunneling in Lieb lattice

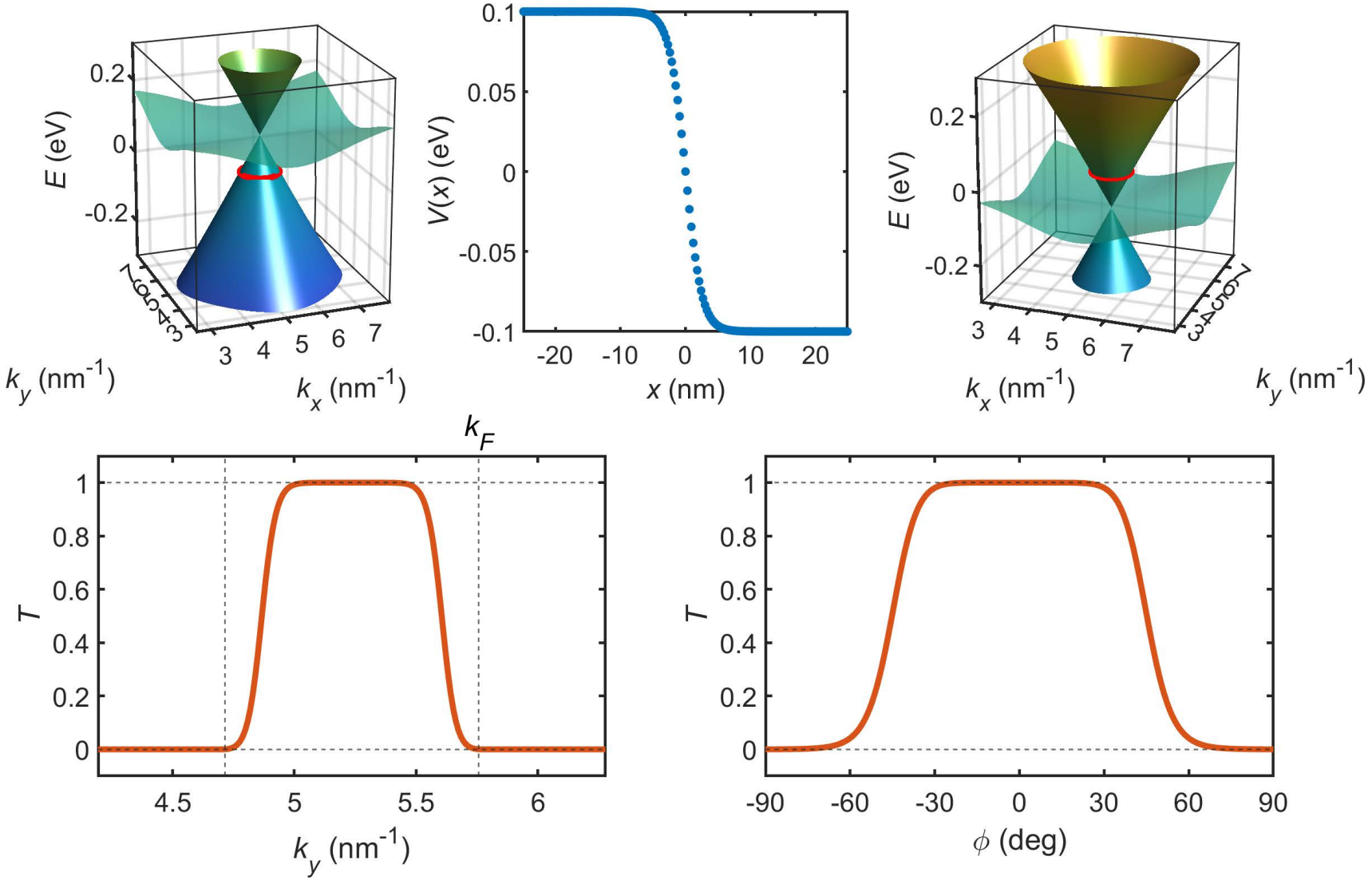

Summary

Basics

- Landauer-Büttiker formalism
- Real-space Green's function method
- Lead self-energy
- Peierls substitution
- Gauge transformation for vector potential
- Semiclassical motion of Bloch electrons

Applications

- 2DEG & MoS_2
- Graphene
- Bilayer graphene
- Lieb lattice

Acknowledgments

Special thanks: Aitor Garcia-Ruiz, Alina Mreńca-Kolasińska, Szu-Chao Chen, Wun-Hao Kang

- Financial: National Science and Technology Council of Taiwan
- Computational: National Center for High-performance Computing
- Prof. Dr. Klaus Richter for hosting my sabbatical in Uni Regensburg